AD-A158 844 THEORETICAL INVESTIGATION OF SINGLE-FREQUENCY 8-ELEMENT 1/3
LOCALIZER SIGNAL..(U) OHIO UNIV ATHENS AVIONICS
ENGINEERING CENTER W D PHIPPS MAY 85 OU/AEC/EER-59-4
UNCLASSIFIED DOT/FAA/PM-85/4 DTFA01-82-C-10050 F/G 17/7 NL

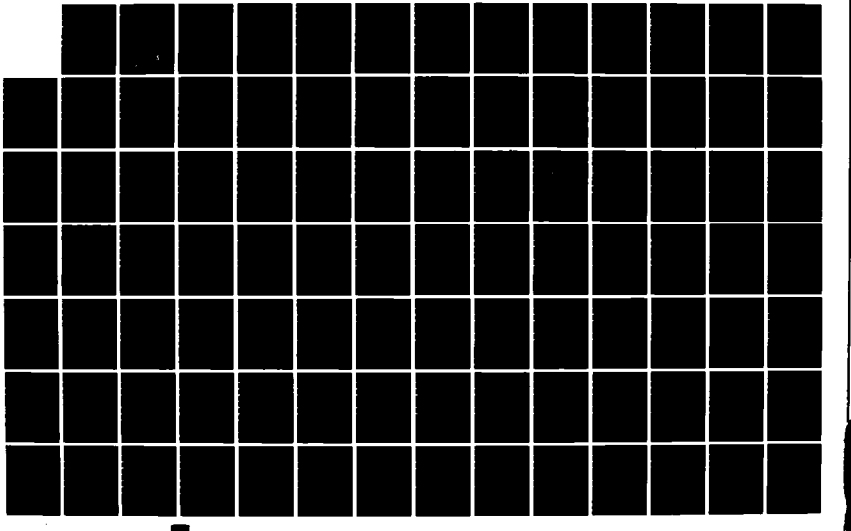

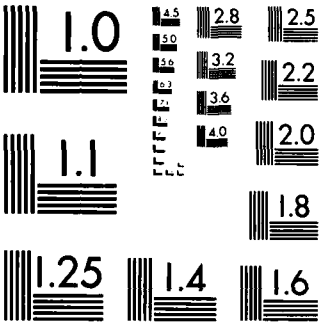

MICROCOPY RESOLUTION TEST CHART

)ARDS-1963-A

DOT/FAA/PM-85/4

Program Engineering
and Maintenance Service
Washington, D.C. 20591

Theoretical Investigation of Single-Frequency 8-Element Localizer Signal Scattering For Critical Area Determination

AD-A158 844

Walter D. Phipps

Avionics Engineering Center
Department of Electrical and Computer Engineering
Ohio University
Athens, Ohio 45701

May 1985

Final Report

DTIC FILE COPY

This Document is available to the public through the National Technical Information Service, Springfield, Virginia 22161.

DTIC ELECTE AUG 2 9 1985 S D G

DISTRIBUTION STATEMENT A
Approved for public release;
Distribution Unlimited

U.S. Department of Transportation
Federal Aviation Administration

85 8 20 101

NOTICE

This document is disseminated under the sponsorship of the Department of Transportation in the interest of information exchange. The United States Government assumes no liability for the contents or use thereof.

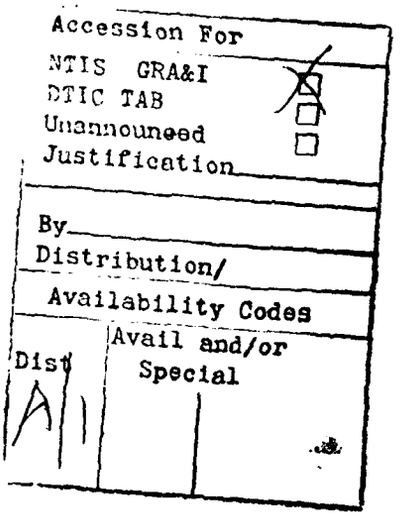

Technical Report Documentation Page

1. Report No.	2. Government Accession No.	3. Recipient's Catalog No.
DOT/FAA/RD/82/4	AD-A158 844	

4. Title and Subtitle
THEORETICAL INVESTIGATION OF SINGLE-FREQUENCY 8-ELEMENT LOCALIZER SIGNAL SCATTERING FOR CRITICAL AREA DETERMINATION

5. Report Date

6. Performing Organization Code
OU/AEC/EER 82-4

7. Author(s)
Walter L. Fripps

8. Performing Organization Report No.

9. Performing Organization Name and Address
Avionics Engineering Center
Dept. of Electrical and Computer Engineering
Ohio University
Athens, Ohio 45701

10. Work Unit No. (TRAIS)

11. Contract or Grant No.
DTFA01-82-C-10050

12. Sponsoring Agency Name and Address
U.S. Department of Transportation
Federal Aviation Administration
Program Engineering and Maintenance Service
Washington, D.C. 20591

13. Type of Report and Period Covered
FINAL REPORT

14. Sponsoring Agency Code

15. Supplementary Notes

16. Abstract

A theoretical investigation of the log-periodic, 8-element, single-frequency localizer has been performed to establish critical area criteria for all categories of ILS operation. Contour maps are provided which predict the peak localizer CDI perturbation in each ILS zone for various sizes, locations, and orientations of scatterer aircraft in the vicinity of the localizer transmitting array. Also, plots are provided indicating locations at which the presence of an interfering aircraft will cause the radiated signal of the 8-element localizer to exceed Category I, Category II, or Category III tolerances, specified in U.S. Flight Inspection Manual 8200.1. Additionally, comparative data for the log-periodic, 14-element, single-frequency localizer are presented.

17. Key Words	18. Distribution Statement
LOCALIZER, CRITICAL AREA, 8-ELEMENT, 14-ELEMENT, CONTOUR MAPS, MATHEMATICAL MODELING	This document is available to the U.S. public through the National Technical Information Service, Springfield, Virginia 22161.

19. Security Classif. (of this report)	20. Security Classif. (of this page)	21. No. of Pages	22. Price
NONE	UNCLASSIFIED	191	

Form DOT F 1700.7 (8-72) Reproduction of completed page authorized

English/Metric Conversion Factors

Length

From \ To	Cm	m	Km	in	ft	s mi	nmi
Cm	1	0.01	$1x10^{-5}$	0.3937	0.0328	$6.21x10^{-6}$	$5.39x10^{-6}$
m	100	1	0.001	39.37	3.281	0.0006	0.0005
Km	100,000	1000	1	39370	3281	0.6214	0.5395
in	2.540	0.0254	$2.54x10^{-5}$	1	0.0833	$1.58x10^{-5}$	$1.37x10^{-5}$
ft	30.48	0.3048	$3.05x10^{-4}$	12	1	$1.89x10^{-4}$	$1.64x10^{-4}$
S mi	160,900	1609	1.609	63360	5280	1	0.8688
nmi	185,200	1852	1.852	72930	6076	1.151	1

Area

From \ To	Cm^2	m^2	Km^2	in^2	ft^2	S mi^2	nmi^2
Cm^2	1	0.0001	$1x10^{-10}$	0.1550	0.0011	$3.86x10^{-11}$	$5.11x10^{-11}$
m^2	10,000	1	$1x10^{-6}$	1550	10.76	$3.86x10^{-7}$	$5.11x10^{-7}$
Km^2	$1x10^{10}$	$1x10^{6}$	1	$1.55x10^{9}$	$1.08x10^{7}$	0.3861	0.2914
in^2	6.452	0.0006	$6.45x10^{-10}$	1	0.0069	$2.49x10^{-10}$	$1.88x10^{-10}$
ft^2	929.0	0.0929	$9.29x10^{-8}$	144	1	$3.59x10^{-8}$	$2.71x10^{-8}$
S mi^2	$2.59x10^{10}$	$2.59x10^{6}$	2.590	$4.01x10^{9}$	$2.79x10^{7}$	1	0.7548
nmi^2	$3.43x10^{10}$	$3.43x10^{6}$	3.432	$5.31x10^{9}$	$3.70x10^{7}$	1.325	1

Volume

From \ To	Cm^3	Liter	m^3	in^3	ft^3	yd^3	fl oz	fl pt	fl qt	gal
Cm^3	1	0.001	$1x10^{-6}$	0.0610	$3.53x10^{-5}$	$1.31x10^{-6}$	0.0338	0.0021	0.0010	0.0002
liter	1000	1	0.001	61.02	0.0353	0.0013	33.81	2.113	1.057	0.2642
m^2	$1x10^{6}$	1000	1	61,000	35.31	1.308	33,800	2113	1057	264.2
in^3	16.39	0.0163	$1.64x10^{-5}$	1	0.0006	$2.14x10^{-5}$	0.5541	0.0346	2113	0.0043
ft^3	28,300	28.32	0.0283	1728	1	0.0370	957.5	59.84	0.0173	7.481
yd^3	765,000	764.5	0.7646	46700	27	1	25900	1616	807.9	202.0
fl oz	29.57	0.2957	$2.96x10^{-5}$	1.805	0.0010	$3.87x10^{-5}$	1	0.0625	0.0312	0.0078
fl pt	473.2	0.4732	0.0005	28.88	0.0167	0.0006	16	1	0.5000	0.1250
fl qt	946.3	0.9463	0.0009	57.75	0.0334	0.0012	32	2	1	0.2500
gal	3785	3.785	0.0038	231.0	0.1337	0.0050	128	8	4	1

Mass

From \ To	g	Kg	oz	lb	ton
g	1	0.001	0.0353	0.0022	$1.10x10^{-6}$
Kg	1000	1	35.27	2.205	0.0011
oz	28.35	0.0283	1	0.0625	$3.12x10^{-5}$
lb	453.6	0.4536	16	1	0.0005
ton	907,000	907.2	32,000	2000	1

Temperature

$°C = 5/9 (°F - 32)$

$°F = 9/5 (°C) + 32$

TABLE OF CONTENTS

LIST OF FIGURES

LIST OF FIGURES (continued)

LIST OF TABLES

I. CONCLUSIONS

The following conclusions are based on the theoretical work performed to examine the effects of scatterer aircraft on the performance of an 8-element, single-frequency localizer using LPD antennas.

1. The 8-element, single-frequency localizer has significantly larger critical areas for Category I, Category II, and Category III operations than a 14-element, single-frequency localizer. The boundaries of the critical areas in the direction perpendicular to the runway centerline are approximately twice as large for an 8-element array.

2. B-727 and smaller size aircraft have very limited effect on an 8-element, single frequency localizer. The worst case causes out-of-tolerance conditions for CAT III operations only within an area 1000 feet in front of the localizer array, and 250 feet from runway centerline.

3. Critical area size is strongly dependent on the overall size of the scatterer aircraft. No specific formula is sufficient to fully define this relationship.

4. When the fuselage of the scatterer aircraft is perpendicular to runway centerline, the largest contributor to path structure perturbations is the tail section of the scatterer.

5. When the fuselage of the scatterer aircraft is parallel to runway centerline, the tail section and the fuselage contribute approximately equal amounts of structure perturbations.

6. For B-727 and smaller aircraft, the oscillations from a parallel scatterer at least 1000 feet in front of the localizer array not exceed tolerances for any ILS category.

7. The worst case orientation for a scatterer aircraft in terms of overall derogation of the localizer signal is perpendicular to runway centerline, with tail towards centerline such as is the case when a landing aircraft exits the runway. This typically causes much larger and longer-term perturbations than the parallel case.

8. Increasing the localizer coursewidth decreases the size of the critical area.

9. Reducing the path structure requirement from 5 to 10 μA between ILS Point B and ILS Point E greatly reduces the size of the critical area for larger aircraft.

10. The effect of multiple reflectors is too complex to quantify. In general terms, the perturbations caused by N scatterers is no greater than N times the perturbations caused by a single scatterer.

11. It is very difficult to determine critical area boundaries as a function of the position of the landing aircraft. Because of the very large number of cases examined, it has been necessary to develop an automated process of analyzing path structure. This process of examining the entire path structure to determine if it is out-of-tolerance begins 3000 feet in front of the array (ILS Point E) and proceeds outbound. The procedure is terminated once the path structure exceeds simulated flight check tolerances and no further analysis is conducted.

II. INTRODUCTION AND BACKGROUND

The term critical area is defined for purposes of this study as that area in which the presence of any portion of a scatterer aircraft will cause aberrations in the radiated ILS localizer signal which exceed tolerances specified in U.S. Flight Inspection Manual 8200.1.

These aberrations are normally evident to a pilot flying an instrument approach as undesired movements in the localizer CDI indicator. Short term irregularities are usually only an inconvenience, although they may cause some autopilots to disengage. Long term aberrations are very undesirable, and can in an extreme case, produce unsafe conditions.

An examination of nearly any airport layout will reveal areas where parked, holding, or taxiing aircraft will be in remarkably close proximity to ILS antenna arrays. It is intuitively obvious that any large conducting object placed near an antenna transmitting electromagnetic radiation will have an effect on the transmitting system and its radiation patterns. It is therefore necessary to determine what restrictions or prohibitions should be implemented with respect to the real estate surrounding ILS transmitting arrays in order to insure that the signals serving user aircraft on approach remain adequate and safe.

Numerous experimental and theoretical investigations, both in the U.S. and abroad, have attempted to examine the effects of aircraft near both the localizer and glide slope transmitting arrays. In 1974, Ohio University published the first comprehensive work [1] on mathematical modeling of large aircraft near the ILS transmitting antennas. This work was validated with on-site measurements using the Boeing 747 and the Lockheed C-5A. The math model was also checked against data collected [2] at Heathrow Airport, London, England. Additional studies at Ohio University [3] [4] [5] served to refine the technique of mathematical modeling. More recently, reports published by Ohio University have provided both experimental and theoretical data to establish the minimum critical area required for the GRN-27 dual frequency localizer [6] and the 8-element and 14-element single-frequency localizers [7] operating under Category III tolerances. Both of these studies deal with the scattering effects of wide-body aircraft such as the B-747.

While previous studies have provided valuable information towards establishing minimum requirements for critical areas, the combination of Category III operating tolerances and wide-body scatterer aircraft yield values only for the nominal worst case. There are many airports where ILS facilities operate on less than Category III tolerances and where wide-body aircraft are scarce or non-existent. Consequently, considerable interest is justified in what critical areas may exist for more typical combinations of operating tolerances and aircraft sizes. The purpose of this study is to expand on previous work by examining localizer critical area determination under other than worst case conditions.

III. OBJECTIVE OF WORK

The broad objective of the work presented in this report is to identify areas of the earth's surface near the localizer transmitting array where the presence of an aircraft will cause unacceptable derogation of the localizer radiated signal. The identification process consists of using a mathematical model, which has been validated through the use of flight measurements, to predict the values of perturbations in the localizer CDI signal. These predictions will be used to define an appropriate critical area that will allow pilots and air traffic controllers to take appropriate holding actions to prevent out-of-tolerance path anomalies from occurring in space.

Within the broad purpose of this work there are several specific objectives to be achieved. These are:

1. Obtaining the typical relationship by which the critical area can be estimated from the size of the interfering aircraft.

2. Determining the critical area size relationship to the localizer coursewidth (runway length).

3. Measuring the impact of relaxing the course structure tolerances from 5 to 10 microamps between ILS points B and E for Category III operation.

4. Discussing, in general terms, the impact of multiple aircraft.

IV. APPROACH TO SOLUTION

The basic approach to the solution of this problem is to use the math model described in Section V to produce calculations of localizer CDI perturbations caused by aircraft in the vicinity of the localizer transmitting array.

A previous study [8] has demonstrated good agreement between experimental and calculational results for the localizer. Because of the expense and difficulty in collecting a large number of samples experimentally, a calculational approach has been found to be the most effective and efficient method of systematically studying localizer critical areas.

There are some difficulties even with this approach. For example, there are an infinite number of locations where a scatterer aircraft can be placed for the simulated approach. To make the problem tractable, the area used for scatterer location is broken into a grid, and a simulated localizer approach is calculated with a scatterer present at each of the grid locations in turn.

An additional difficulty is choosing a sampling interval along the simulated approach that will provide sufficient data to analyze the approach, and yet keep the number of necessary calculations at a reasonable level. It should be noted that the current implementation of the Physical Optics Mathematical Model is designed to deal with a maximum of 500 points.

The sampling interval was initially chosen to be 100 feet. This means that an imaginary localizer receiver is placed at a position along the approach, all the calculations necessary to determine localizer CDI at that point are performed, and the receiver position is advanced 100 feet. This process was started at a distance of 53000 feet from the array, and was halted 3000 feet from the array (ILS Point E). This gives 500 data points along the approach. Each data point is assumed to be valid for a 100 foot segment of the approach, or 50 feet each side of the computed point.

This approach normally gives reasonable results, but a problem arises in the case of an aircraft scatterer parallel to runway centerline. Parallel scatterers tend to introduce small but rapid oscilations into ILS Zone 4 or 5. These oscillations are so rapid that a sample taken only every 100 feet along the approach will yield erroneous conclusions about path structure. Consequently, the sampling interval was decreased to 50 feet, and the simulation was made in two sections. Section 1 covers the range of 53000 feet to 28000 feet and section 2 covers the range of 28000 feet to 3000 feet. This allows the maximum resolution of 500 data points in each section. Decreasing the sampling interval further did not affect the results in any cases studied.

A final difficulty lies in determining a suitable filter which can be applied to the calculated data in order to make it compatible with standard flight inspection techniques. The time constant of the deviation recording system for flight inspection work is specified by ICAO [9] as

being 50/V seconds, where V is the aircraft speed in knots. The speed of the aircraft is assumed to be 200 ft/sec for all simulations in this study. This converts to 118 knots, and yields a recommended time constant of .42 seconds.

This is normally achieved in ILS receivers by means of a large capacitor across the meter loads. Each receiver is designed with the capability of driving a certain load impedance, and resistors are usually connected in parallel with the meter movements as needed to achieve the desired impedance. For example, a typical ILS receiver might be designed to drive a load of 333 ohms. Since 333 ohms represents the parallel combination of three 1000 ohm resistors, the receiver can drive up to three separate meter movements, with 1000 ohm resistors substituted for unused meters.

The formula for the time constant of this circuit is given by

$$TC = R \times C$$

where,

TC is the time constant in microseconds,
R is the resistance in ohms,
C is the capacitance in microfarads.

Using a 1200 μF capacitor with the 333 ohm load in the example above will give a time constant of .40 seconds. This is in very good agreement with the time constant specified by ICAO for flight inspection work.

While a low-pass filter of this sort is easily implemented using physical components such as capacitors and resistors, it is considerably more difficult to derive a mathematical formula which will apply these filter characteristics to calculated data. The basic formula for such a filter has been derived and can be expressed as

$$FX(i)=(SP*(X(i)+X(i-1))-(FX(i-1)*(SP-2.0*TC)))/(SP+2.0*TC)$$

where,

i = receiver position number,
X = input (unfiltered) data,
FX = Filtered value of X,
SP = Sampling Period of data in seconds,
TC = Time Constant desired for filter.

In this study, calculations for CDI are made in 50 foot increments along the approach path. The aircraft velocity is 200 ft/sec, so the sampling period is .25 seconds. The desired time constant is .42 seconds. Substitution of the input data values for X will yield the filtered output data. Since this formula represents a specified standard, all calculations will be based on use of this filter. Derivation of this formula is presented in Appendix 1.

Since an aircraft is nominally on runway centerline during an approach, the localizer perturbations are examined only in terms of path structure. The localizer CDI values are analyzed for the entire approach to determine if they exceed any of the structure tolerances specified in U.S. Flight Inspection Manual 8200.1,Section 217.5. Path structure analysis is a computerized process. New programs and EXEC's have been written which apply standard flight check tolerances to each simulated approach for all categories of ILS operation. This has increased the number of cases which can be analyzed by a factor of about 100. Additionally, the peak CDI perturbations are predicted with respect to specific ILS Zones, viz, 1,2,3,4 and 5 [10]. Since different tolerances sometimes are applied for different zones, this distinction is considered desirable.

In order to determine the typical relationship by which the critical area can be estimated from the size of the interfering aircraft, three different sizes of aircraft were initially included. However, the gap in size between the two largest aircraft made it impossible to establish the form of the relationship. Consequently, two additional sizes of aircraft have been included. This creates a data base comprised of 5 aircraft sizes, ranging from DC-9 through B-747. In order of overall increasing scatterer size, they are:

1. DC-9
2. B-727
3. B-707
4. L-1011
5. B-747

The orientation of the scatterer aircraft involves 8 discrete cases. Previous studies have been limited primarily to modeling the scatterer aircraft either perpendicular or parallel to the runway centerline. There is insufficient evidence to prove that these two orientations produce the worst-case critical area, so additional modeling of aircraft situated at angles of 30 and 60 degrees with respect to runway centerline is included. Each of these four orientations is also repeated with the aircraft heading rotated 180 degrees.

The critical area size relationship to localizer coursewidth (runway length) is demonstrated by generating input data files for the math model which differ only in the runway length value. The values for runway length are chosen such that the extremes for localizer path width (3.0 degrees to 6.0 degrees) are achieved.

The impact of relaxing the course structure requirement from 5 to 10 microamps between ILS points B and E for Category III operation is easily implemented by adding an additional version of the Fortran computer program which applies flight check tolerances to each simulated approach. This program calculates allowable CDI perturbations based on this relaxed course structure specification, and the resulting critical area maps can be directly compared with the the normal Category III maps.

The impact of multiple aircraft is examined by calculating the CDI perturbations caused by two scatterer aircraft in the vicinity of the loca-

lizer array at the same time. Approaches are simulated with the aircaft in several locations and orientations.

V. MATHEMATICAL MODEL DESCRIPTION

This effort has been completed through the use of the same model as Longworth [11] [12] and McFarland [13], which is an updated version of the 1974 model used by Rondini [14] and earlier by Chin et.al. [15].

The model operates using the physical optics principles by considering the aircraft as a target or reflector. The target can be satisfactorily modeled by considering it as a collection of flat plates whose profile is that of the specific aircraft. The plates are assumed to be perfectly conducting and located with a specified orientation at a specific location in an area through which the localizer signals are propagating.

The plates are broken into incrementally small areas, and currents flowing in the incremental plates become source currents for the scattered signals. An integration of the contributions produced by the incremental plates is accomplished, and summed with the direct radiation from the localizer.

An in-depth description [16] of the physical optics approach to modeling was published by Ohio University in 1963. A user's guide [17] to the math model is also available.

VI. CALCULATION WORK

The final product of this work is intended to be a set of maps delineating those locations where a certain size and orientation of interfering aircraft will cause the localizer to exceed certain tolerances specified in U.S. Flight Inspection Manual 8200.1, Section 217.1.

The scope of this particuliar work is larger than most previous studies of critical area. The data is analyzed with respect to four separate tolerance categories for each of 5 sizes of scatterers. Each of the specific objectives listed in section III has the potential of doubling again the number of cases to be considered. Since most of these specific objectives require the determination of trends and relationships, it is intuitive that processing larger quantities of data will make these trends and relationships more obvious. Several steps have been taken to allow processing the largest bulk of data possible.

Computer programs and EXEC's have been written allowing the calculations to be performed on one computer while the results are spooled to a second computer for examination and processing into files which can be plotted. This arrangement requires no operator intervention, and allows the first computer to generate data almost continously. It also drastically reduces the data storage requirements, since only the results are spooled to the second computer.

In order to obtain the objectives of this study, approximately 30,000 simulated approaches have been calculated and analyzed. This consumed a total of about 400 hours of CPU time on an IBM Model 4341 computer. Approximately 600 plots were produced, with about 125 included in this report.

While the general approach to the solution is outlined in section III, there are many variables yet to be defined. The math model outlined in section V requires a data file which is used as an input to the model for purposes of defining these variables. Since many of these are somewhat arbitrary, they are presented here in hopes that future work can be standardized. Table 1 summarizes the values assigned.

In addition to the variables displayed in table 1, additional data is required to define the type of localizer array being modeled. This data includes the spacing (in wavelengths) of each element from the center of the array, the carrier-plus-sideband (CSB) relative amplitude and phase for each element, and the sideband-only (SBO) relative amplitude and phase for each element. The values for the 8-element single frequency localizer are given in table 2.

The final definition of variables required to specify fully all required inputs to the math model is the actual radiating pattern of the individual array elements. The element used in all calculations for this report is the Log-Periodic Dipole (LPD). The values used to simulate the LPD radiation pattern are given in table 3. The radiation pattern is assumed to be symmetrical, so only one side of the pattern needs to be specified.

Localizer Frequency	110.0 Mhz
Antenna Element Type	Log-Periodic
Length of Runway	10000 Ft
Distance from Array to Stop End of Runway	1000 Ft
Distance from Array to ILS Point E	3000 Ft
Distance from Array to ILS Point D	8000 Ft
Distance from Array to Threshold	11000 Ft
Distance from Array to ILS Point C	11950 Ft
Distance from Array to ILS Point B	14500 Ft
Distance from Array to ILS Point A	35320 Ft
Starting Distance of Simulation	53000 Ft
Sampling Rate of Simulation	50 Ft
Localizer Antenna Height	5.57 Ft
Elevation Angle of Approach	3.00 Deg
Azimuth Angle of Approach	0.00 Deg
Speed of Approach	200 Ft/Sec

Table 1. Assumptions and variables utilized as input data for all calculations.

ELEMENT	CSB LEVEL	CSB PHASE	SBO LEVEL	SBO PHASE	WAVELENGTH SPACING (λ)
4R	.055	180.00	.416	180.00	-2.55
3R	.143	0.00	.700	180.00	-1.80
2R	.363	0.00	.890	180.00	-1.05
1R	1.000	0.00	1.000	180.00	-0.30
1L	1.000	0.00	1.000	0.00	0.30
2L	.363	0.00	.890	0.00	1.05
3L	.143	0.00	.700	0.00	1.80
4L	.055	180.00	.416	0.00	2.55

Table 2. Nominal values used to represent an 8-element single-frequency localizer.

Azimuth angle (degrees)	Relative Signal Level
0.0	1.000
10.0	.930
20.0	.780
30.0	.570
40.0	.330
50.0	.180
60.0	.080
70.0	.040
80.0	.020
90.0	.000
100.0	.000
110.0	.000
120.0	.000
130.0	.010
140.0	.010
150.0	.010
160.0	.020
170.0	.030
180.0	.050

Table 3. Nominal radiation pattern used for modeling LPD antennas

Three size groupings of aircraft were originally chosen as scatterers. These groupings were DC-9 and smaller, B-727 and smaller, and the B-747 and smaller. The tremendous gap in overall size between the B-727 and the B-747 made it difficult to quantify the trends and relationships of critical area as a function on aircraft size, so two additional aircraft have been added. These two are the B-707 and the L-1011. This provides a larger range of sizes, and makes interpreting the data easier. The dimensions of the scattering plates used to simulate 5 types of aircraft are shown in figure 1. Although the B-707 is being phased out of usage, it represents a particular size of scatterer which fills a gap in the calculations.

Figure 2 represents the locations and dimensions of the area in which the aircraft were placed. The left boundary of the plot represents the runway centerline, the center of the localizer array is at the bottom left. The first position for which a simulated approach is calculated is on runway centerline, 1000 feet in front of the array. As each simulation is completed, the filter formula described in Section IV is applied. Figure 3 demonstrates the relationship of the filtered and unfiltered data for a typical simulated approach. The CDI values for the entire approach as well as the peak values for each ILS zone are then stored in computer memory. The program then increments the location of the scatterers to the next position, and a new simulation begins. The computer program continues this operation until approaches have been calculated for all 204 points on the grid.

All 204 approaches are then analyzed to determine if they exceed any of the structure requirements specified for each of the ILS categories. With the exception of Category III-X, all tolerance limits applied to localizer structure are obtained from the U.S. Flight Inspection Manual 8200.1. The tolerance limits for Category III-X are an arbitrary experiment and replicate the limits for Category III with the exception of relaxed requirements in ILS zones 4 and 5. Table 4 summarizes the structure tolerances for all categories of ILS operation.

A plot, similar to figure 2, is produced for each ILS category (including 3X) with a dot at every location where the presence of a particular size and orientation of scatterer causes the path structure to exceed tolerance limits. These maps serve to define the critical area for each case studied. The reference point on the aircraft for these maps is the center of the base of the fuselage as derived from figure 1.

In addition to the critical area maps, a contour map is prepared for each ILS zone. These maps represent the peak CDI that occured within that particular zone for each of the 204 approaches. Contour maps also are based on filtered data as described earlier. Since each of the 204 approaches is represented by a specific point on the grid of figure 2, the peak CDI value for each point forms a scalar field which allows a contour map to be drawn. From an examination of these contour maps, it is possible to determine what an aircraft placed in a certain location with a certain orientation will produce in terms of maximum path perturbation, as well as the ILS zone in which the perturbation occurs. By knowing the tolerance

(continued on page 19)

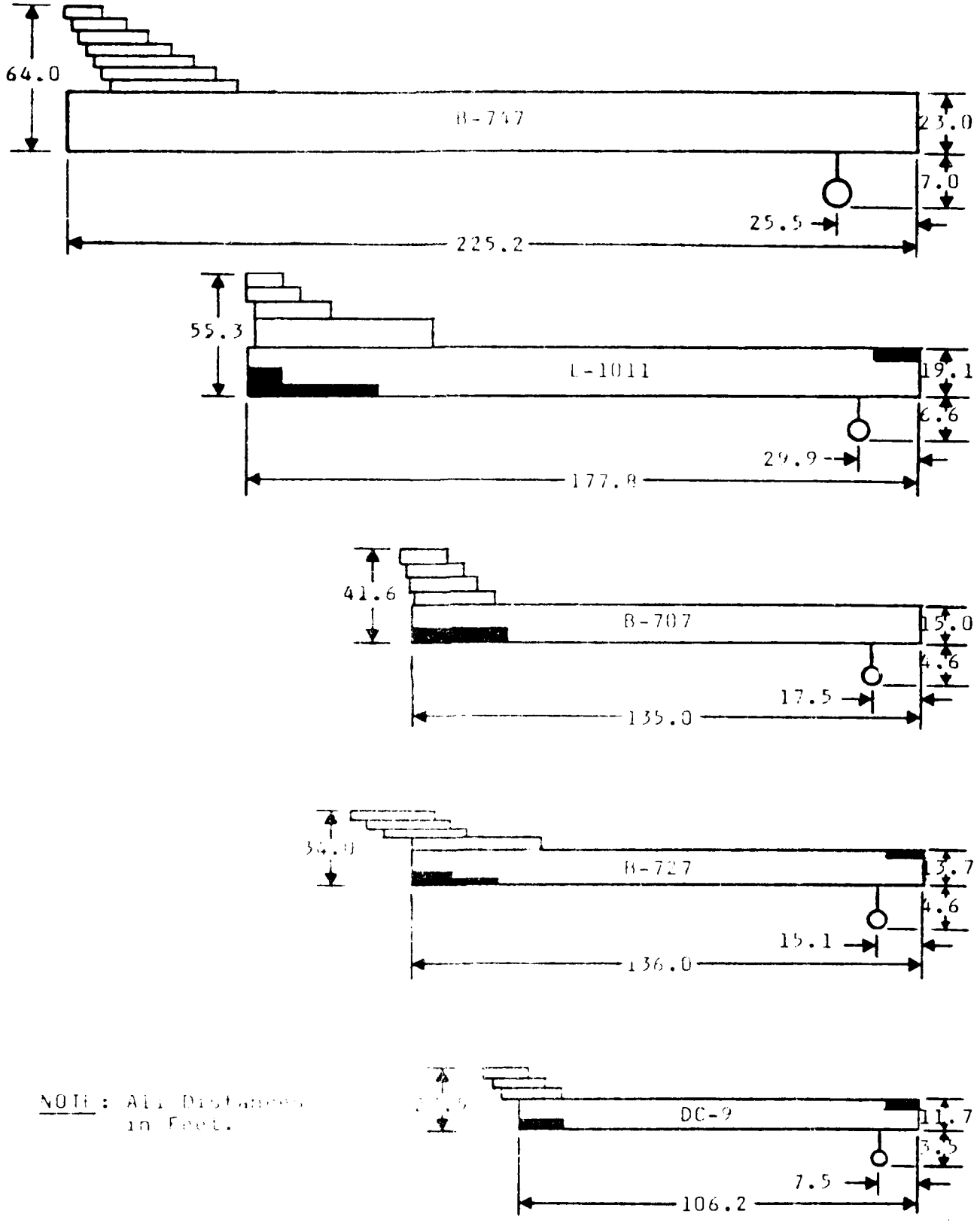

NOTE: All Distances in Feet.

Figure 1 Overall dimensions of scattering plates used to simulate specific aircraft.

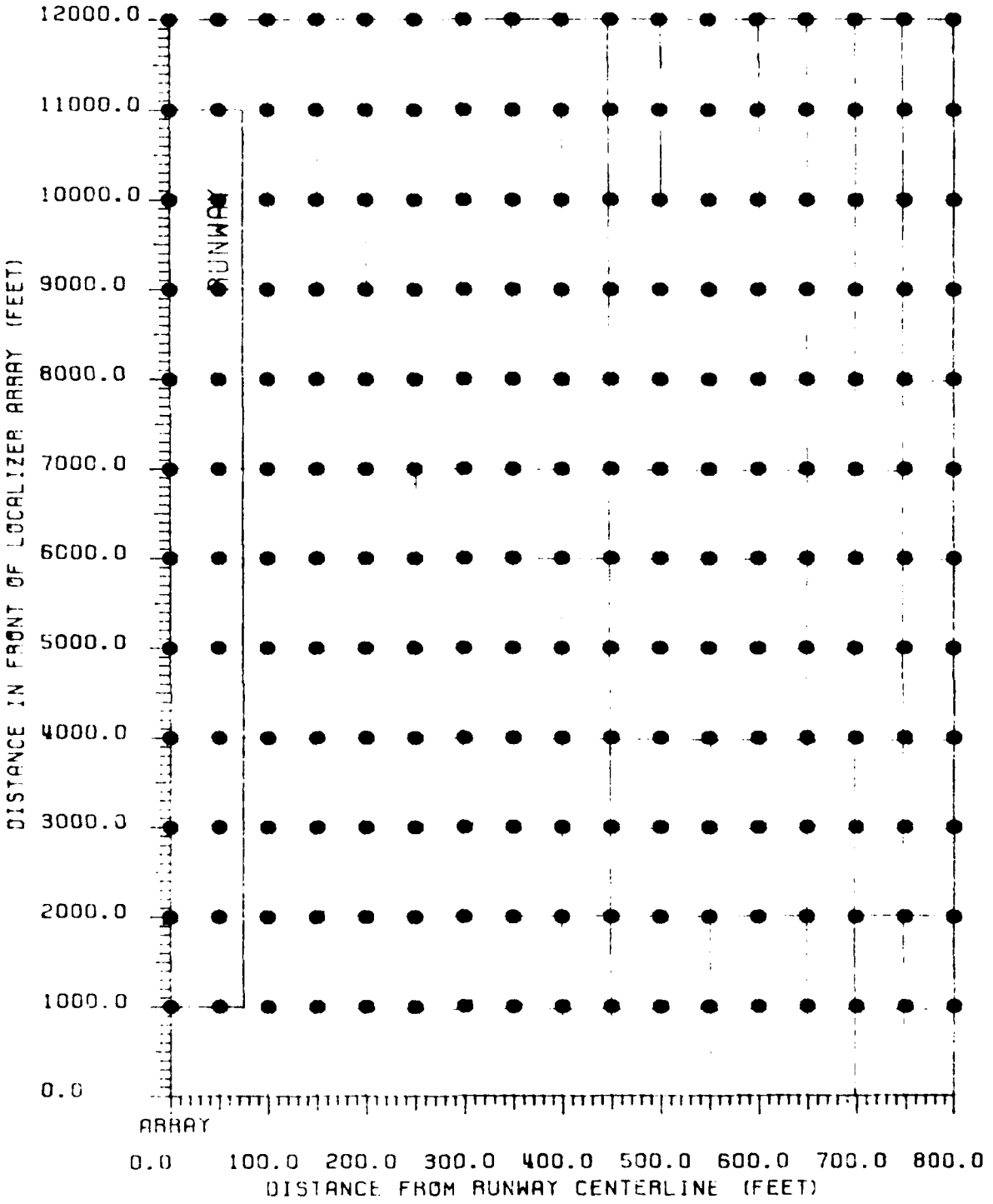

Figure [illegible] rid locations of scatterer aircraft for which an pproach is calculated. The dots are also used to enote out-of-tolerance conditions on the critical areas maps.

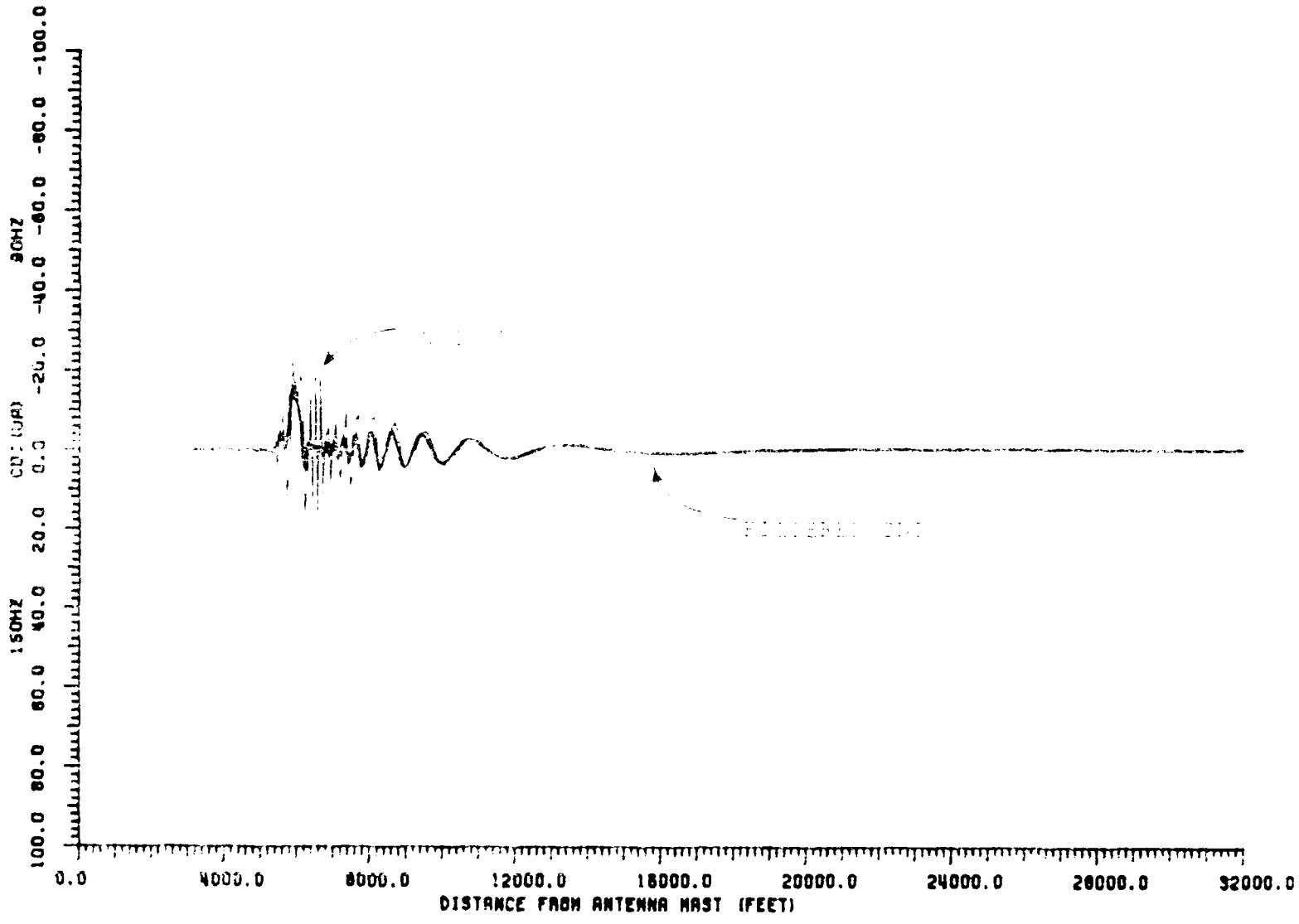

Effects of digital filter on a typical CDI plot.

CAT I	Zone 1: ± 30 μA to Point A Zone 2: ± 30 μA at Point A, linear decrease to ± 15 μA at Point B Zone 3: ± 15 μA from Point B to Point C Zone 4: No structure requirements for CAT I Zone 5: No structure requirements for CAT I
CAT II	Zone 1: ± 30 μA to Point A Zone 2: ± 30 μA at Point A, linear decrease to ± 5 μA at Point B Zone 3: ± 5 μA from Point B to Threshold Zone 4: ± 5 μA from Threshold to Point D Zone 5: No structure requirements for CAT II
CAT III	Zone 1: ± 30 μA to Point A Zone 2: ± 30 μA at Point A, linear decrease to ± 5 μA at Point B Zone 3: ± 5 μA from Point B to Threshold Zone 4: ± 5 μA from Threshold to Point D Zone 5: ± 5 μA at Point D, linear increase to ± 10 μA at Point E
CAT III-X	Zone 1: ± 30 μA to Point A Zone 2: ± 30 μA at Point A, linear decrease to ± 10 μA at Point B Zone 3: ± 10 μA from Point B to Threshold Zone 4: ± 10 μA from Threshold to Point D Zone 5: ± 10 μA from Point D to Point E

NOTE: Zone 1 structure is measured from average course signal. Zones 2,3,4, and 5 are measured from actual course alignment.

Table 4. Summary of structure tolerances for all categories of ILS operation.

limit for a particular ILS zone, it is possible to determine the general outlines for critical areas directly from the contour maps. The task is complicated by the fact that the tolerance limits in some zones have tapered brackets and that FAA Flight Inspection Manual 8200.1 makes exceptions for brief out-of-tolerance conditions. These conditions cannot readily be determined from the contour maps, but are automatically taken into consideration for the critical area maps. The contour maps also are based on a reference point in the center of the base of the fuselage for each scatterer.

Figure 4 is a sample of the CDI information that is calculated for each of the 204 grid locations for a particular scatterer. The scatterer in this instance is a B-747 with the center of the fuselage located 3000 feet in front of the localizer array, and 200 feet from runway centerline. The B-747 fuselage is perpendicular to the runway centerline, with the tail towards the runway. The CDI trace on this plot demonstrates what the pilot of an aircraft on approach would see under these conditions. The other brackets on the plot demonstrate the structure tolerance limits for Category III operations. The structure obviously exceeds these limits, since the perturbation reaches a peak value of 35 μA at a distance from the array of about 5000 feet. Figure 5 is a sample contour map based on the same conditions as figure 4. It provides the peak CDI perturbation in ILS Zone 2 for 204 positions of a perpendicular B-747. By locating the point on the contour map that corresponds to the position (2000,300) of the B-747 used to calculate figure 4, one can see that the closest contour line is the same as the peak value in figure 4, namely, 35 μA.

Figure 6 also represents the same conditions as figure 4, except that only the tail of the B-747 is considered as a scatterer. This shows that the major contribution to the structure perturbations are due to the tail. When scattering from only the fuselage is considered, as in figure 7, it is obviously much smaller. This is often the case, but there are exceptions. Figure 8 represents the case of a B-747 located 5000 feet on front of the array and 600 feet from centerline. The aircraft is parallel to the runway with the tail facing the localizer array. Figure 9 demonstrates the contributions from the tail of the plane, while figure 10 shows scattering due to the fuselage. At this location, the amount of scattering from the tail and the fuselage is more nearly equal.

The following critical area maps and contour plots are arranged in order of overall increasing scatterer size, which is as follows:

1. DC-9
2. B-727
3. B-707
4. L-1011
5. B-747

Two orientations are presented for each aircraft size including the worst case orientation with tail towards the runway, the worst case orientation with tail away from the runway, and the worst case parallel orientation. The orientation is indicated on each plot. In each case, the criti-

(continued on page 7)

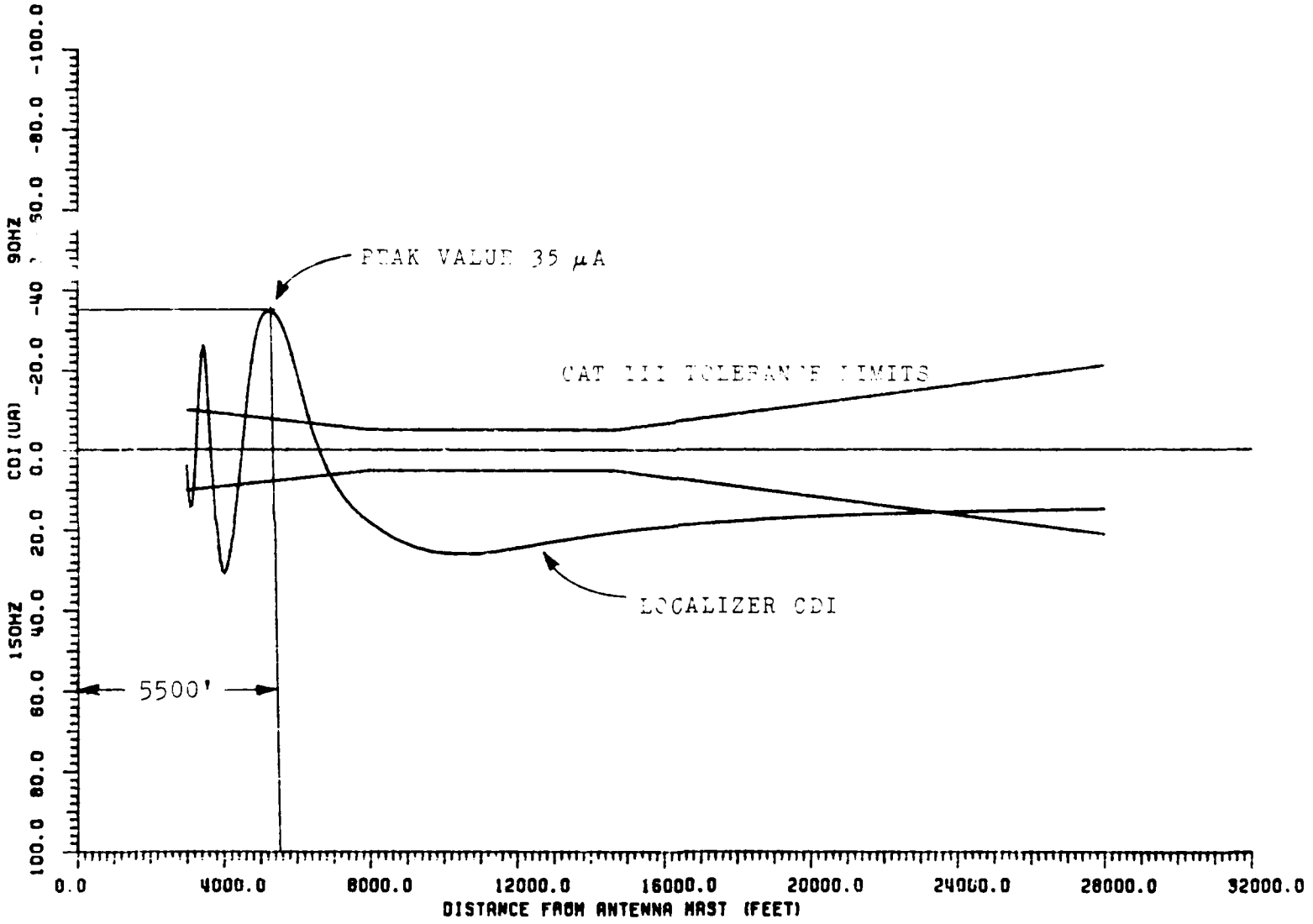

Figure 4 Typical CDI plot showing Cat III tolerance brackets. Perturbations are caused by a B-747 aircraft. Orientation is perpendicular to runway centerline, with tail towards the runway. Center of fuselage is 2000 feet in front of localizer and 300 feet from centerline.

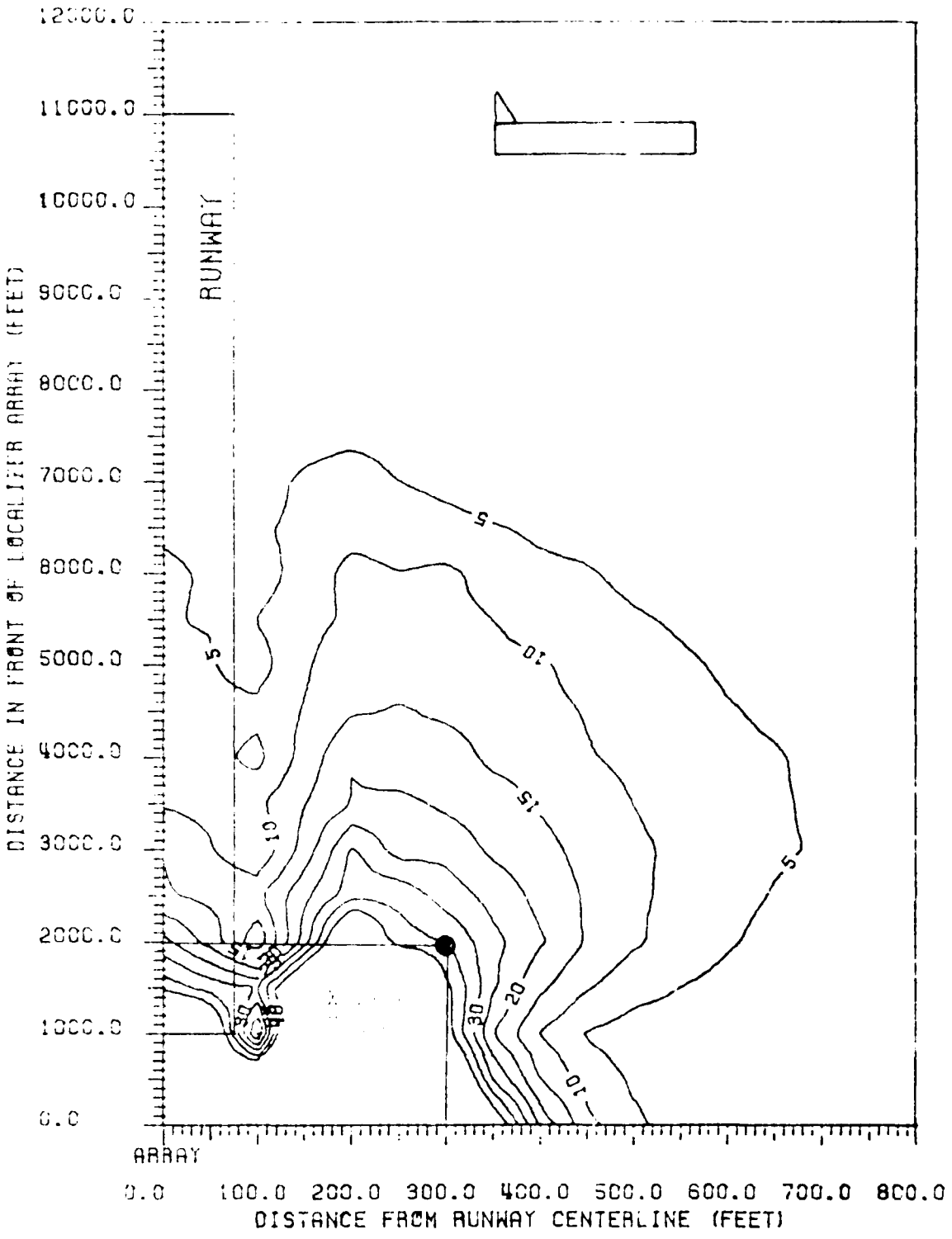
12000.0
11000.0
10000.0
9000.0
8000.0
7000.0
6000.0
5000.0
4000.0
3000.0
2000.0
1000.0
0.0
DISTANCE IN FRONT OF LOCALIZER ARRAY (FEET)
RUNWAY
ARRAY
5
10
15
20
30
0.0
100.0
200.0
300.0
400.0
500.0
600.0
700.0
800.0
DISTANCE FROM RUNWAY CENTERLINE (FEET)

[illegible]

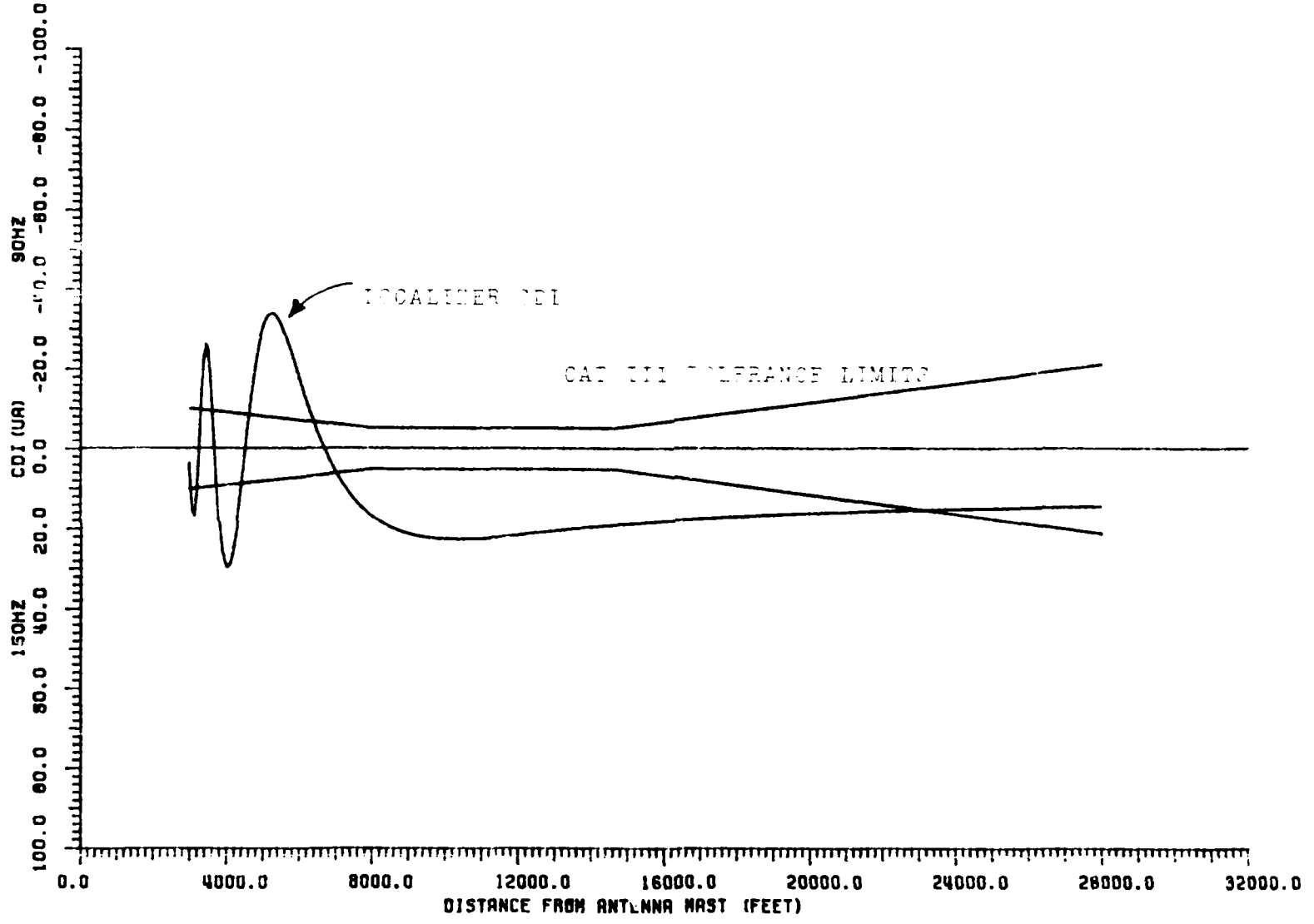

Figure 6 CDI plot with CAT III tolerance trackets. Perturbations are caused by only the tail section of a B-747. Orientation is perpendicular to runway centerline, with tail toward the runway. Center of fuselage is 2000 feet in front of localizer and 300 feet from the centerline.

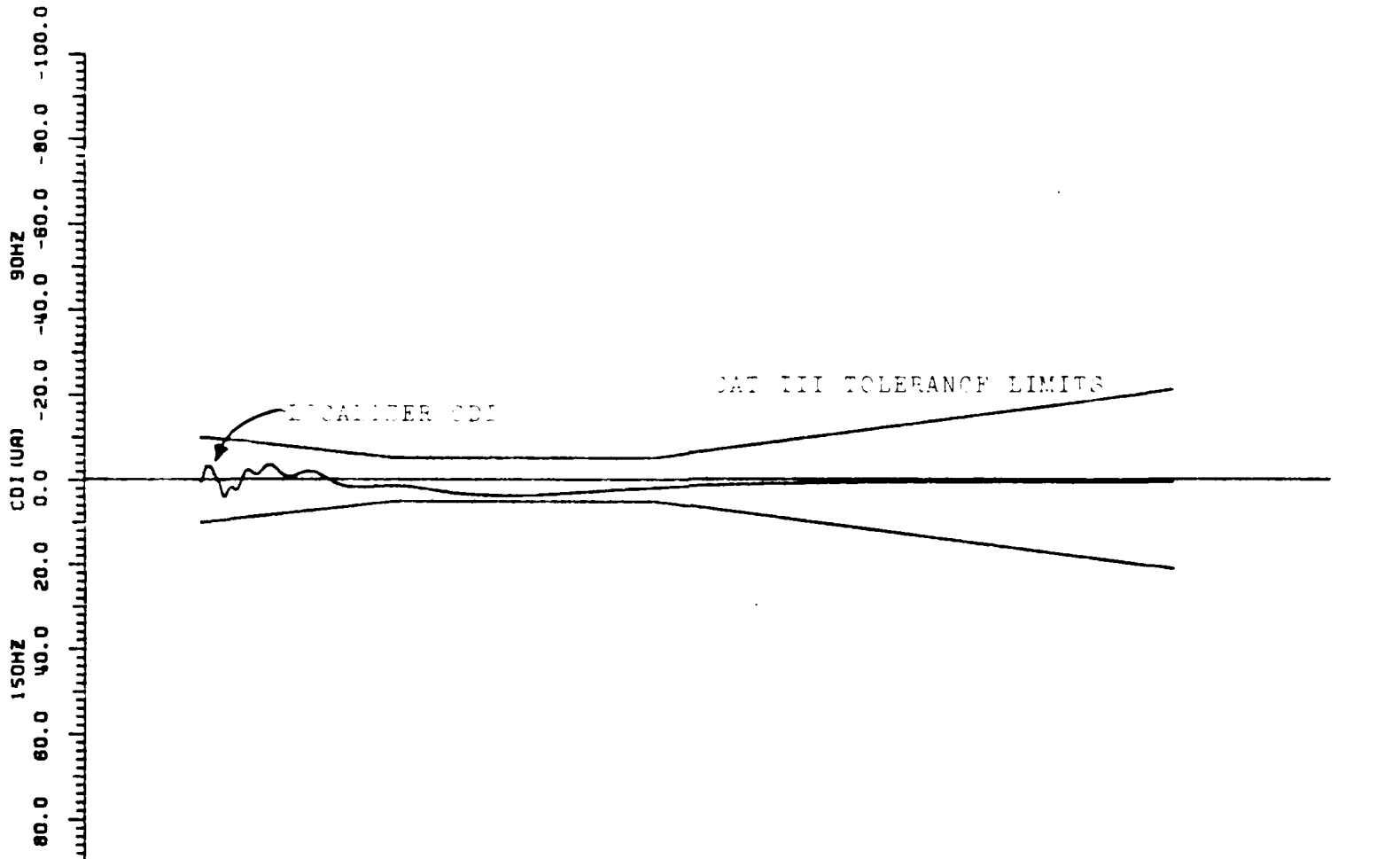

Figure 7 CDI plot with CAT III tolerance brackets. Perturbations are caused by only the fuselage of a B-747. Orientation is perpendicular to runway centerline, with tail towards the runway. Center of fuselage is 2000 feet in front of localizer and 300 feet from centerline.

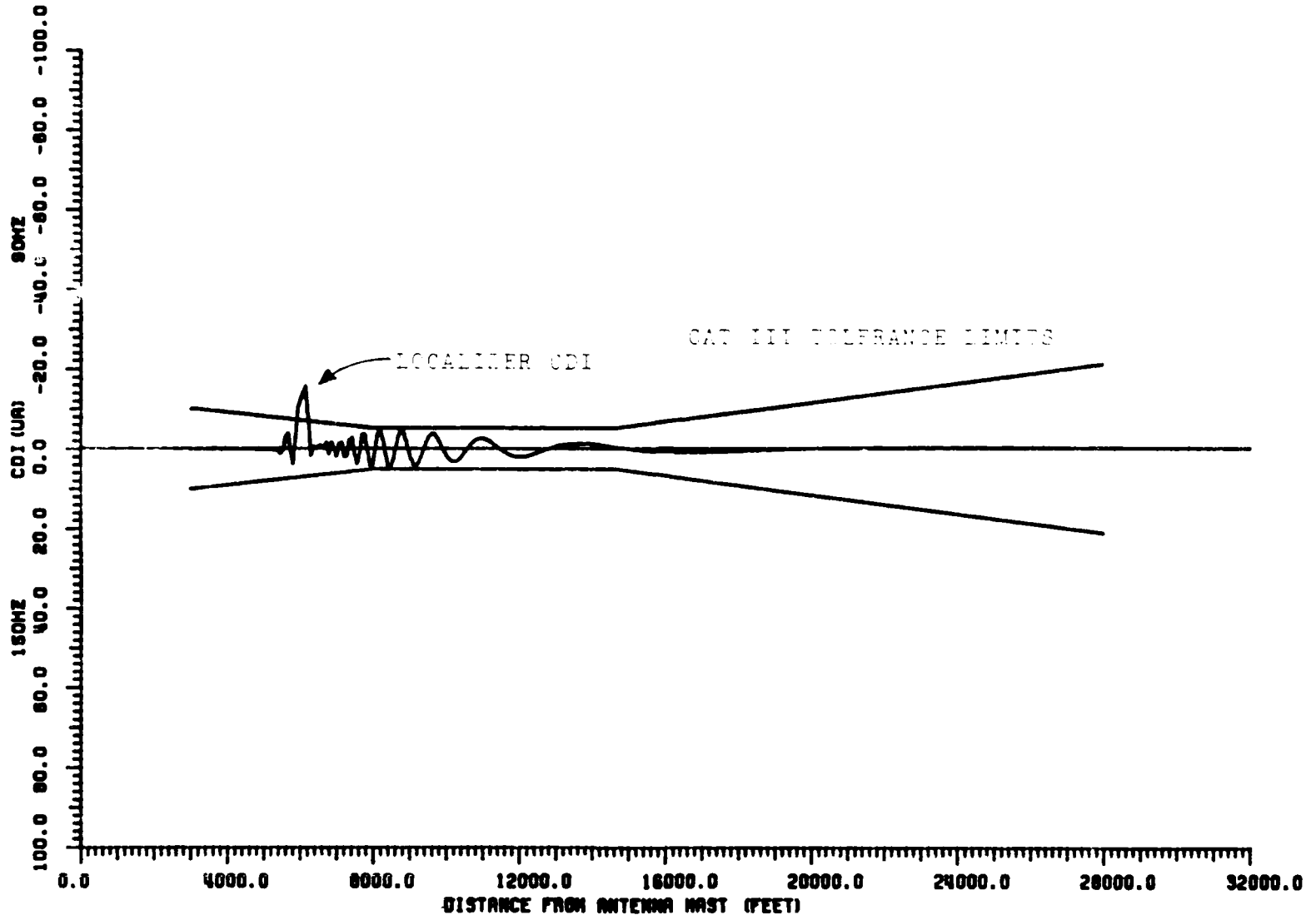

Figure 8 CDI plot showing CAT III tolerance brackets. Perturbations are caused by a B-747 aircraft. Orientation is parallel to runway centerline, with tail towards the array. Center of fuselage is 5000 feet in front of localizer and 400 feet from centerline.

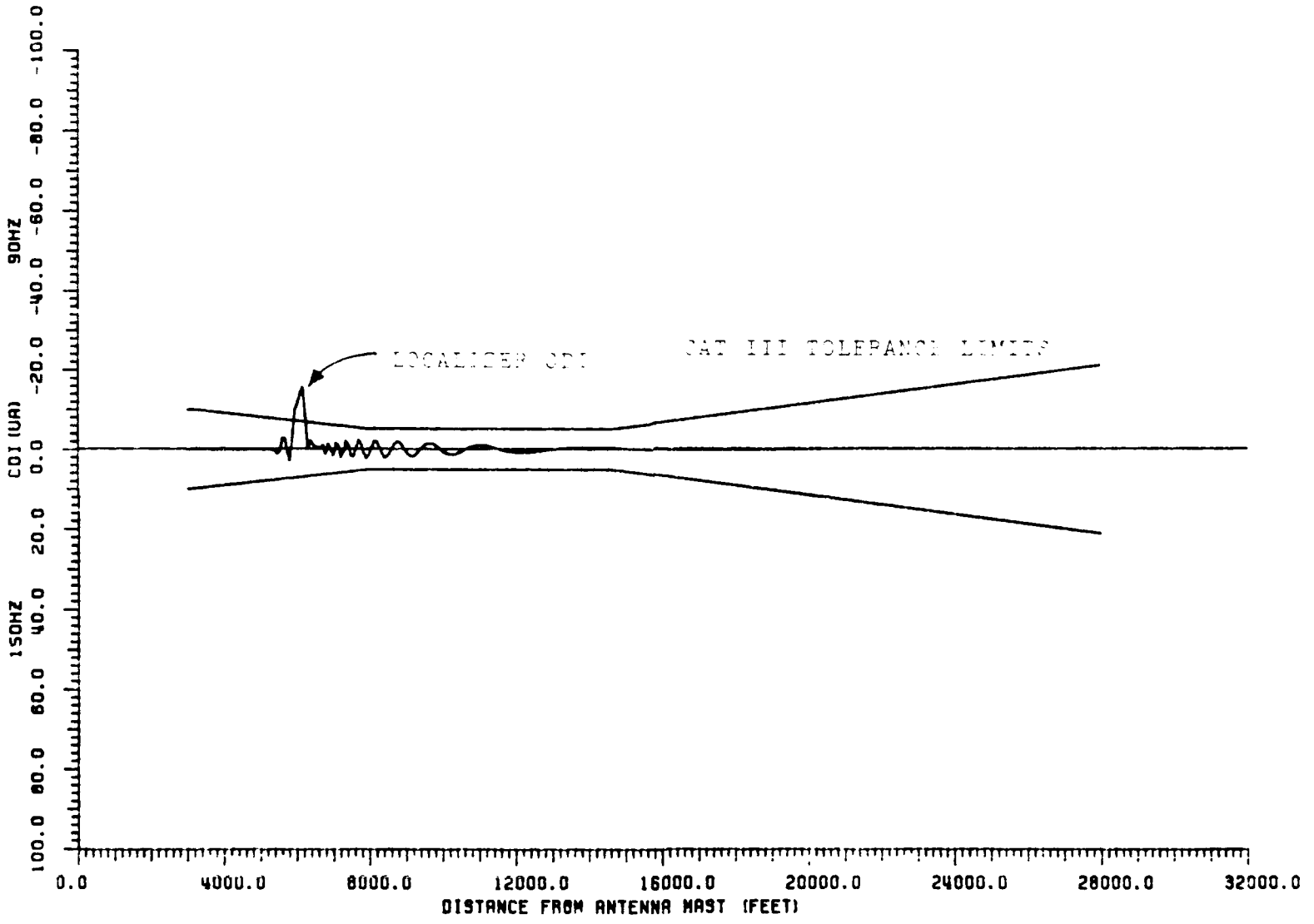

Figure 9 CDI plot with CAT III tolerance brackets. Perturbations are caused by only the tail section of a B-747. Orientation is parallel to runway centerline, with tail towards the array. Center of fuselage is 5000 feet in front of localizer and 600 feet from centerline.

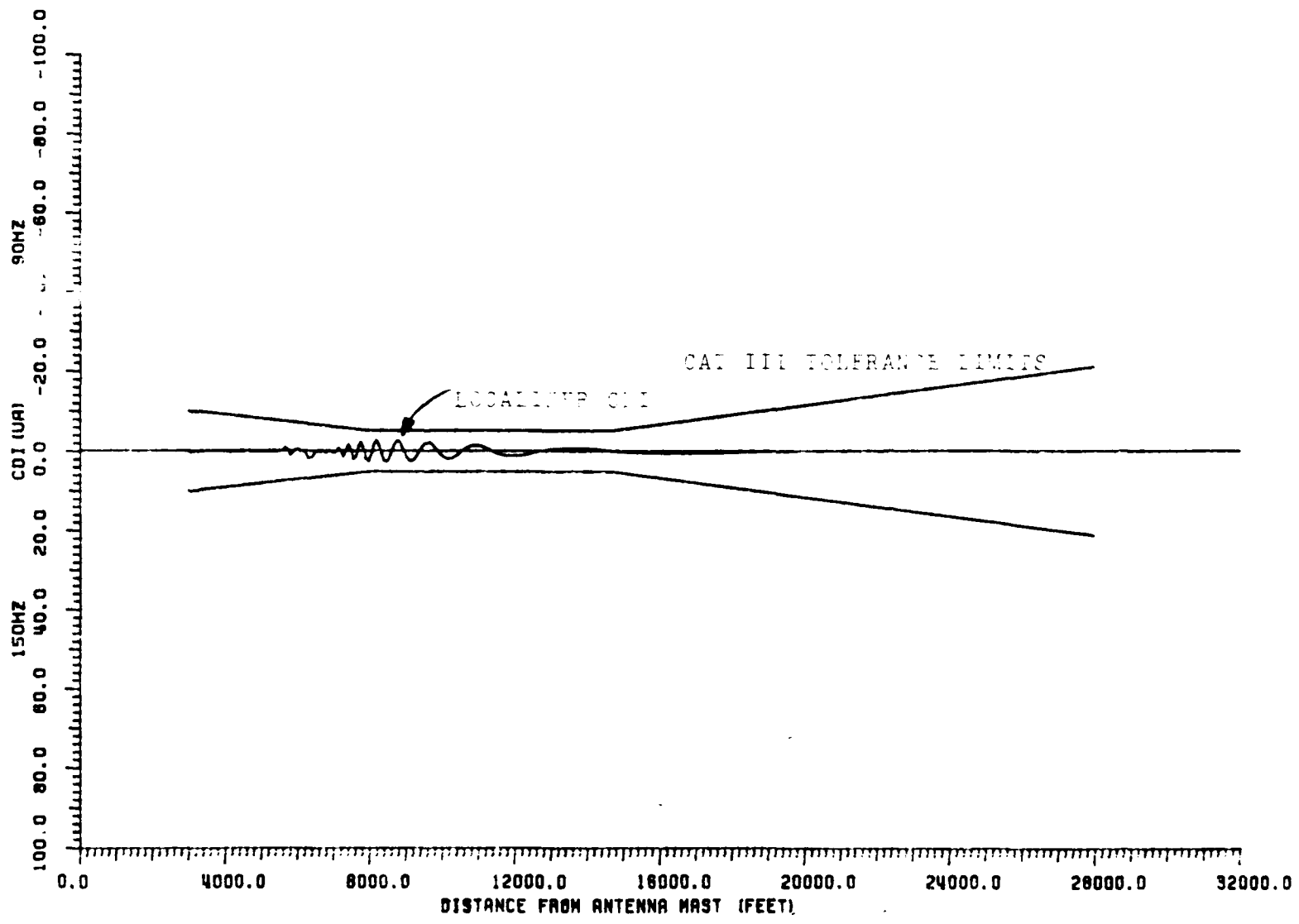

Figure 10 CDI plot with CAT III tolerance brackets. Perturbations are caused by only the fuselage of a B-747. Orientation is parallel to runway centerline, with tail towards array. Center of fuselage is 5000 feet in front of localizer and 600 feet from centerline.

cal area maps are presented first. In some cases, critical area maps may be missing for certain ILS categories. This indicates that there are no locations causing out-of-tolerance conditions for that category. A list of locations for which there are no out-of-tolerance points is shown in table 5. There are also some instances of contour maps not being present for certain ILS zones. This means that the largest perturbation in that zone is less than 5 μA, which is the minimum value of the contours. A list of these contour maps is given in table 6.

The contour lines on each contour map have been chosen such that the entire range of structure tolerance limits are represented. Since the minimum value involved in analyzing the structure of a localizer approach is 5 μA, this is also the value of the the minimum contour shown. The maximum contour was chosen to include at least the largest value involved in structure analysis, or 30 μA. Additional contours are included for 35 and 40 μA. More contour lines than this tend to clutter the plots. The computer programs which calculate the contour lines have the capability to automatically scale the contour intervals to fit the data, but then each contour map is based on different values. This makes it very difficult to compare maps, so the maps in this report are all based on an increment of 5 μA between contours.

The contour maps for ILS Zone 3 are based on CAT II/CAT III dimensions, and extend from ILS Point B to Threshold. This is in contrast to CAT I dimensions, in which ILS Zone 3 extends only from ILS Point B to ILS Point C.

Grid positions for the scatterer aircraft as indicated in figure 2 are measured with respect to the center of the base of the rectangle representing the main fuselage of each aircraft. If it is desired to determine critical area sizes or contour lines with respect to another reference point on the aircraft, it is necessary to refer to figure 1 for aircraft dimensions. Once the distance from the center of the main fuselage section to the new reference point is established, the contour maps and critical area maps can easily be interpreted from this new reference point.

As stated earlier in Section IV, 8 specific orientations of scatterer aircraft are included in the calculations. The results, which are summarized in table 7, reflect the distance (to the next 25 foot interval) from the runway centerline to the nearest point on the aircraft. Therefore, the aircraft lies completely outside the critical area boundaries shown in table 7.

Table 7 may be used to examine the relationship between critical area size and size of the reflector aircraft. A comparison of similar orientations for different size aircraft shows, in general, a clear trend of increasing critical area size as aircraft size increases. Determining the exact nature of the relationship of critical area to scatterer size, however, is complicated by several facts. First, the overall size of the scatterer is not the only factor. In the case of a perpendicular scatterer, figures 4, 6, and 7 demonstrate that the tail section is the primary scatterer. As the aircraft approaches the parallel case, the fuselage

(continued on page 31)

AIRCRAFT	ORIENTATION	ILS ZONES
DC-9	parallel, tail towards the array	1,2,3,4,5
DC-9	perpendicular, tail towards the runway	1,2,3,4
DC-9	perpendicular, tail away from runway	1,2
B-727	parallel, tail towards the array	1,2,3,4
B-707	parallel, tail towards the array	1,2,3,4
L-1011	parallel, tail towards the array	1,2,3
B-747	parallel, tail towards the array	1,2

Table 5. ILS Zones for which no contour maps are presented. Maximum contours are less than 5 μA.

AIRCRAFT	ORIENTATION	ILS CATEGORIES
DC-9	parallel, tail towards the array	I,II,III,III-X
DC-9	perpendicular, tail towards the runway	I,II,III,III-X
DC-9	perpendicular, tail away from runway	I,III-X
B-727	parallel, tail towards the array	I,II,III,III-X
B-727	60 degrees to runway CL, tail towards the array	I
B-727	perpendicular, tail towards the runway	I
B-707	parallel, tail towards the array	I,II,III,III-X
L-1011	parallel, tail towards the array	I,II
B-747	parallel, tail towards the array	I

Table 6. ILS categories for which no critical area maps are presented. No out-of-tolerance locations identified for X > 1000 feet and Y > 0 feet.

	CAT I x, y*	CAT II x, y*	CAT III x, y*	CAT III-A x, y*
DC-9 perp, tail away CL	--	1000,50	1000,50	--
DC-9 perp, tail to CL	--	--	--	--
DC-9 para, tail away array	--	--	--	--
DC-9 para, tail to array	--	--	--	--
DC-9 30°, tail to array	--	--	--	--
DC-9 30°, tail away array	--	--	--	--
DC-9 60°, tail to array	--	--	--	--
DC-9 60°, tail away array	--	--	--	--
B-727 perp, tail away CL	--	1000,0	1000,0	1000,0
B-727 perp, tail to CL	--	1000,175	1000,175	1000,125
B-727 para, tail away array	--	--	--	--
B-727 para, tail to array	--	--	--	--
B-727 30°, tail to array	--	975,25	975,75	975,75
B-727 30°, tail away array	--	975,125	975,125	975,125
B-727 60°, tail to array	--	950,75	950,75	950,25
B-727 60°, tail away array	--	950,125	950,175	950,175
B-707 perp, tail away CL	--	2000,200	2000,200	2000,100
B-707 perp, tail to CL	1000,100	2000,400	2000,400	2000,250
B-707 para, tail away array	--	--	--	--
B-707 para, tail to array	--	--	--	--
B-707 30°, tail to array	--	975,150	975,150	975,100
B-707 30°, tail away array	--	975,200	975,250	975,150
B-707 60°, tail to array	950,75	1950,275	1950,275	1950,125
B-707 60°, tail away array	--	1950,325	1950,375	1950,275
L-1011 perp, tail away CL	1000,75	4000,375	4000,375	3000,225
L-1011 perp, tail to CL	1000,225	5000,575	6000,575	3000,375
L-1011 para, tail away array	--	--	1925,400	1925,300
L-1011 para, tail to array	--	--	2925,350	1925,350
L-1011 30°, tail to array	975,0	2975,275	2975,275	1975,125
L-1011 60°, tail to array	925,75	2925,375	3925,375	1925,275
L-1011 60°, tail away array	925,225	3925,525	4925,575	2925,425
B-747 perp, tail away CL	1000,0	7000,300	7000,300	4000,150
B-747 perp, tail to CL	2000,300	9000,550	9000,550	5000,400
B-747 para, tail away array	--	--	3900,700	2900,450
B-747 para, tail to array	--	4900,650	4900,700	2900,500
B-747 30°, tail to array	950,25	3950,425	4950,425	2950,225
B-747 30°, tail away array	950,175	5950,325	5950,325	2950,225
B-747 60°, tail to array	1925,100	5925,350	6925,350	3925,200
B-747 60°, tail away array	1925,300	7925,600	7925,600	3925,450

* x - distance in front of localizer array to nearest point on aircraft longitudinal axis

y = distance perpendicular to runway centerline to nearest point on aircraft longitudinal axis

-- = no identified out-of-tolerance locations for X > 1000' and Y > 0'

Table 7. Critical area vs. aircraft orientation for 8-element single-frequency array.

assumes more importance. The relative proportions of tail and fuselage vary even among aircraft of very similar size.

As a further complication, the data represents only perturbations along runway centerline at a normal elevation angle of approach. This is a reasonable limitation when examining the effects the scatterers will have on an aircraft making an approach, but is not optimum when determining relationships to scatterer size. Some scatterers may have their maximum impact along something other than a nominal approach.

Finally, while the resolution of the results demonstrated in table 7 is 25 feet for x and 25 feet for y, the grid increments as shown in figure 2 are 1000 feet for x and 50 feet for y. This masks small differences in critical area size. In spite of these limitations, the trend of increasing critical area size with increasing scatterer size is readily apparent in table 7.

The impact of relaxing course structure requirements from 5 to 10 μA in ILS Zones 3 and 4 is also apparent in table 7. Category III-X has a much smaller associated critical area for the B-707, L-1011, and B-747 than Category III. In some instances, the critical areas for CAT III-X are smaller than those for CAT II.

Tables 8 and 9 demonstrate the critical area size relationship to localizer coursewidth (runway length) for perpendicular and parallel cases respectively. The shortest runway lengths are not operationally feasible, but are included for completeness. Wider coursewidths greatly reduce the critical area size in both the perpendicular case and parallel case.

In order to reduce the number of figures presented to a reasonable number, plots are presented for only three orientations. These include:

1. Worst case orientation with tail towards the runway.
2. Worst case orientation with tail away from the runway.
3. Worst case orientation parallel to runway centerline (CL).

This is intended to represent aircraft leaving, entering, and taxiing parallel to the runway. Figures 11 through 98 illustrate the critical area boundaries and show the contour maps of the peak perturbation based on the center of the fuselage of the scatterer.

The subject of multiple aircraft can only be discussed in general terms. The addition of more aircraft to the reflecting area adds significant complication. The combinations of position and orientation become impractically large. When simple superposition of the electromagnetic field in space is considered, it is apparent that certain placements will produce additive effects, and other placements will produce some amount of cancellation.

Figures 99 through 105 demonstrate the impact of one series of multiple reflector aircraft. Figure 99 demonstrates the locations and orientations of the scatterer aircraft used in this discussion. Figures 100

(continued on page 123)

RUNWAY LENGTH (feet)	COURSE WIDTH (degrees)	CAT I x,y* (feet)	CAT II x,y* (feet)	CAT III x,y* (feet)	CAT III-X x,y* (feet)
5000	6.00	1000,150	4000,400	4000,400	3000,300
6000	5.72	1000,150	4000,400	5000,400	3000,300
7000	5.01	2000,200	6000,450	6000,450	4000,350
8000	4.45	2000,200	7000,500	7000,500	4000,350
9000	4.01	2000,200	8000,550	8000,550	5000,350
10000	3.64	2000,300	9000,550	9000,550	5000,400
11000	3.34	2000,300	10000,600	10000,600	6000,400
12000	3.08	2000,300	11000,600	11000,600	6000,450

* x = distance in front of array to nearest point on aircraft longitudinal axis

y = distance perpendicular from centerline to nearest point on aircraft longitudinal axis

Table 8. Critical area size as a function of runway length for a B-747. B-747 fuselage is perpendicular to runway centerline, with tail towards the runway.

RUNWAY LENGTH (feet)	COURSE WIDTH (degrees)	CAT I x,y* (feet)	CAT II x,y* (feet)	CAT III x,y* (feet)	CAT III-X x,y* (feet)
5000	6.00	--	--	1900,350	1900,350
6000	5.72	--	--	1900,400	1900,350
7000	5.01	--	--	2900,400	1900,400
8000	4.45	--	--	3900,650	2900,400
9000	4.01	--	--	4900,700	2900,450
10000	3.64	--	4900,650	4900,700	2900,500
11000	3.34	--	4900,750	5900,800	2900,500
12000	3.08	--	4900,800	5900,800	3900,600

* x = distance in front of array to nearest point on aircraft longitudinal axis

y = distance perpendicular from centerline to nearest point on aircraft longitudinal axis

-- = no out-of-tolerance conditions identified for X > 1000' and Y > 0'

Table 9. Critical area size as a function of runway length for a B-747. B-747 fuselage is parallel to runway centerline, with tail towards the array.

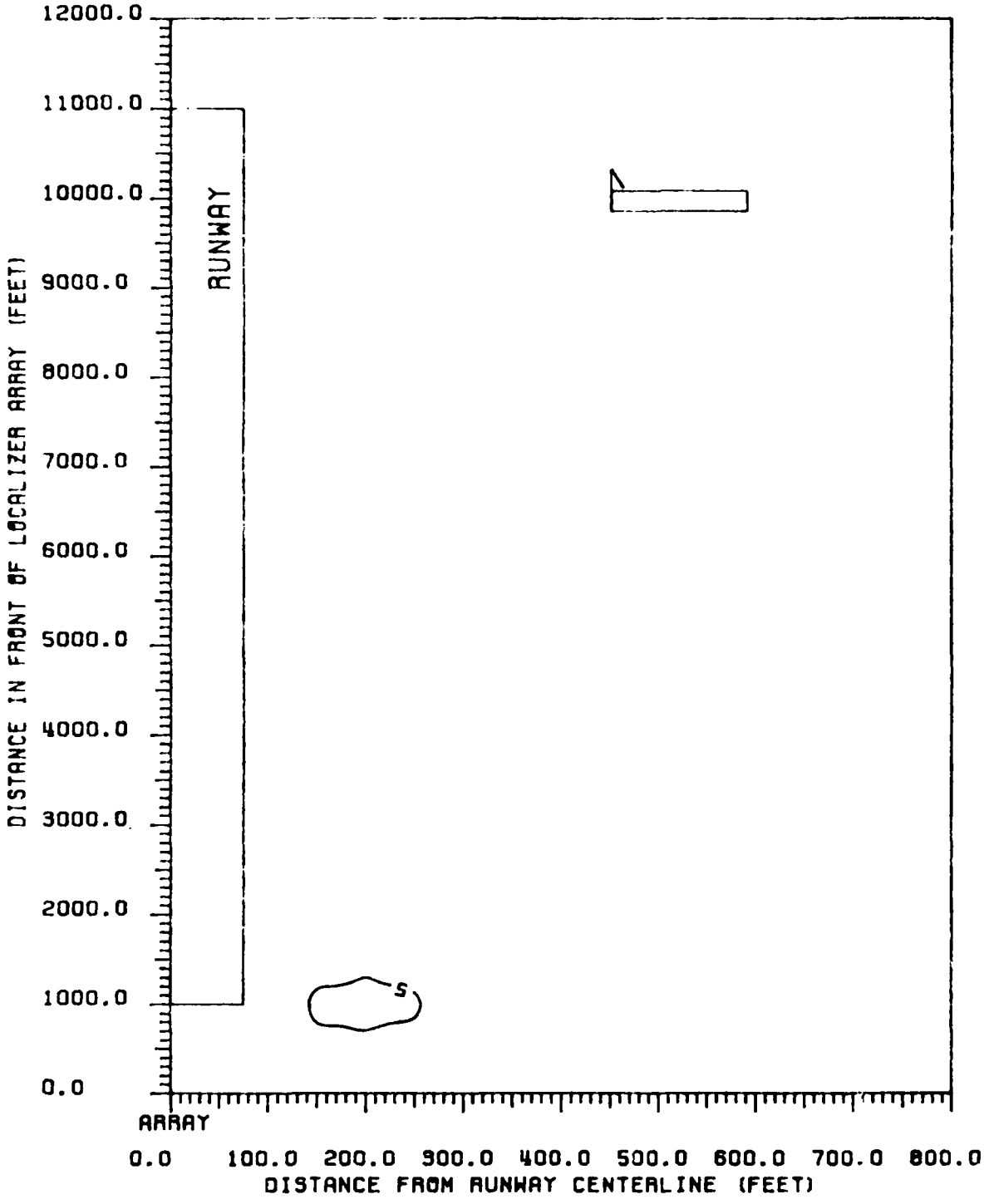

Figure 11 Contours of peak CDI values produced in ILS Zone 5 for a DC-9. DC-9 fuselage is perpendicular to runway centerline, with tail towards the runway. 8-element single-frequency array, LPD antennas.

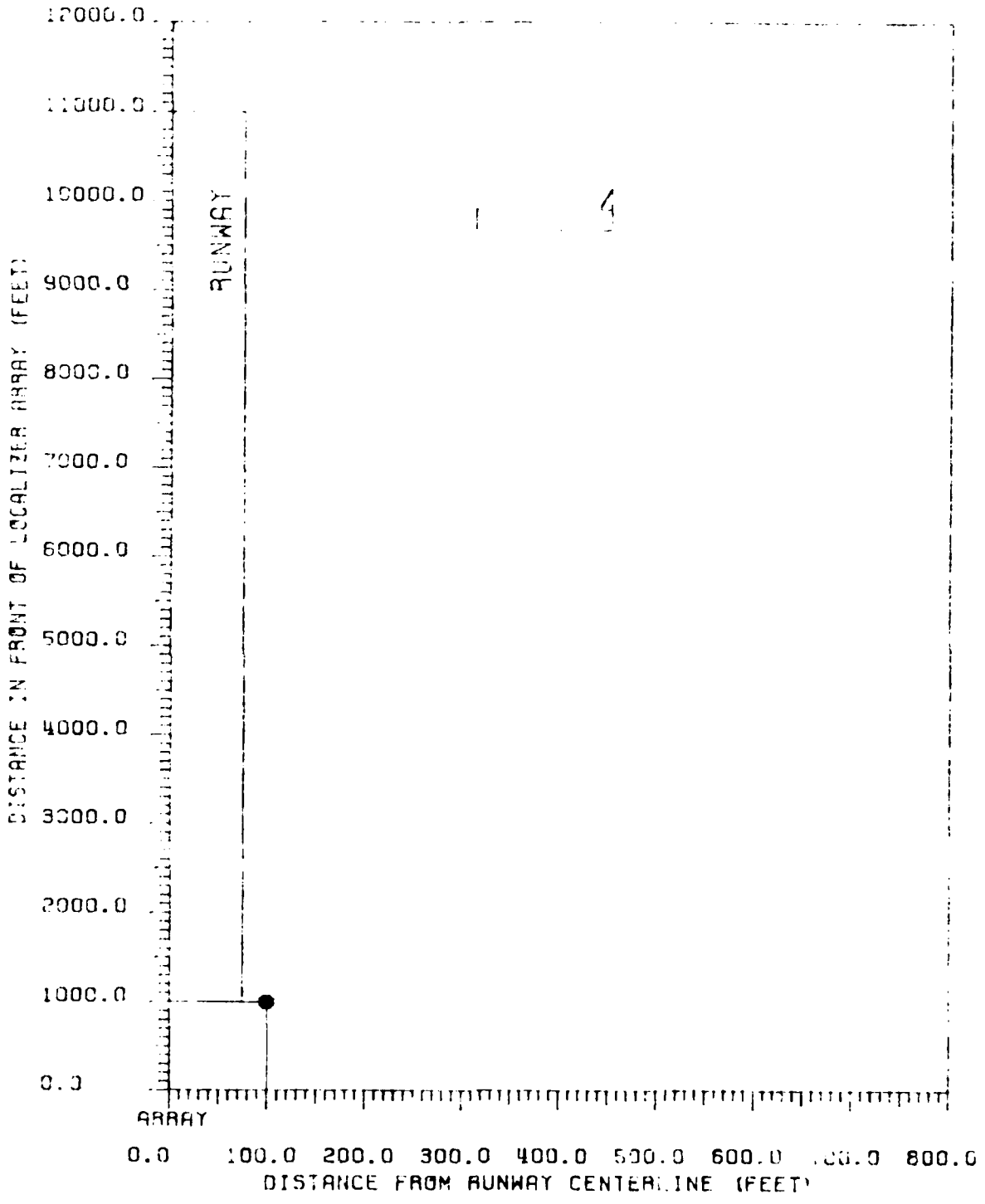

Figure 1. Critical area map for CAT II tolerances relative to DC-9 aircraft. DC-9 fuselage is perpendicular to runway centerline with tail away from runway. Nine element single-frequency array, LPD antennas.

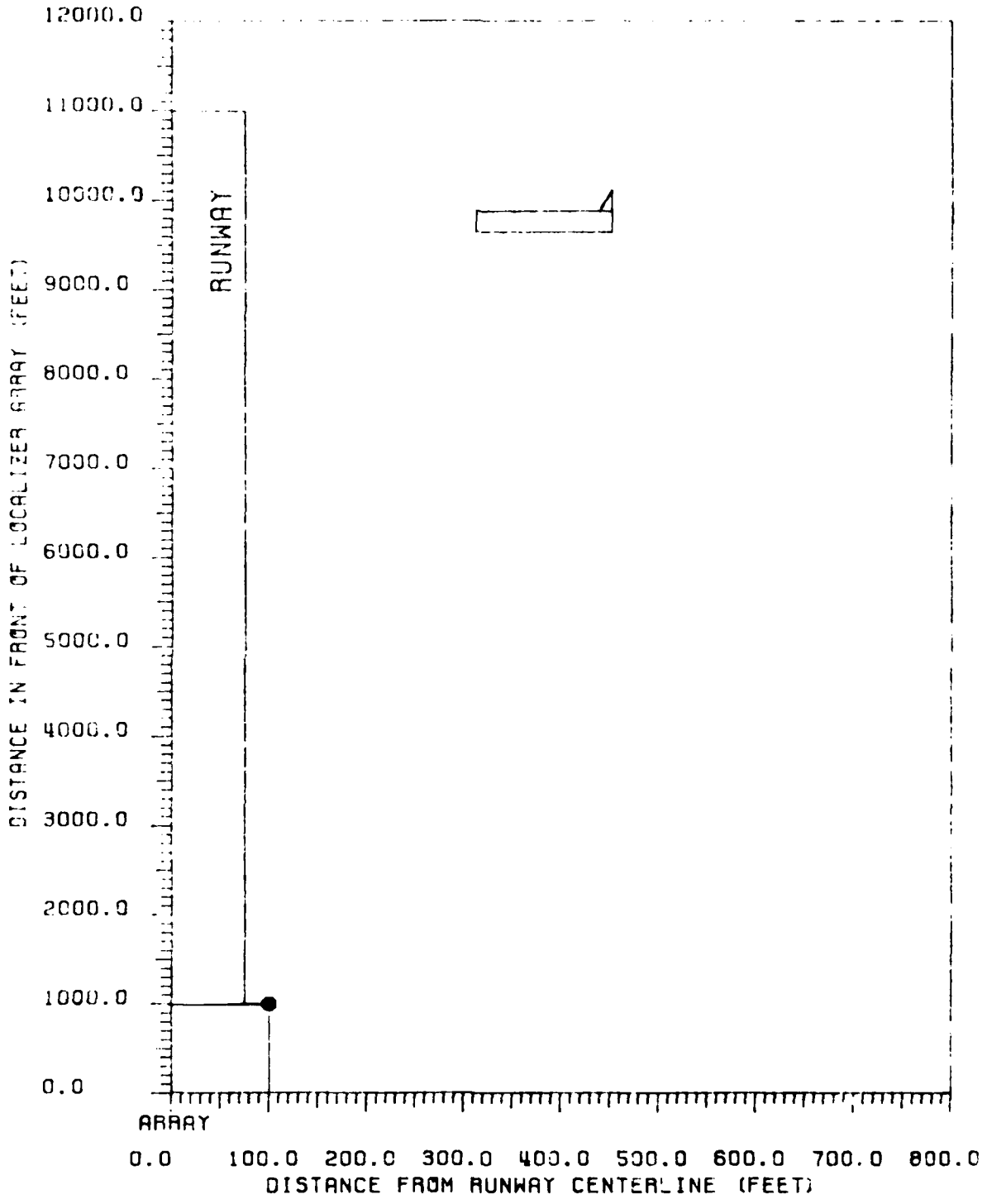

Figure 13 Critical area map for CAT III tolerances relating to DC-9 aircraft. DC-9 fuselage is perpendicular to runway centerline with tail away from runway. 8-element single-frequency array, LPD antennas.

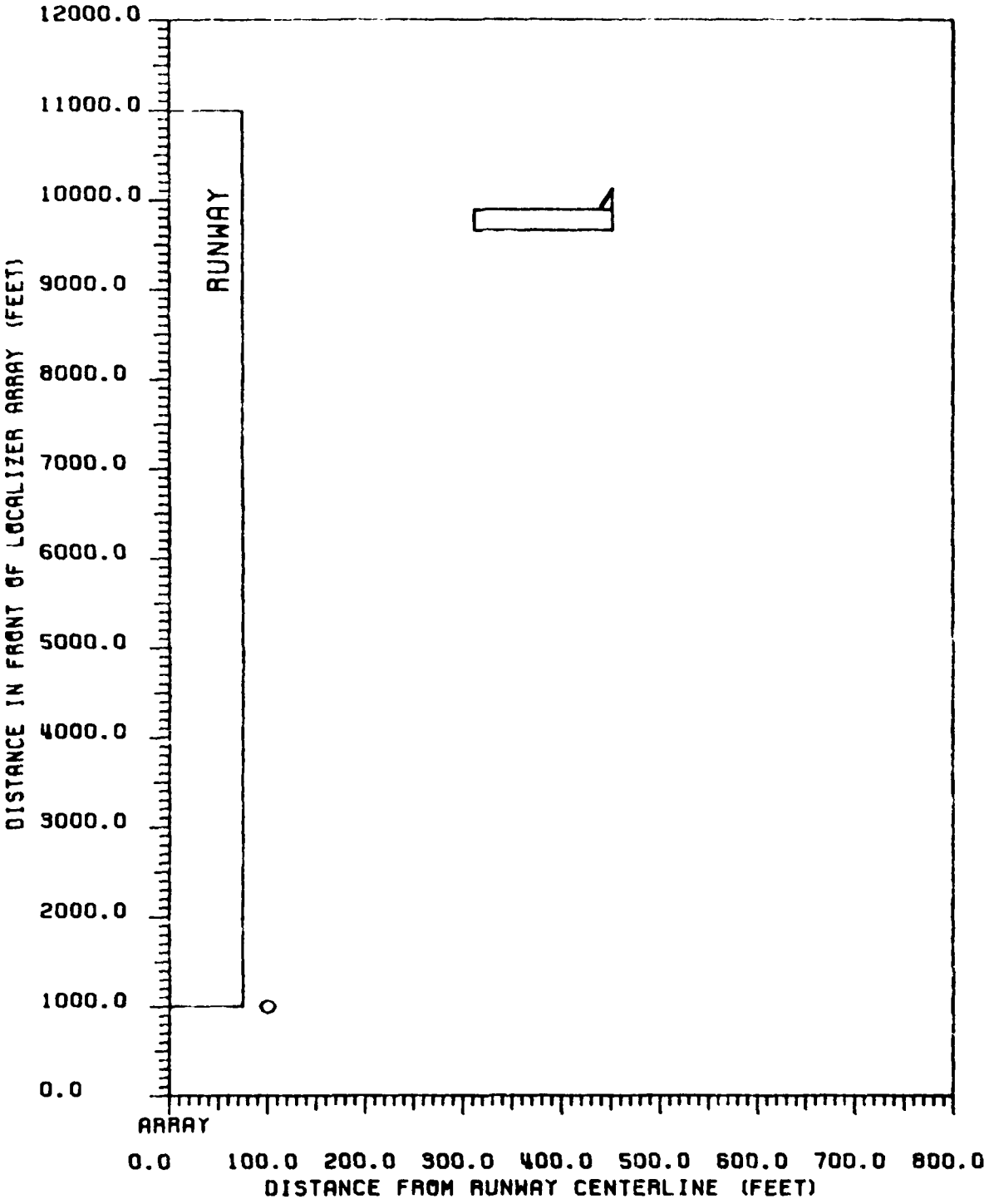

Figure 1 Contours of peak CDI values produced in ILS Zone 3 for a DC-9. DC-9 fuselage is perpendicular to runway centerline, with tail away from the runway. 8-element single-frequency array, LPD antennas.

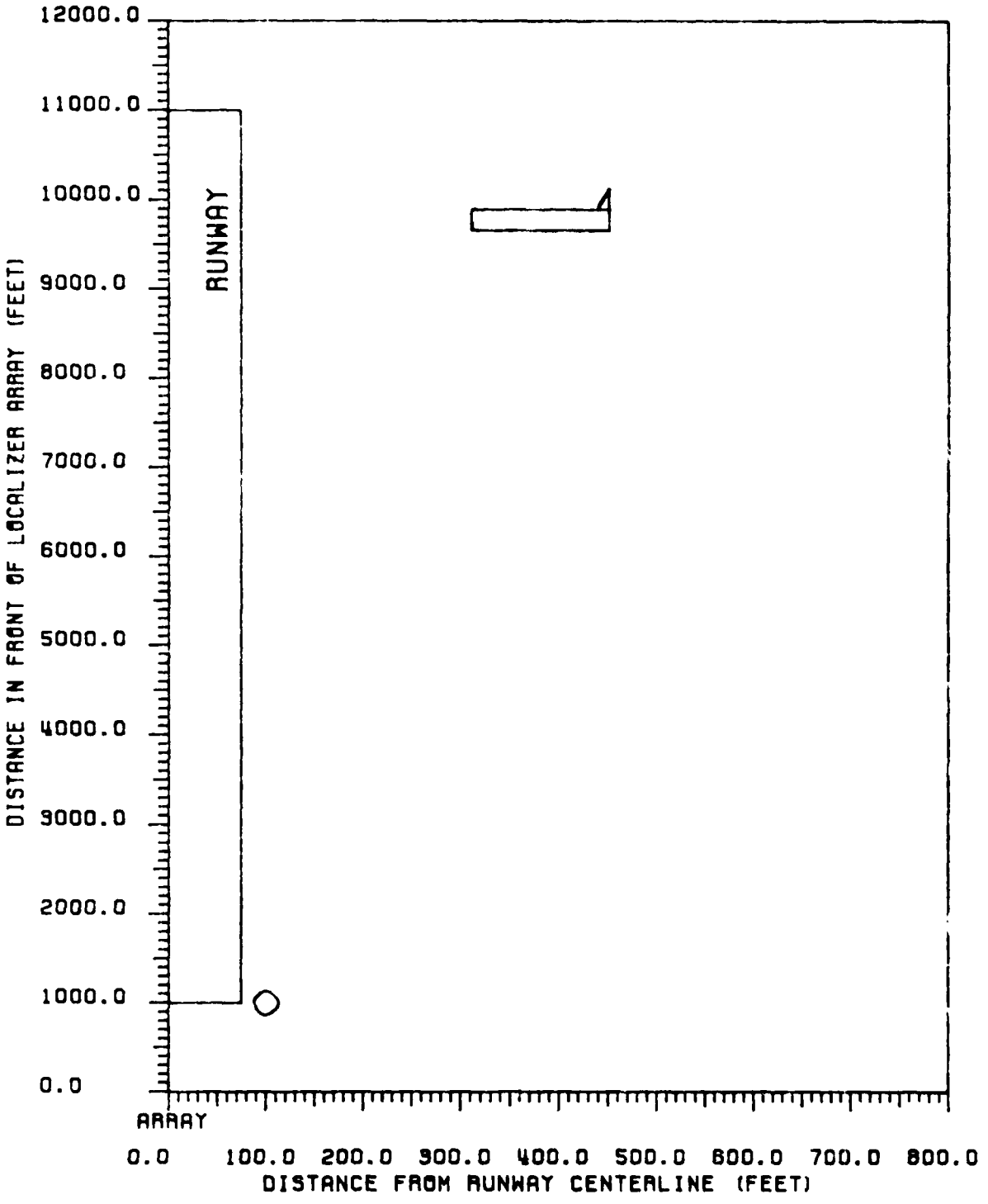

Figure 15 Contours of peak CDI values produced in ILS Zone 4 for a DC-9. DC-9 fuselage is perpendicular to runway centerline, with tail away from the runway. 8-element single-frequency array, LPD antennas.

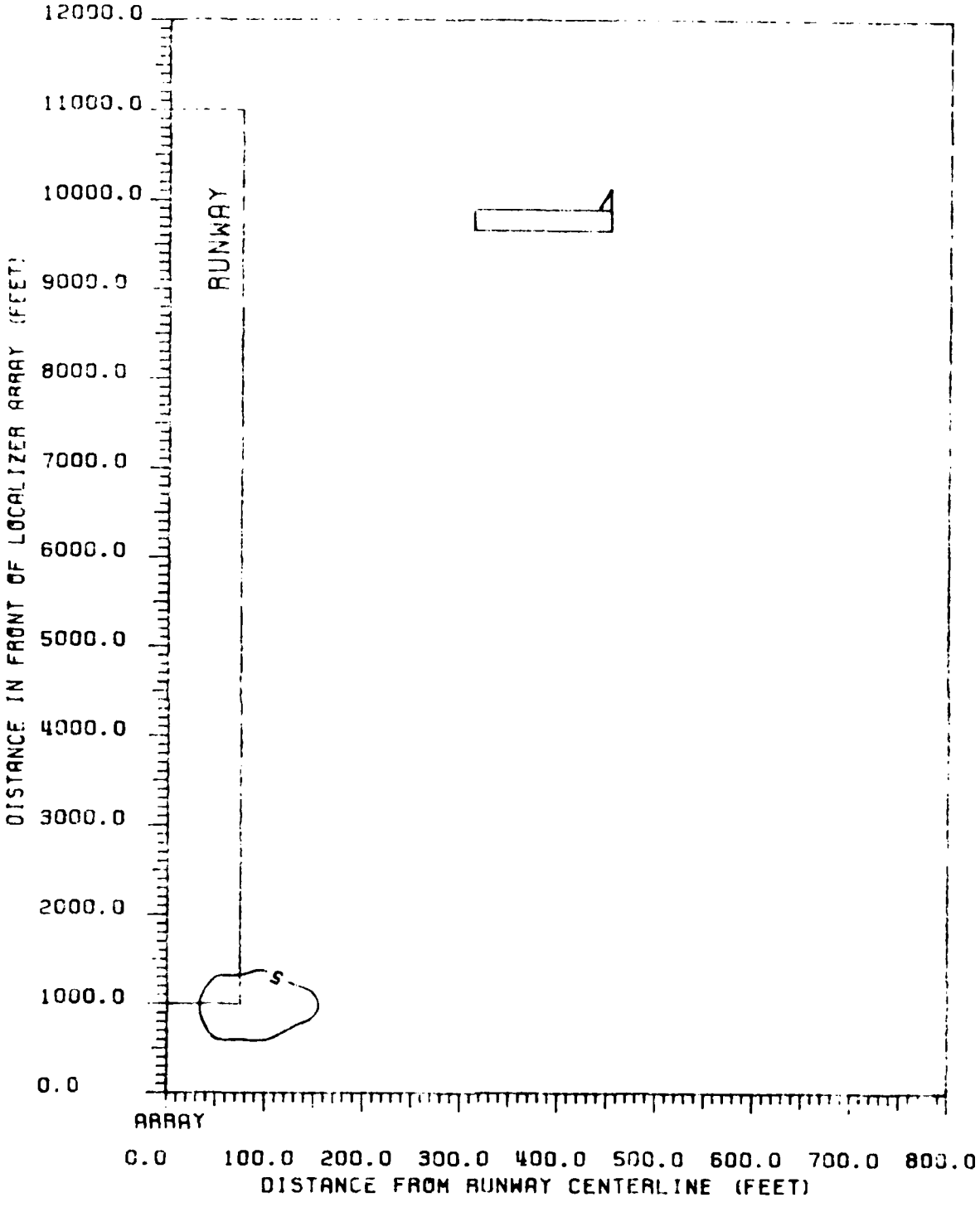

Figure 5. Contours of peak CSF values produced in ILS Zone 5 by a DC-9. DC-9 fuselage is perpendicular to runway centerline, with tail away from the runway. 5-element single-frequency array, LPD antennas.

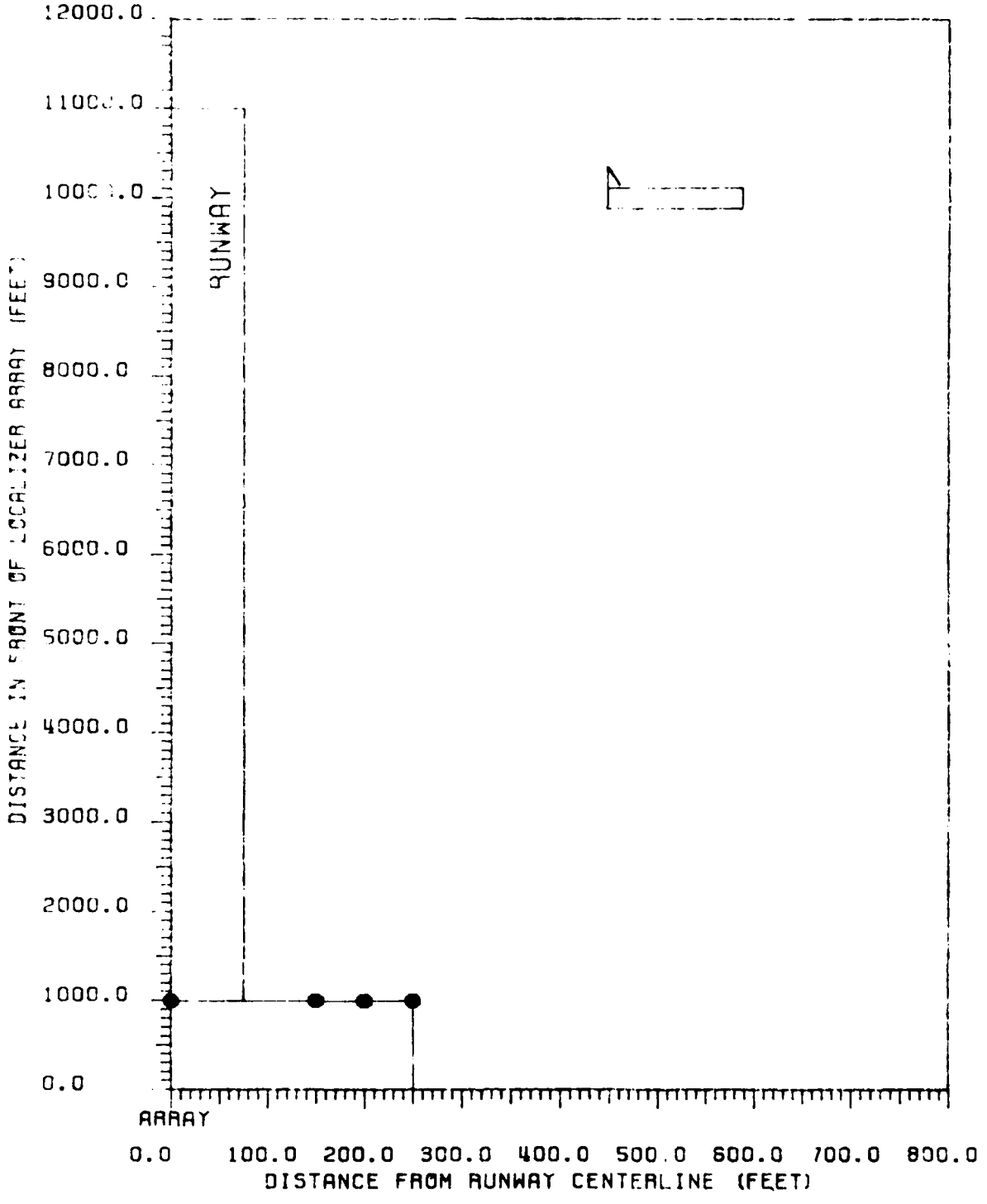

Figure 17 Critical area map for CAT II tolerances relating to B-727 aircraft. B-727 fuselage is perpendicular to runway centerline with tail towards the runway. 8-element single-frequency array, LPD antennas.

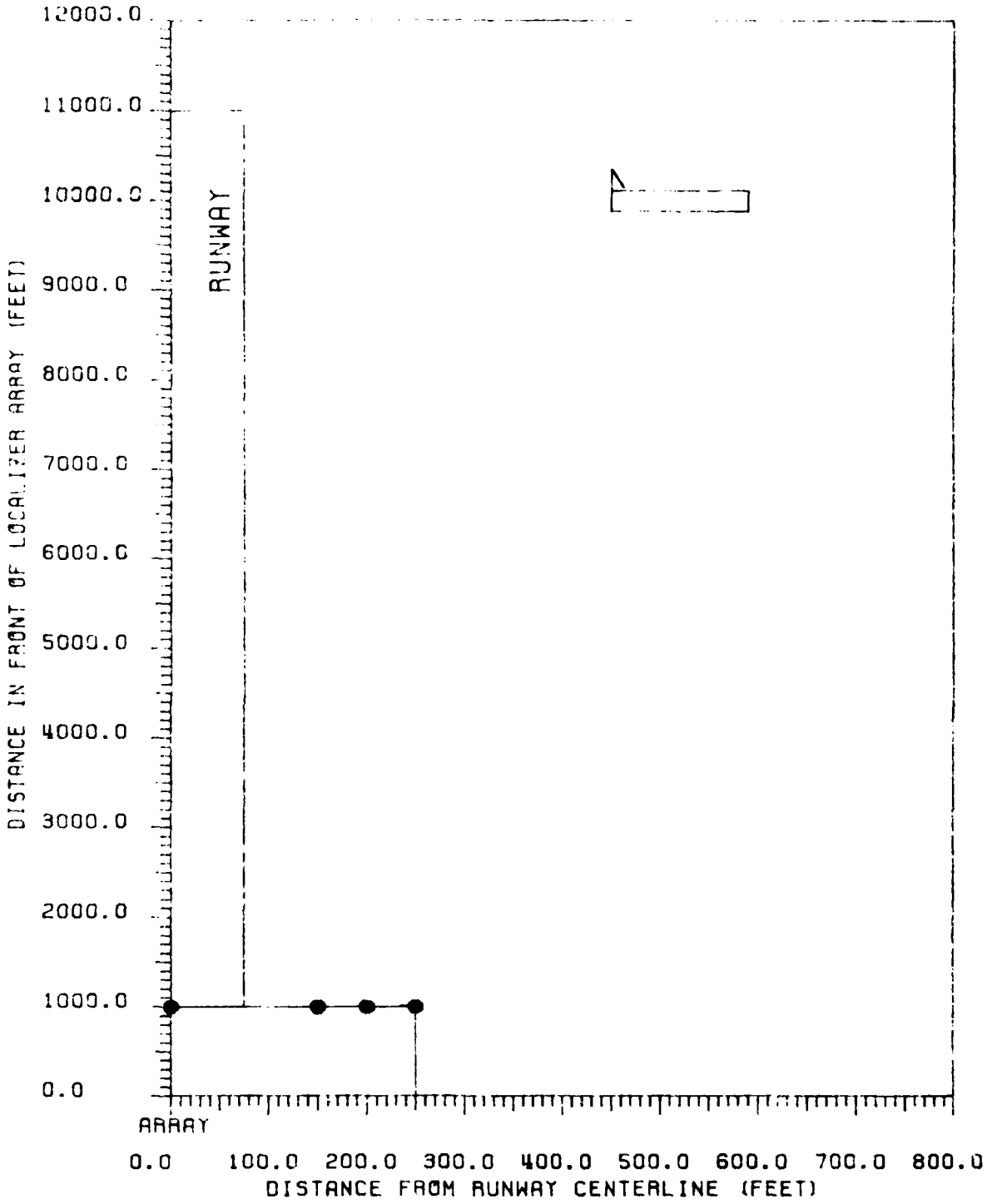

Figure 6. Critical area map for CAT III tolerances relating to B-727 aircraft. B-727 fuselage is perpendicular to runway centerline with tail towards the runway. 8-element single-frequency array, LPD antennas.

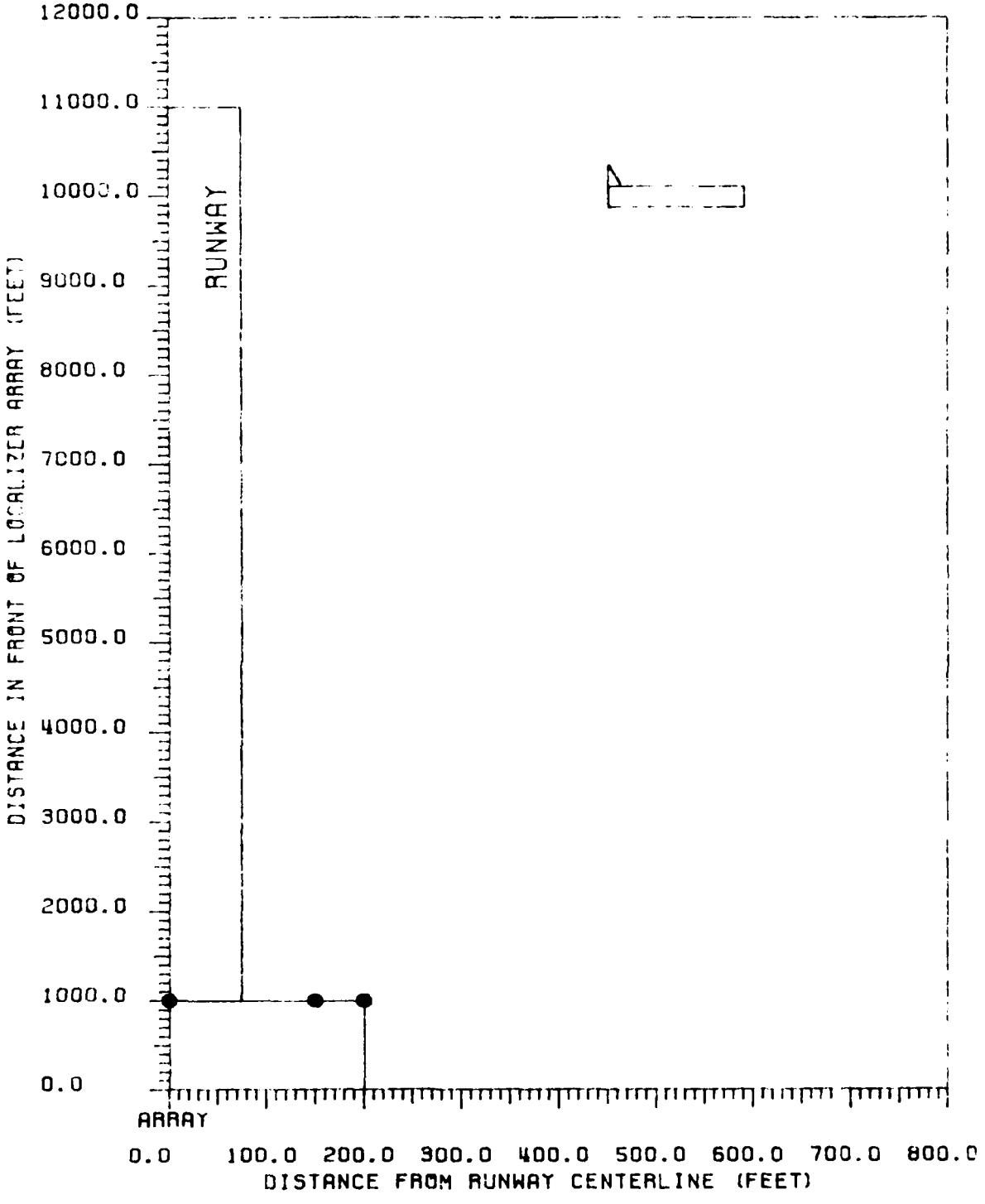

Figure 19 Critical area map for CAT III-X tolerances relating to B-727 aircraft. B-727 fuselage is perpendicular to runway centerline with tail towards the runway. 8-element single-frequency array, LPD antennas.

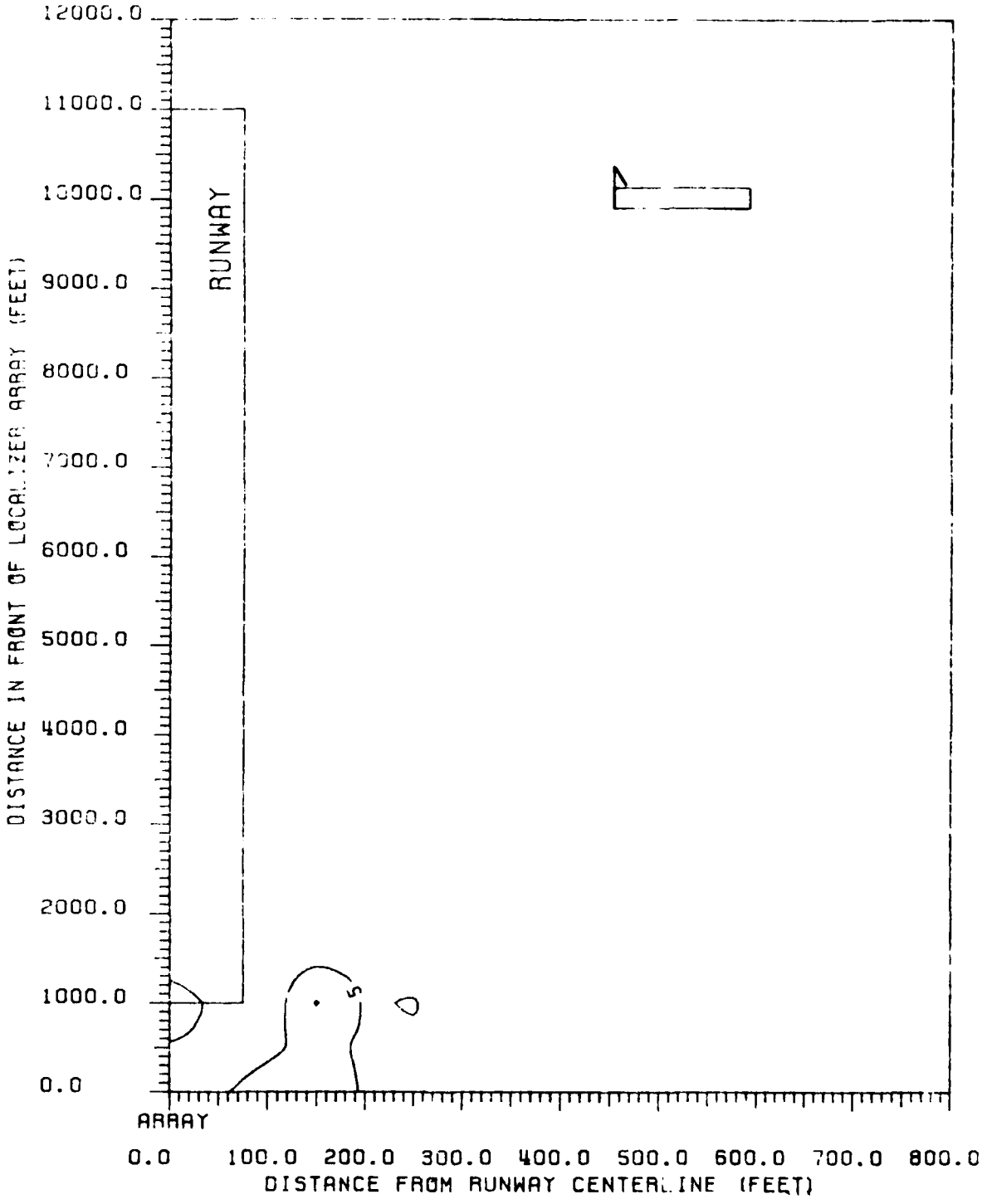

Figure 20 Contours of peak CDI values produced in ILS Zone 1 for a B-727. B-727 fuselage is perpendicular to runway centerline, with tail towards the runway. 8-element single-frequency array, LPD antennas.

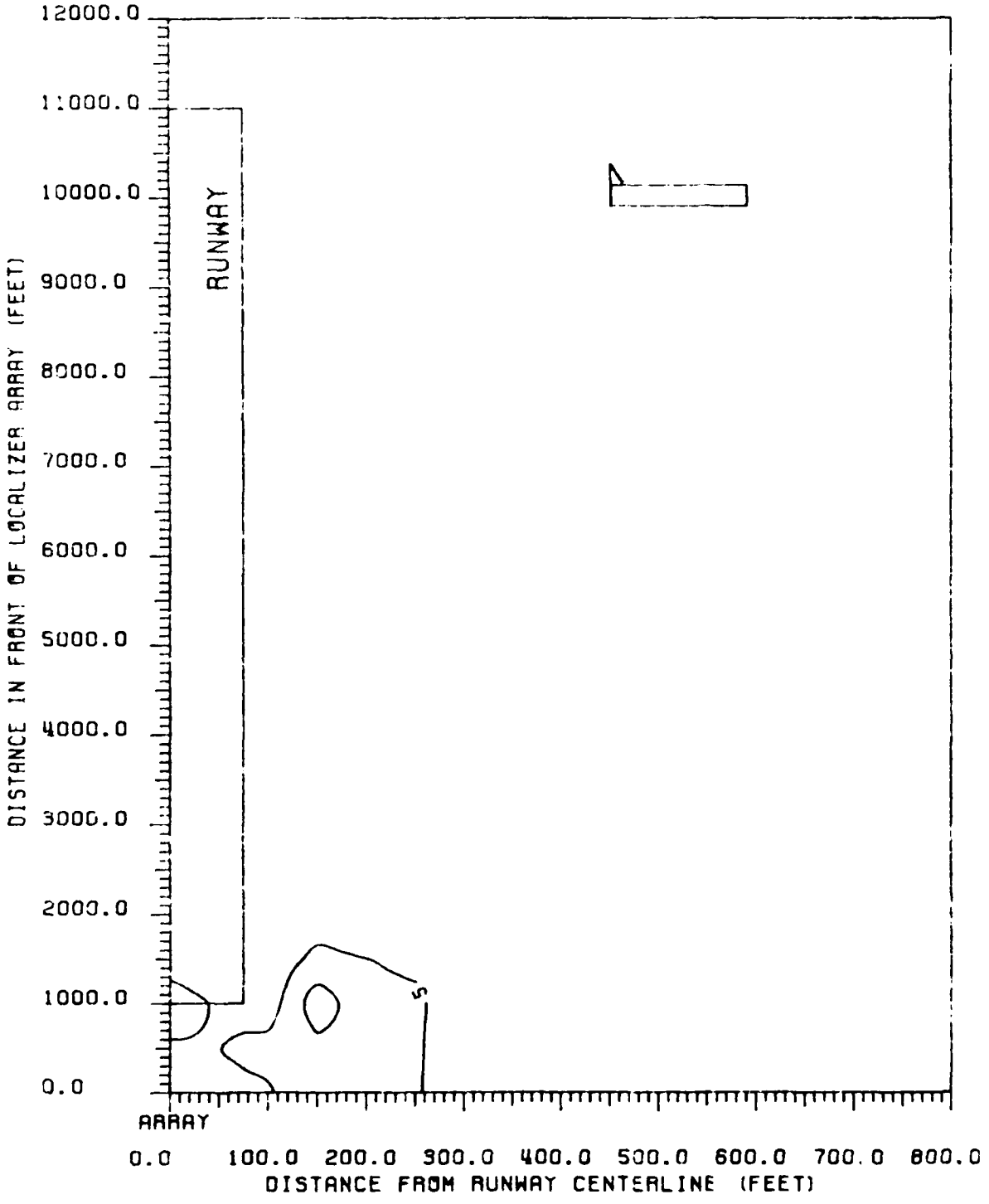

Figure 21 Contours of peak CDI values produced in ILS Zone 2 for a B-727. B-727 fuselage is perpendicular to runway centerline, with tail towards the runway. 8-element single-frequency array, LPD antennas.

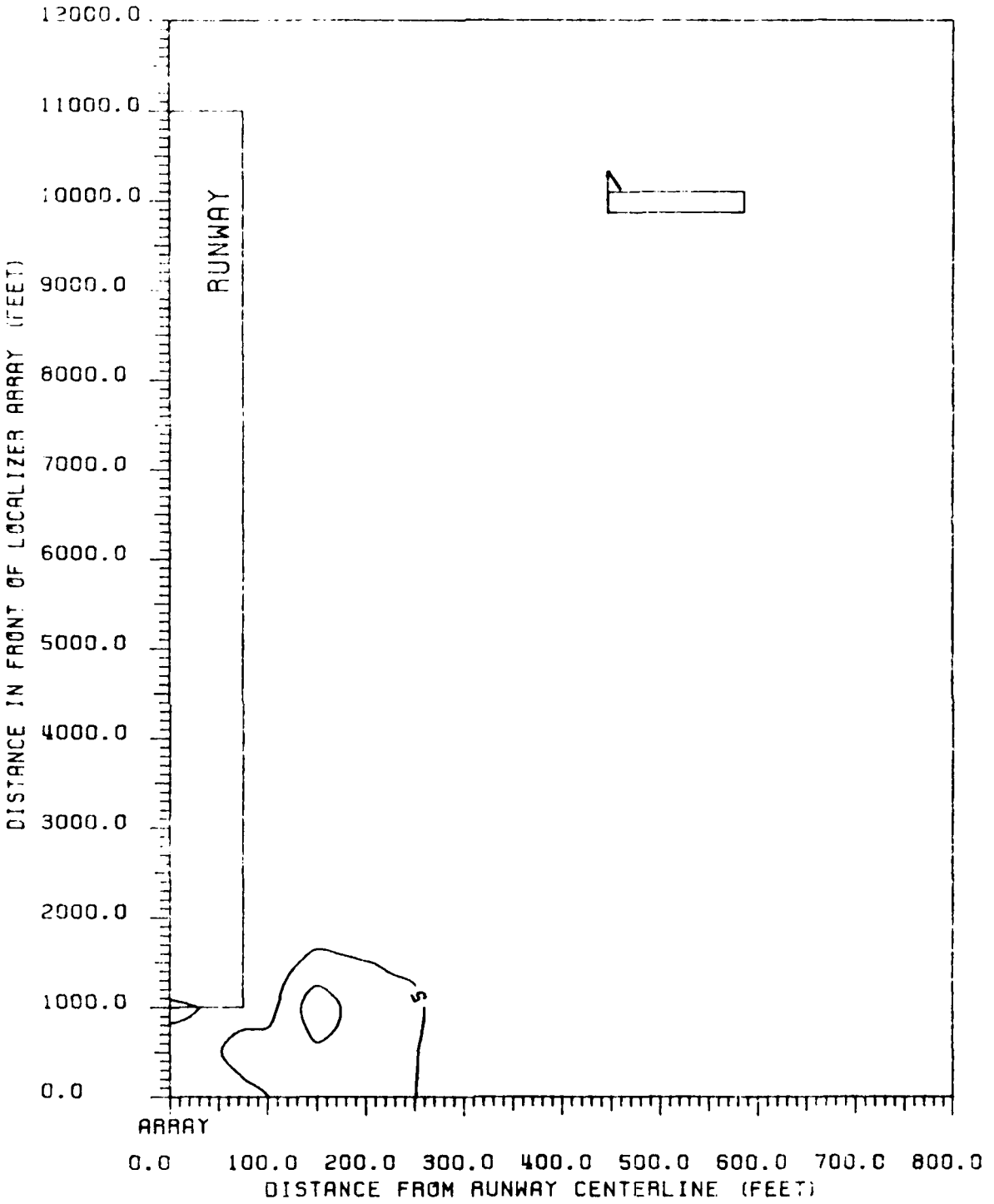

Figure 22 Contours of peak CDI values produced in ILS Zone 3 to Threshold for a B-727. B-727 fuselage is perpendicular to runway centerline, with tail towards the runway. 8-element single-frequency array, LPD antennas.

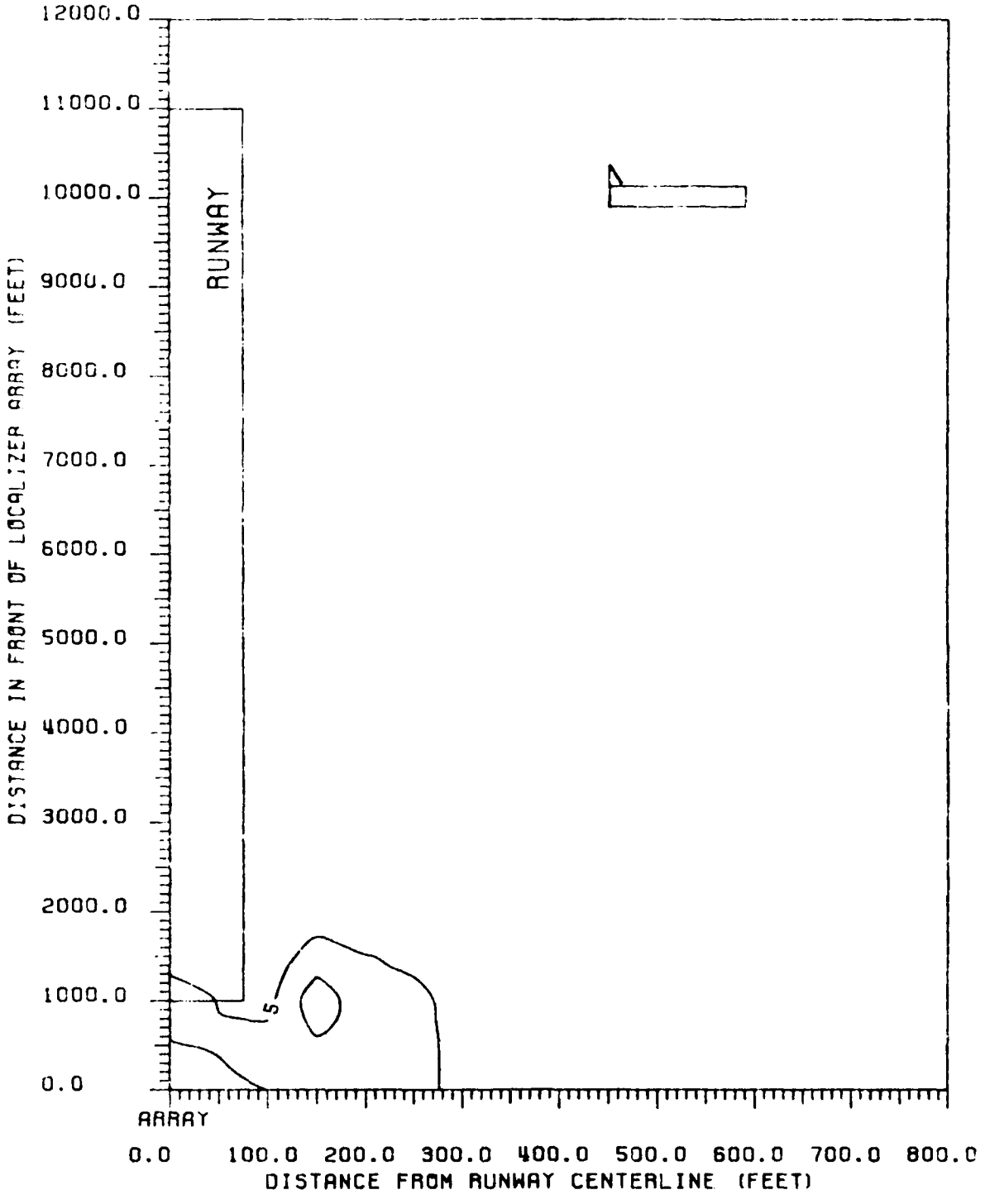

Figure 23 Contours of peak CDI values produced in ILS Zone 4 for a B-727. B-727 fuselage is perpendicular to runway centerline, with tail towards the runway. 8-element single-frequency array, LPD antennas.

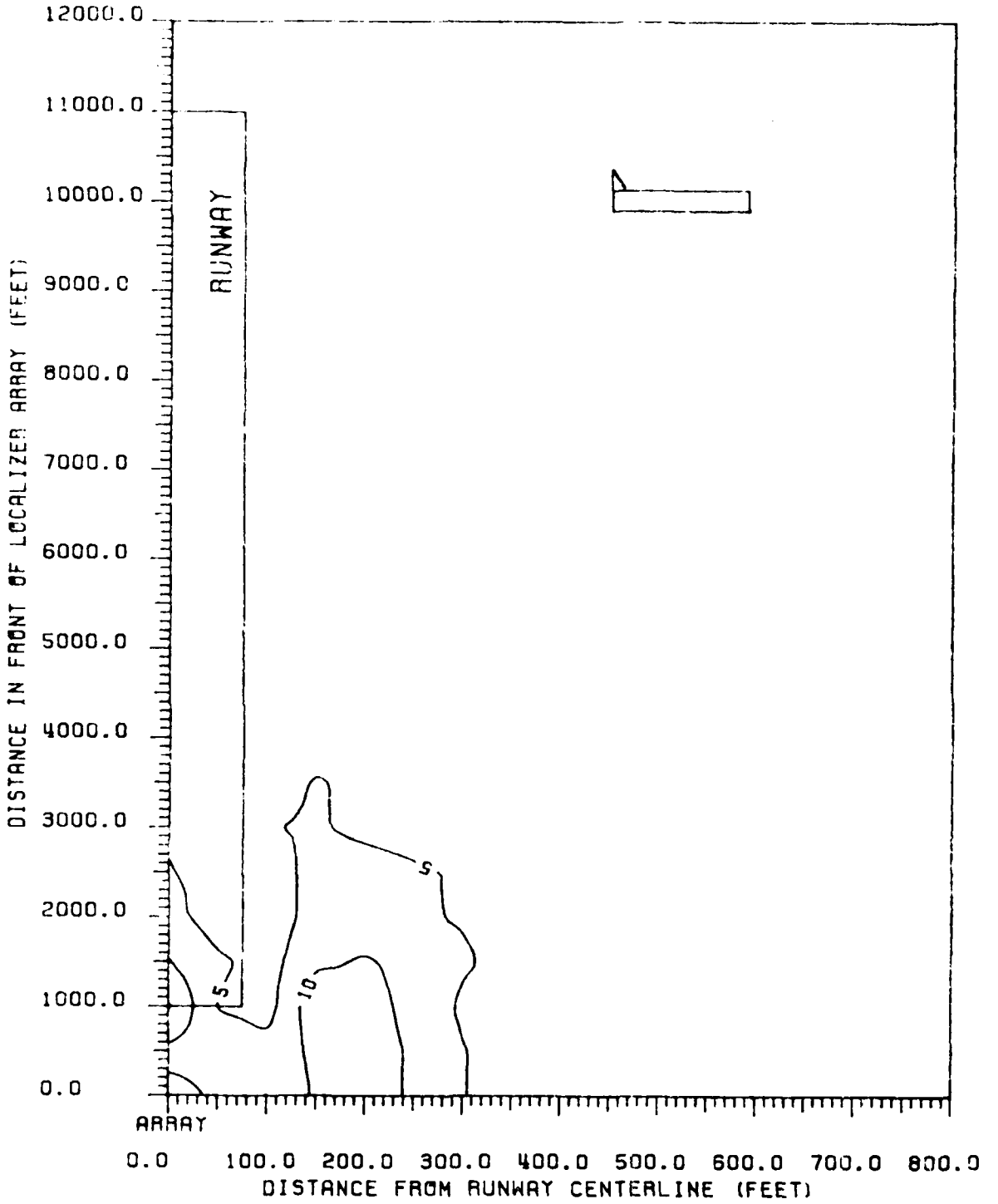

Figure 24 Contours of peak CDI values produced in ILS Zone 5 for a B-727. B-727 fuselage is perpendicular to runway centerline, with tail towards the runway. 8-element single-frequency array, LPD antennas.

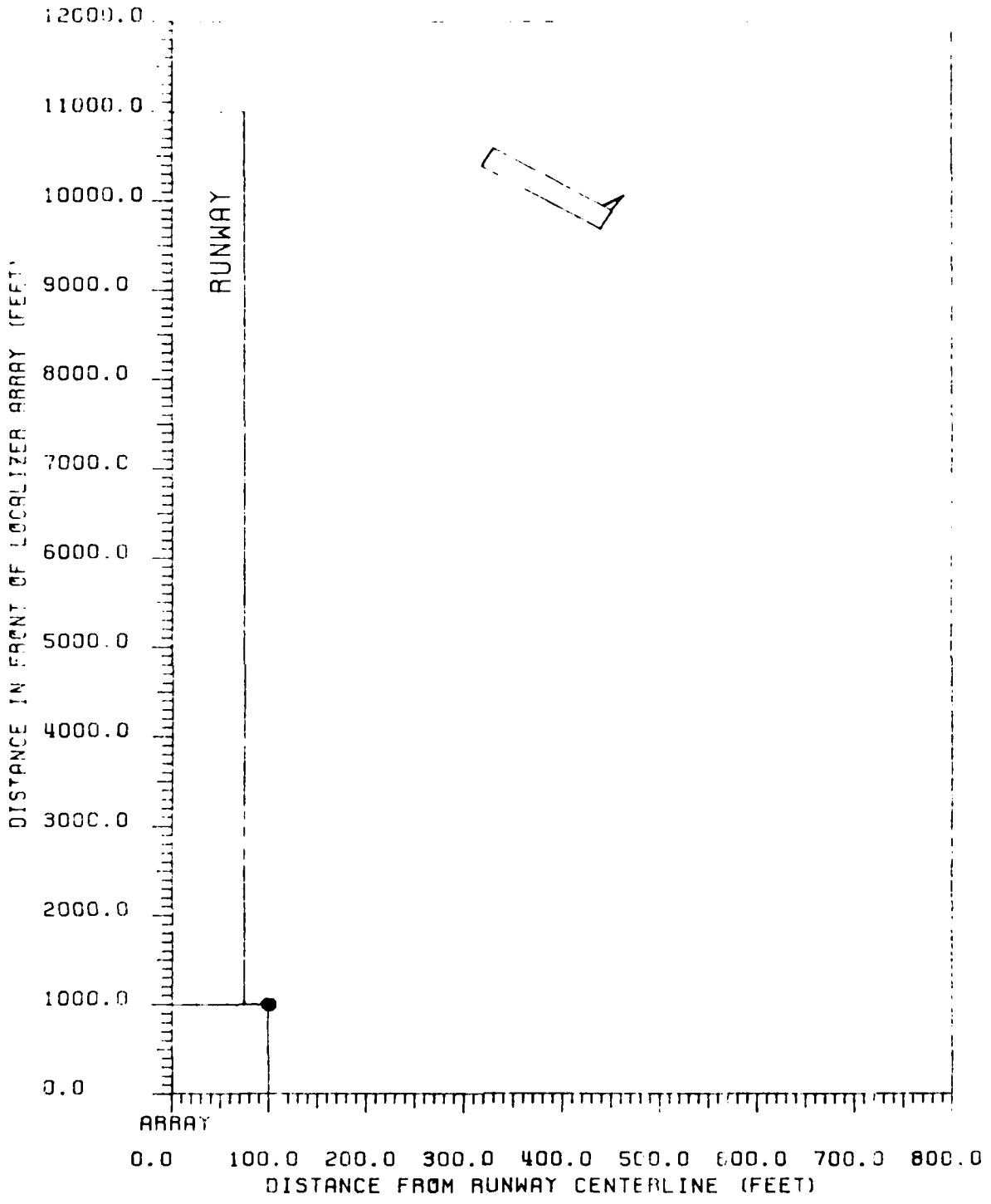

Figure 25 Critical area map for CAT II tolerances relating to B-727 aircraft. B-727 fuselage is oriented 60 degrees to runway centerline with tail towards the array. 8-element single-frequency array, LPD antennas.

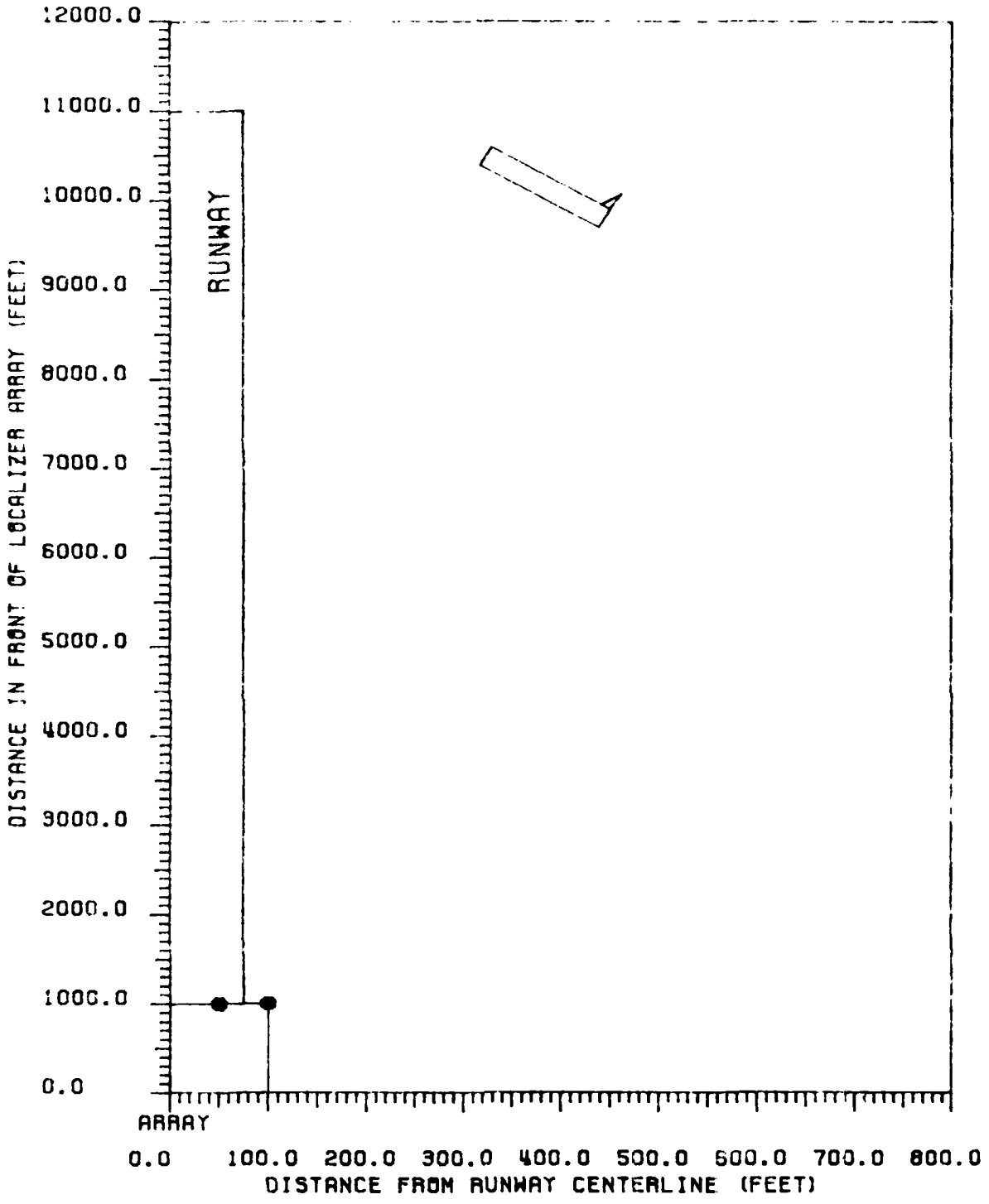

Figure 26 Critical area map for CAT III tolerances relating to B-727 aircraft. B-727 fuselage is oriented 60 degrees to runway centerline with tail towards the array. 8-element single-frequency array, LPD antennas.

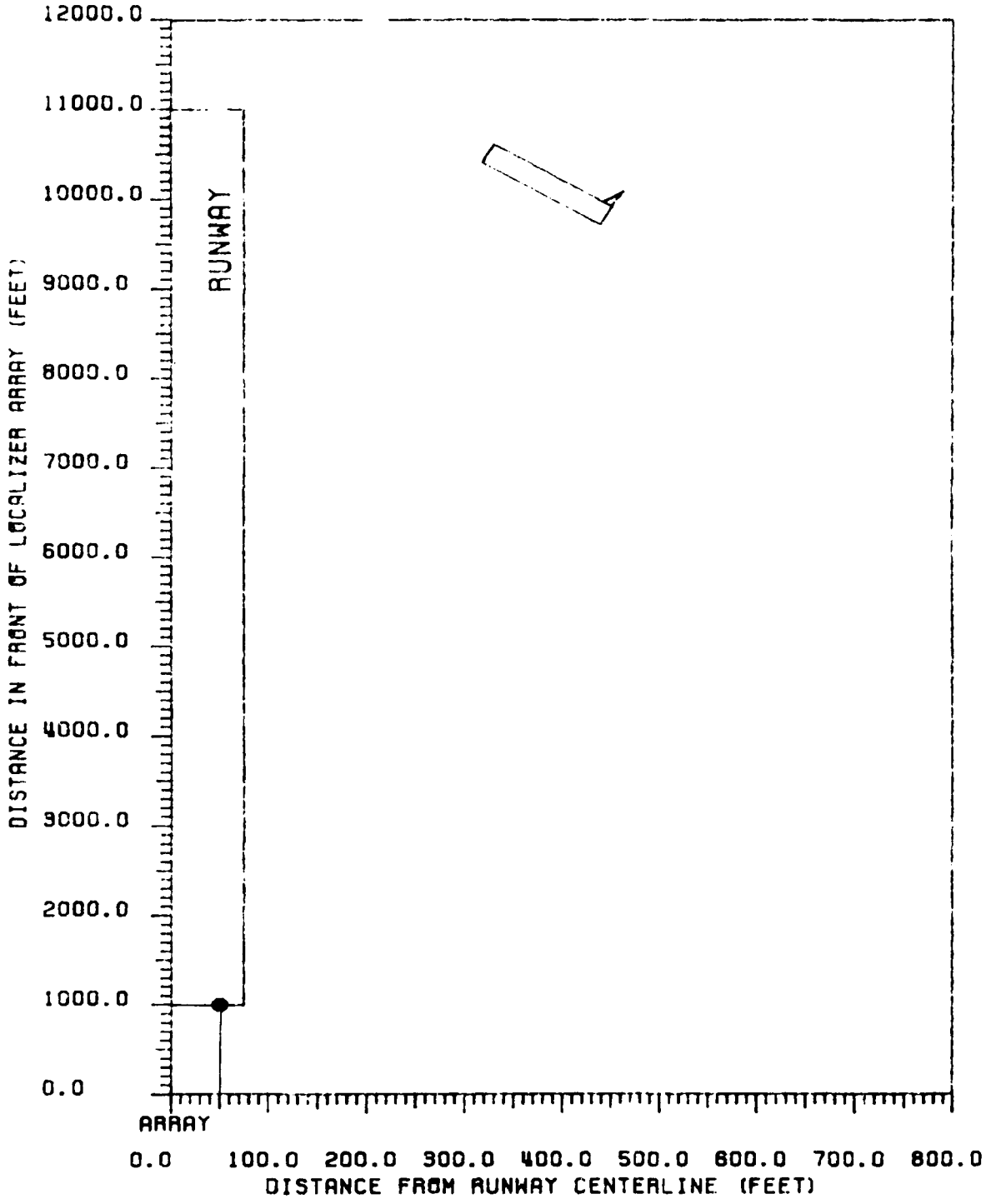

Figure 27 Critical area map for CAT III-X tolerances relating to B-727 aircraft. B-727 fuselage is oriented 60 degrees to runway centerline with tail towards the array. 8-element single-frequency array, LPD antennas.

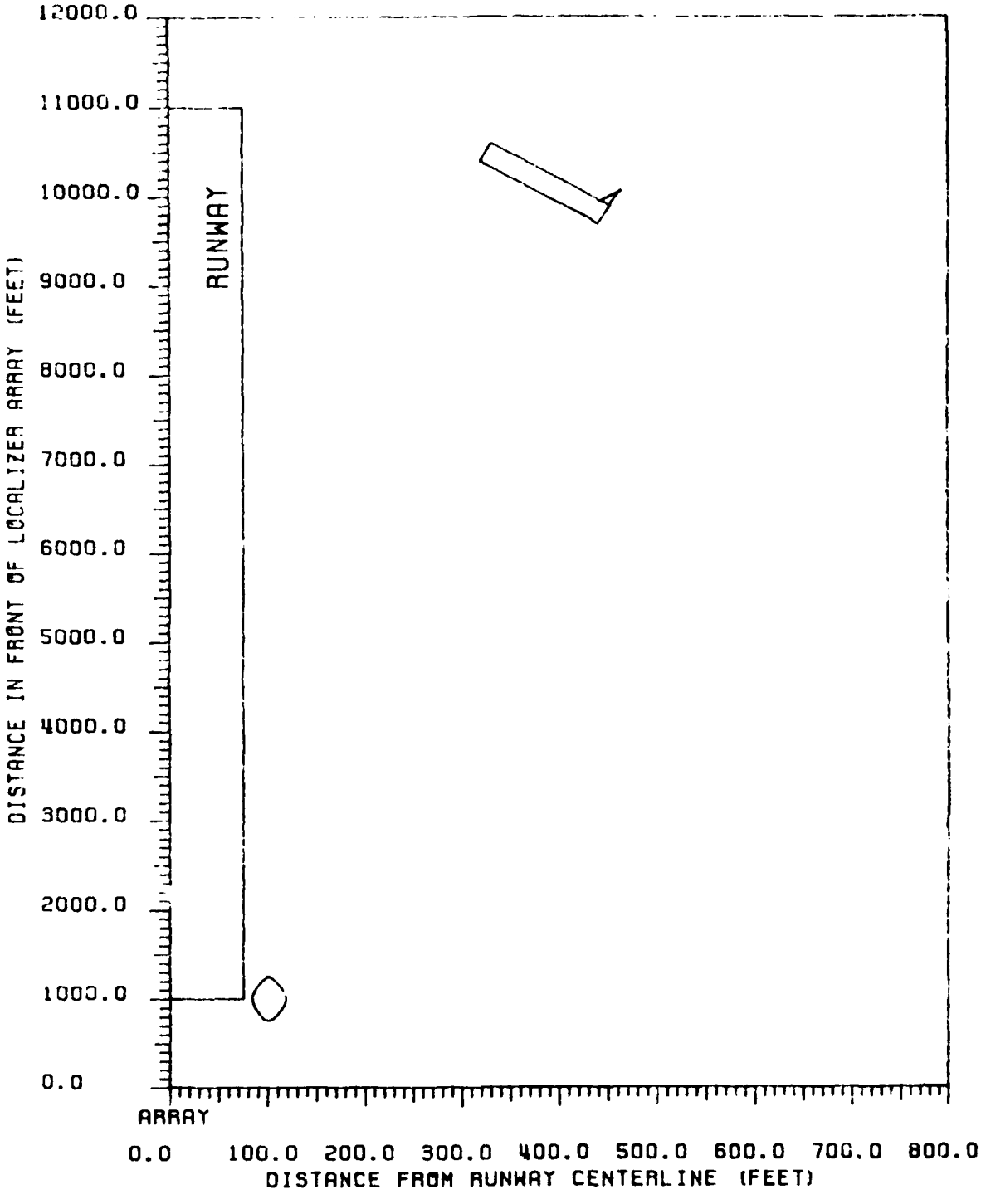

Figure 28 Contours of peak CDI values produced in ILS Zone 1 for a B-727. B-727 fuselage is oriented 60 degrees to runway centerline, with tail towards the array. 8-element single-frequency array, LPD antennas.

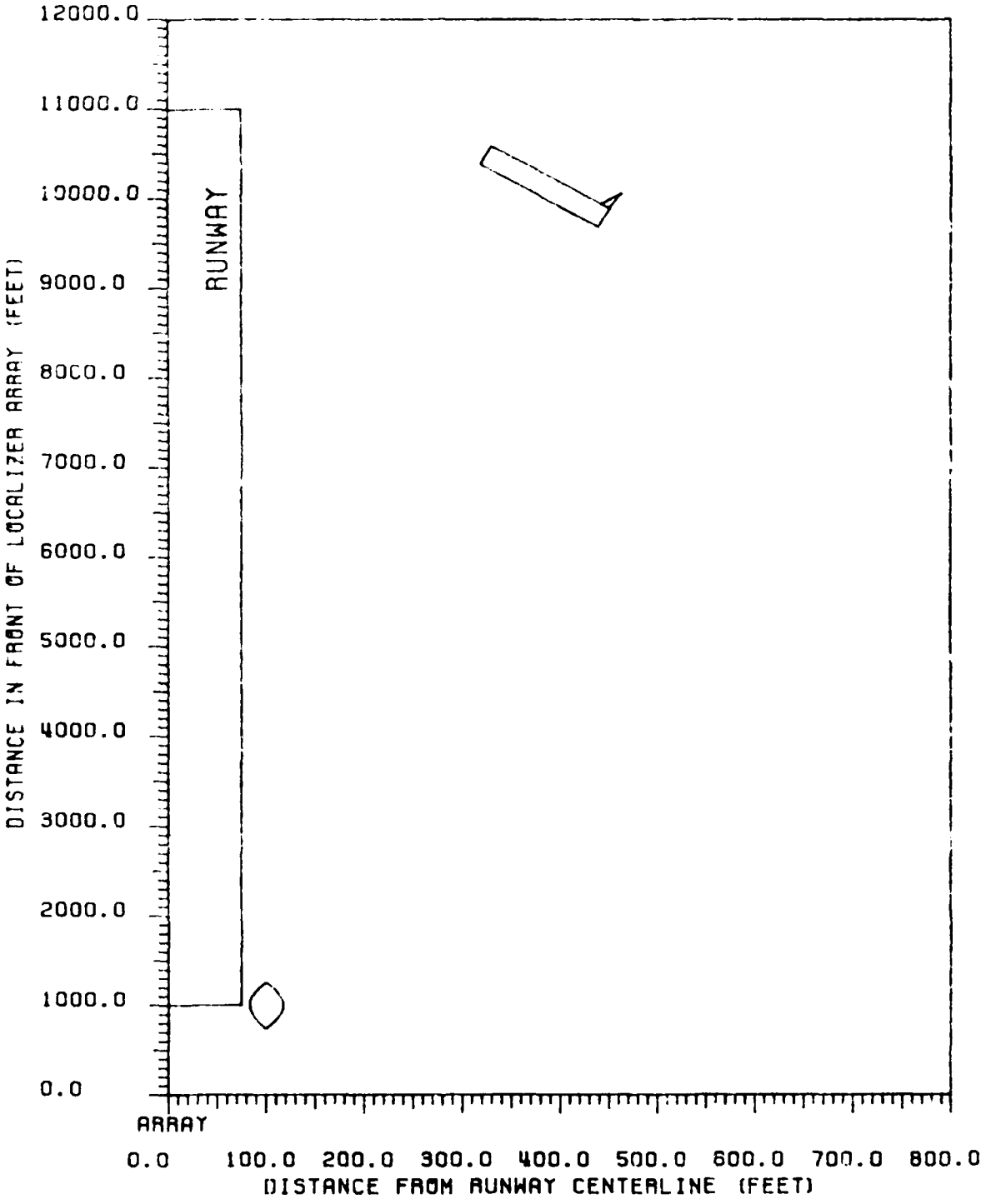

Figure 29 Contours of peak CDI values produced in ILS Zone 2 for a B-727. B-727 fuselage is oriented 60 degrees to runway centerline, with tail towards the array. 8-element single-frequency array, LPD antennas.

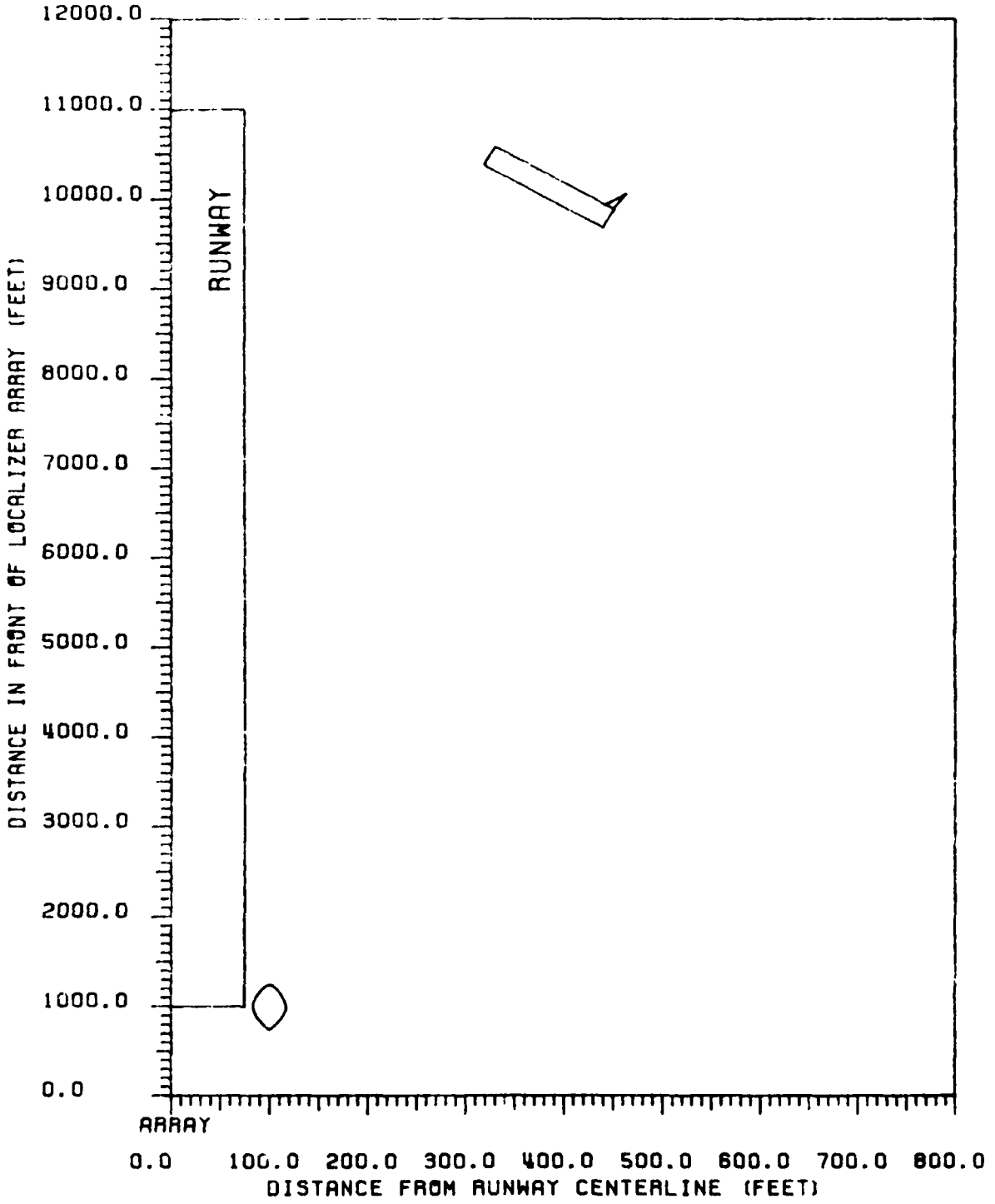

Figure 30 Contours of peak CDI values produced in ILS Zone 3 to Threshold for a B-727. B-727 fuselage is oriented 60 degrees to runway centerline, with tail towards the array. 8-element single-frequency array, LPD antennas.

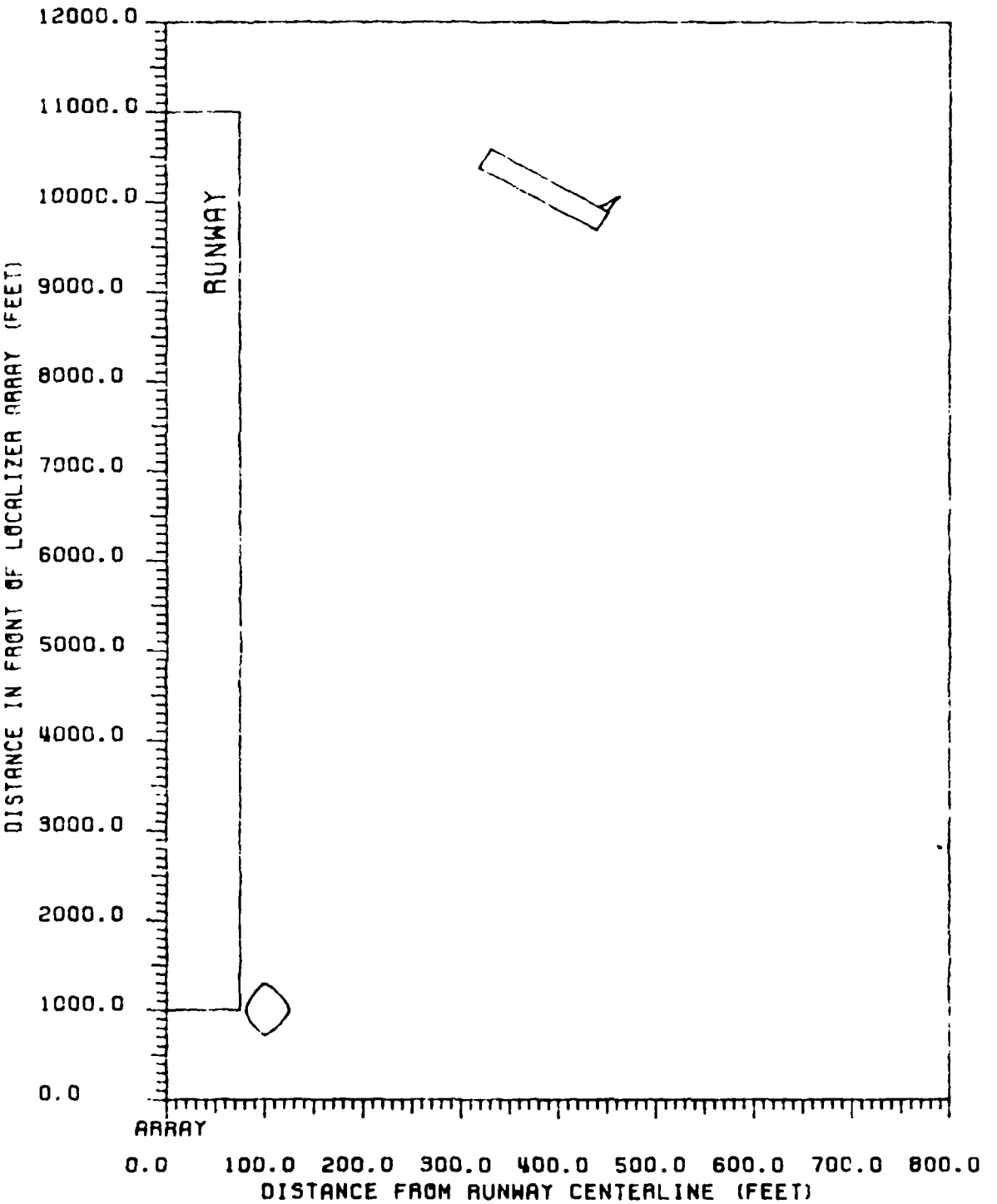

Figure 31 Contours of peak CDI values produced in ILS Zone 4 for a B-727. B-727 fuselage is oriented 60 degrees to runway centerline, with tail towards the array. 8-element single-frequency array, LPD antennas.

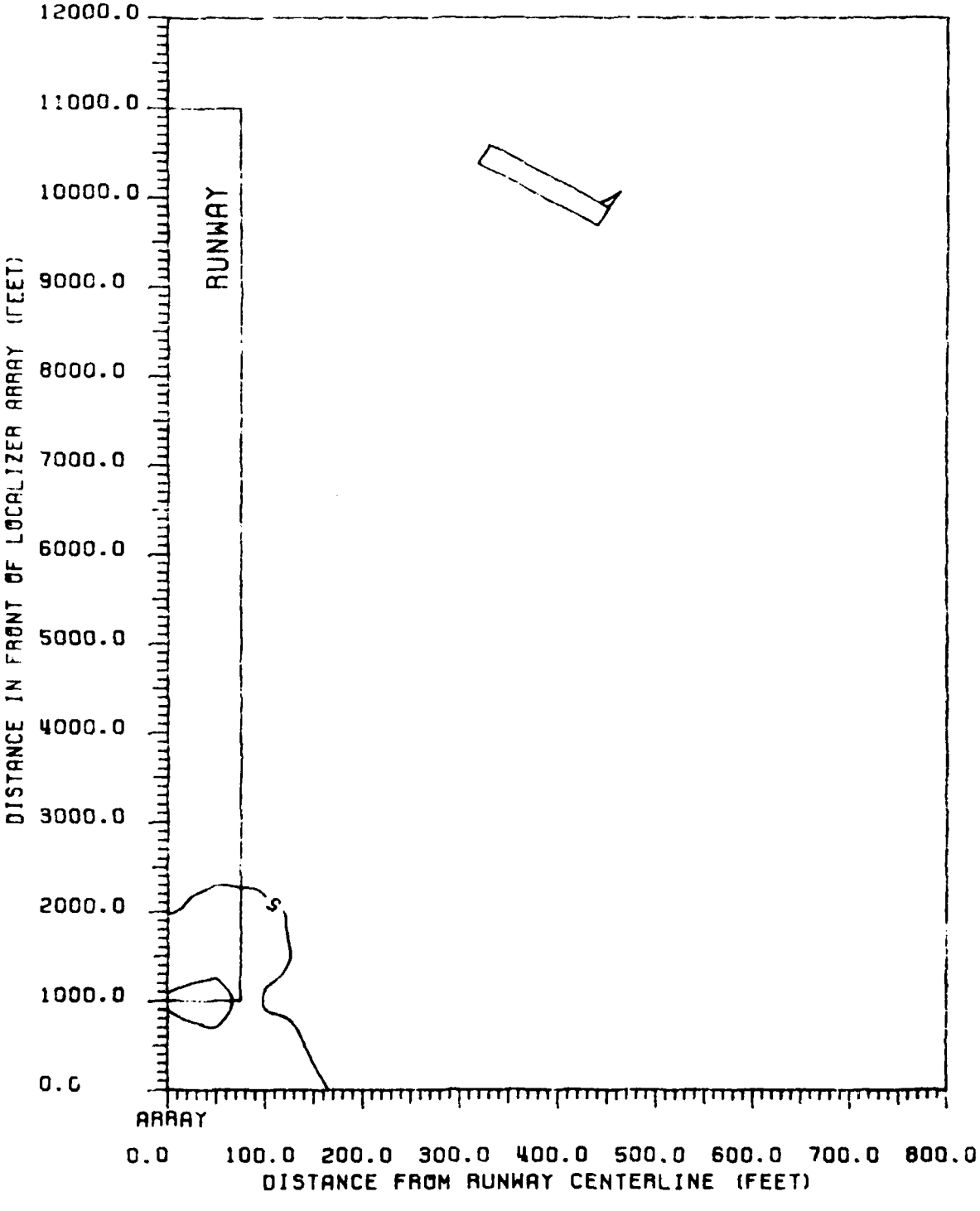

Figure 32 Contours of peak CDI values produced in ILS Zone 5 for a B-727. B-727 fuselage is oriented 60 degrees to runway centerline, with tail towards the array. 8-element single-frequency array, LPD antennas.

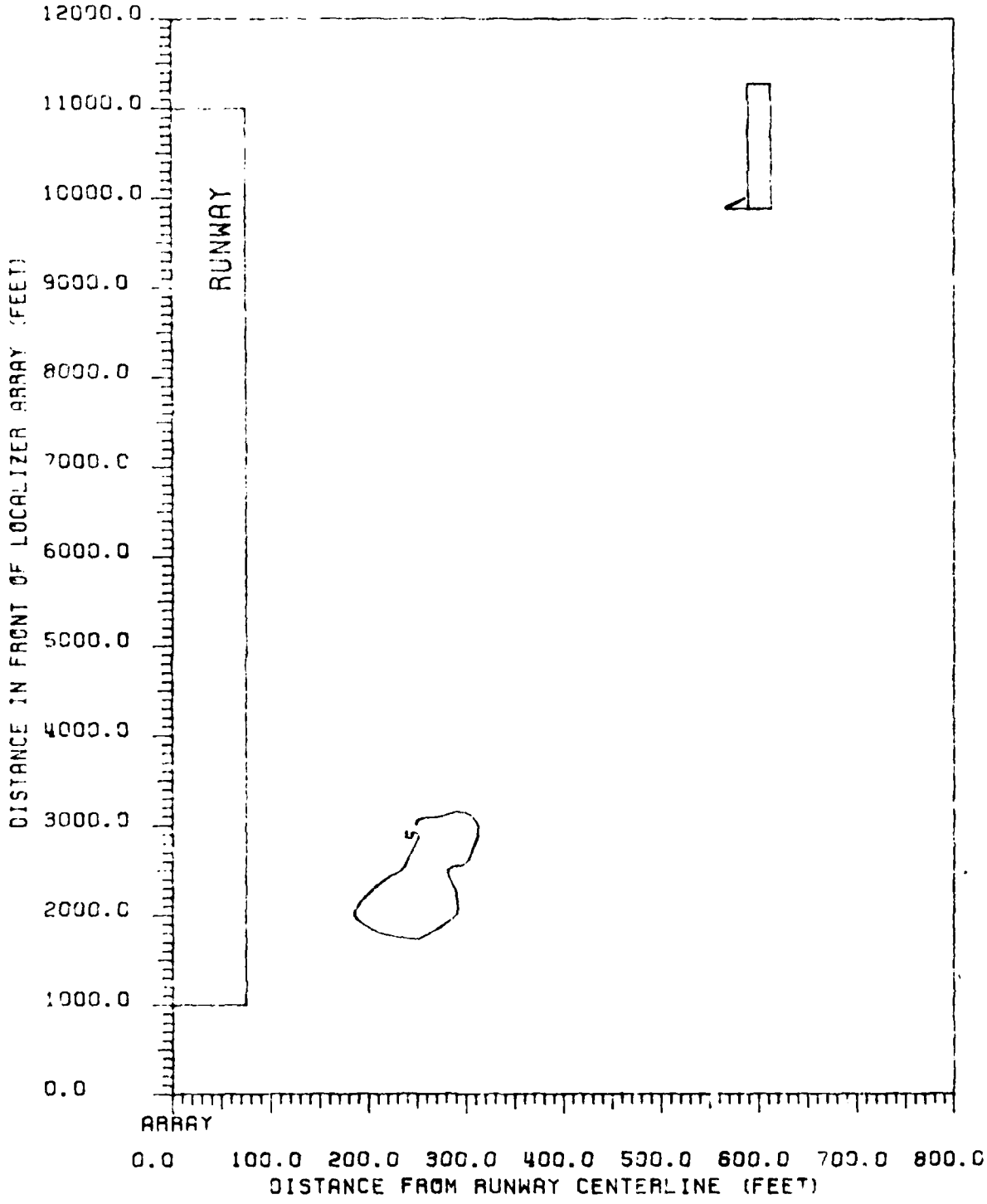

Figure 33 Contours of peak CDI values produced in ILS Zone 5 for a B-727. B-727 fuselage is parallel to runway centerline, with tail towards the array. 8-element single-frequency array, LPD antennas.

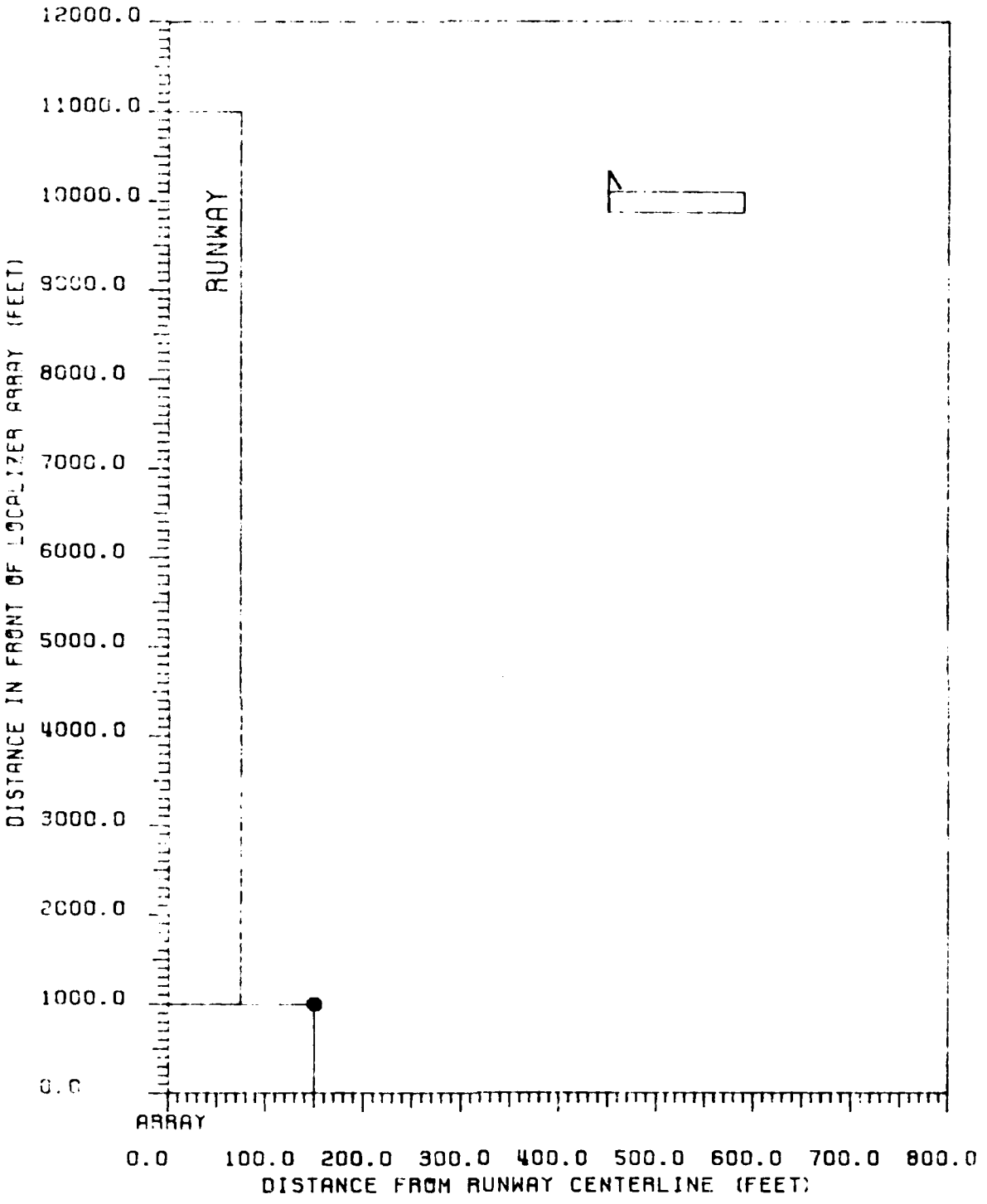

Figure 34 Critical area map for CAT I tolerances relating to B-707 aircraft. B-707 fuselage is perpendicular to runway centerline with tail towards the runway. 8-element single-frequency array, LPD antennas.

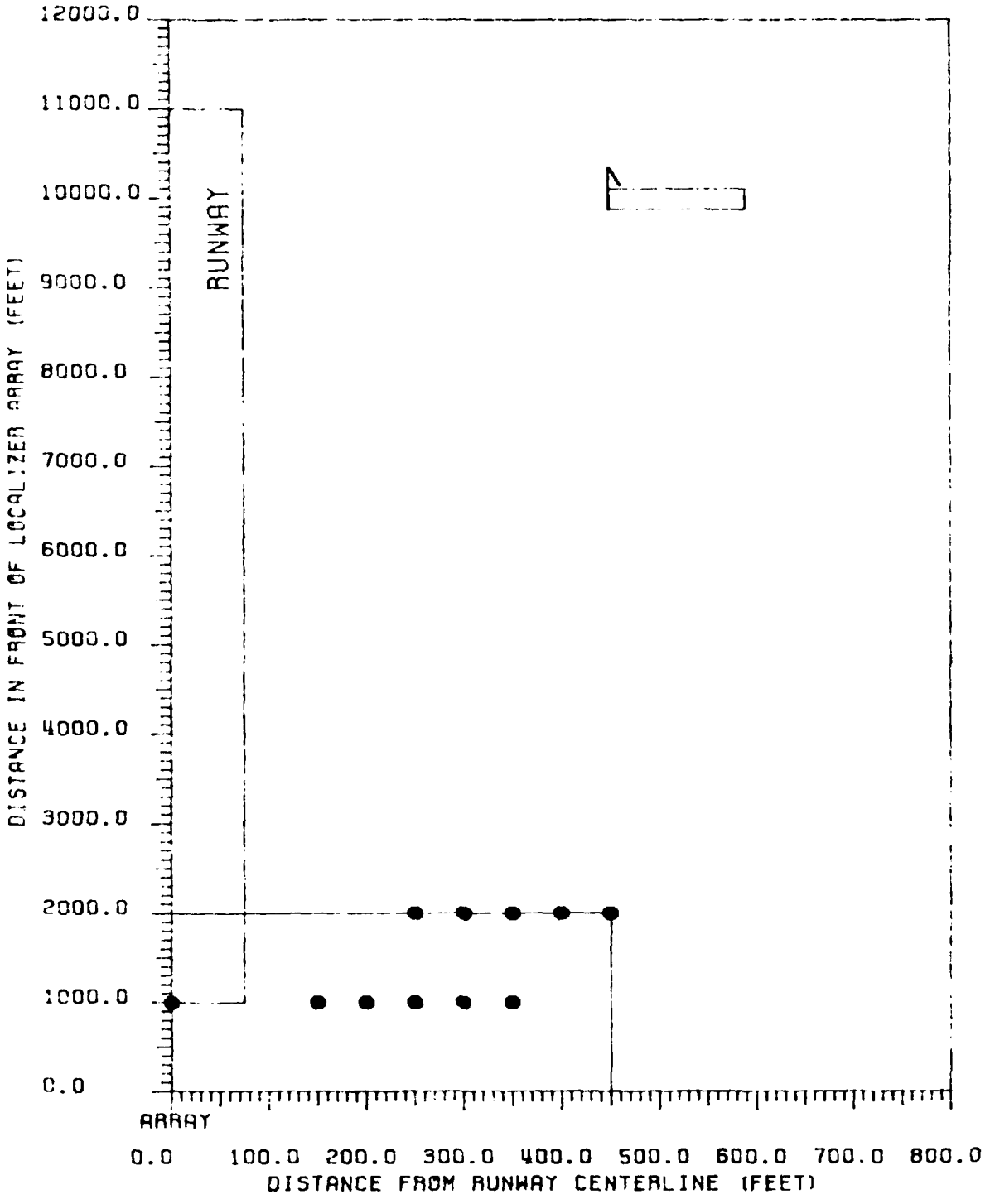

Figure 35 Critical area map for CAT II tolerances relating to B-707 aircraft. B-707 fuselage is perpendicular to runway centerline with tail towards the runway. 8-element single-frequency array, LPD antennas.

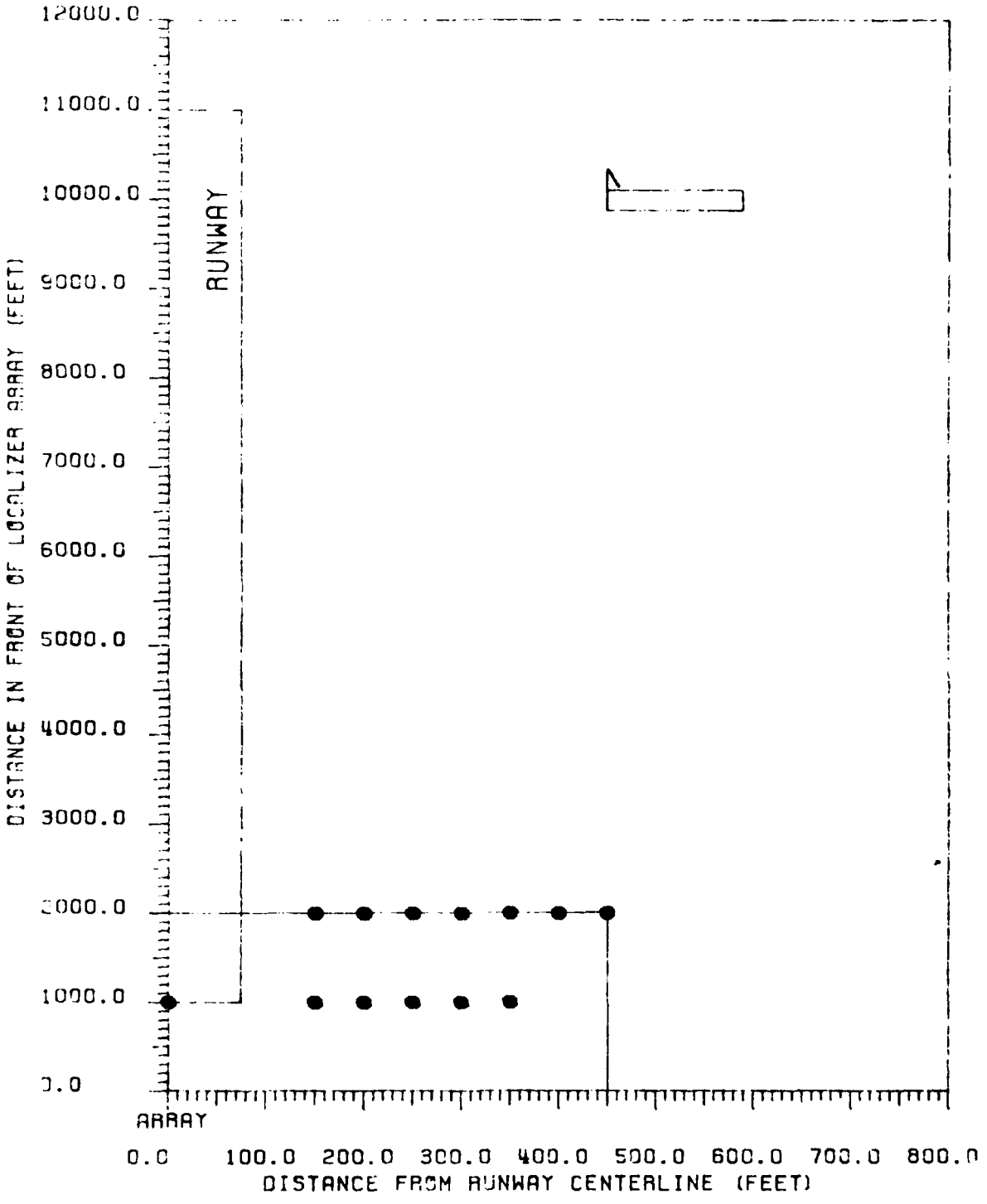

Figure 36 Critical area map for CAT III tolerances relating to B-707 aircraft. B-707 fuselage is perpendicular to runway centerline with tail towards the runway. 8-element single-frequency array, LPD antennas.

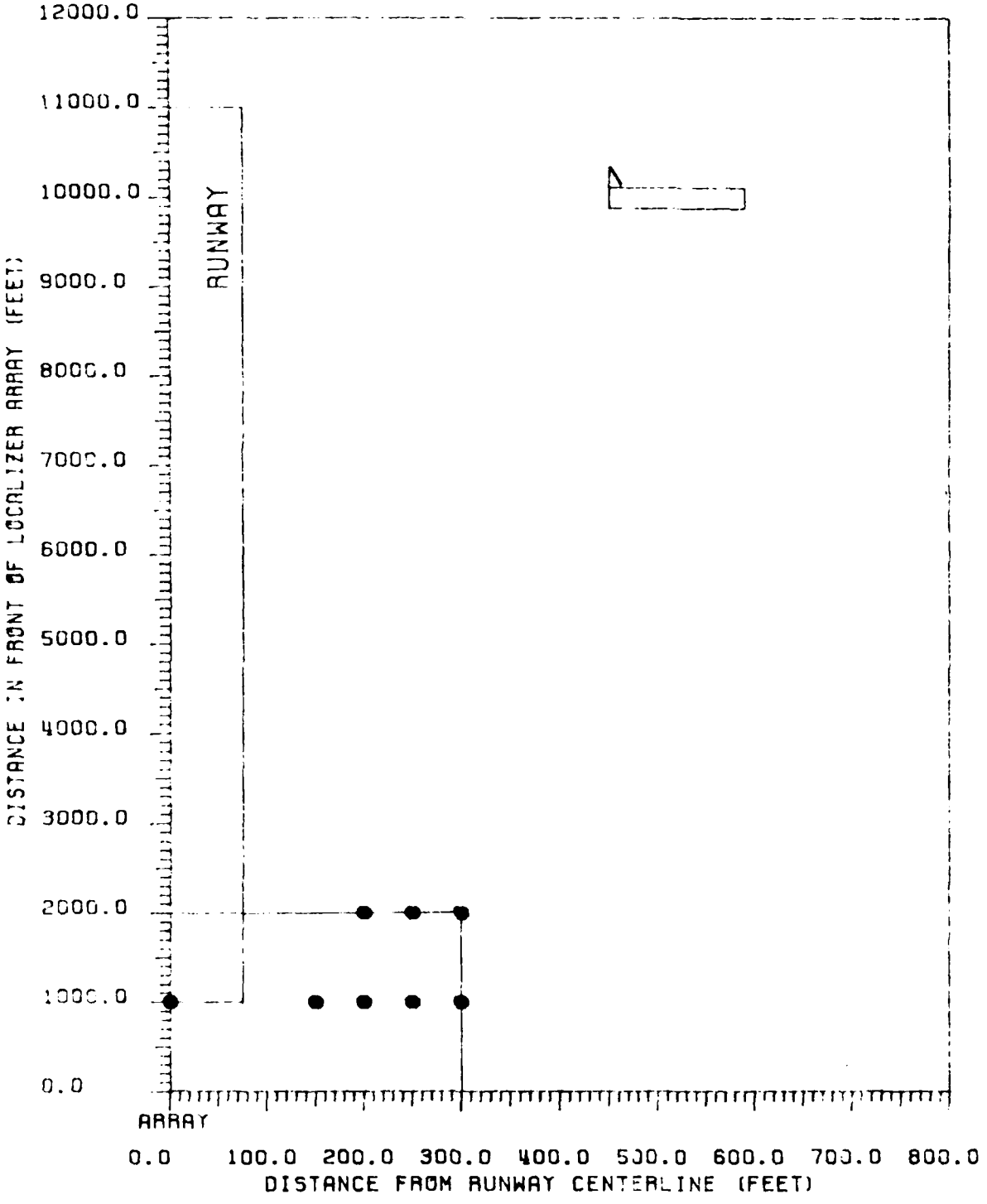

Figure 37 Critical area map for CAT III-X tolerances relating to B-707 aircraft. B-707 fuselage is perpendicular to runway centerline with tail towards the runway. 8-element single-frequency array, LPD antennas.

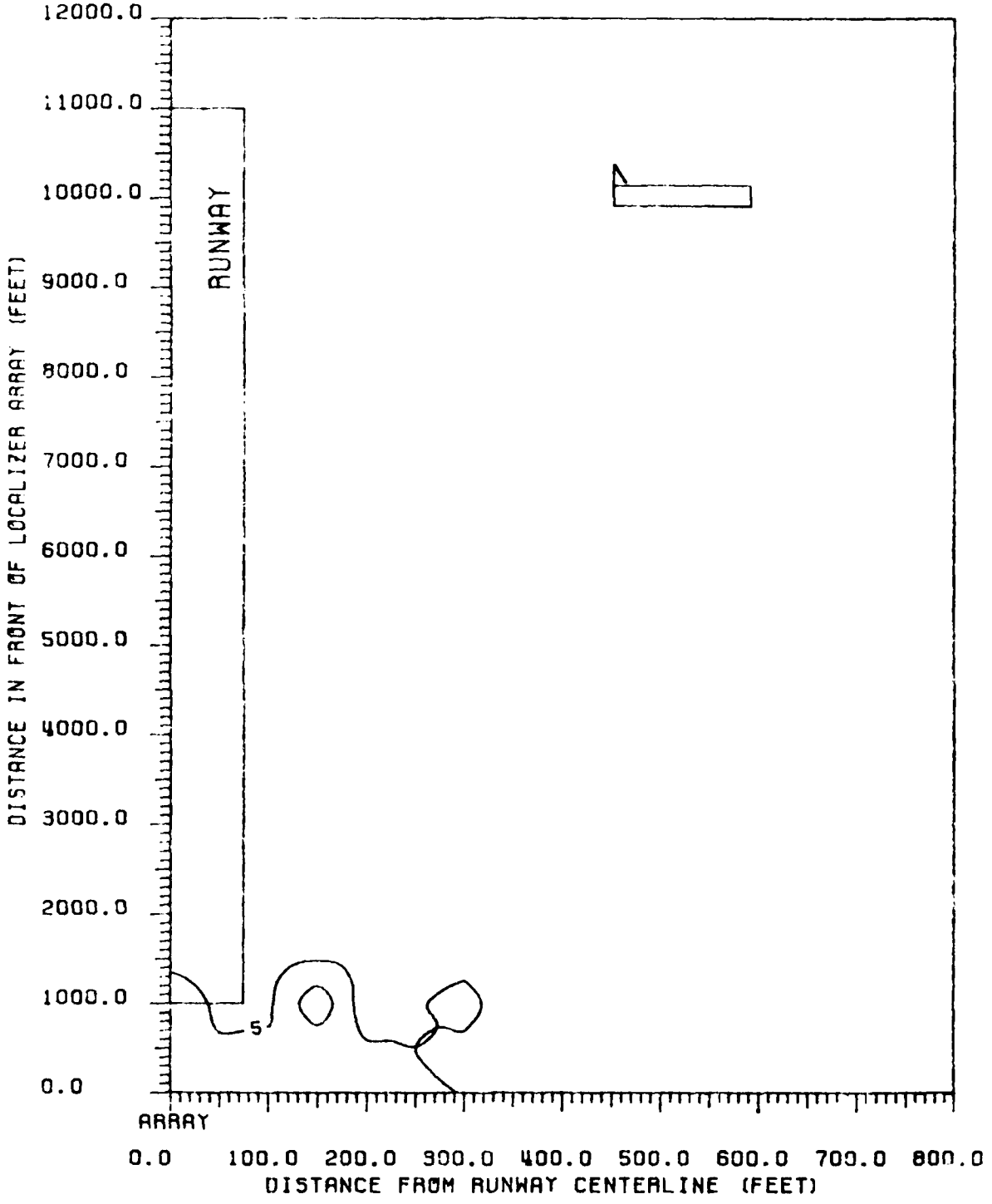

Figure 38. Contours of peak CDI values produced in ILS Zone 1 for a B-707. B-707 fuselage is perpendicular to runway centerline, with tail towards the runway. 8-element single-frequency array, LPD antennas.

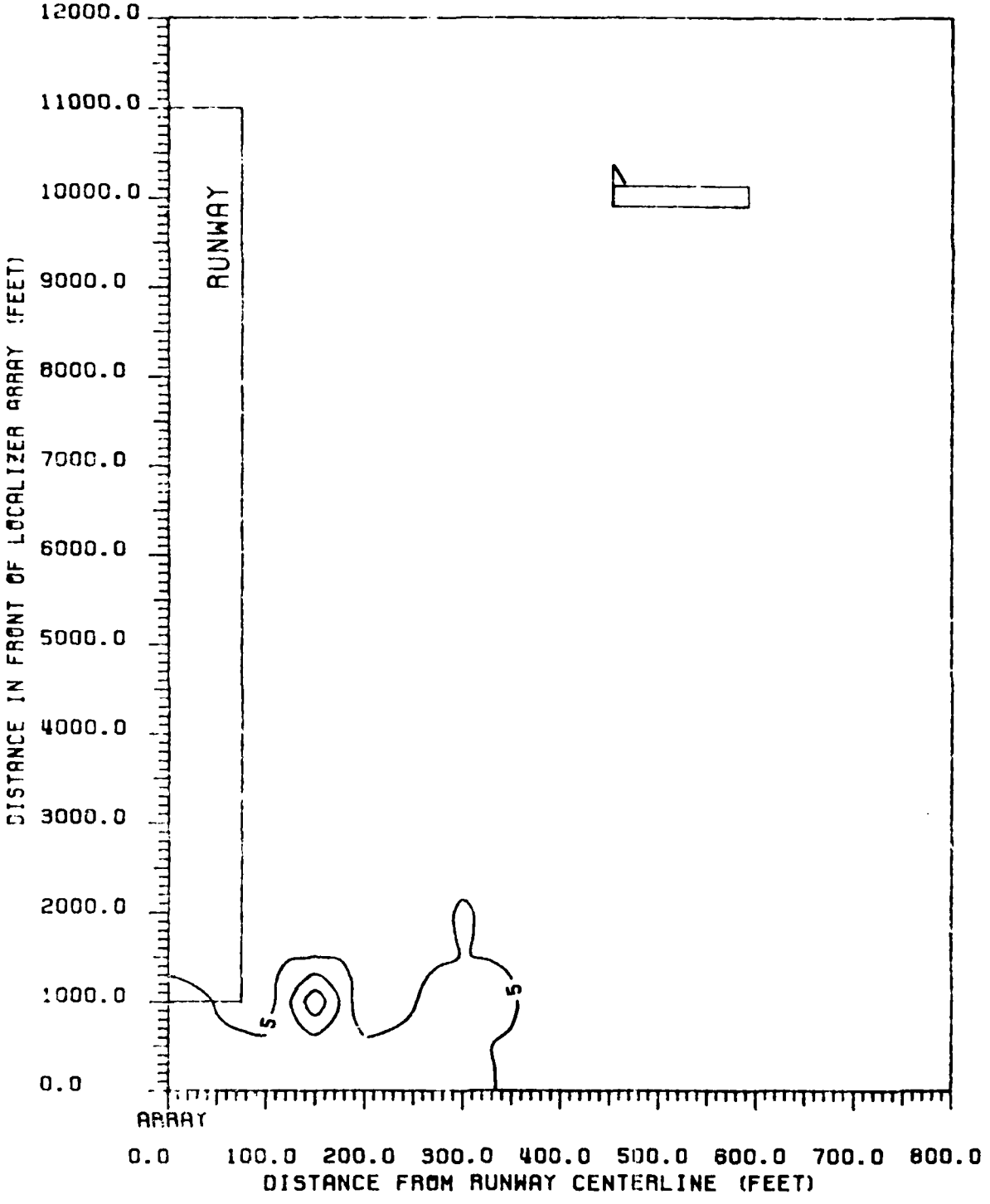

Figure 39 Contours of peak CDI values produced in ILS Zone 2 for a B-707. B-707 fuselage is perpendicular to runway centerline, with tail towards the runway. 8-element single-frequency array, LPD antennas.

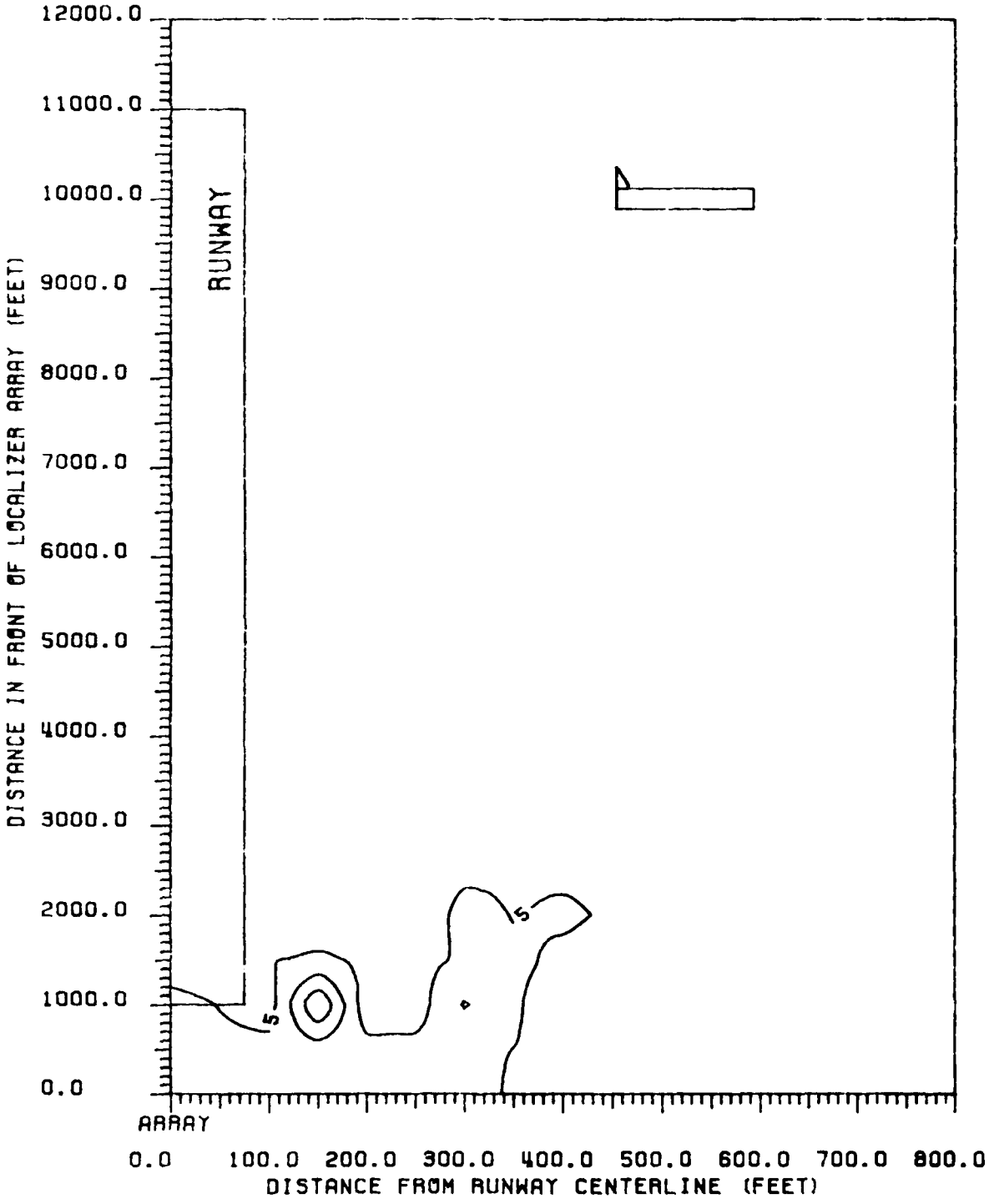

Figure 40 Contours of peak CDI values produced in ILS Zone 3 to Threshold for a B-707. B-707 fuselage is perpendicular to runway centerline, with tail towards the runway. 8-element single-frequency array, LPD antennas.

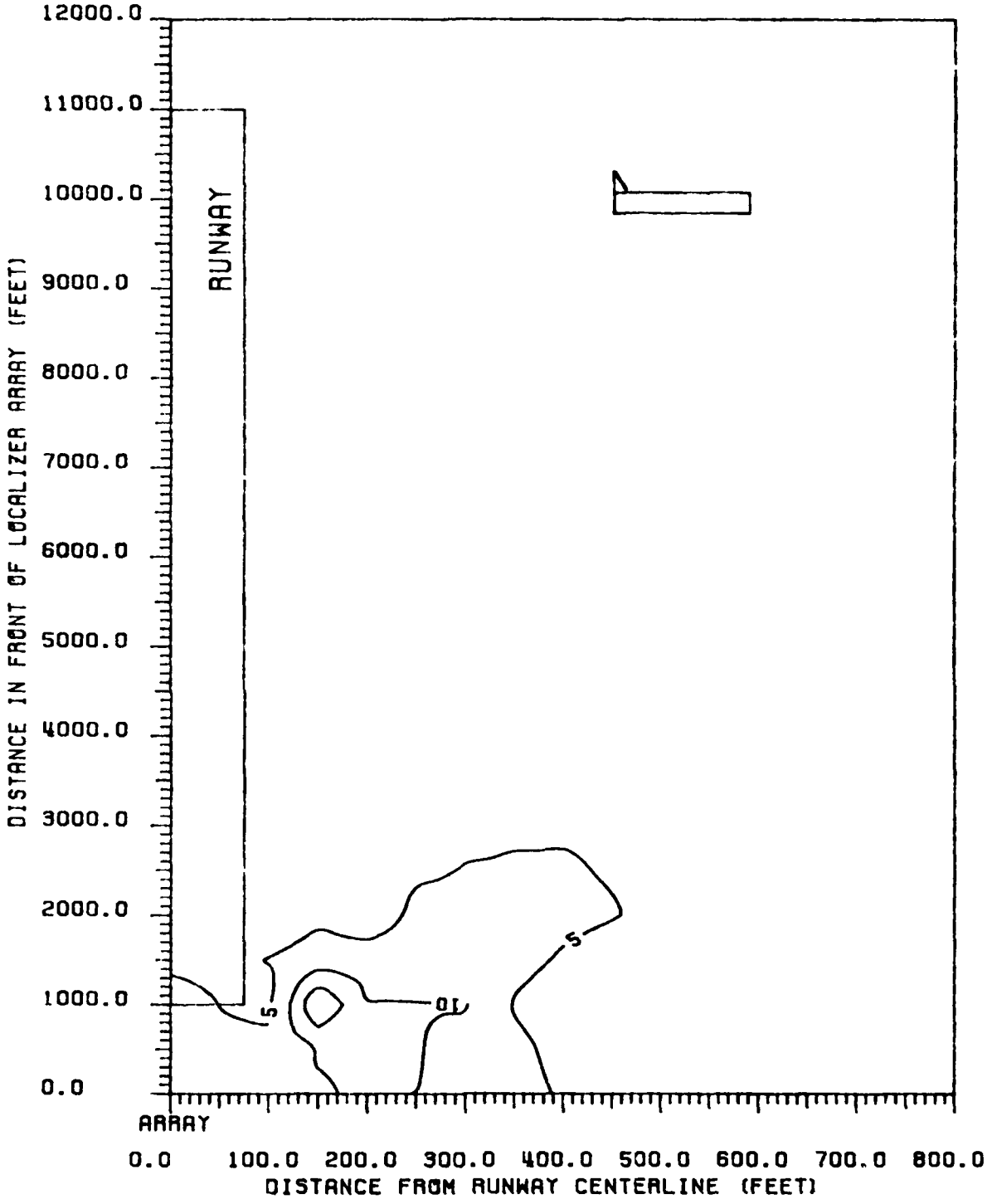

Figure 41 Contours of peak CDI values produced in ILS Zone 4 for a B-707. B-707 fuselage is perpendicular to runway centerline, with tail towards the runway. 8-element single-frequency array, LPD antennas.

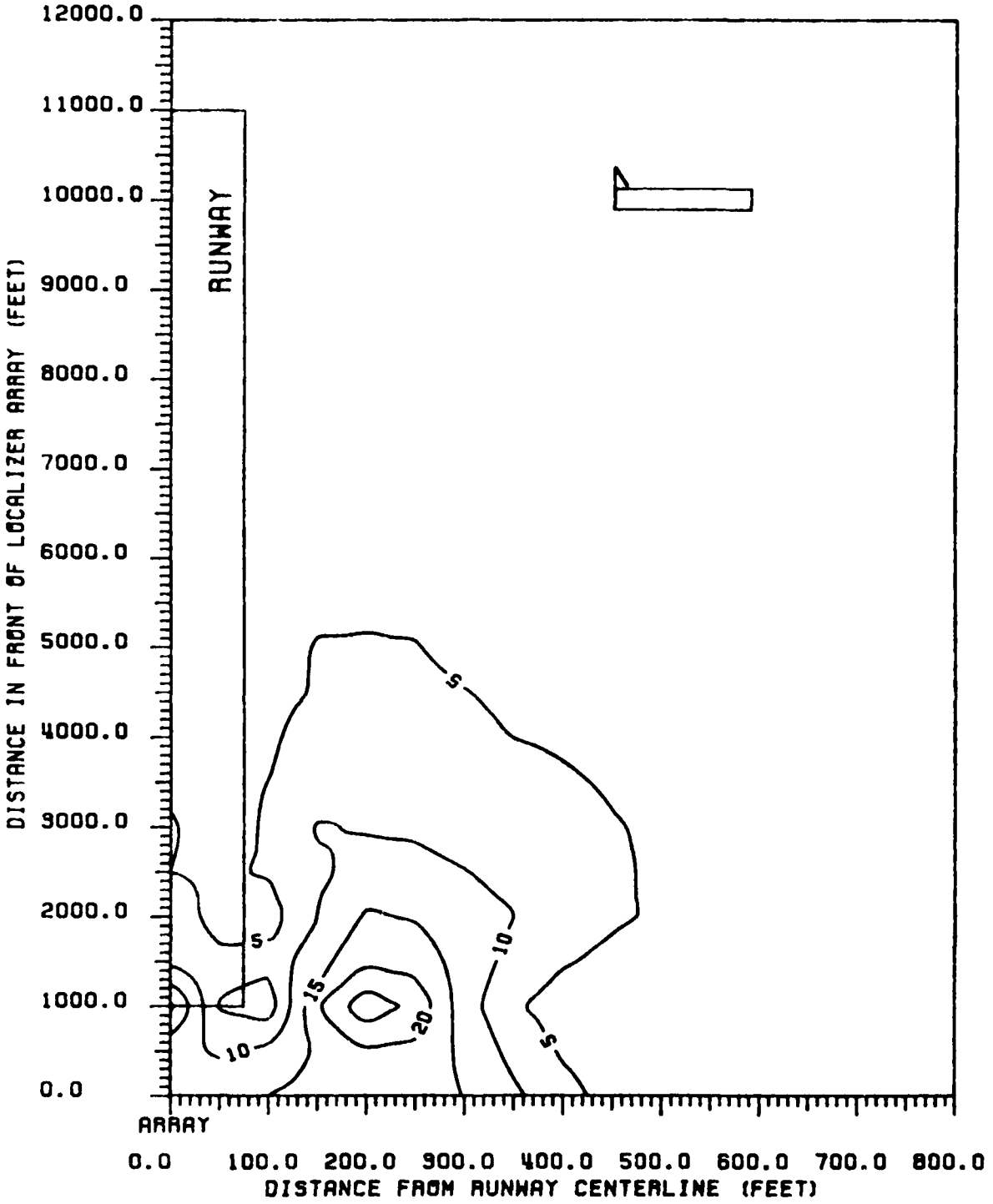

Figure 42 Contours of peak CDI values produced in ILS Zone 5 for a B-707. B-707 fuselage is perpendicular to runway centerline, with tail towards the runway. 8-element single-frequency array, LPD antennas.

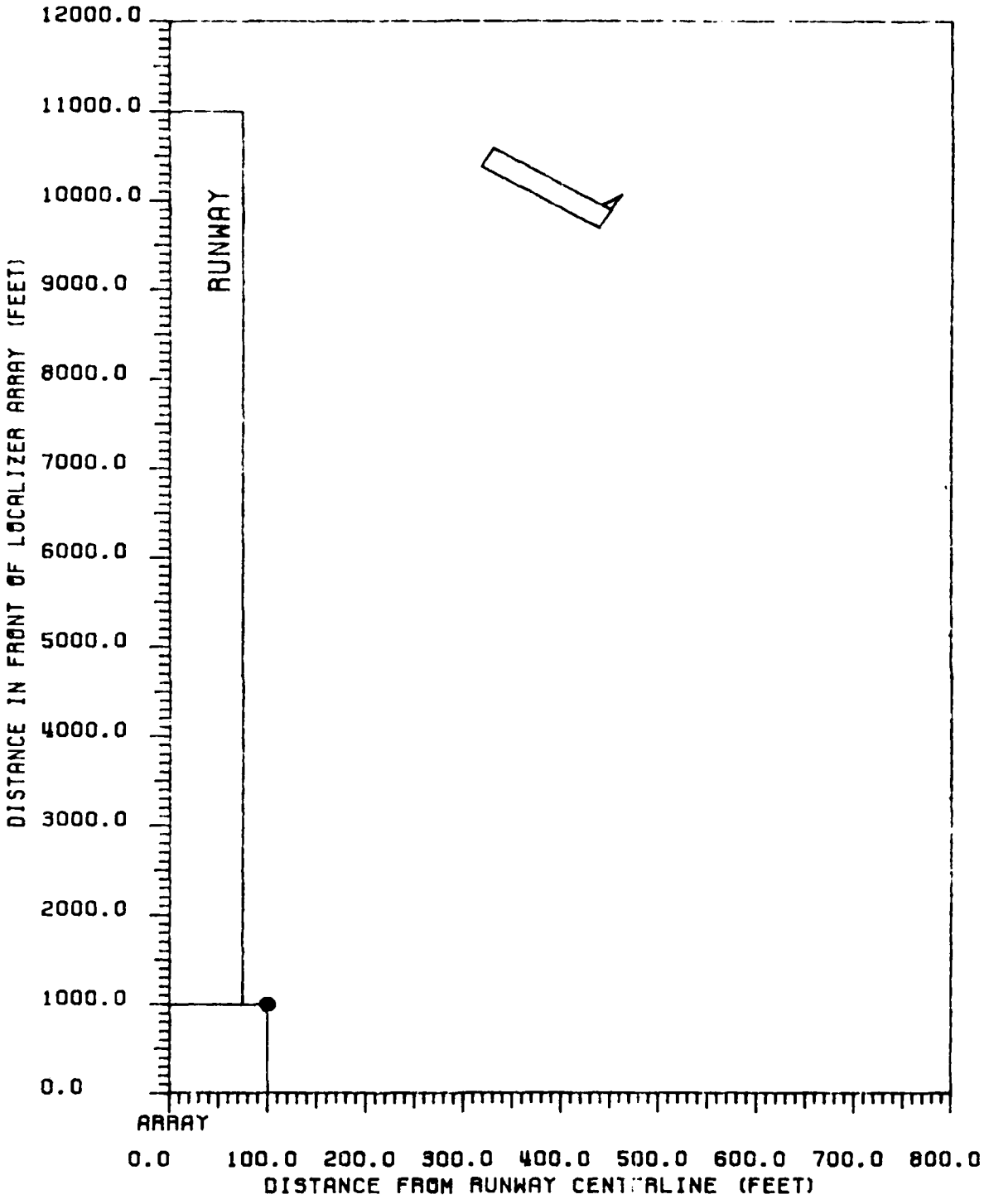

Figure 43 Critical area for CAT I tolerances relating to B-707 aircraft. B-707 fuselage is oriented 60 degrees to runway centerline, with tail towards the array. 8-element single-frequency array, LPD antennas.

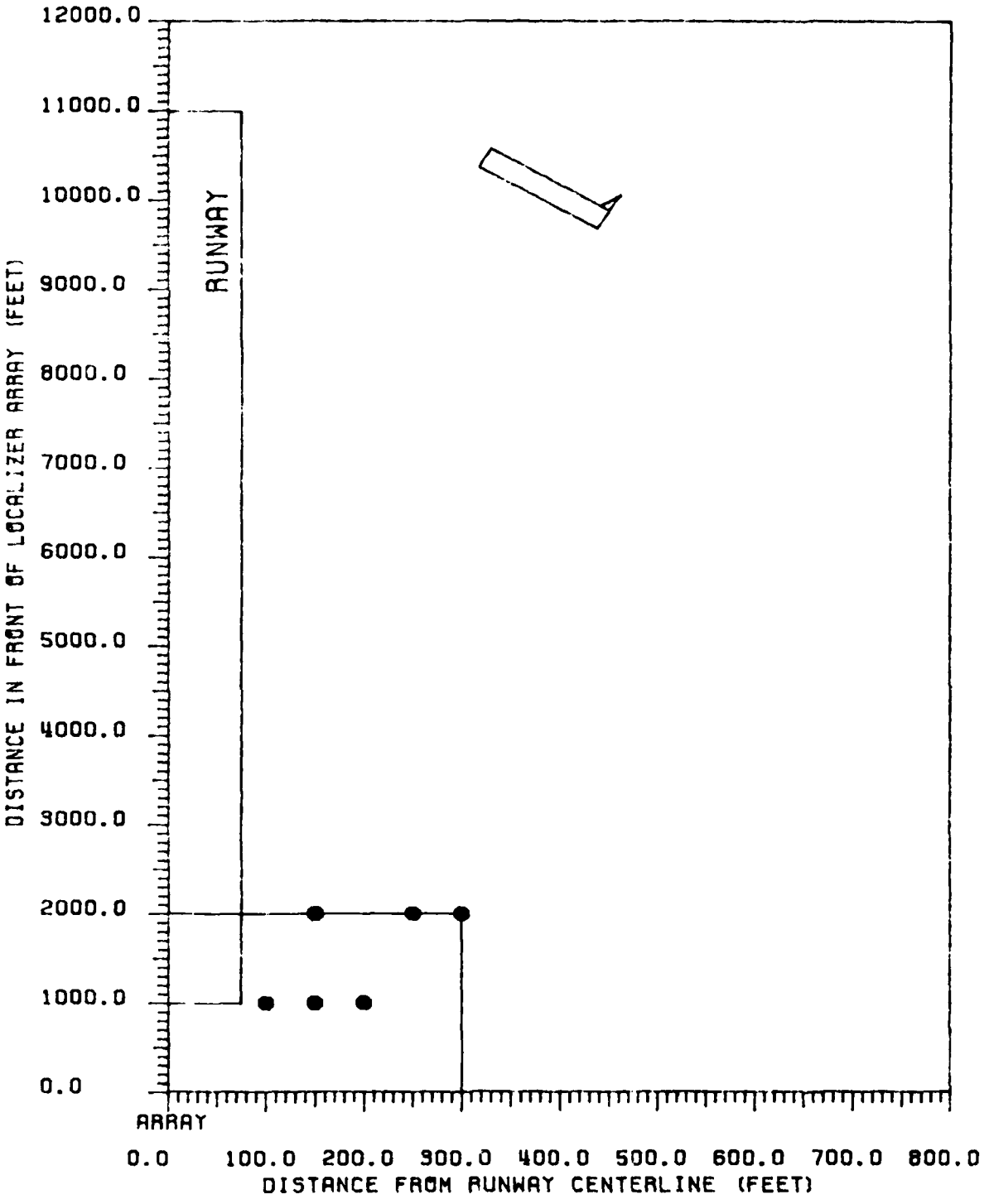

Figure 44 Critical area for CAT II tolerances relating to B-707 aircraft. B-707 fuselage is oriented 60 degrees to runway centerline, with tail towards the array. 8-element single-frequency array, LPD antennas.

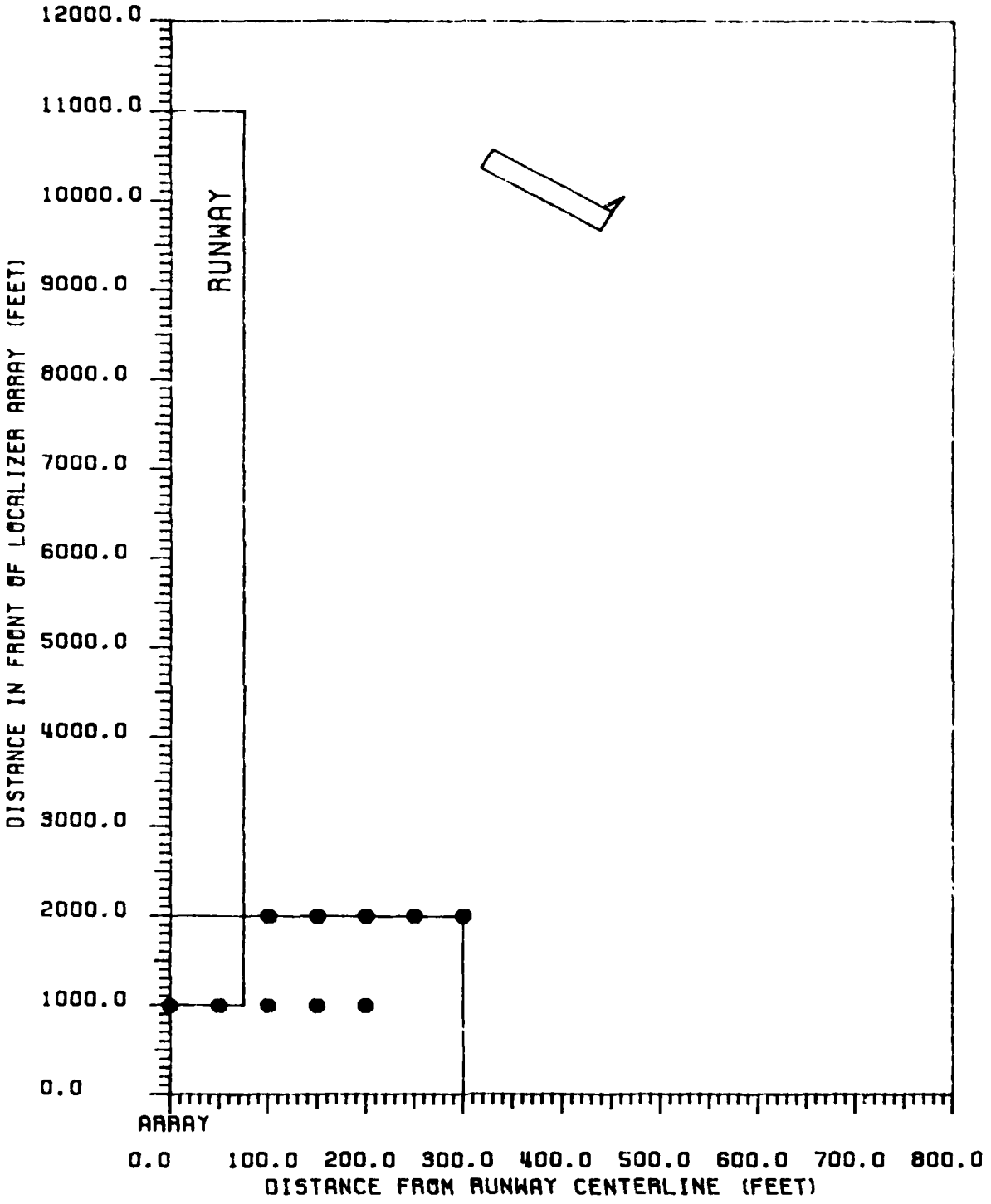

Figure 45 Critical area for CAT III tolerances relating to B-707 aircraft. B-707 fuselage is oriented 60 degrees to runway centerline, with tail towards the array. 8-element single-frequency array, LPD antennas.

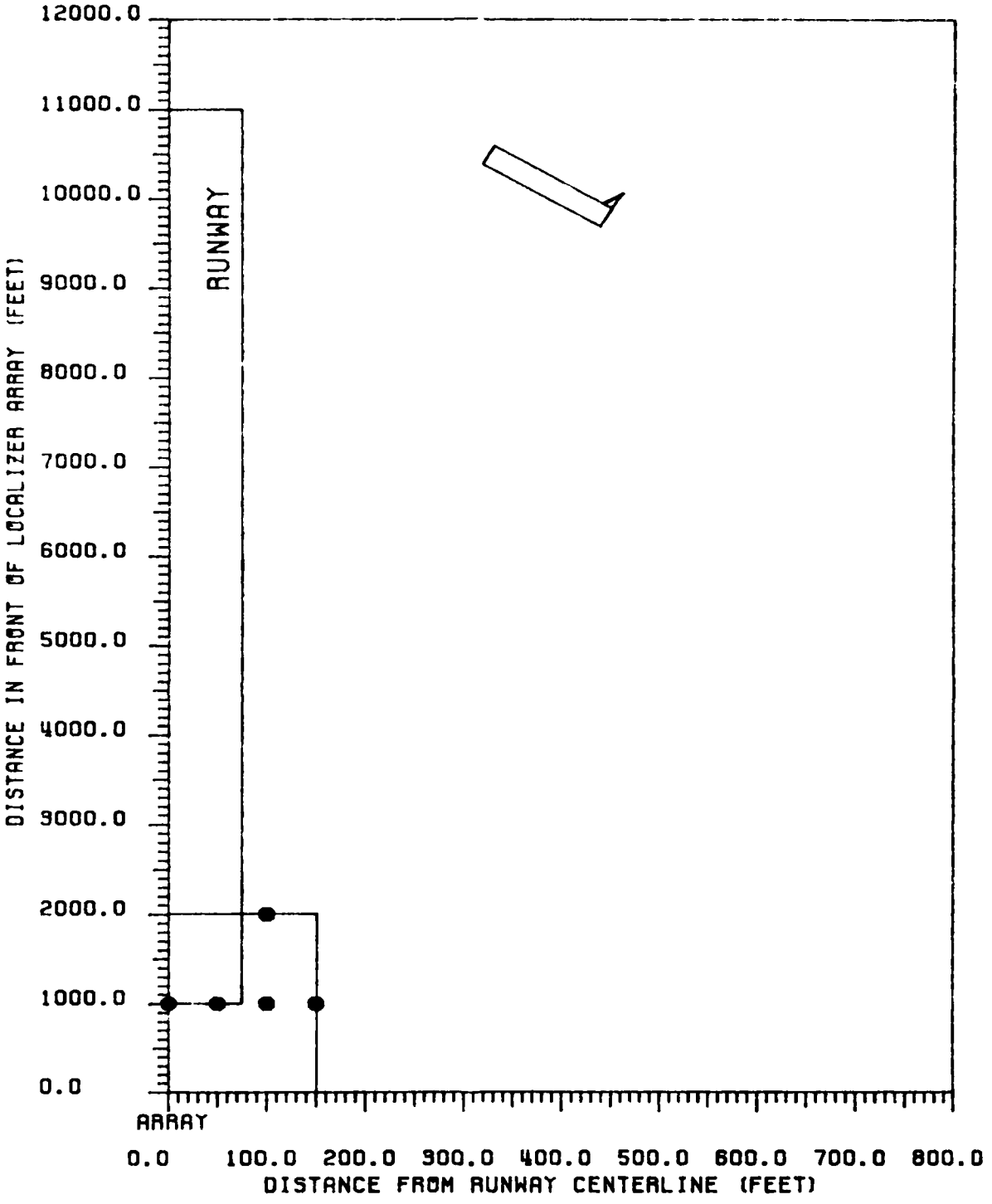

Figure 46 Critical area for CAT III-X tolerances relating to B-707 aircraft. B-707 fuselage is oriented 60 degrees to runway centerline, with tail towards the array. 8-element single-frequency array, LPD antennas.

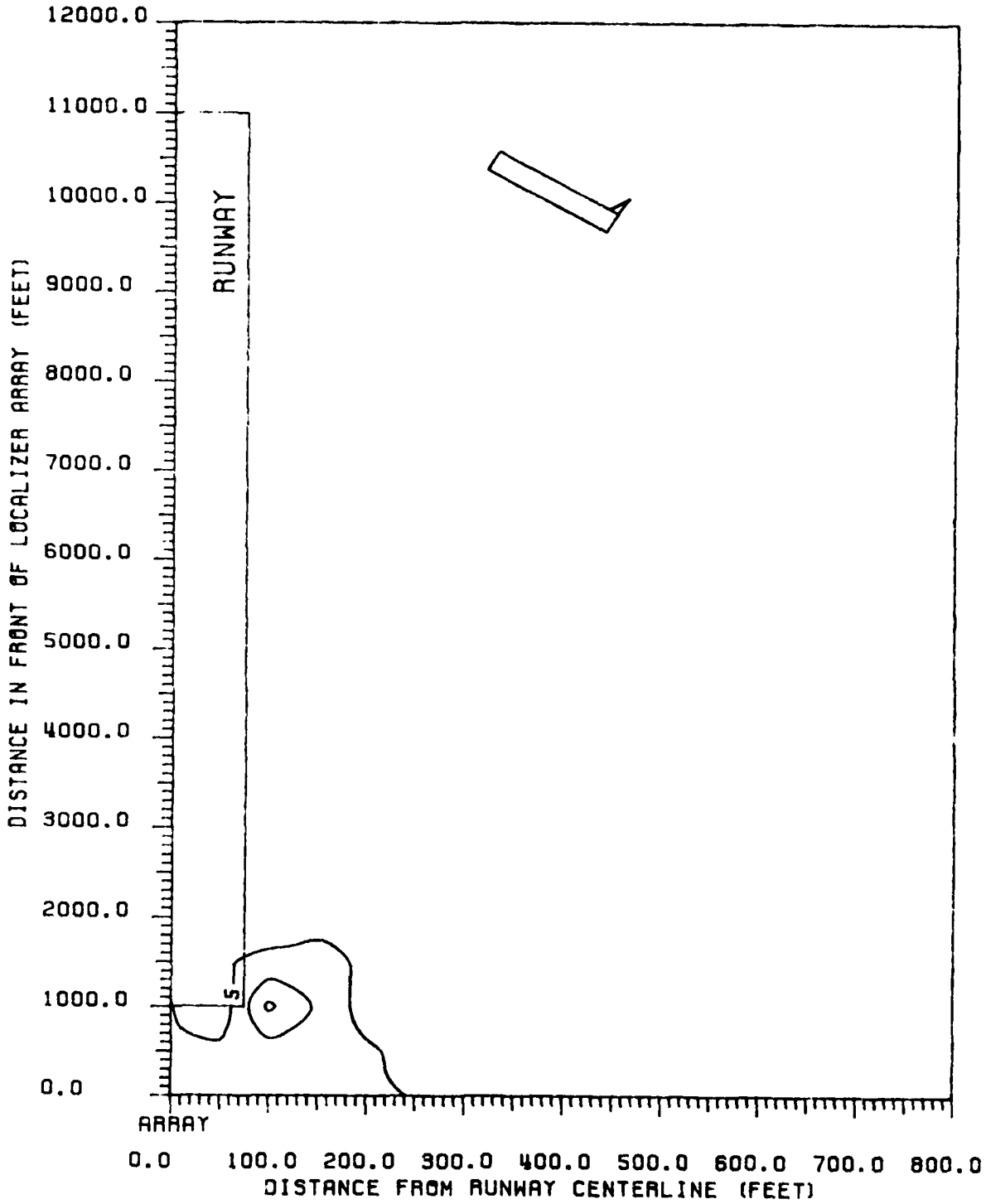

Figure 47 Contours of peak CDI values produced in ILS Zone 1 for a B-707. B-707 fuselage is oriented 60 degrees to runway centerline, with tail towards the array. 8-element single-frequency array, LPD antennas.

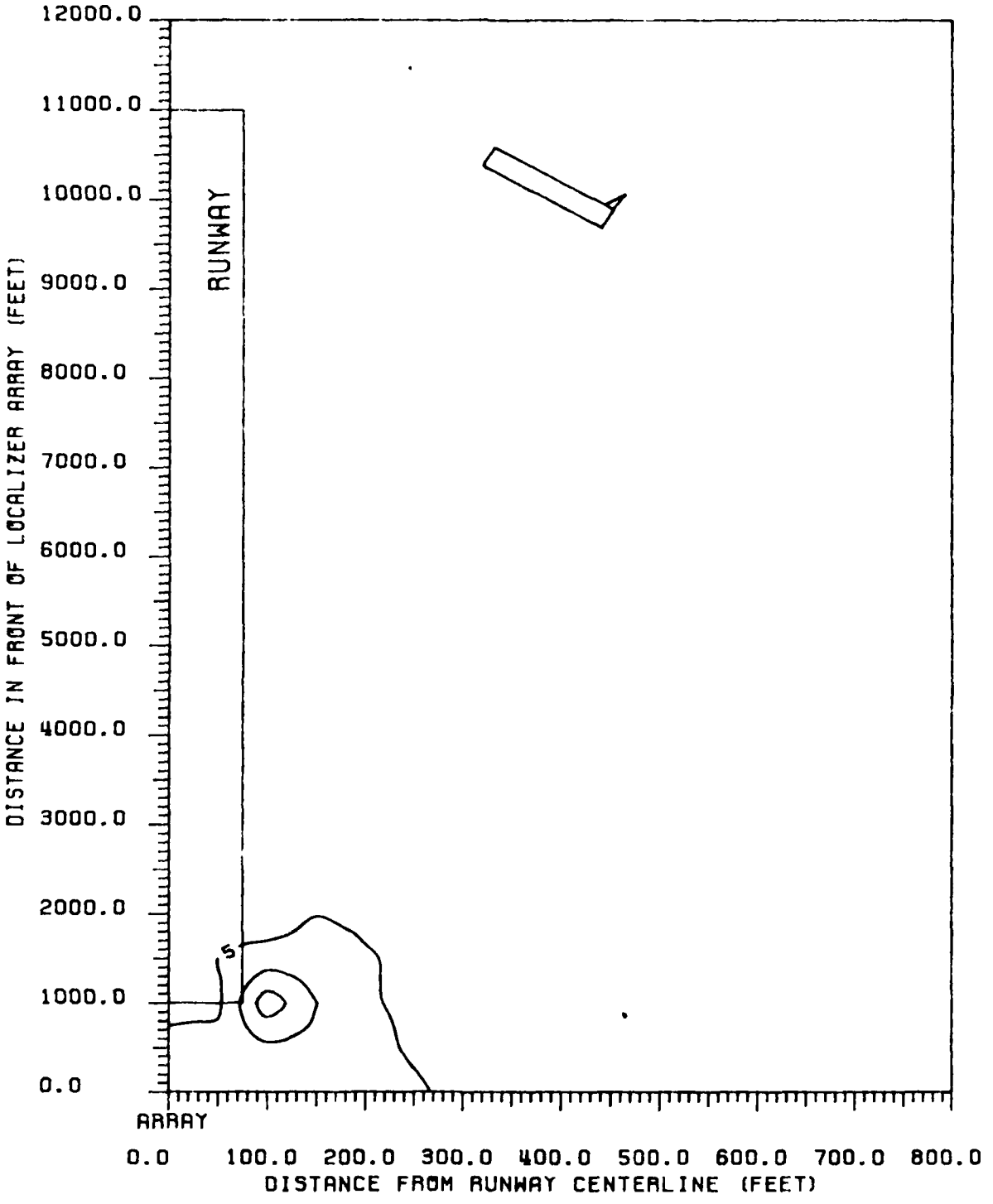

Figure 48 Contours of peak CDI values produced in ILS Zone 2 for a B-707. B-707 fuselage is oriented 60 degrees to runway centerline, with tail towards the array. 8-element single-frequency array, LPD antennas.

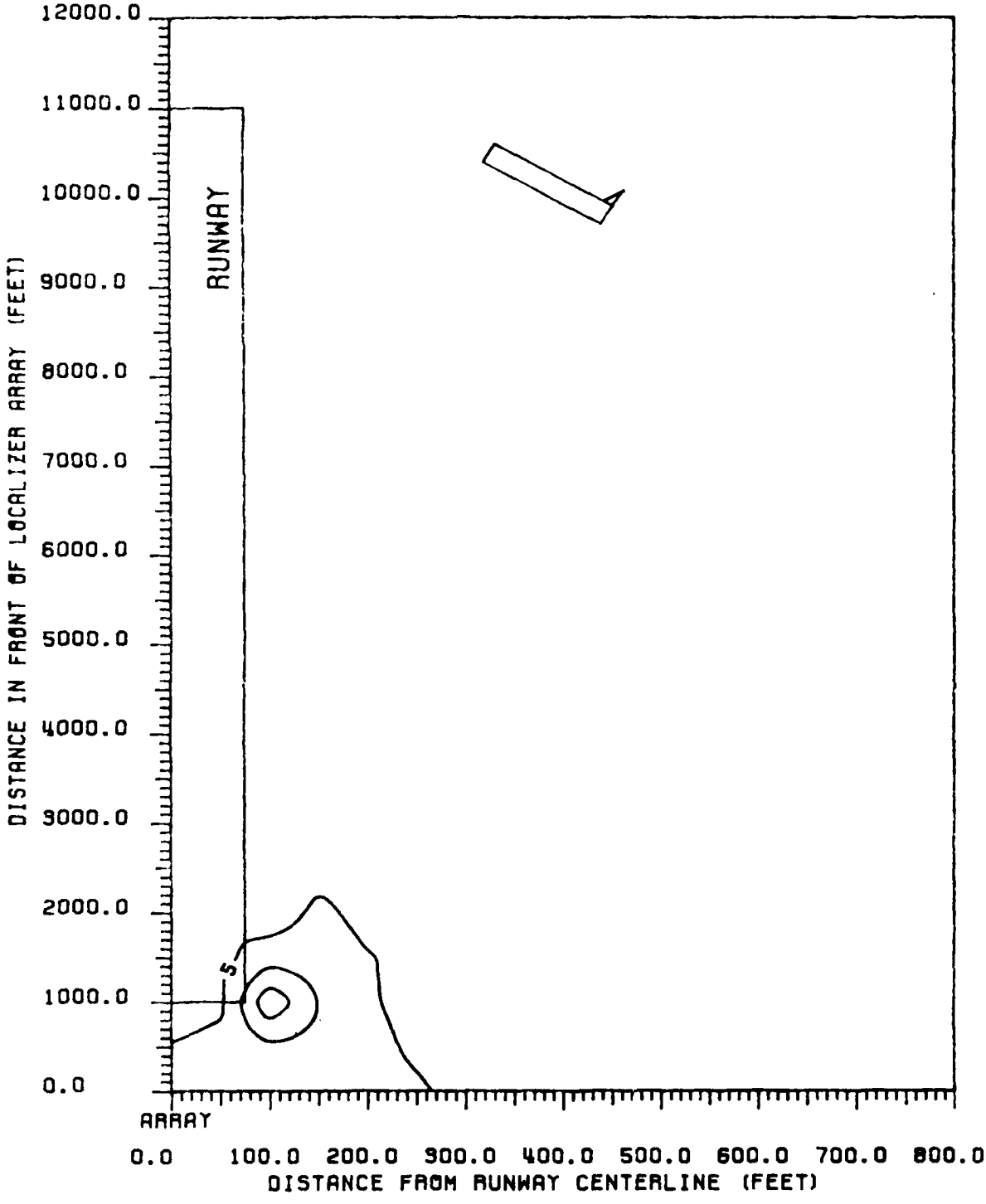

Figure 49 Contours of peak CDI values produced in ILS Zone 3 to Threshold for a B-707. B-707 fuselage is oriented 60 degrees to runway centerline, with tail towards the array. 8-element single-frequency array, LPD antennas.

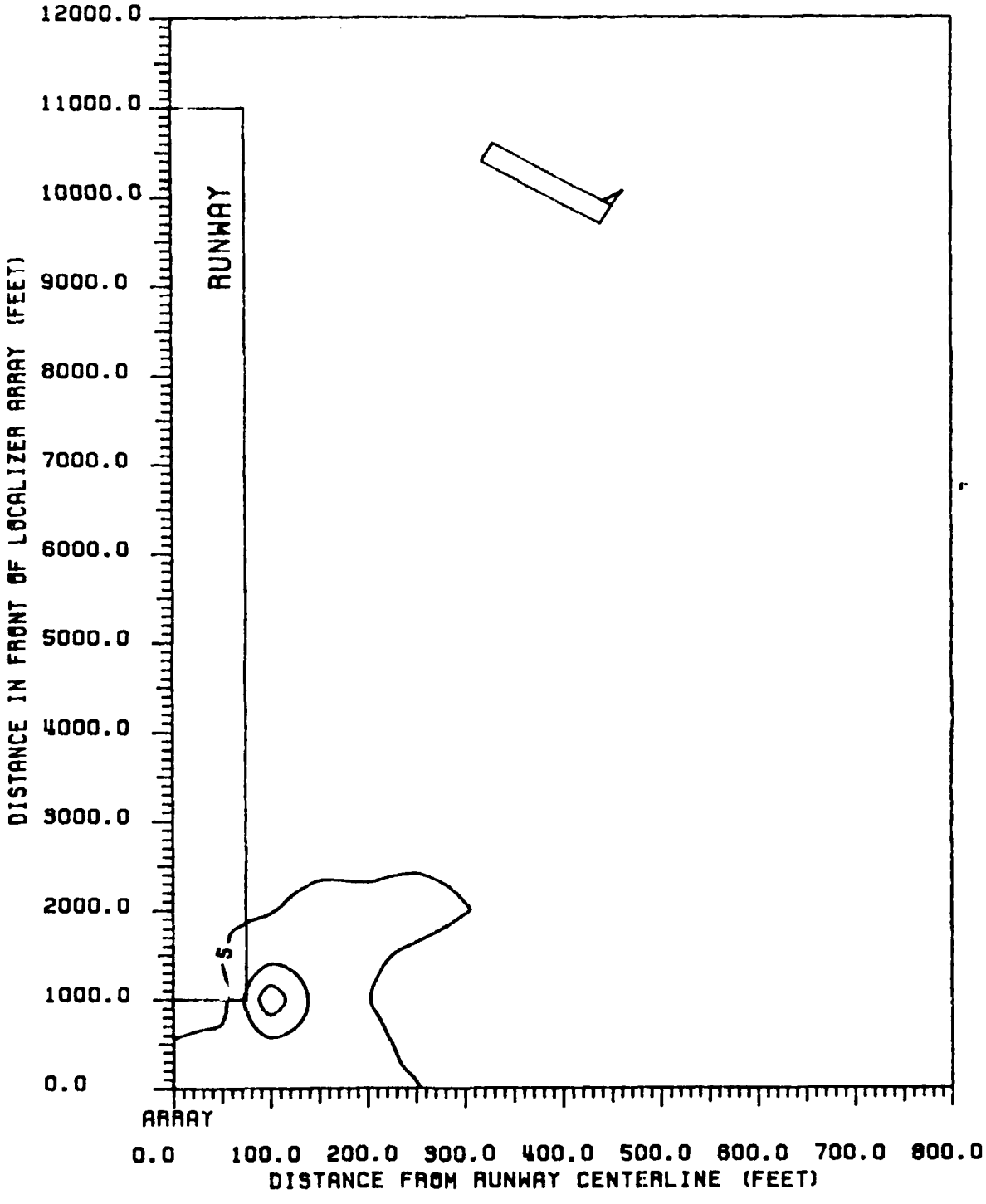

Figure 50 Contours of peak CDI values produced in ILS Zone 4 for a B-707. B-707 fuselage is oriented 60 degrees to runway centerline, with tail towards the array. 8-element single-frequency array, LPD antennas.

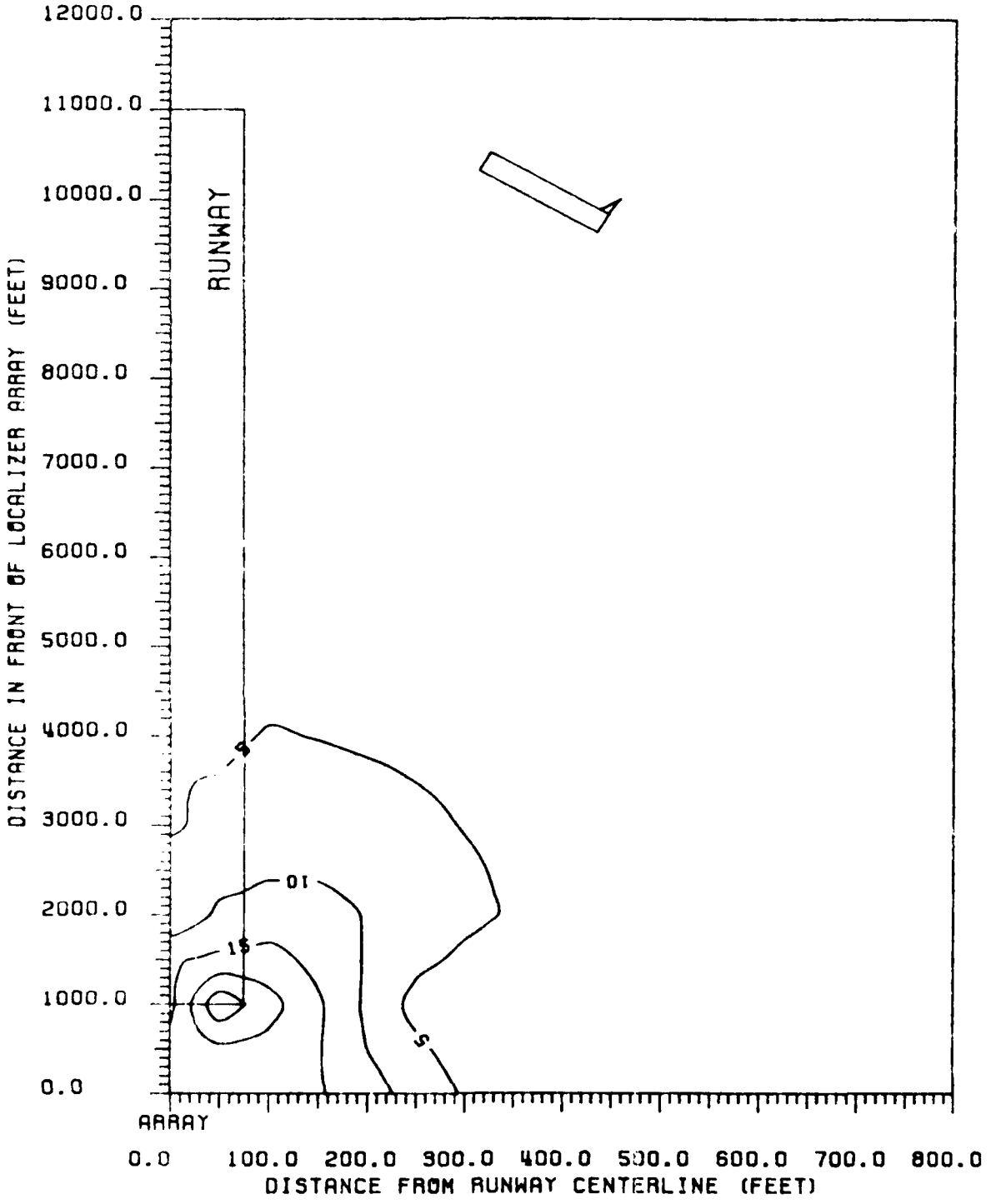

Figure 51. Contours of peak CDI values produced in ILS Zone 5 for a B-707. B-707 fuselage is oriented 60 degrees to runway centerline, with tail towards the array. 8-element single-frequency array, LPD antennas.

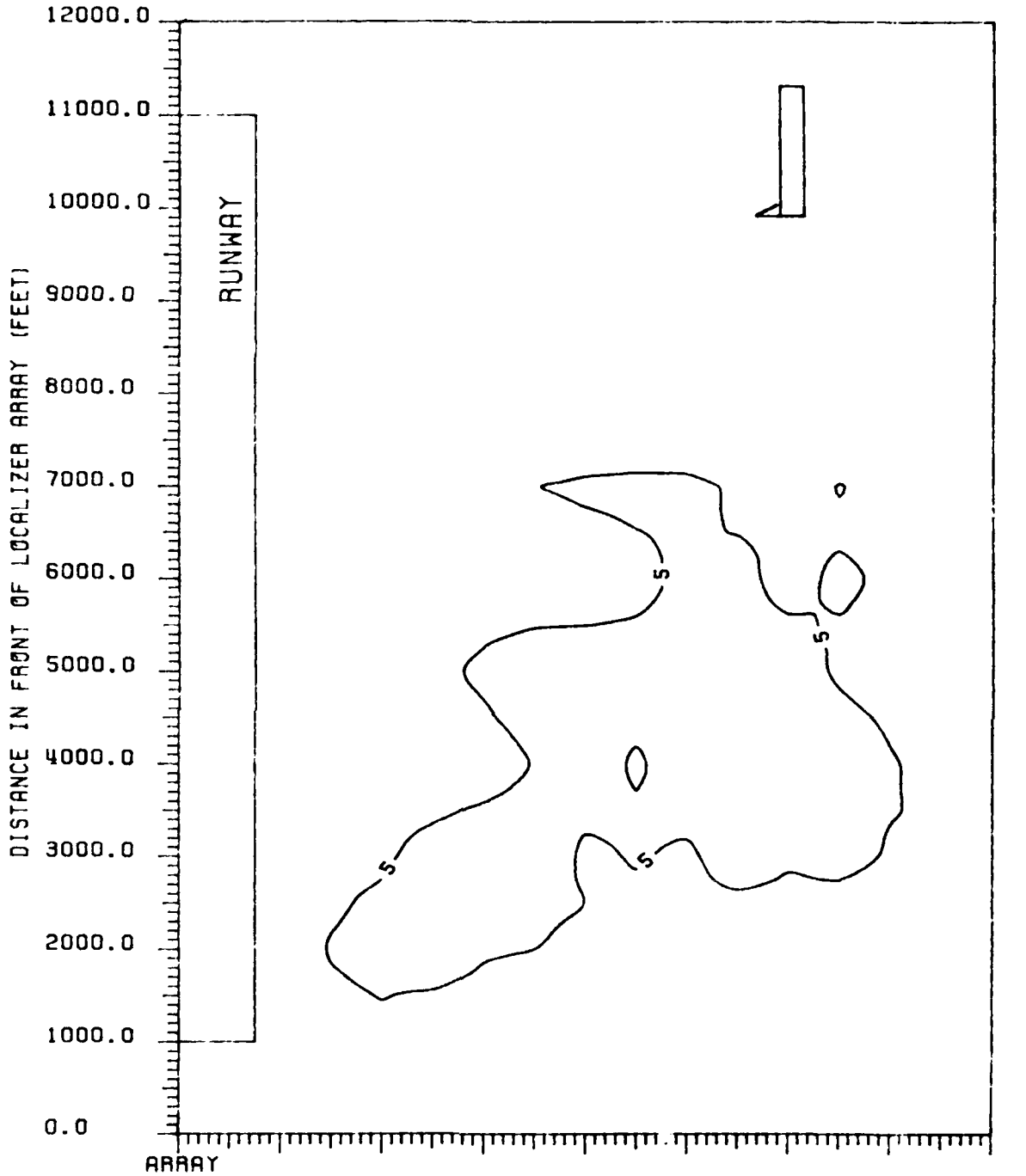

Figure 52 Contours of peak CDI values produced in ILS Zone 5 for a B-707. B-707 fuselage is parallel to runway centerline, with tail towards the array. 8-element single-frequency array, LPD antennas.

AD-A158 844 THEORETICAL INVESTIGATION OF SINGLE-FREQUENCY 8-ELEMENT 2/3
LOCALIZER SIGNAL.. (U) OHIO UNIV ATHENS AVIONICS
ENGINEERING CENTER W D PHIPPS MAY 85 OU/AEC/EER-59-4
UNCLASSIFIED DOT/FAA/PM-85/4 DTFA01-82-C-10050 F/G 17/7 NL

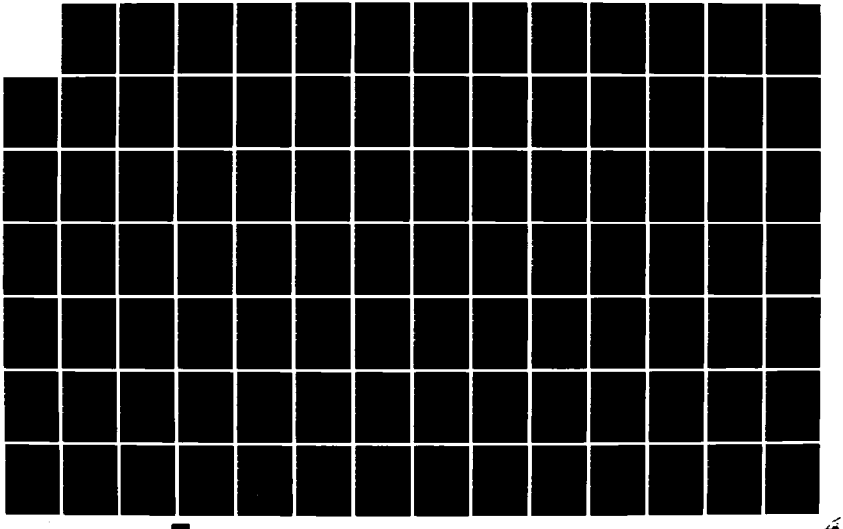

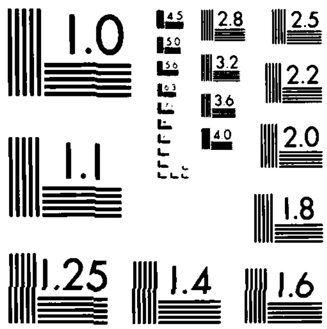

MICROCOPY RESOLUTION TEST CHART
DARDS-1963-A

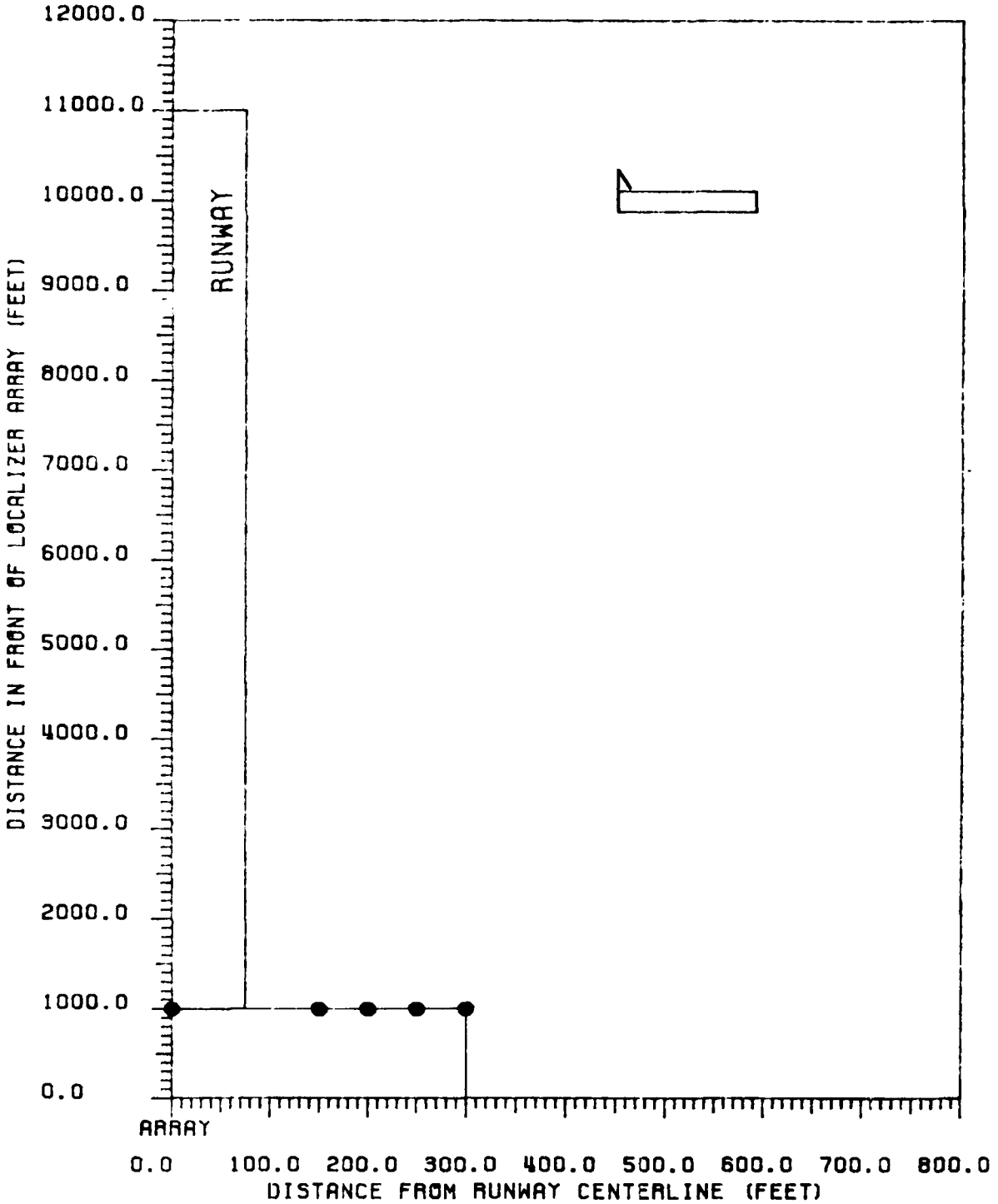

Figure 53 Critical area map for CAT I tolerances relating to L-1011 aircraft. L-1011 fuselage is perpendicular to runway centerline with tail towards the runway. 8-element single-frequency array, LPD antennas.

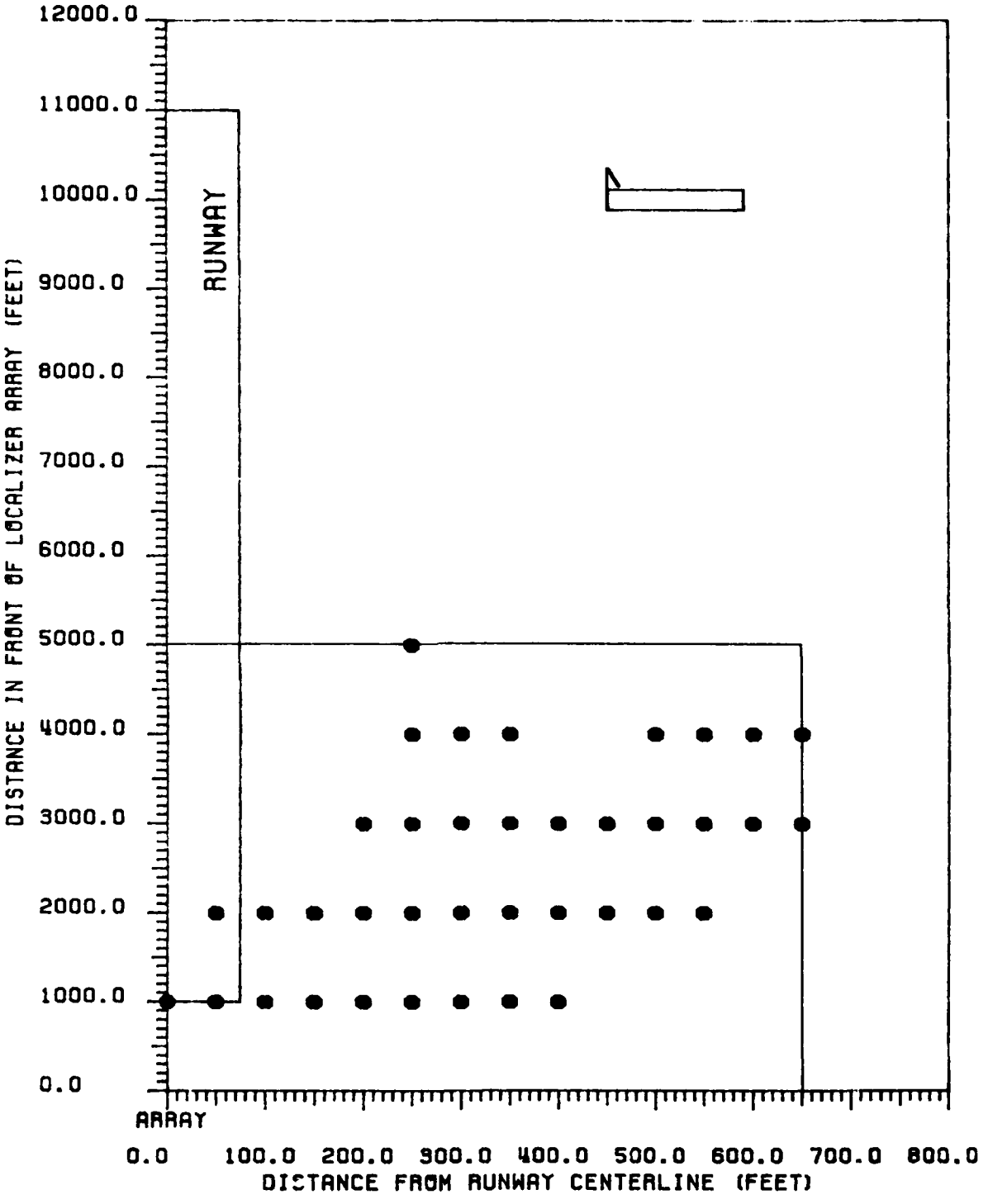

Figure 54 Critical area map for CAT II tolerances relating to L-1011 aircraft. L-1011 fuselage is perpendicular to runway centerline with tail towards the runway. 8-element single-frequency array, LPD antennas.

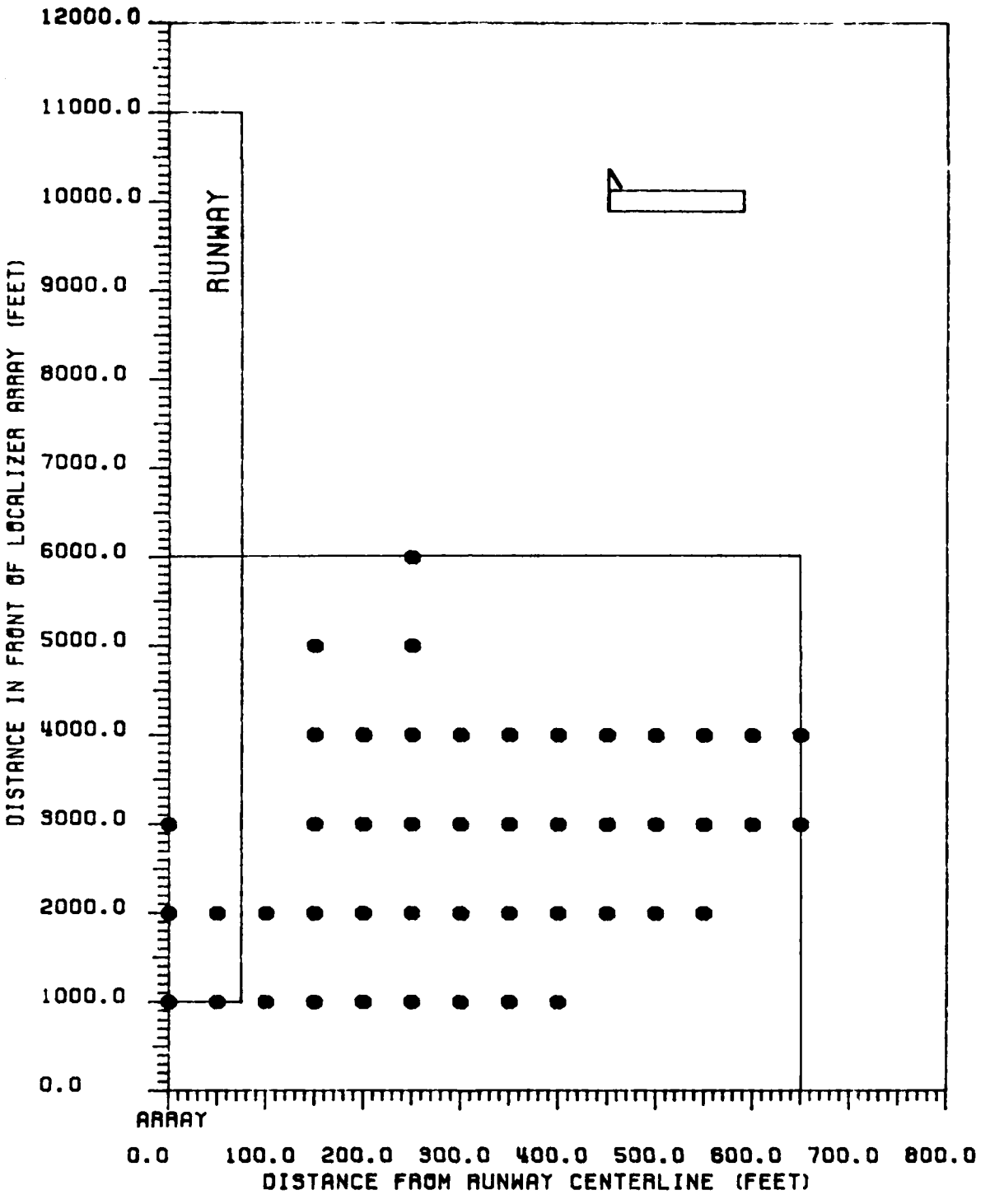

Figure 55 Critical area map for CAT III tolerances relating to L-1011 aircraft. L-1011 fuselage is perpendicular to runway centerline with tail towards the runway. 8-element single-frequency array, LPD antennas.

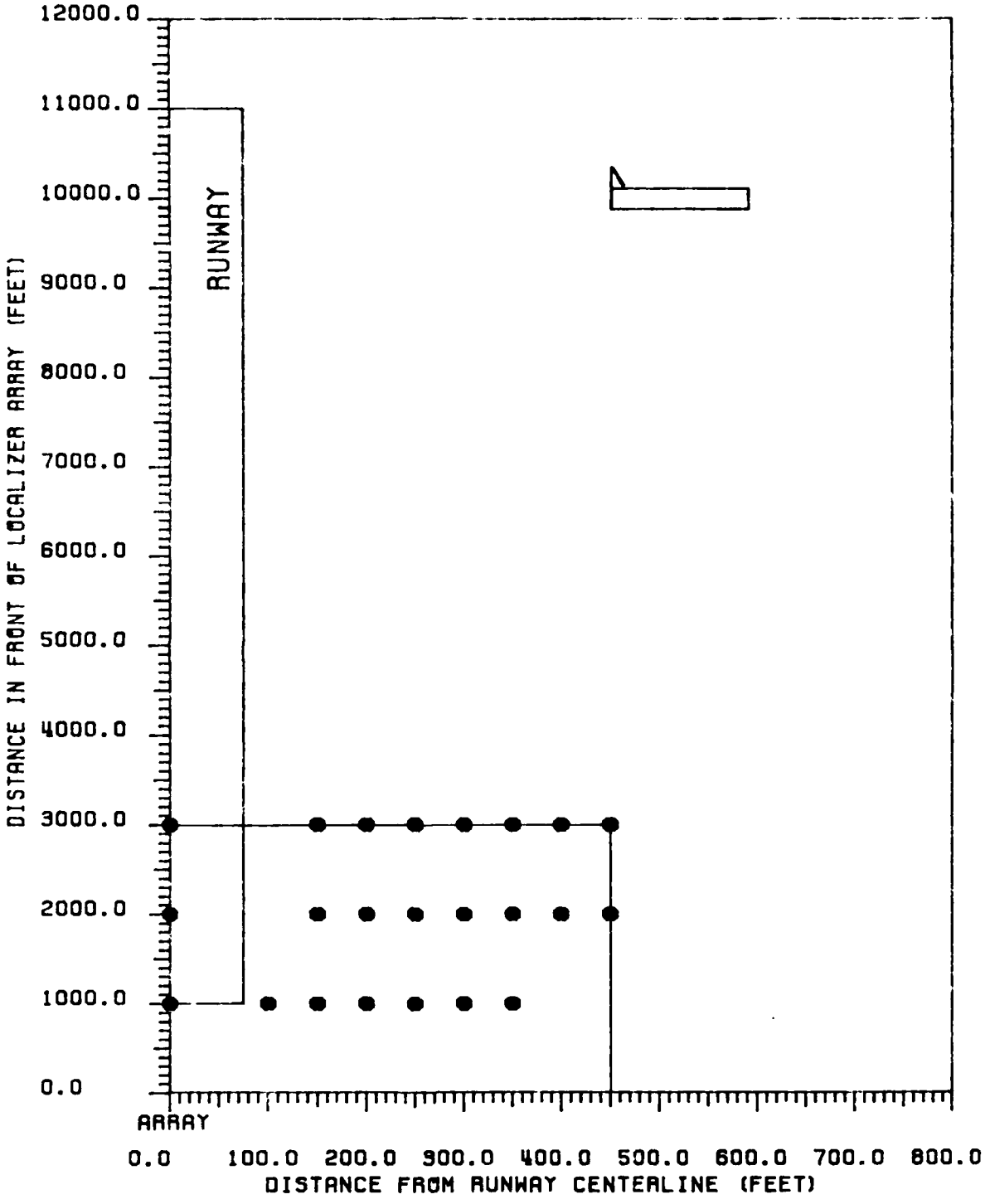

Figure 56 Critical area map for CAT III-X tolerances relating to L-1011 aircraft. L-1011 fuselage is perpendicular to runway centerline with tail towards the runway. 8-element single-frequency array, LPD antennas.

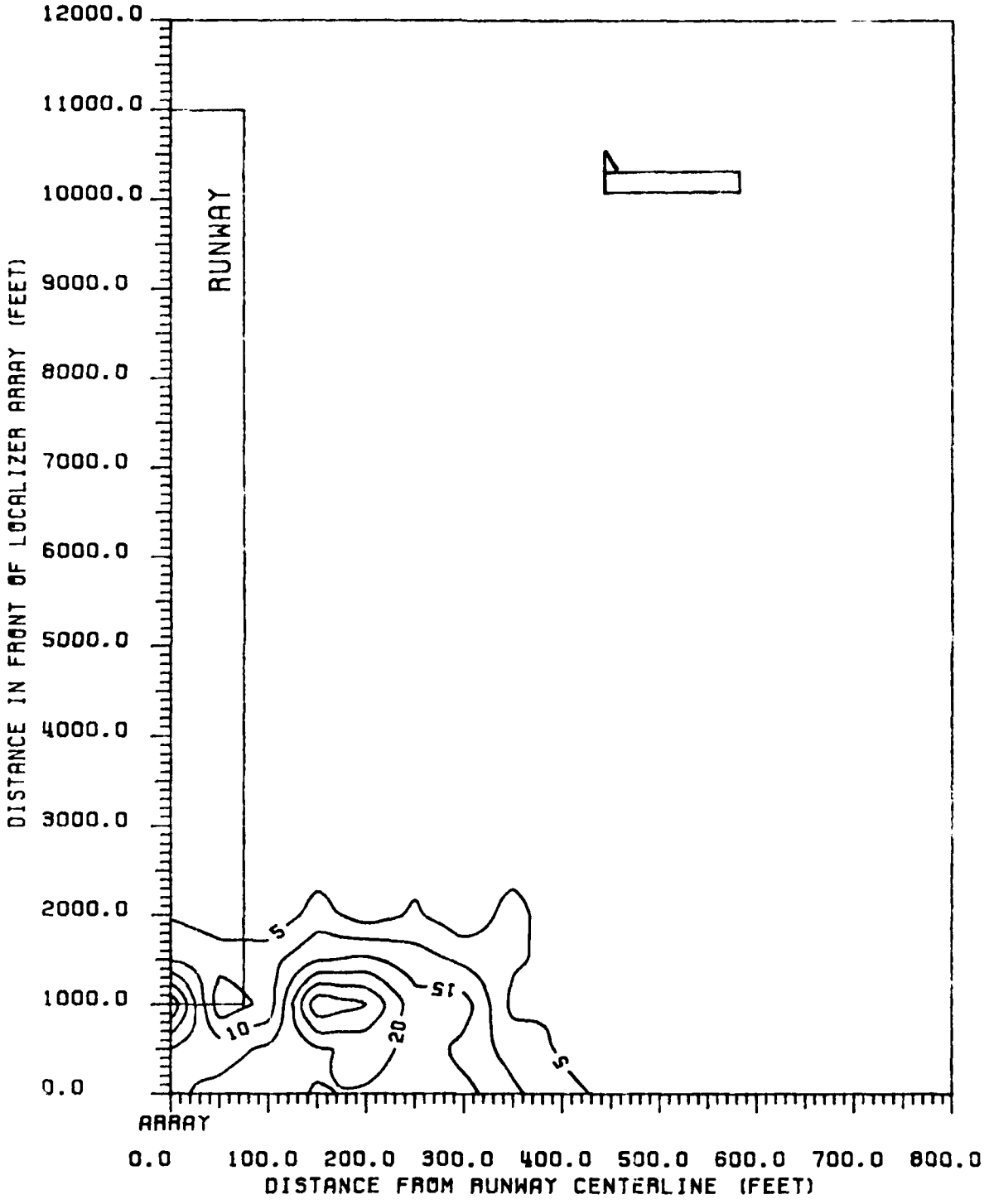

Figure 57 Contours of peak CDI values produced in ILS Zone 1 for a L-1011. L-1011 fuselage is perpendicular to runway centerline, with tail towards the runway. 8-element single-frequency array, LPD antennas.

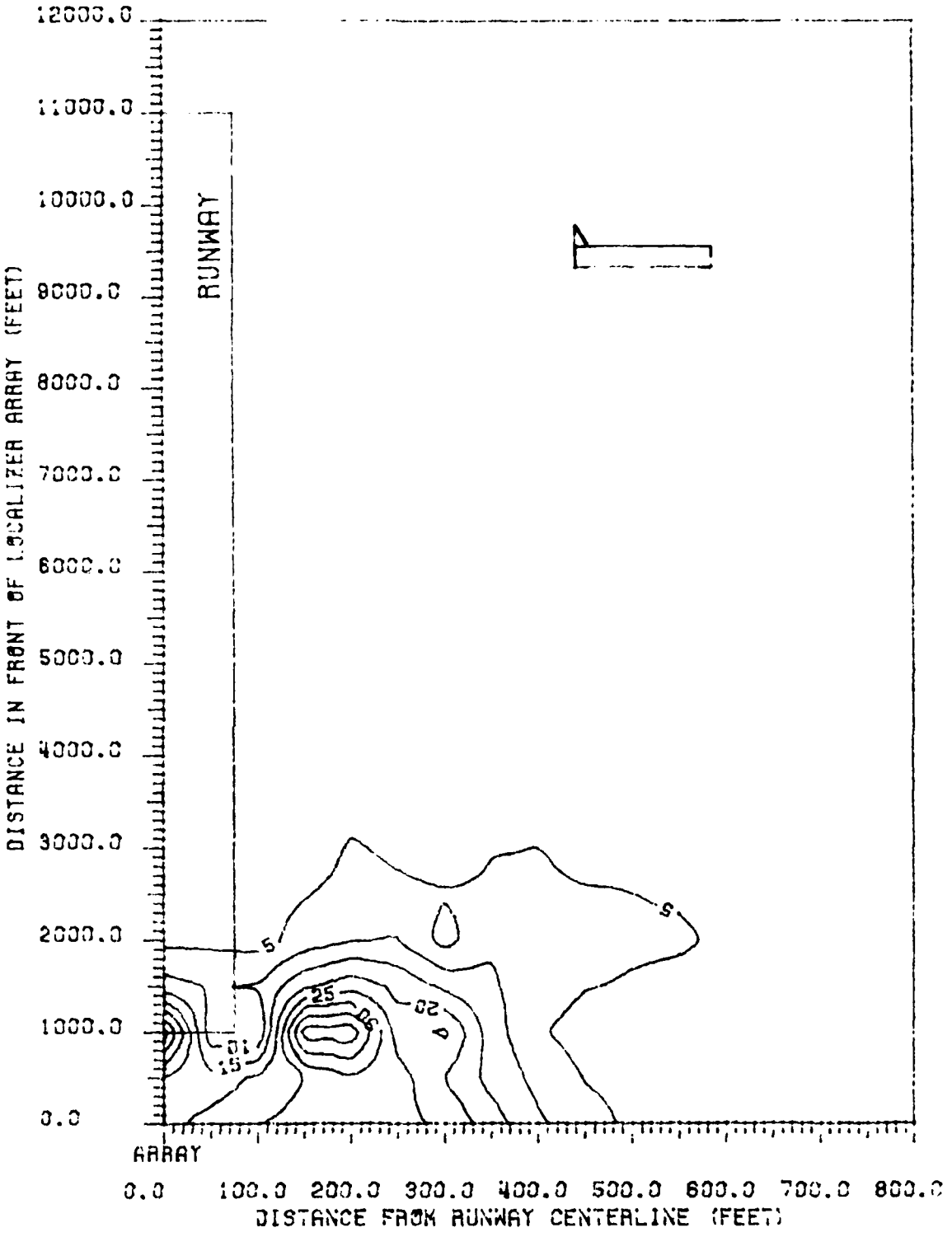

Figure 58 Contours of peak CDI values produced in ILS Zone 2 for a L-1011. L-1011 fuselage is perpendicular to runway centerline, with tail towards the runway. 8-element single-frequency array, LPD antennas.

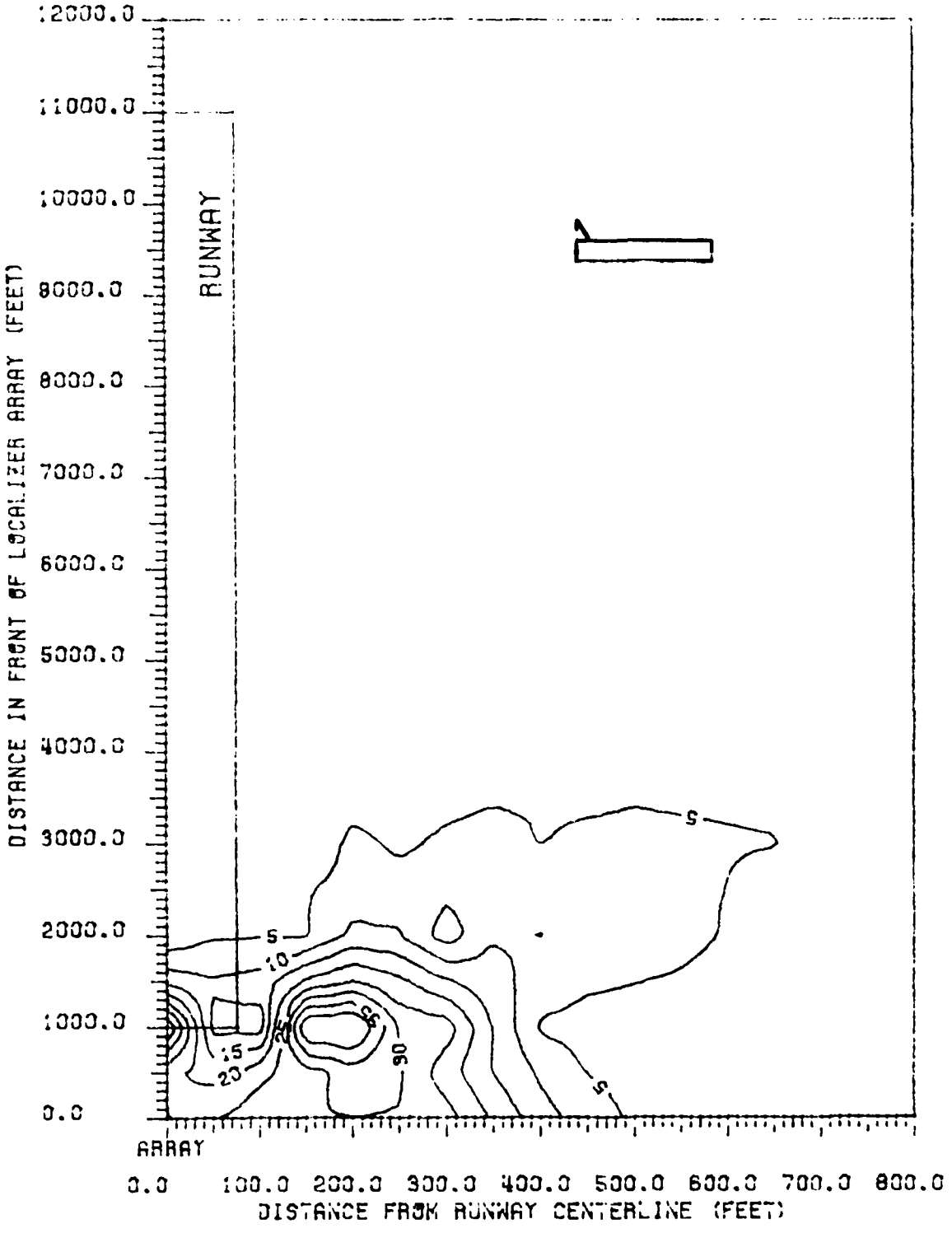

Figure 59 Contours of peak CDI values produced in ILS Zone 3 to Threshold for a L-1011. L-1011 fuselage is perpendicular to runway centerline, with tail towards the runway. 8-element single-frequency array, LPD antennas.

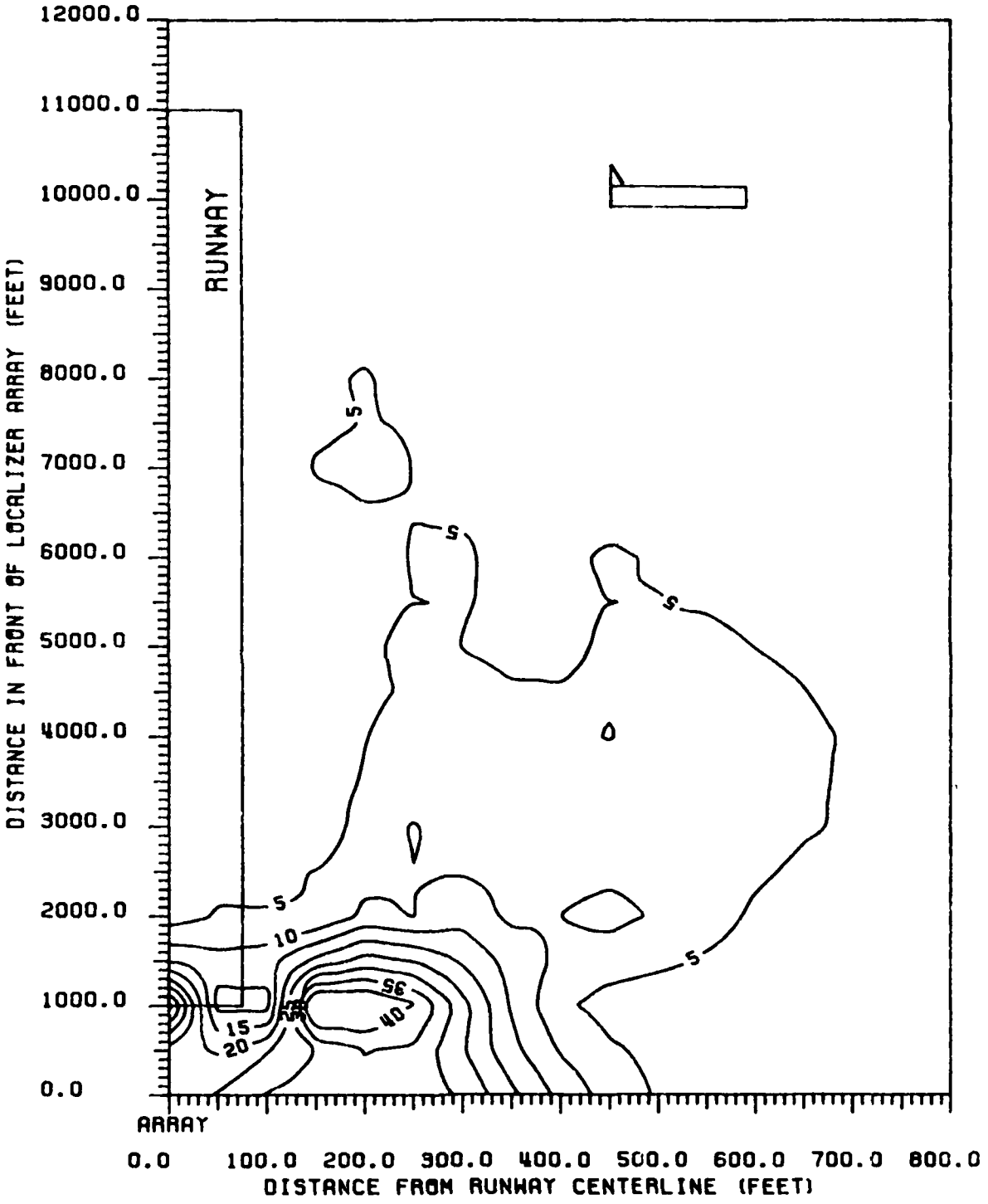

Figure 60 Contours of peak CDI values produced in ILS Zone 4 for a L-1011. L-1011 fuselage is perpendicular to runway centerline, with tail towards the runway. 8-element single-frequency array, LPD antennas.

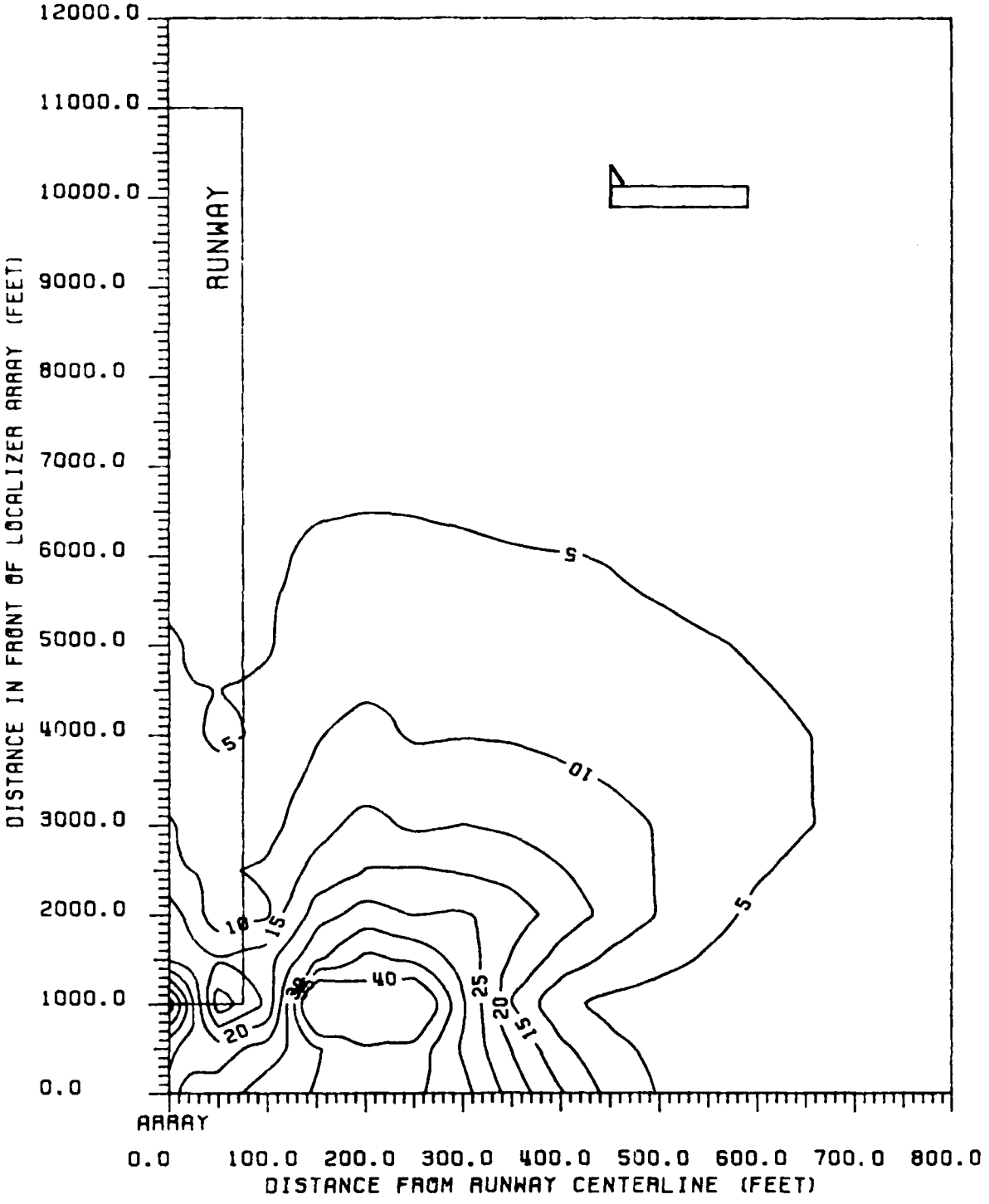

Figure 61 Contours of peak CDI values produced in ILS Zone 5 for a L-1011. L-1011 fuselage is perpendicular to runway centerline, with tail towards the runway. 8-element single-frequency array, LPD antennas.

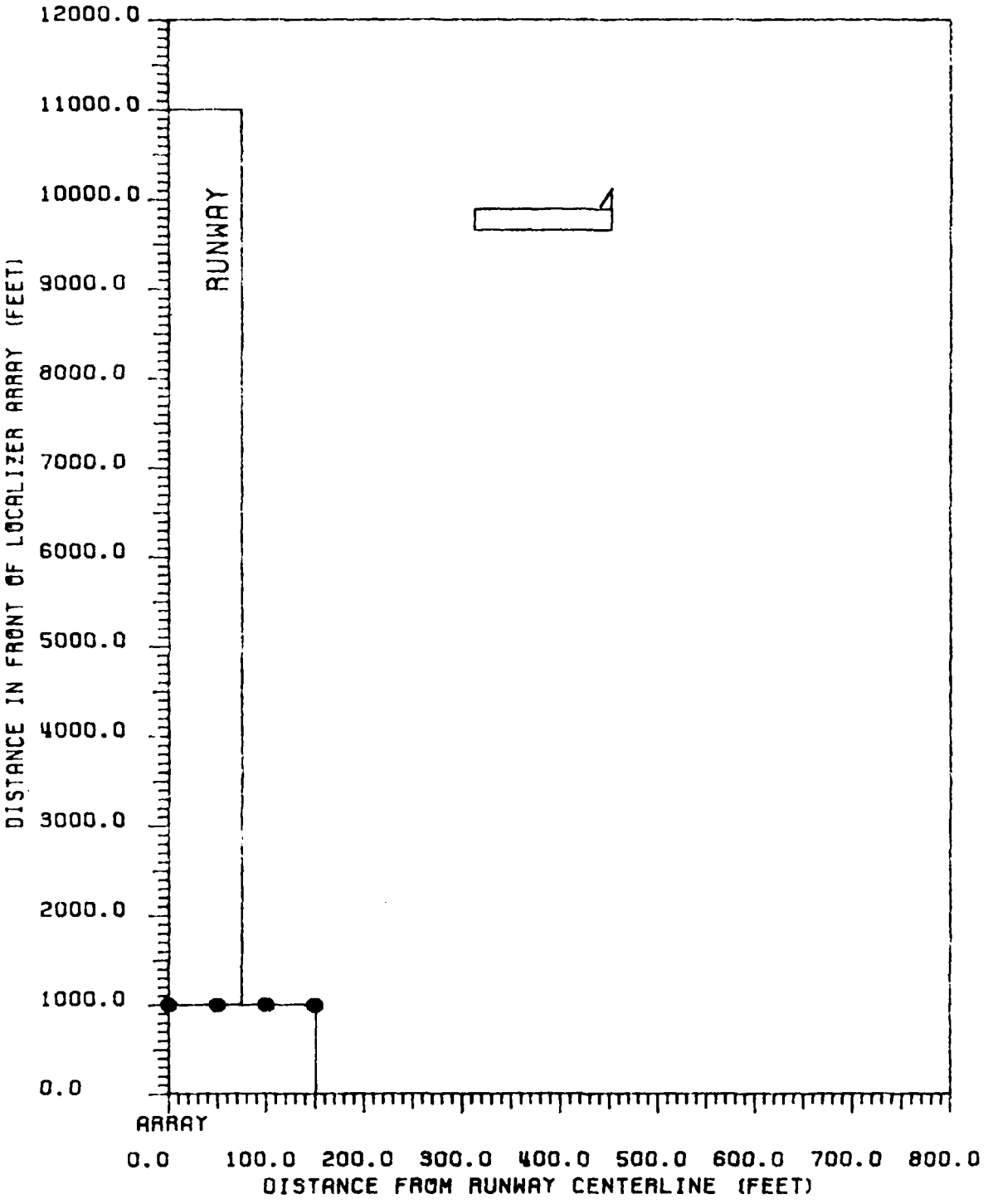

Figure 62 Critical area map for CAT I tolerances relating to L-1011 aircraft. L-1011 fuselage is perpendicular to runway centerline with tail away from runway. 8-element single-frequency array, LPD antennas.

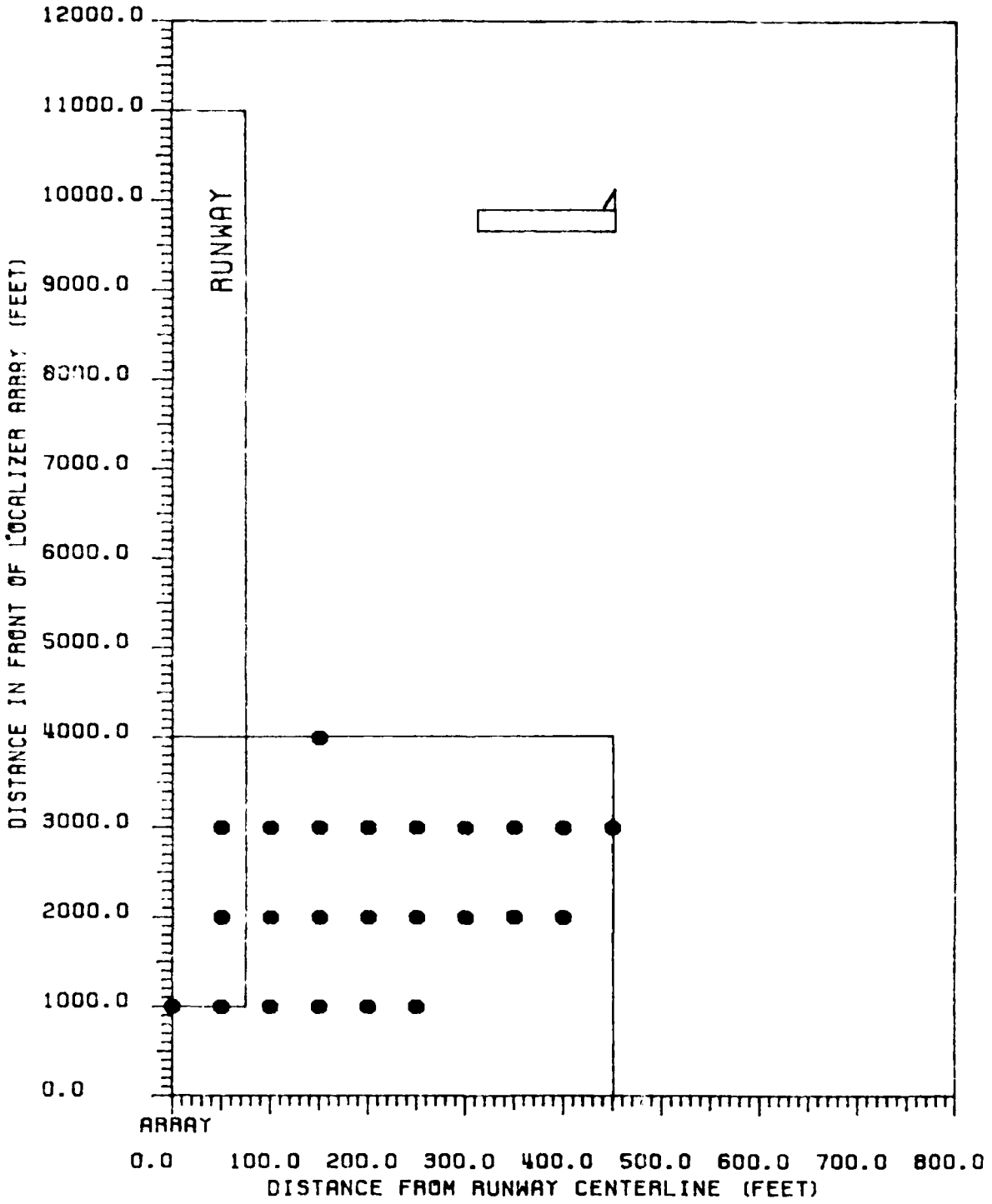

Figure 63 Critical area map for CAT II tolerances relating to L-1011 aircraft. L-1011 fuselage is perpendicular to runway centerline with tail away from runway. 8-element single-frequency array, LPD antennas.

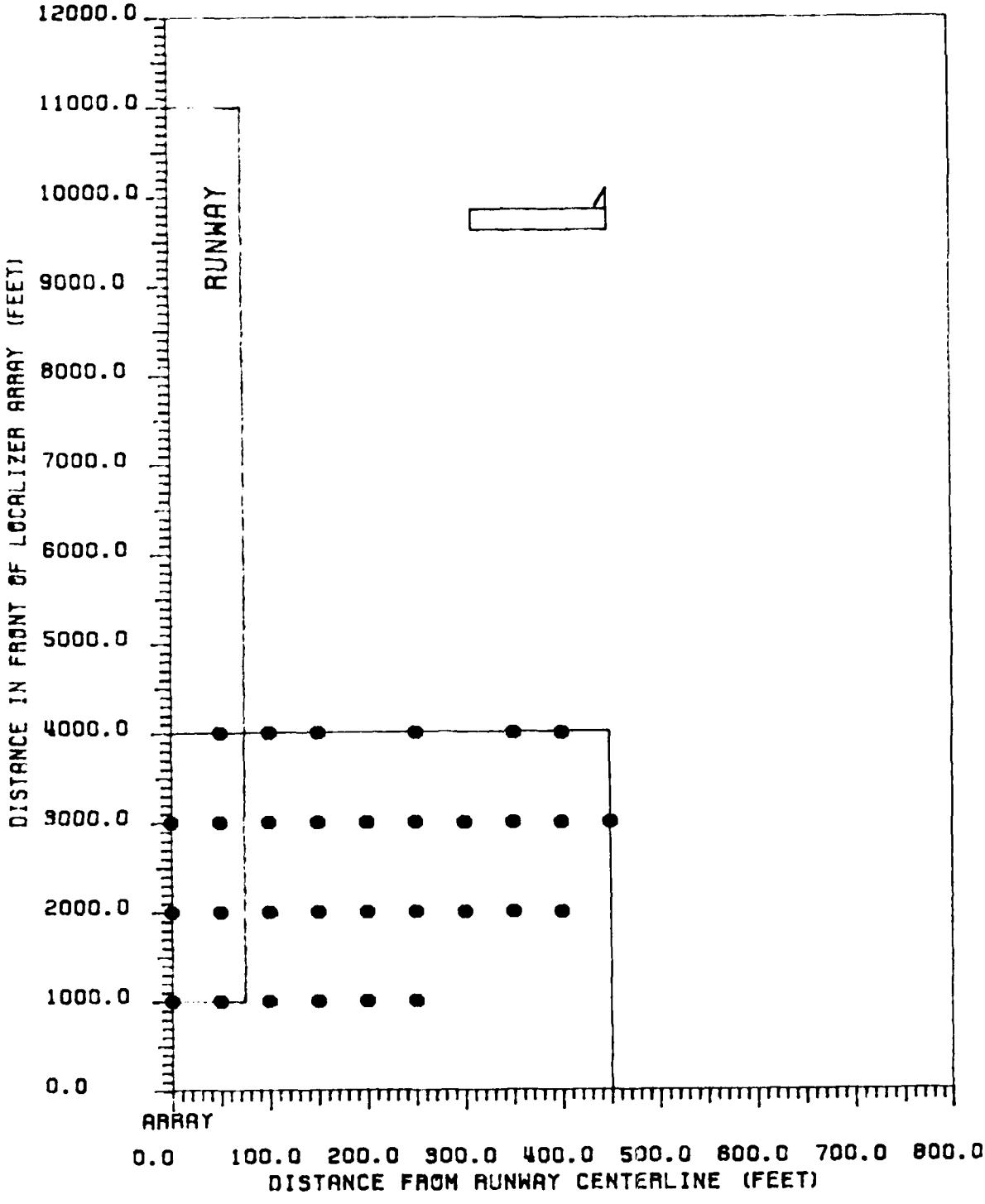

Figure 64 Critical area map for CAT III tolerances relating to L-1011 aircraft. L-1011 fuselage is perpendicular to runway centerline with tail away from runway. 8-element single-frequency array, LPD antennas.

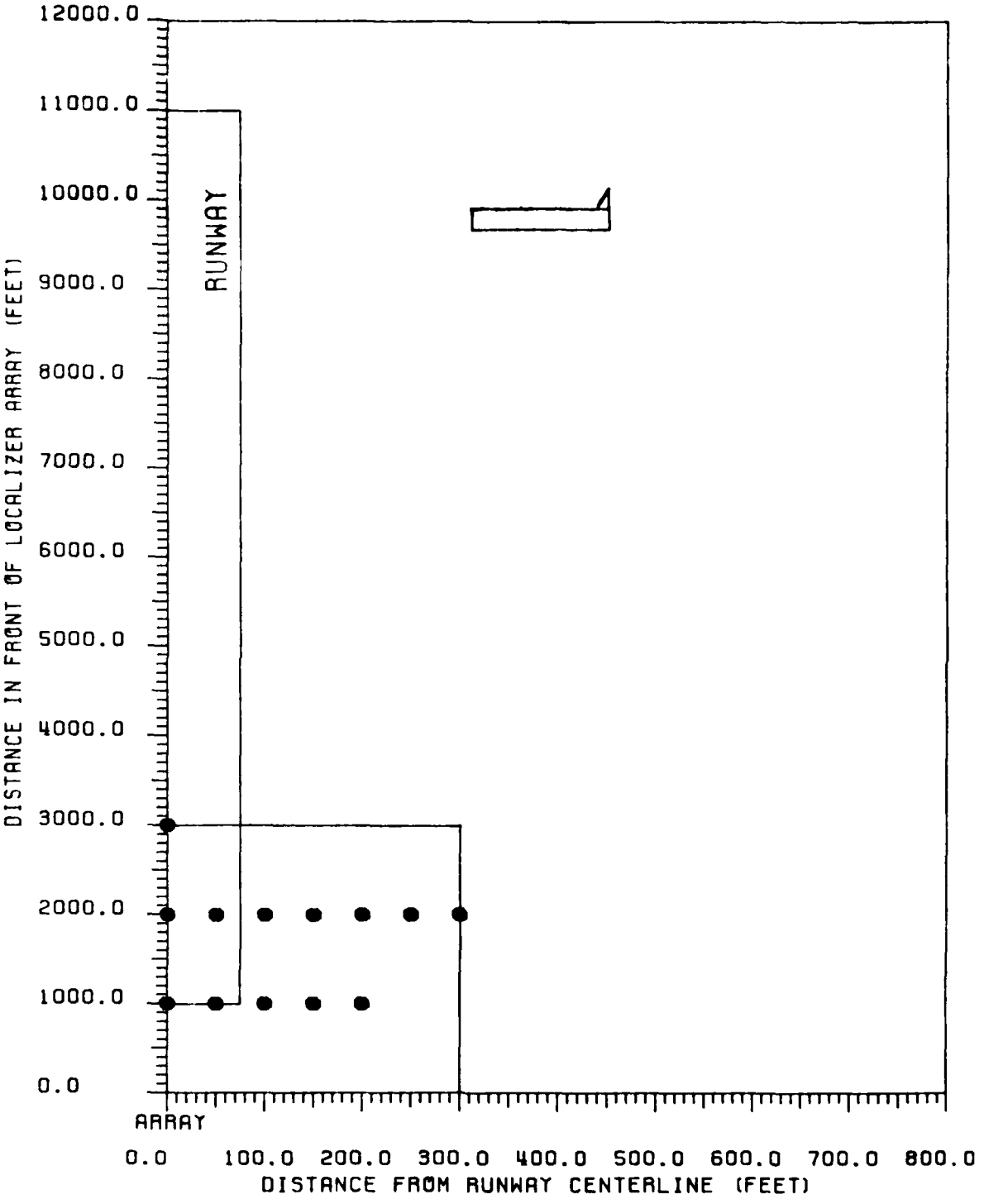

Figure 65 Critical area map for CAT III-X tolerances relating to L-1011 aircraft. L-1011 fuselage is perpendicular to runway centerline with tail away from runway. 8-element single-frequency array, LPD antennas.

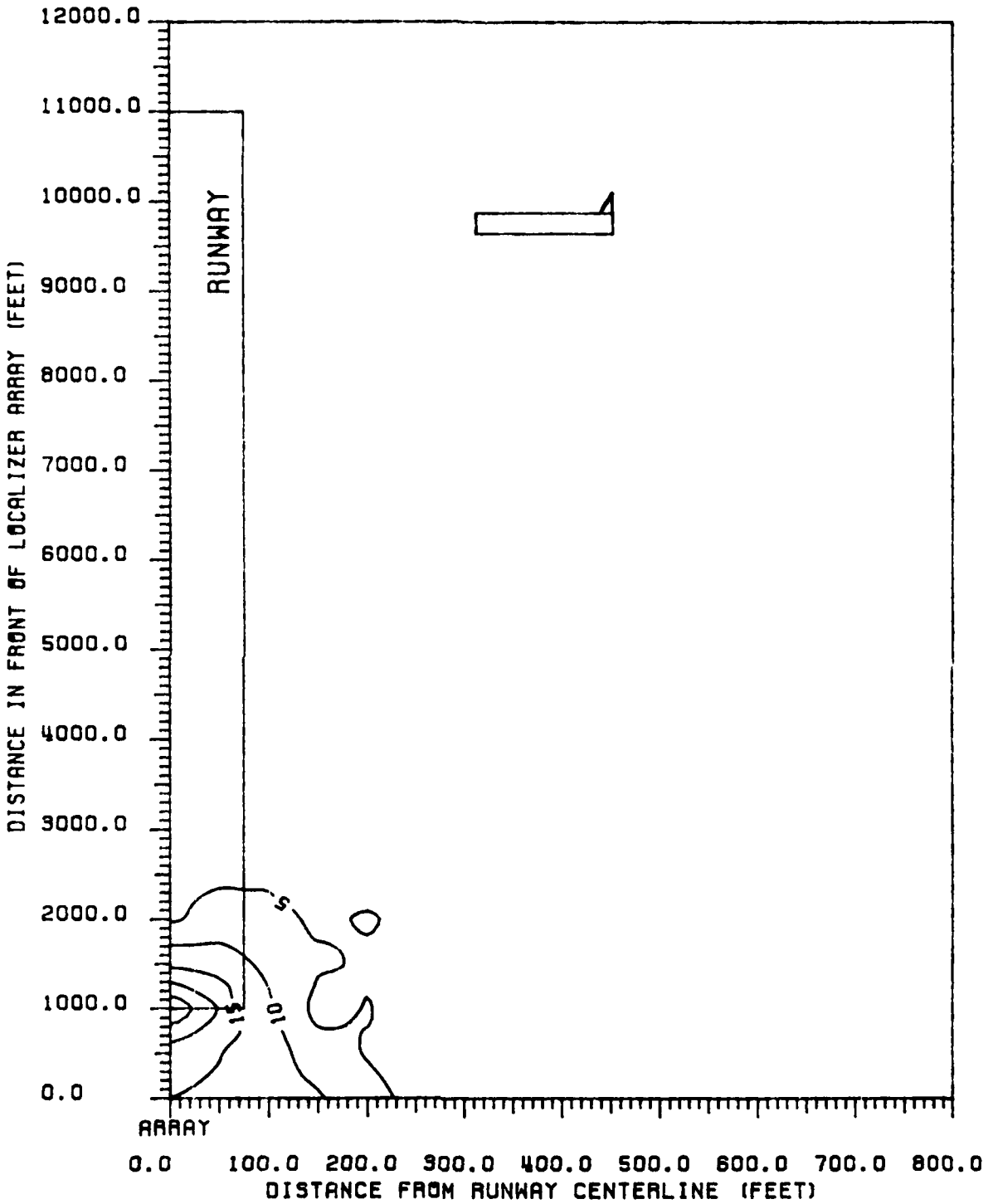

Figure 66 Contours of peak CDI values produced in ILS Zone 1 for a L-1011. L-1011 fuselage is perpendicular to runway centerline, with tail away from runway. 8-element single-frequency array, LPD antennas.

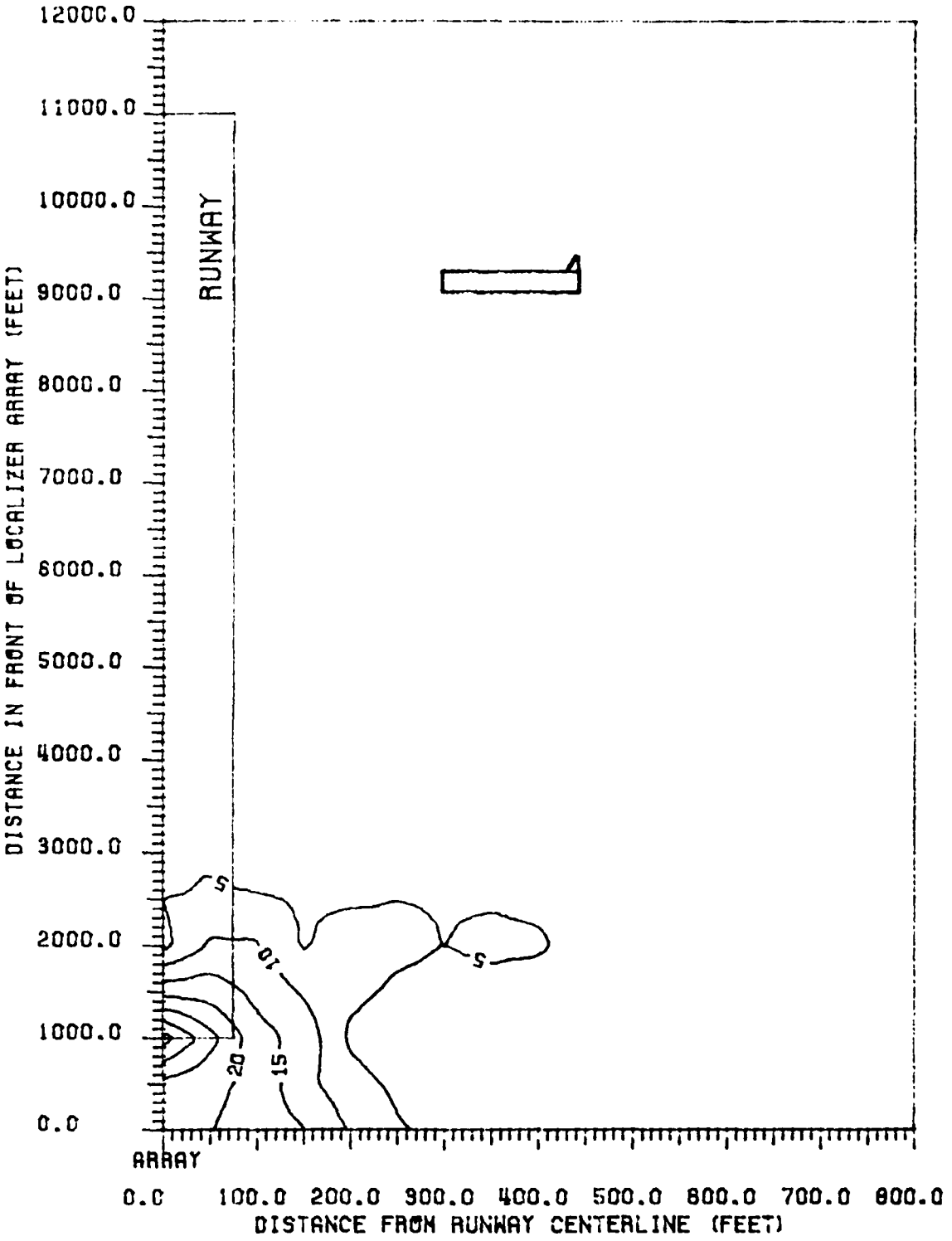

Figure 67 Contours of peak CDI values produced in ILS Zone 2 for a L-1011. L-1011 fuselage is perpendicular to runway centerline, with tail away from runway. 8-element single-frequency array, LPD antennas.

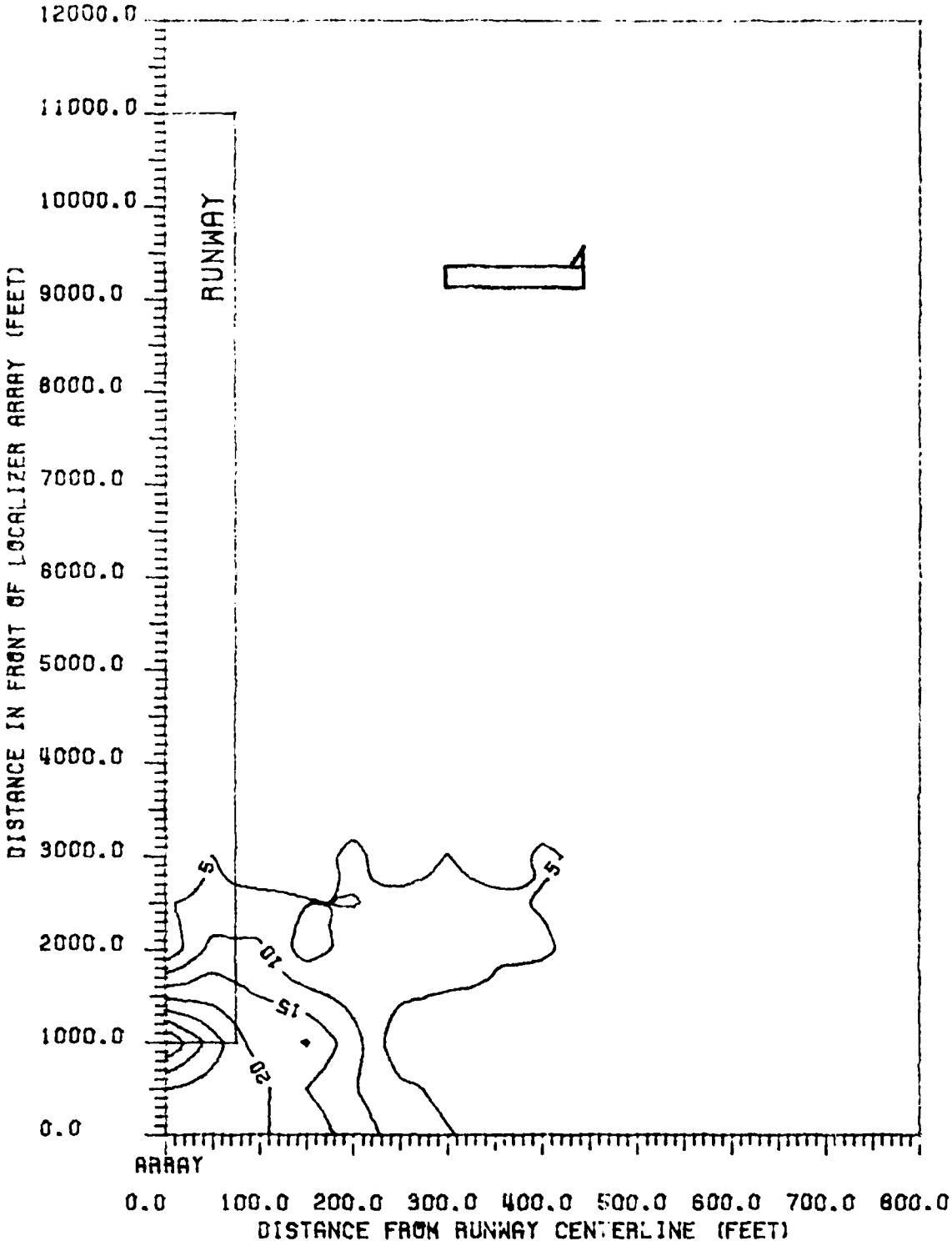

Figure 68 Contours of peak CDI values produced in ILS Zone 3 to Threshold for a L-1011. L-1011 fuselage is perpendicular to runway centerline, with tail away from runway. 8-element single-frequency array, LPD antennas.

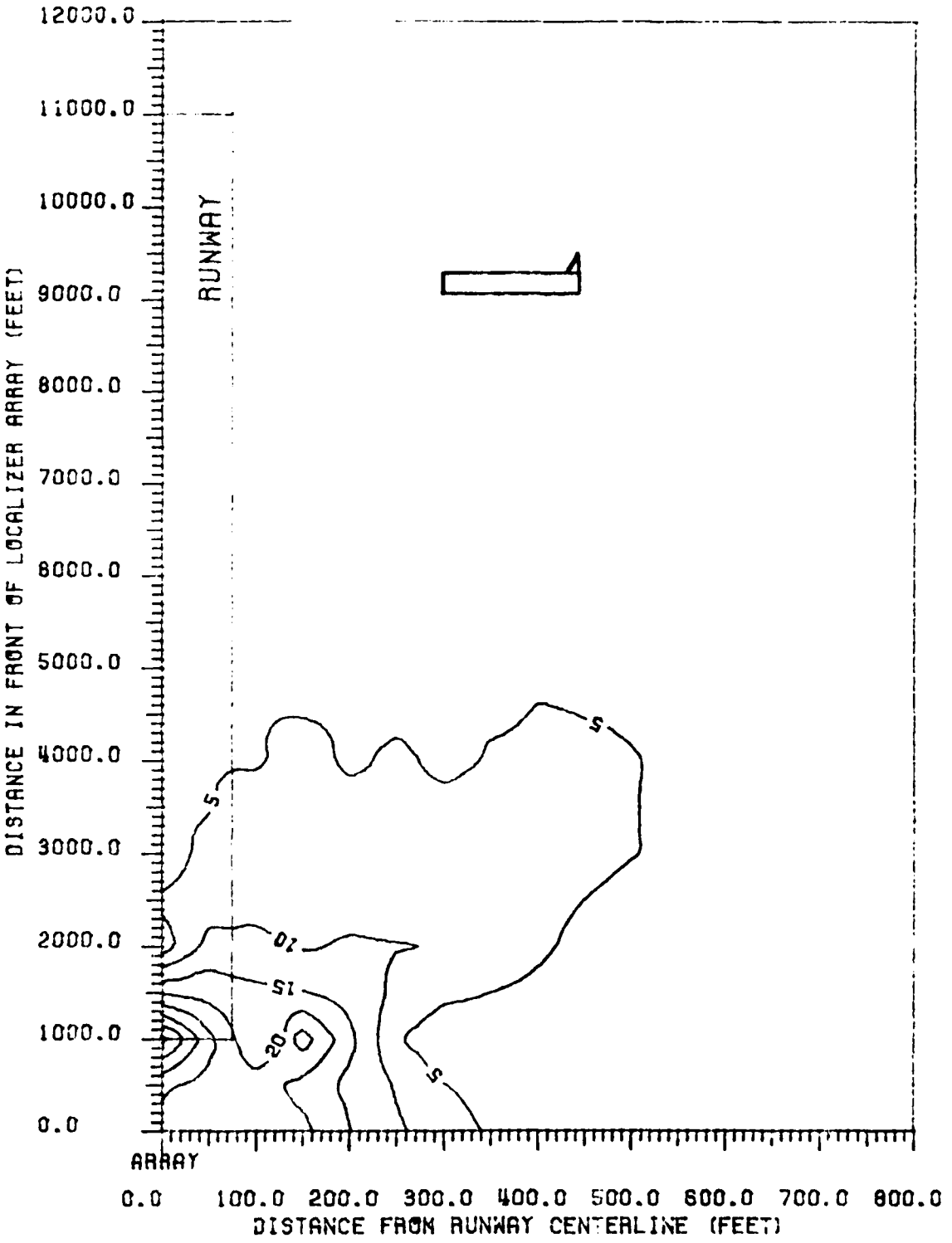

Figure 69 Contours of peak CDI values produced in ILS Zone 4 for a L-1011. L-1011 fuselage is perpendicular to runway centerline, with tail away from runway. 8-element single-frequency array, LPD antennas.

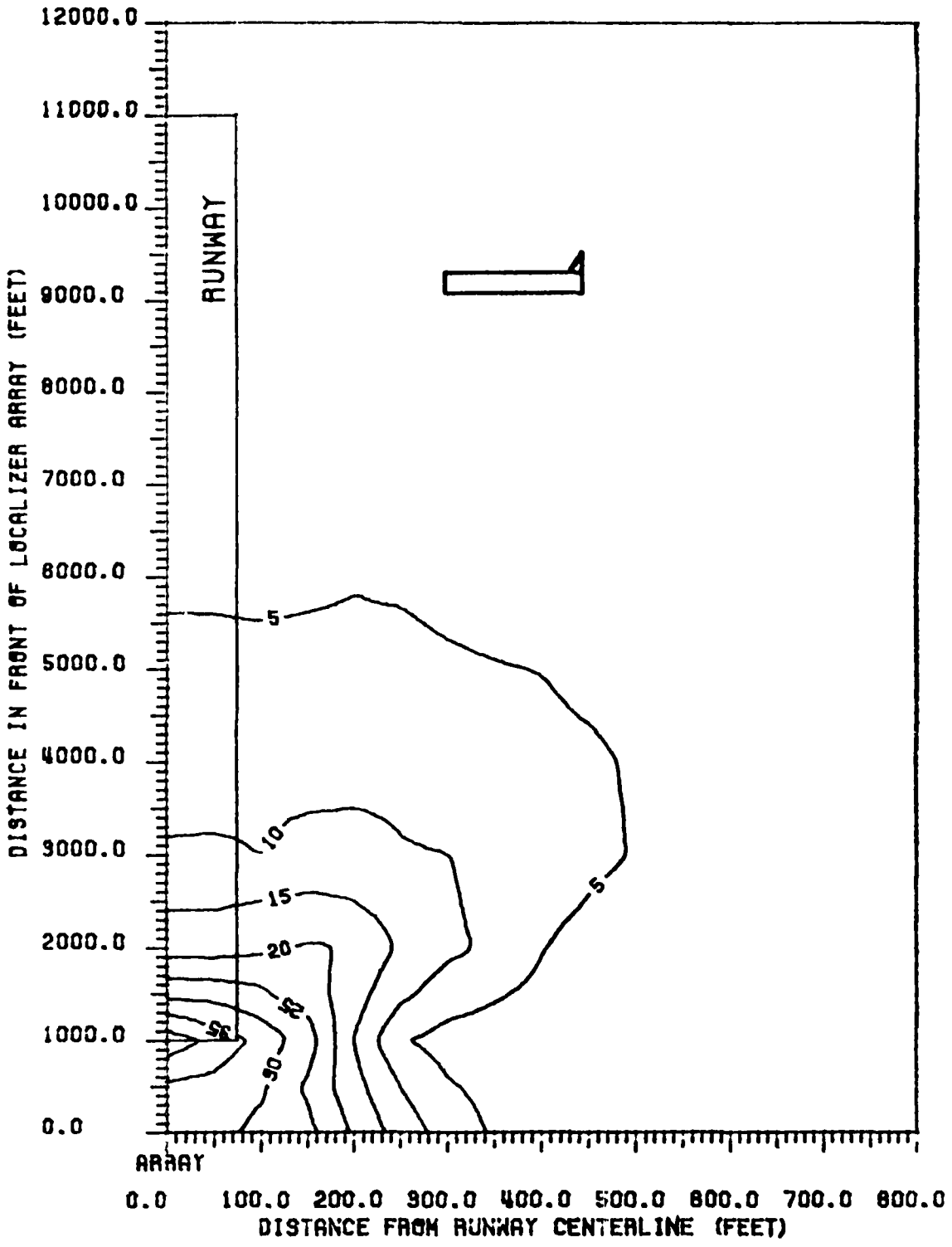

Figure 70 Contours of peak CDI values produced in ILS Zone 5 for a L-1011. L-1011 fuselage is perpendicular to runway centerline, with tail away from ruwnay. 8-element single-frequency array, LPD antennas.

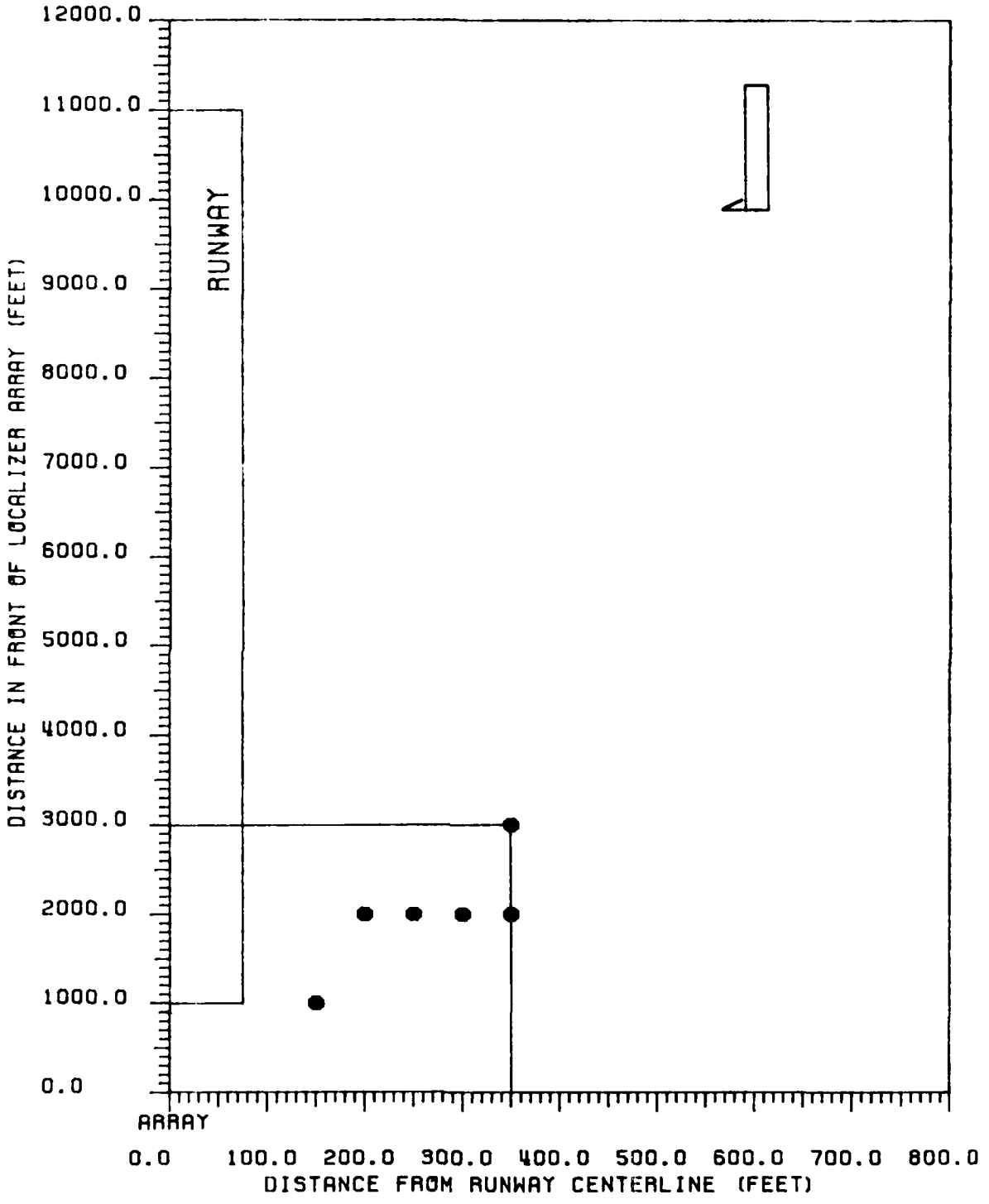

Figure 71 Critical area map for CAT III tolerances relating to L-1011 aircraft. L-1011 fuselage is parallel to runway centerline with tail towards the array. 8-element single-frequency array, LPD antennas.

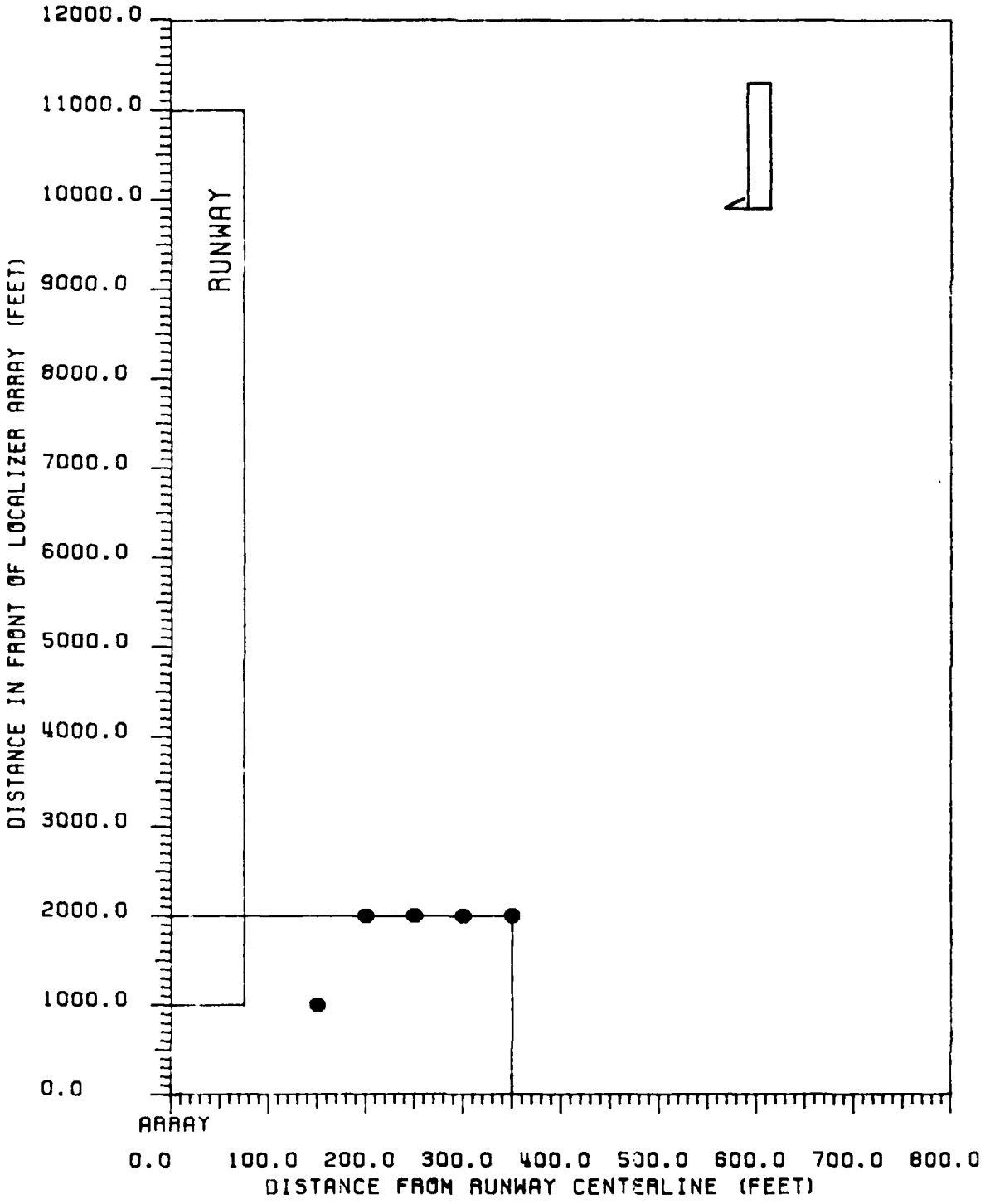

Figure 72 Critical area map for CAT III-X tolerances relating to L-1011 aircraft. L-1011 fuselage is parallel to runway centerline with tail towards the array. 8-element single-frequency array, LPD antennas.

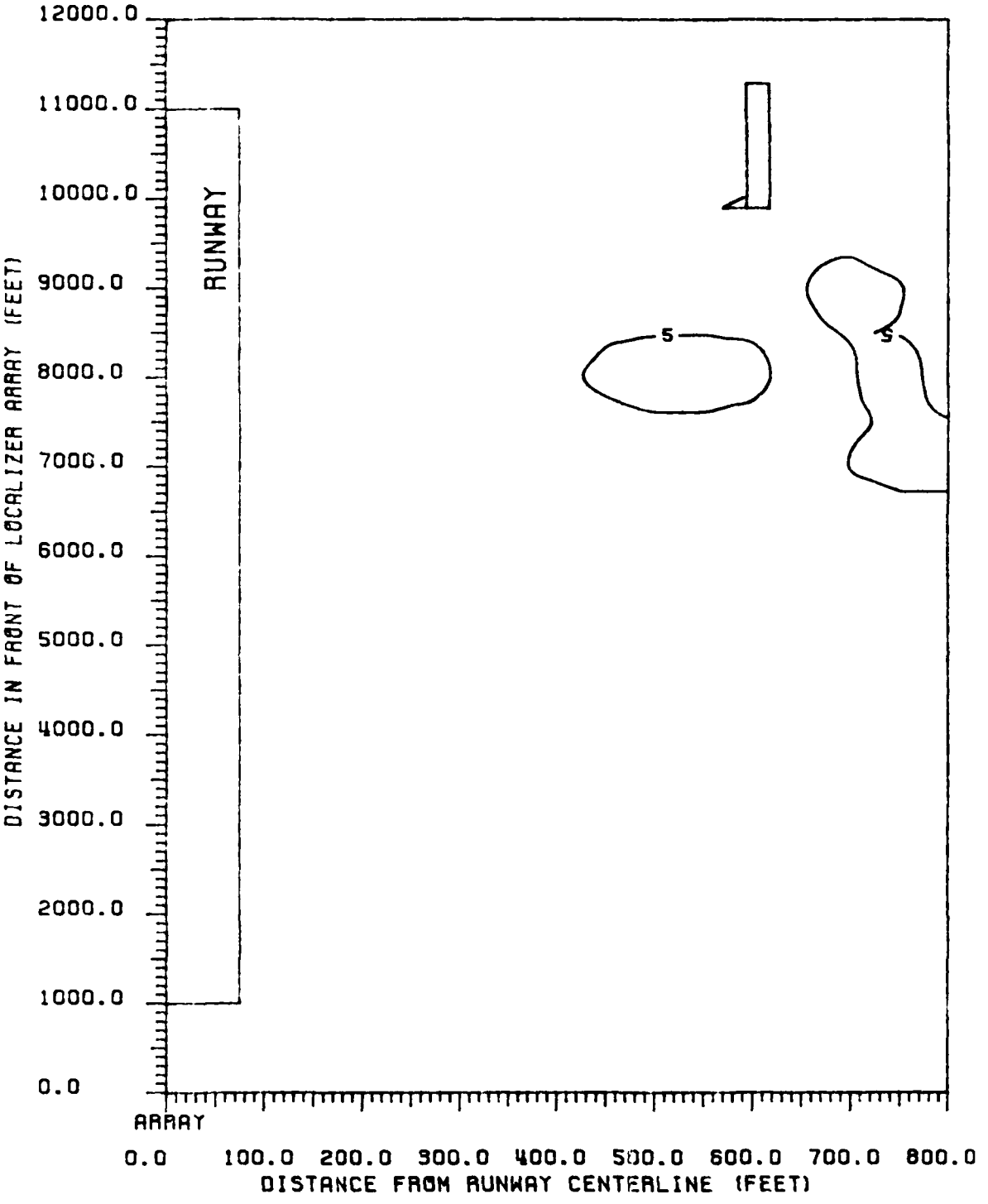

Figure 73 Contours of peak CDI values produced in ILS Zone 4 for a L-1011 parallel to runway centerline, with tail towards the array. 8-element single-frequency array, LPD antennas.

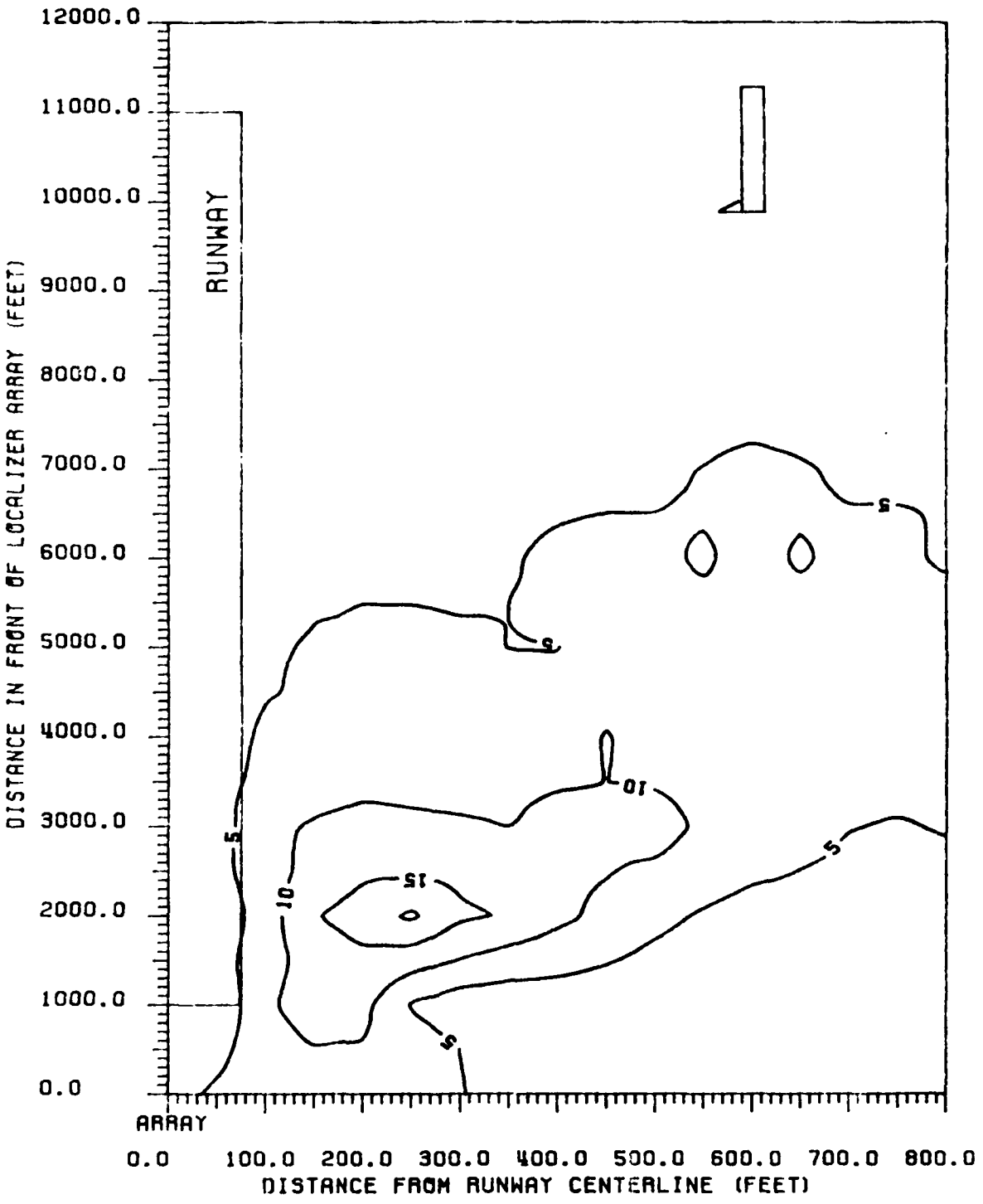

Figure 74 Contours of peak CDI values produced in ILS Zone 5 for a L-1011 parallel to runway centerline, with tail towards the array. 8-element single-frequency array, LPD antennas.

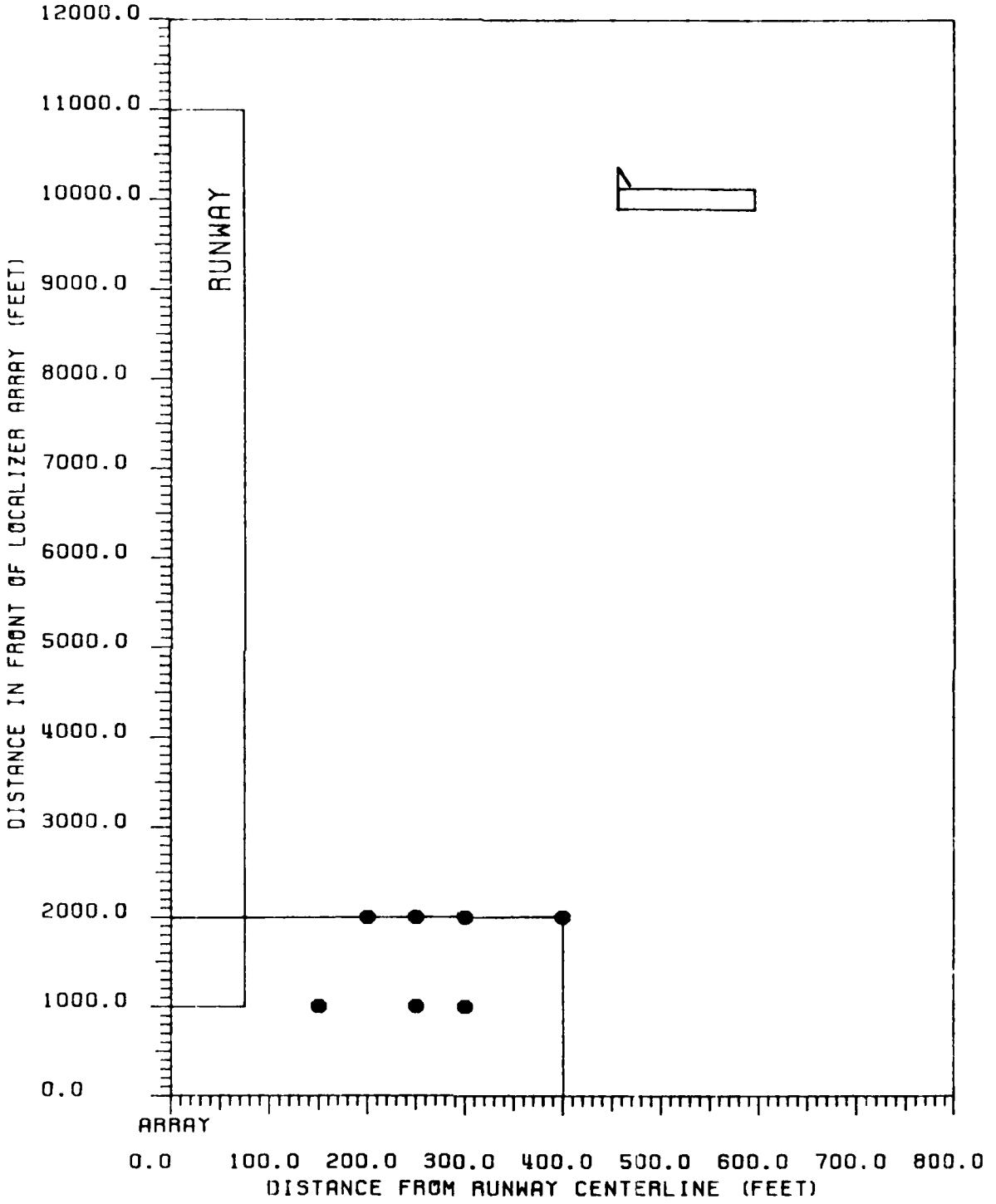

Figure 75 Critical area map for CAT I tolerances relating to B-747 aircraft. B-747 fuselage is perpendicular to runway centerline with tail towards the runway. 8-element single-frequency array, LPD antennas.

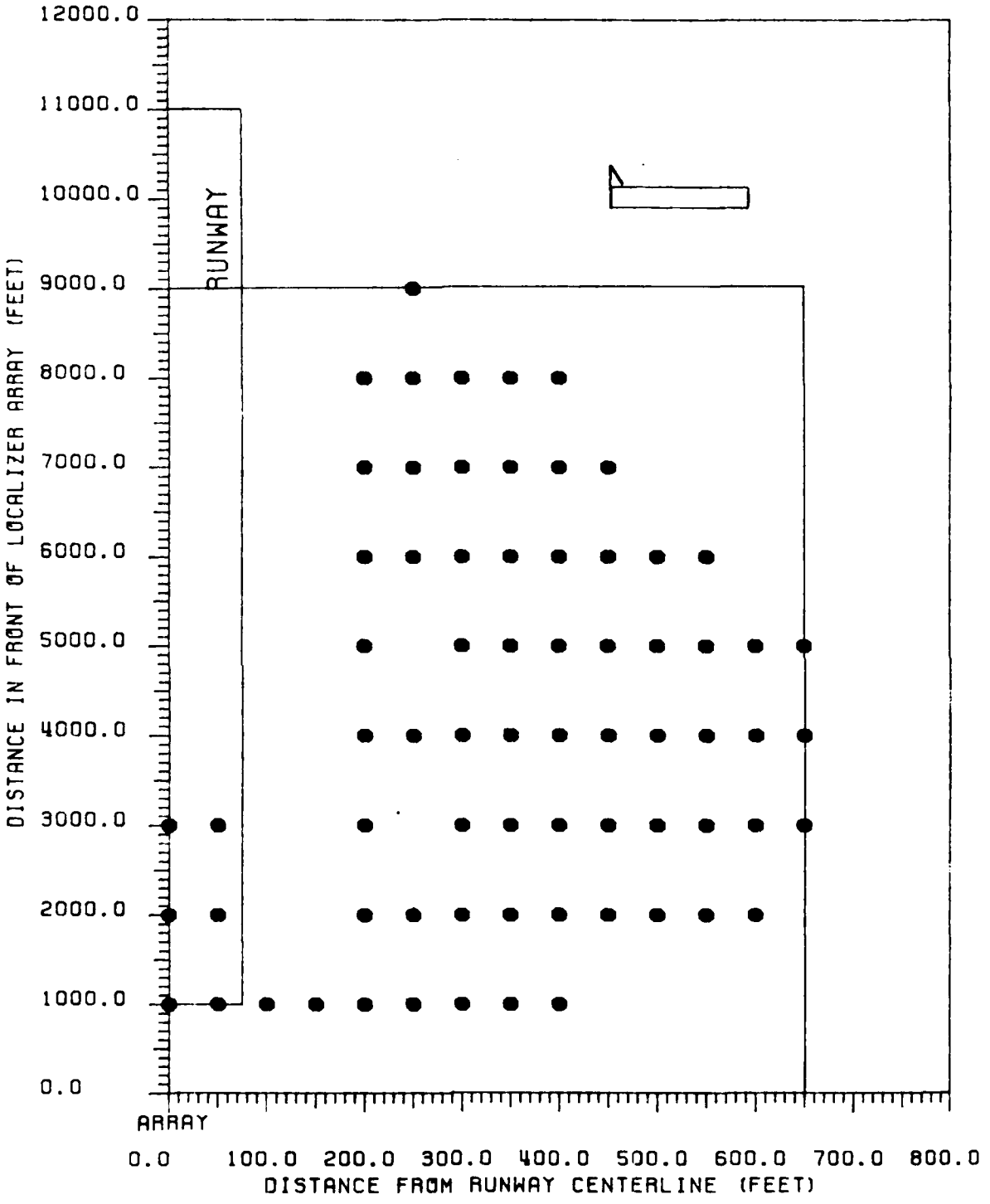

Figure 76 Critical area map for CAT II tolerances relating to B-747 aircraft. B-747 fuselage is perpendicular to runway centerline with tail towards the runway. 8-element single-frequency array, LPD antennas.

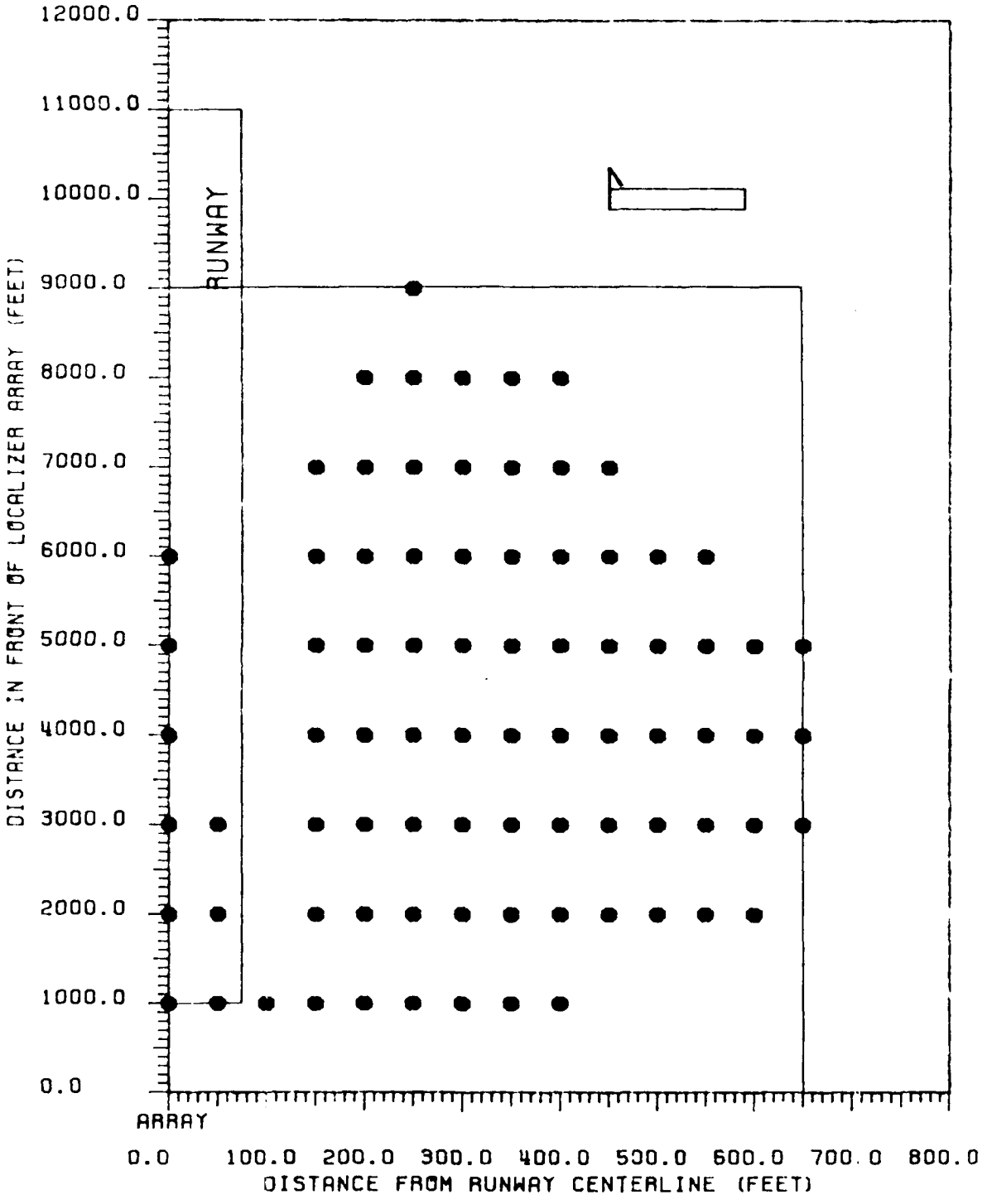

Figure 77 Critical area map for CAT III tolerances relating to B-747 aircraft. B-747 fuselage is perpendicular to runway centerline with tail towards the runway. 8-element single-frequency array, LPD antennas.

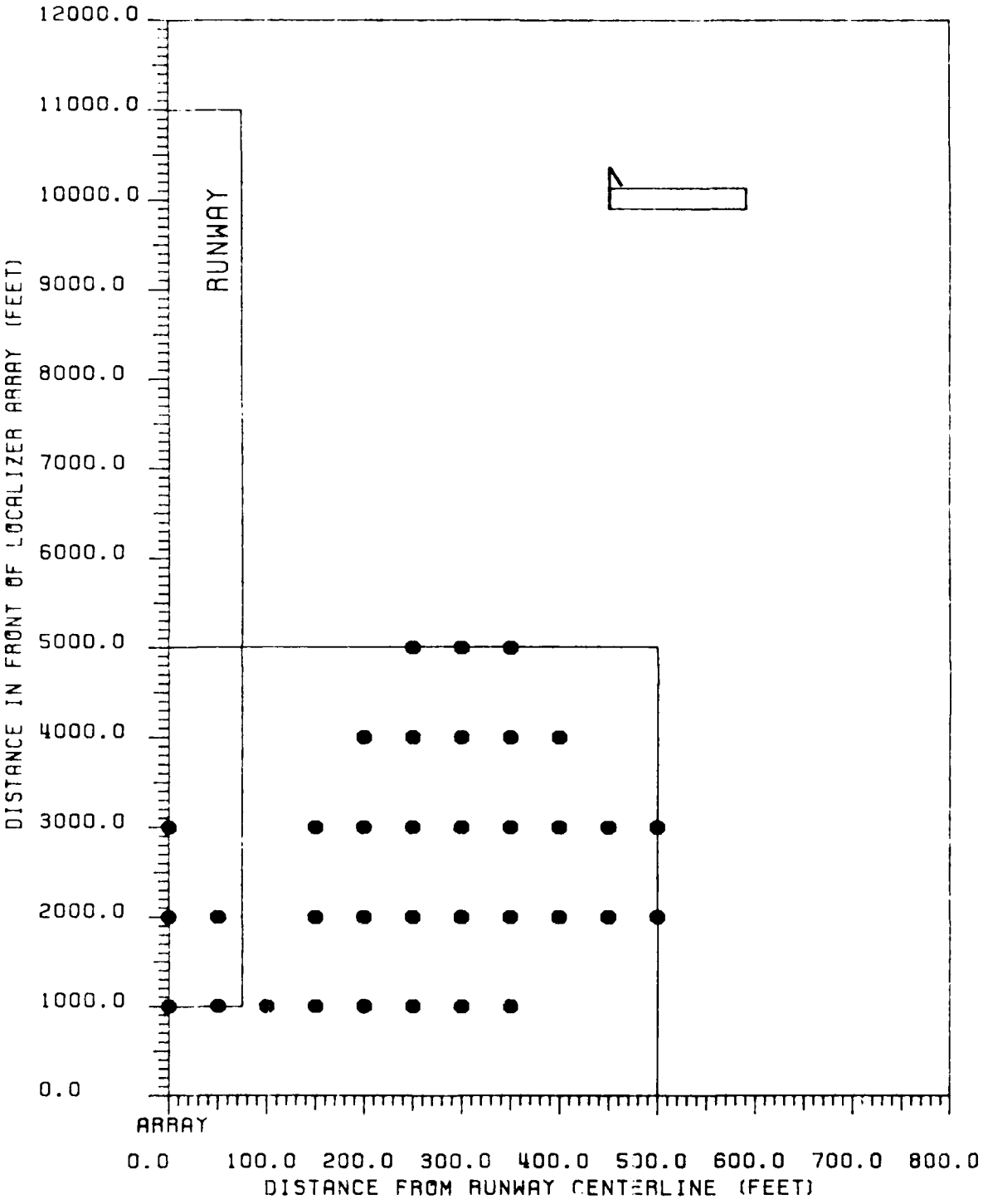

Figure 78 Critical area map for CAT III-X tolerances relating to B-747 aircraft. B-747 fuselage is perpendicular to runway centerline with tail towards the runway. 8-element single-frequency array, LPD antennas.

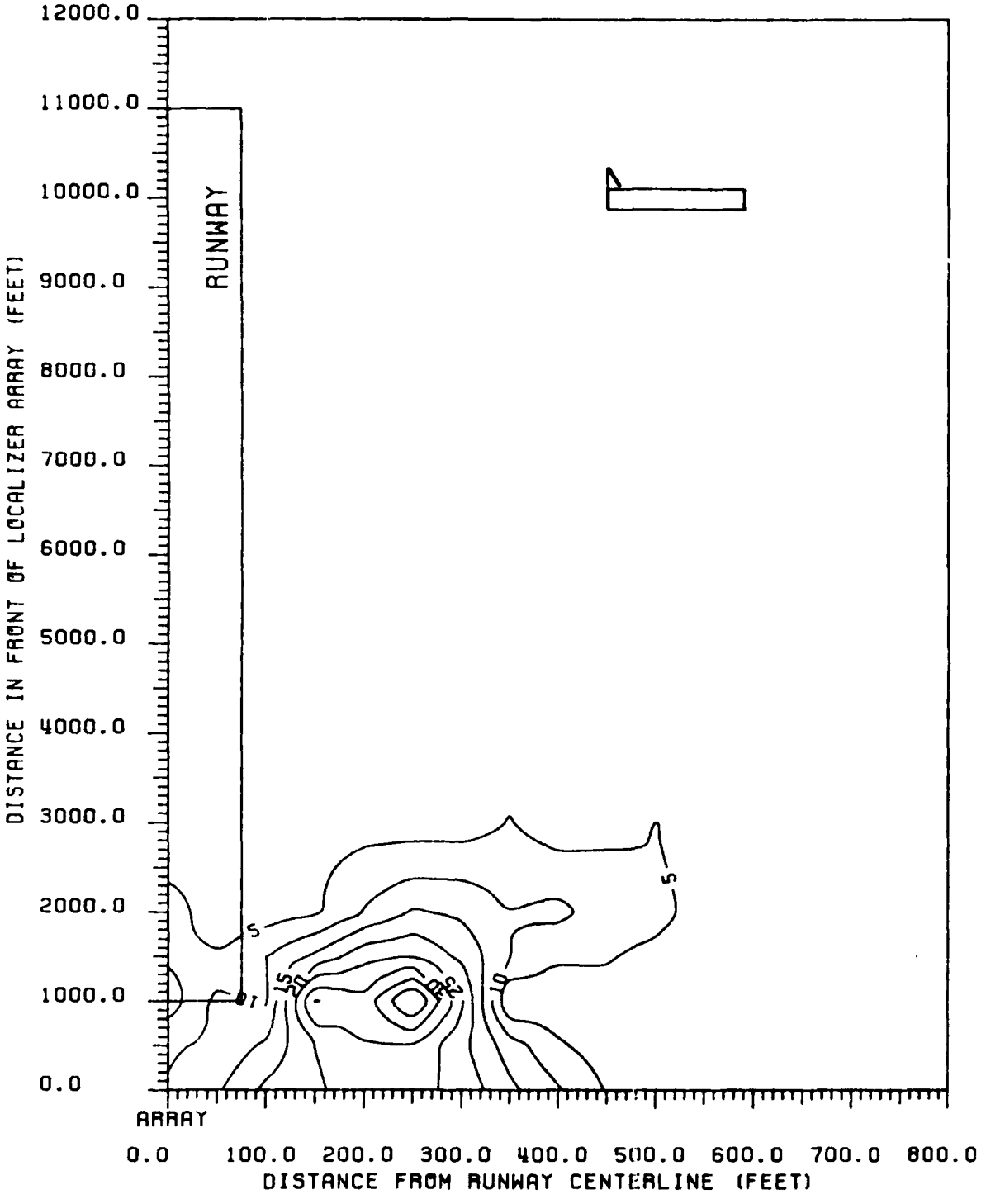

Figure 79 Contours of peak CDI values produced in ILS Zone 1 for a B-747. B-747 fuselage is perpendicular to runway centerline, with tail towards the runway. 8-element single-frequency array, LPD antennas.

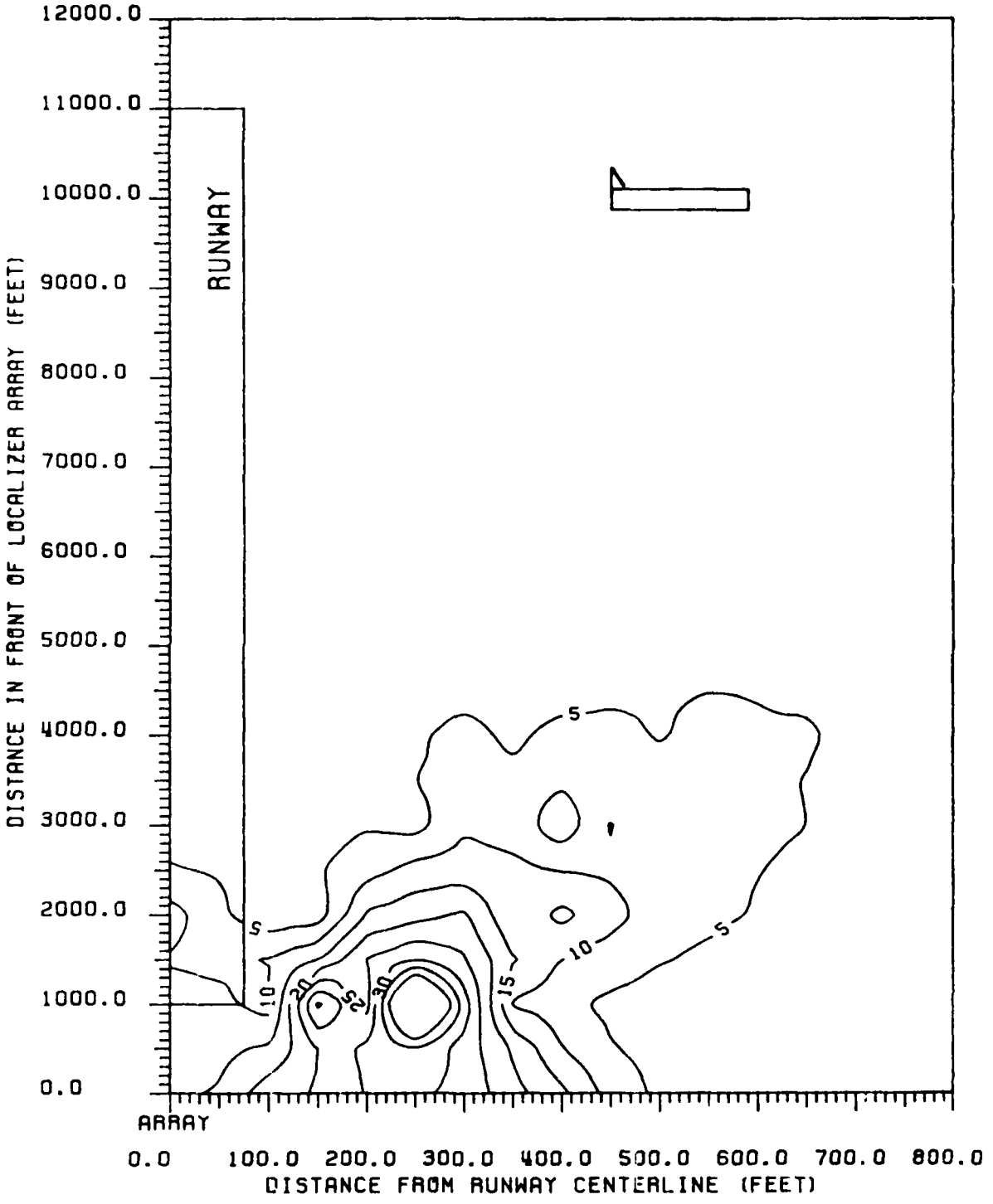

Figure 80 Contours of peak CDI values produced in ILS Zone 2 for a B-747. B-747 fuselage is perpendicular to runway centerline, with tail towards the runway. 8-element single-frequency array, LPD antennas.

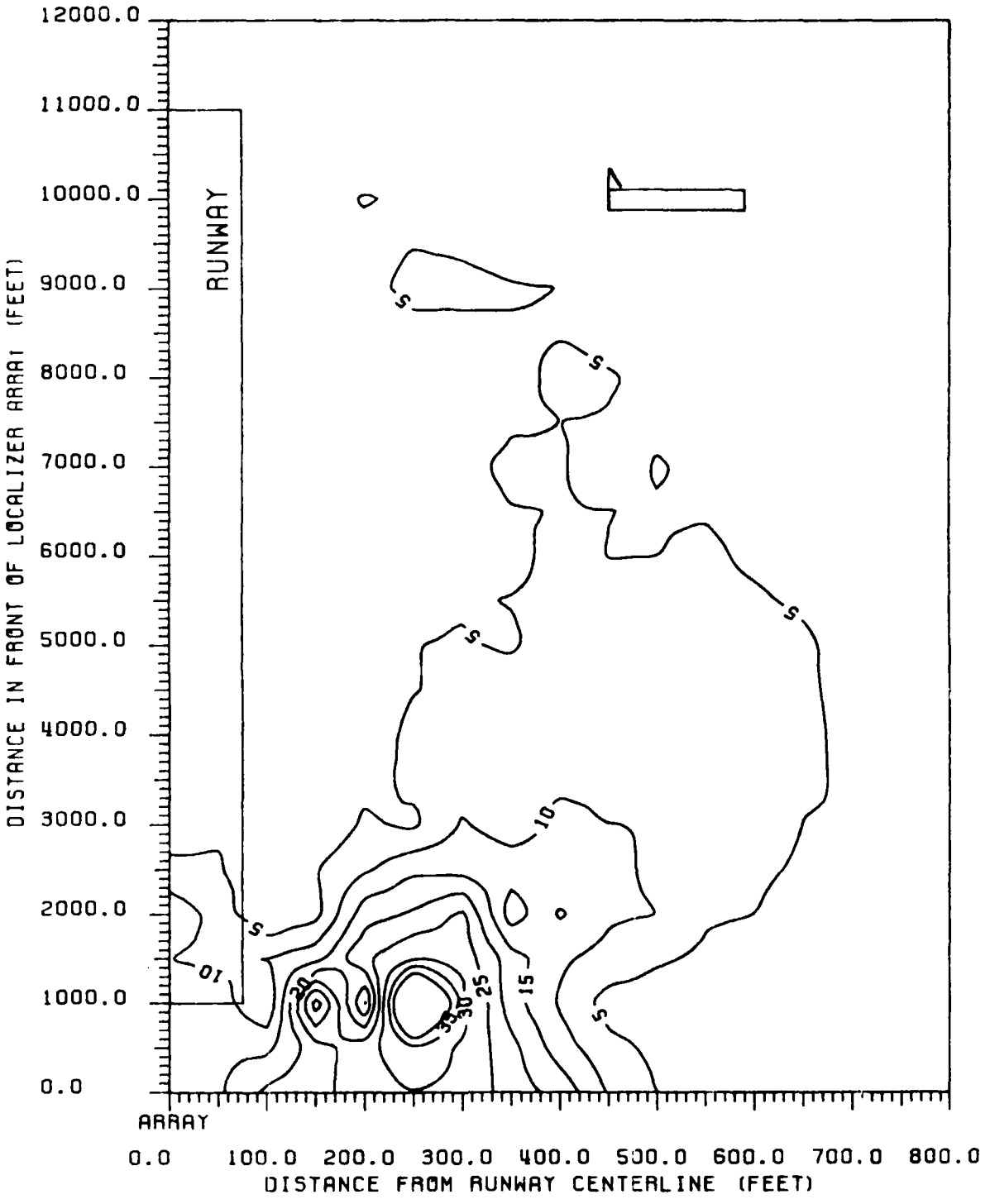

Figure 81 Contours of peak CDI values produced in ILS Zone 3 to Threshold for a B-747. B-747 fuselage is perpendicular to runway centerline, with tail towards the runway. 8-element single-frequency array, LPD antennas.

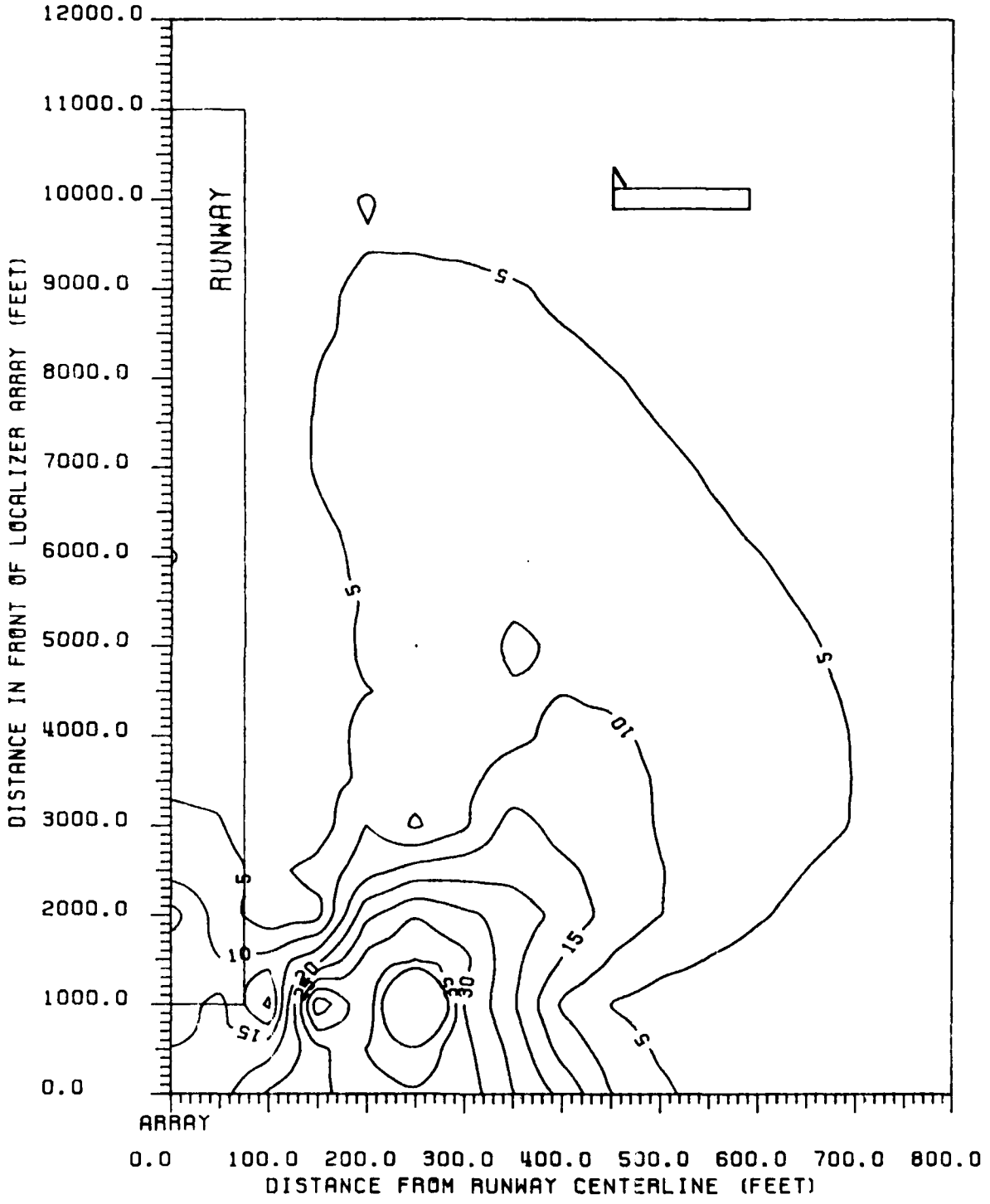

Figure 82 Contours of peak CDI values produced in ILS Zone 4 for a B-747. B-747 fuselage is perpendicular to runway centerline, with tail towards the runway. 8-element single-frequency array, LPD antennas.

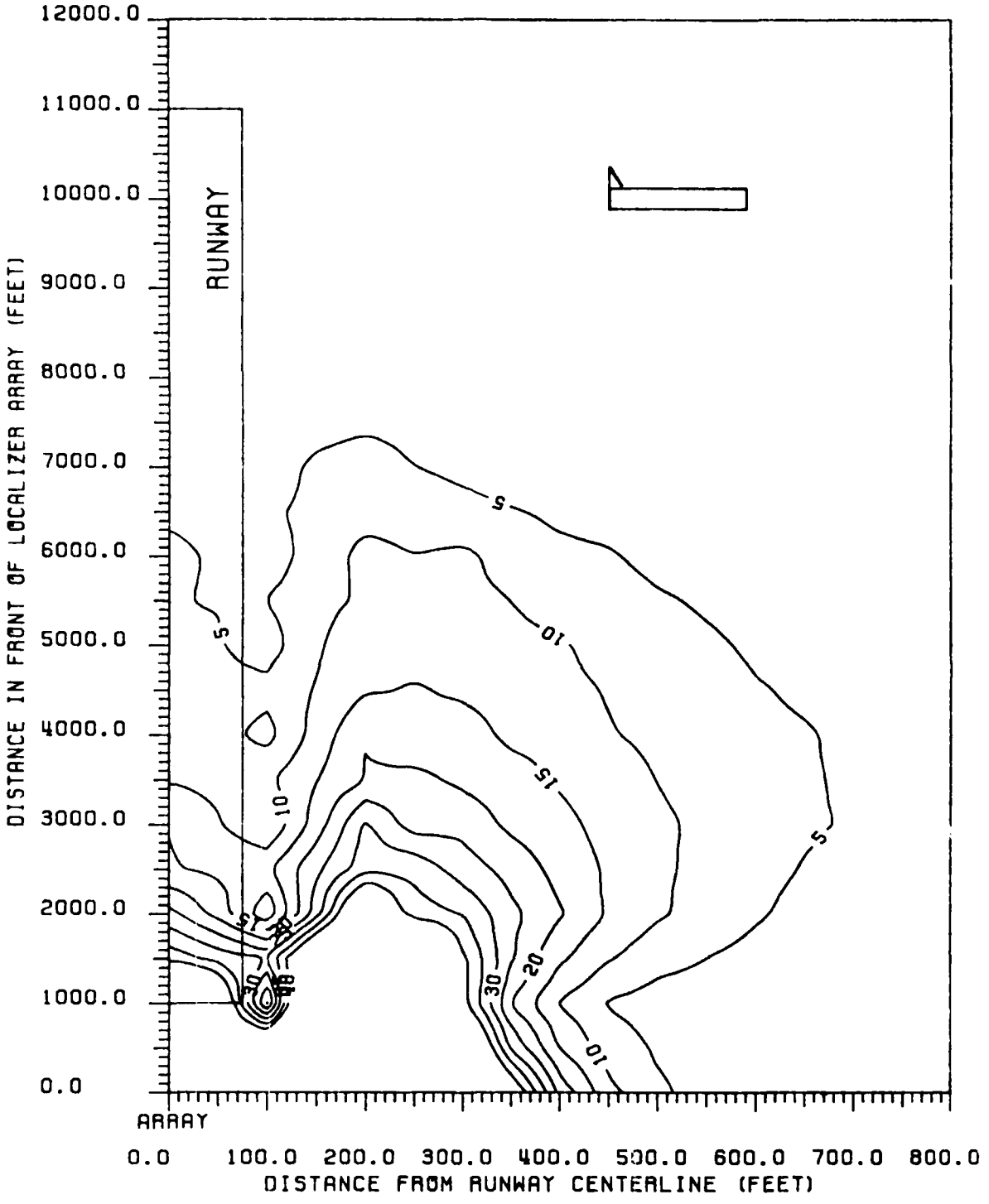

Figure 83 Contours of peak CDI values produced in ILS Zone 5 for a B-747. B-747 fuselage is perpendicular to runway centerline, with tail towards the runway. 8-element single-frequency array, LPD antennas.

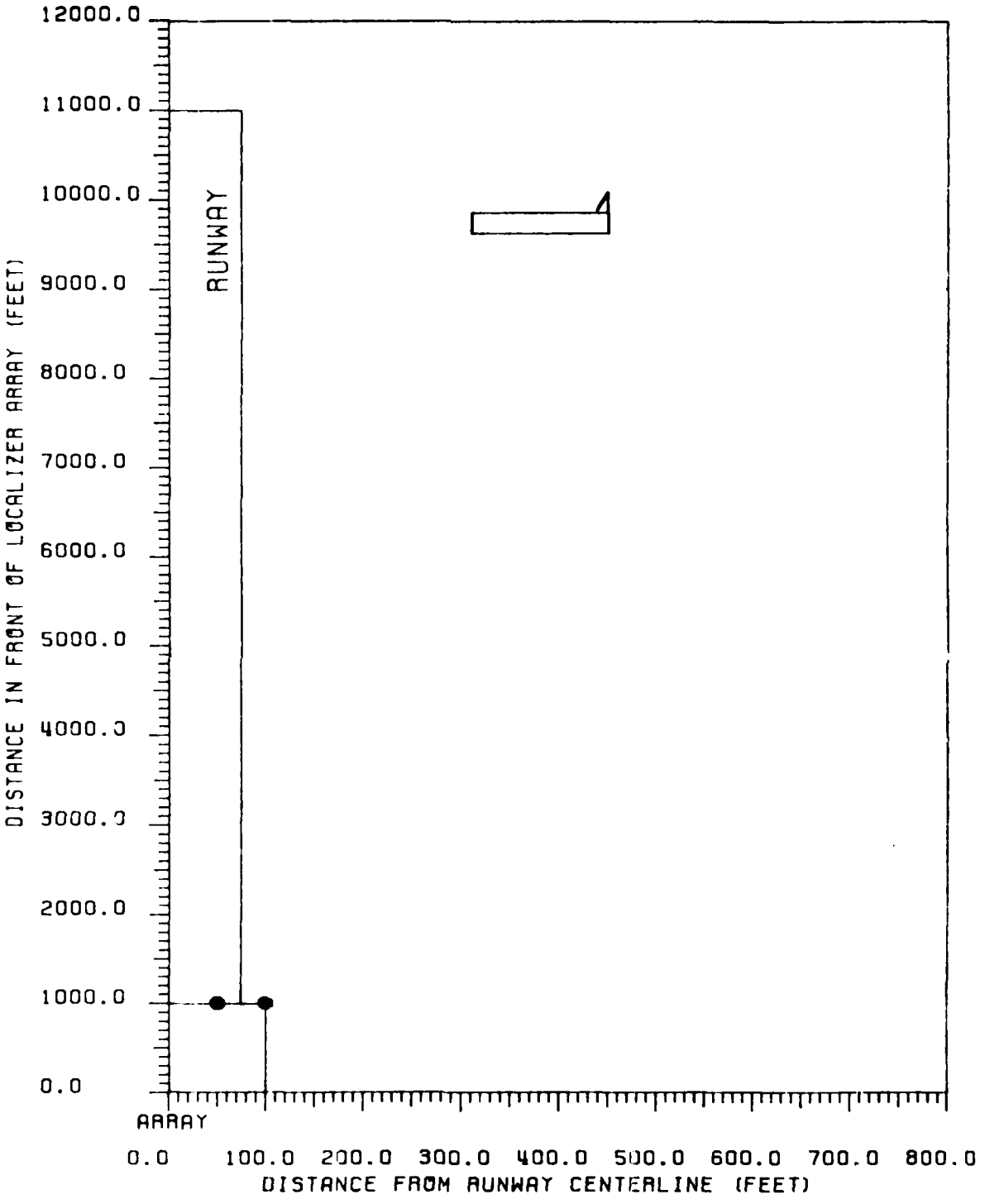

Figure 84 Critical area map for CAT I tolerances relating to B-747 aircraft. B-747 fuselage is perpendicular to runway centerline with tail away from runway. 8-element single-frequency array, LPD antennas.

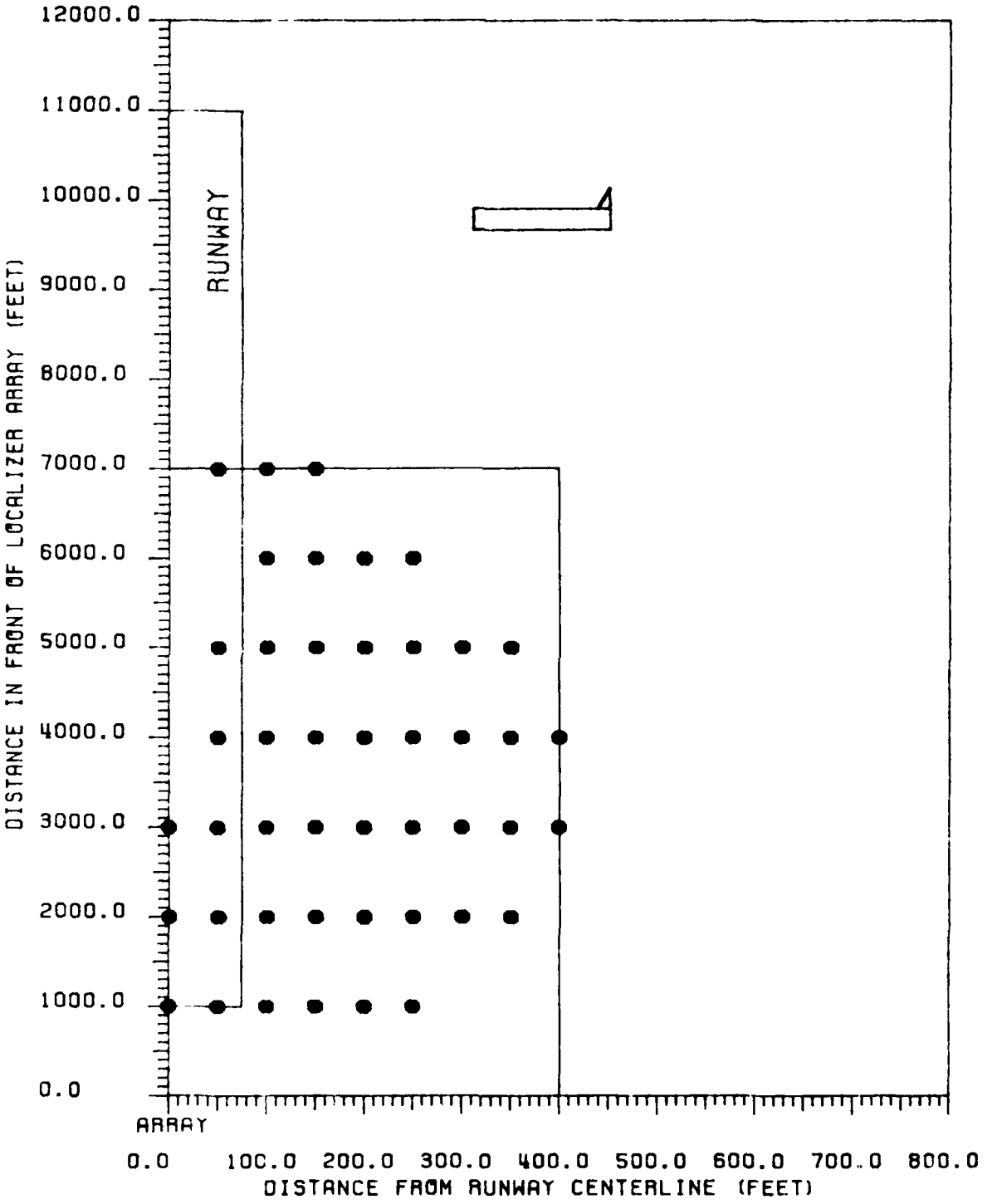

Figure 85 Critical area map for CAT II tolerances relating to B-747 aircraft. B-747 fuselage is perpendicular to runway centerline with tail away from runway. 8-element single-frequency array, LPD antennas.

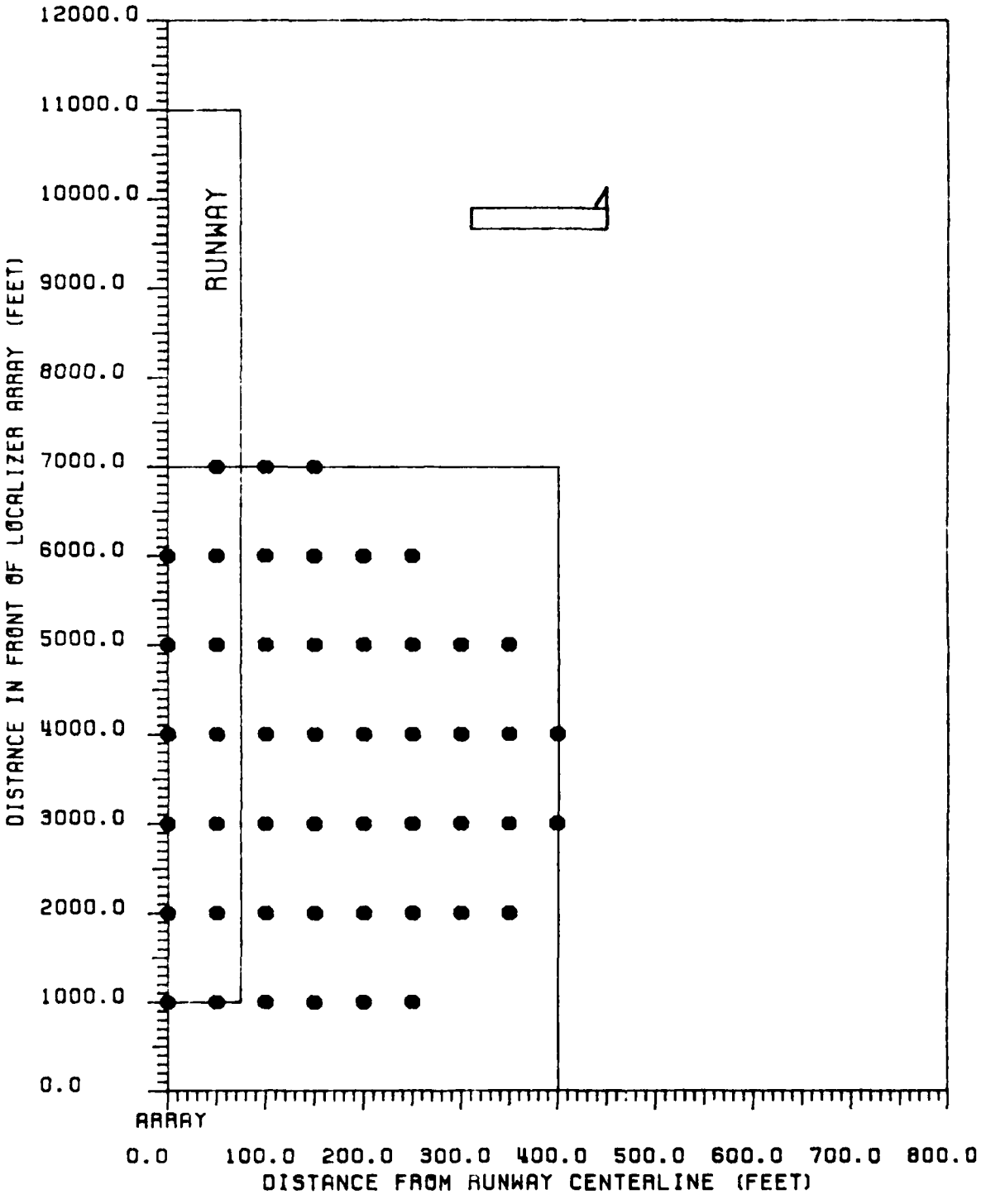

Figure 86 Critical area map for CAT III tolerances relating to B-747 aircraft. B-747 fuselage is perpendicular to runway centerline with tail away from runway. 8-element single-frequency array, LPD antennas.

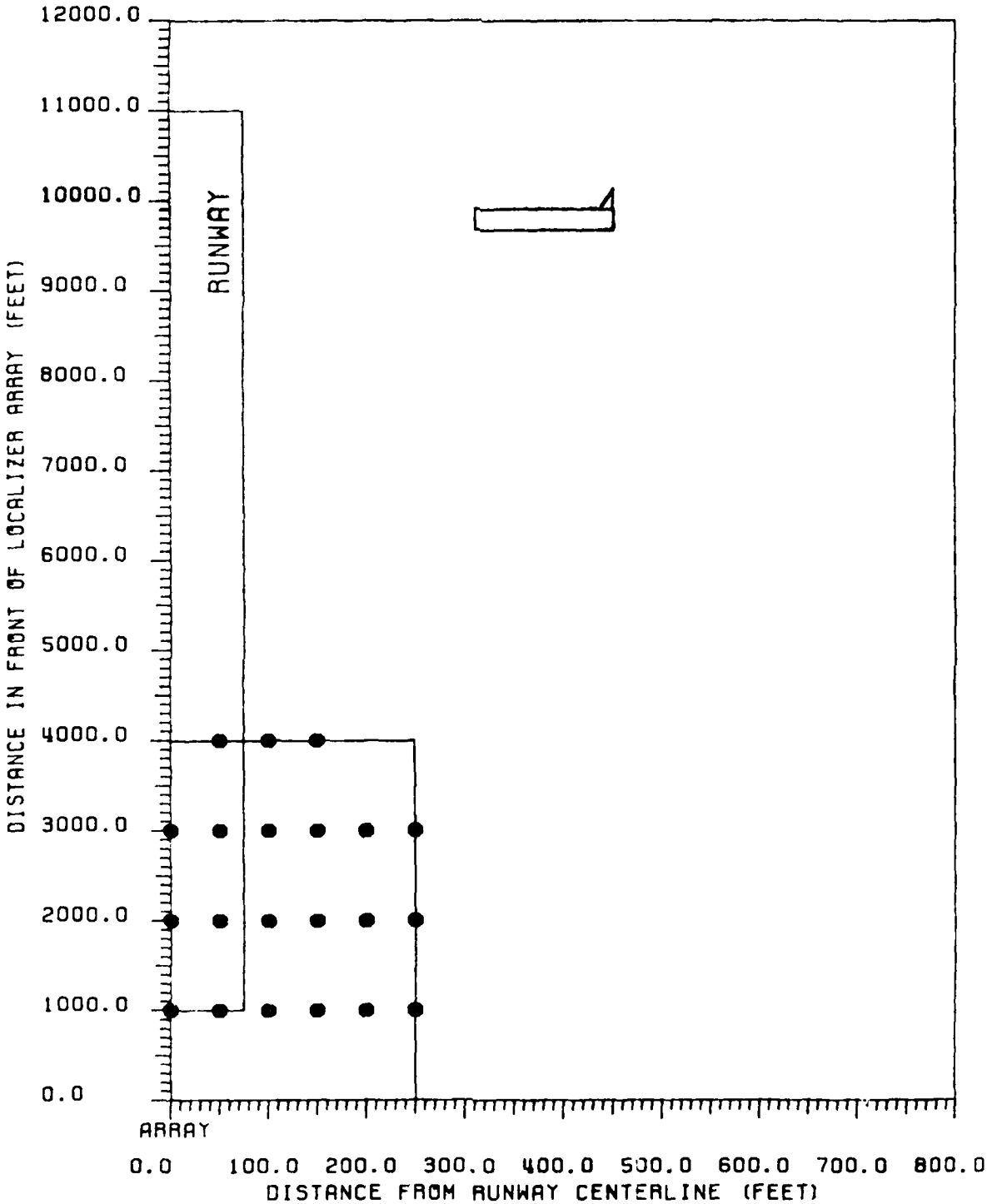

Figure 87 Critical area map for CAT III-X tolerances relating to B-747 aircraft. B-747 fuselage is perpendicular to runway centerline with tail away from runway. 8-element single-frequency array, LPD antennas.

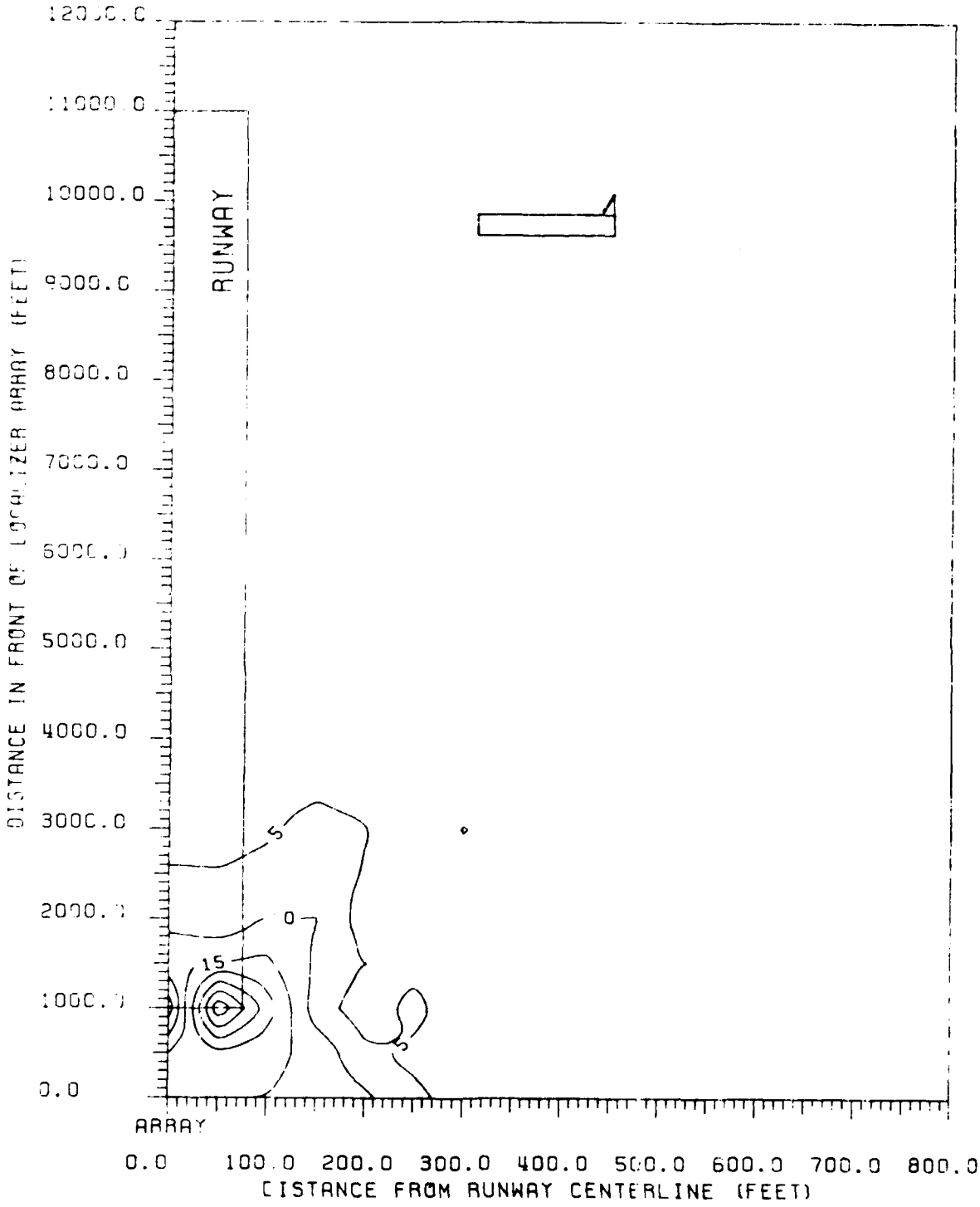

Figure 88 Contours of peak CDI values produced in ILS Zone 1 for a B-747. B-747 fuselage is perpendicular to runway centerline, with tail away from runway. 8-element single-frequency array, LPD antennas.

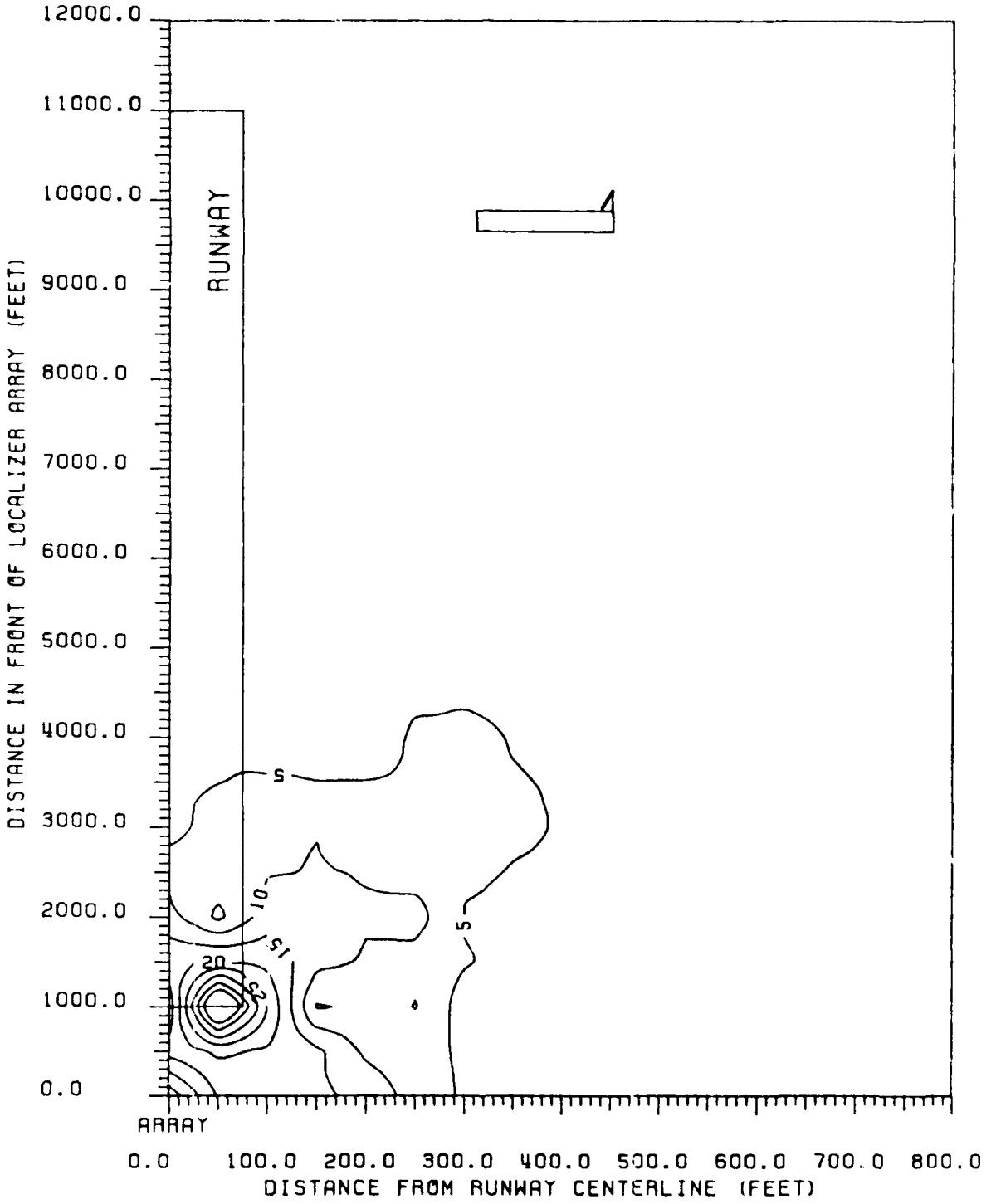

Figure 89 Contours of peak CDI values produced in ILS Zone 2 for a B-747. B-747 fuselage is perpendicular to runway centerline, with tail away from runway. 8-element single-frequency array, LPD antennas.

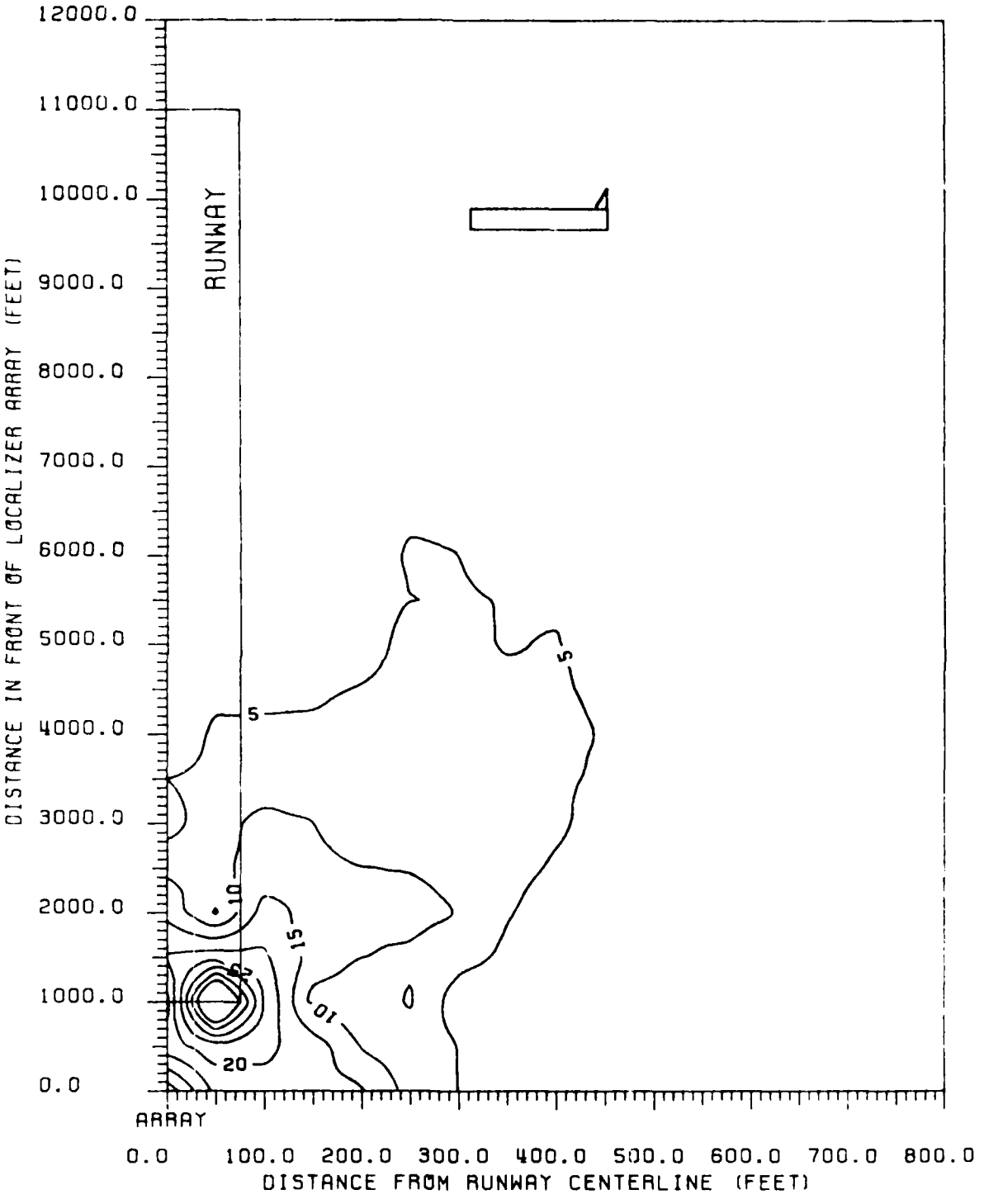

Figure 90 Contours of peak CDI values produced in ILS Zone 3 to Threshold for a B-747. B-747 fuselage is perpendicular to runway centerline, with tail away from runway. 8-element single-frequency array, LPD antennas.

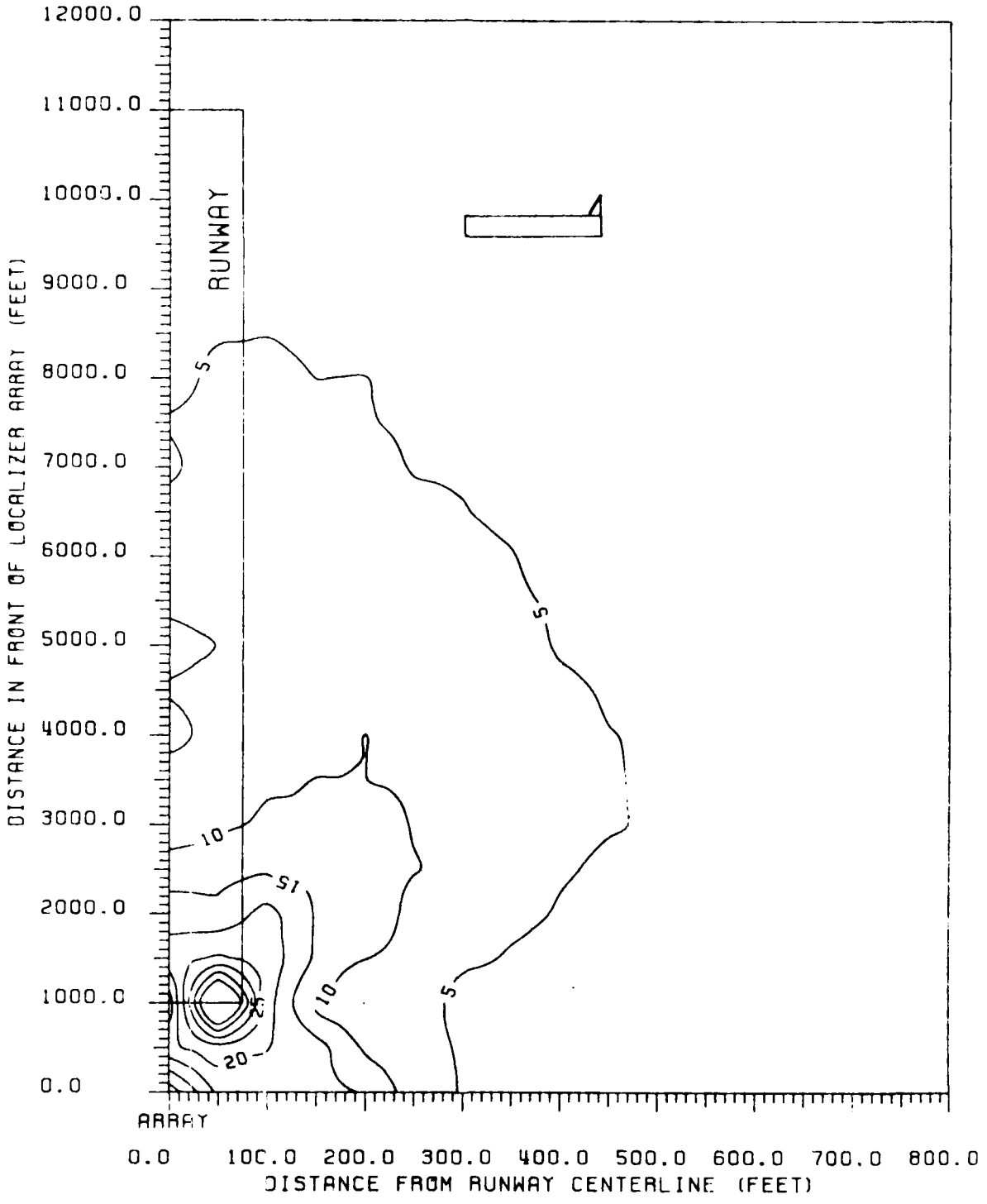

Figure 91 Contours of peak CDI values produced in ILS Zone 4 for a B-747. B-747 fuselage is perpendicular to runway centerline, with tail away from runway. 8-element single-frequency array, LPD antennas.

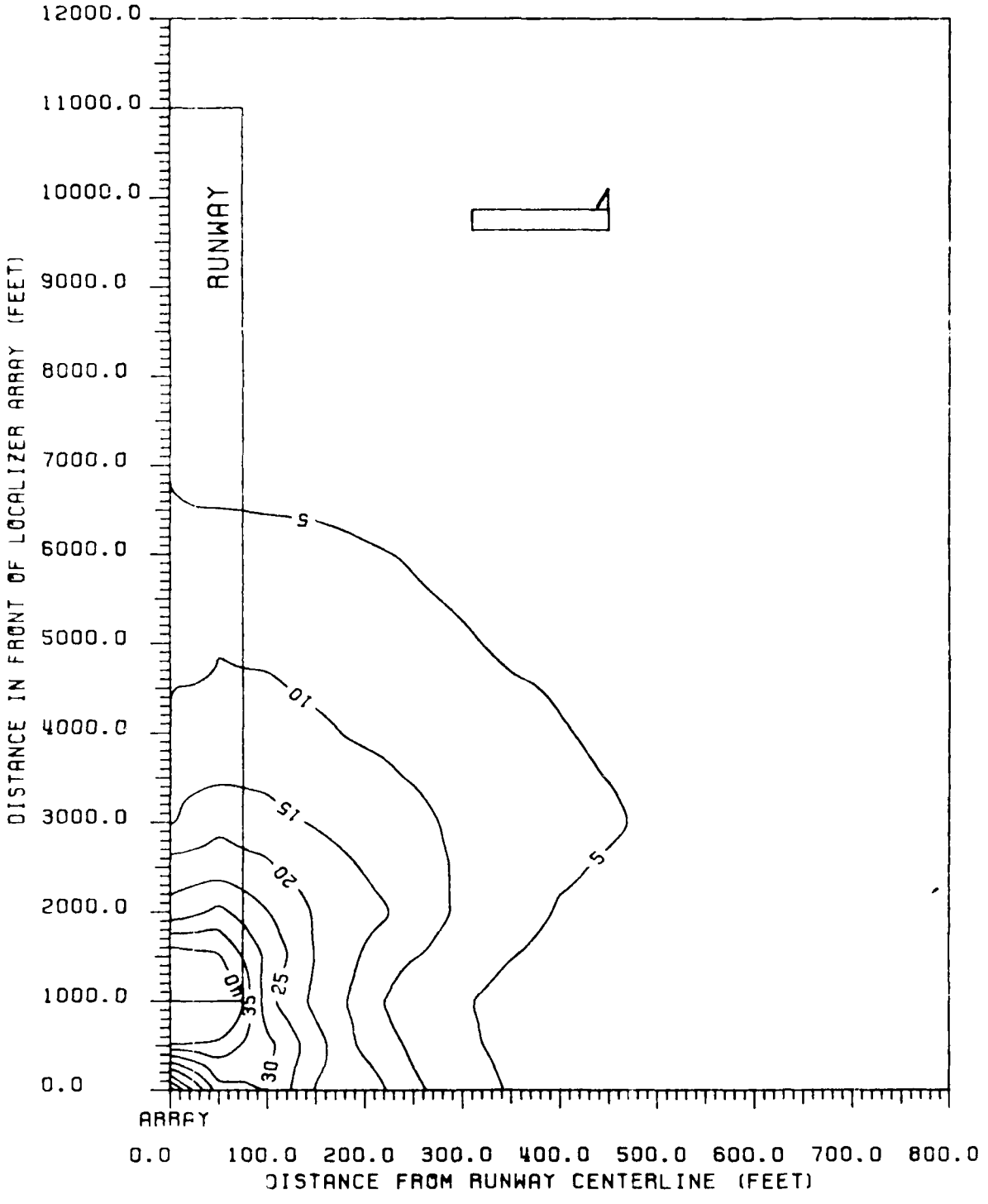

Figure 92 Contours of peak CDI values produced in ILS Zone 5 for a B-747. B-747 fuselage is perpendicular to runway centerline, with tail away from runway. 8-element single-frequency array, LPD antennas.

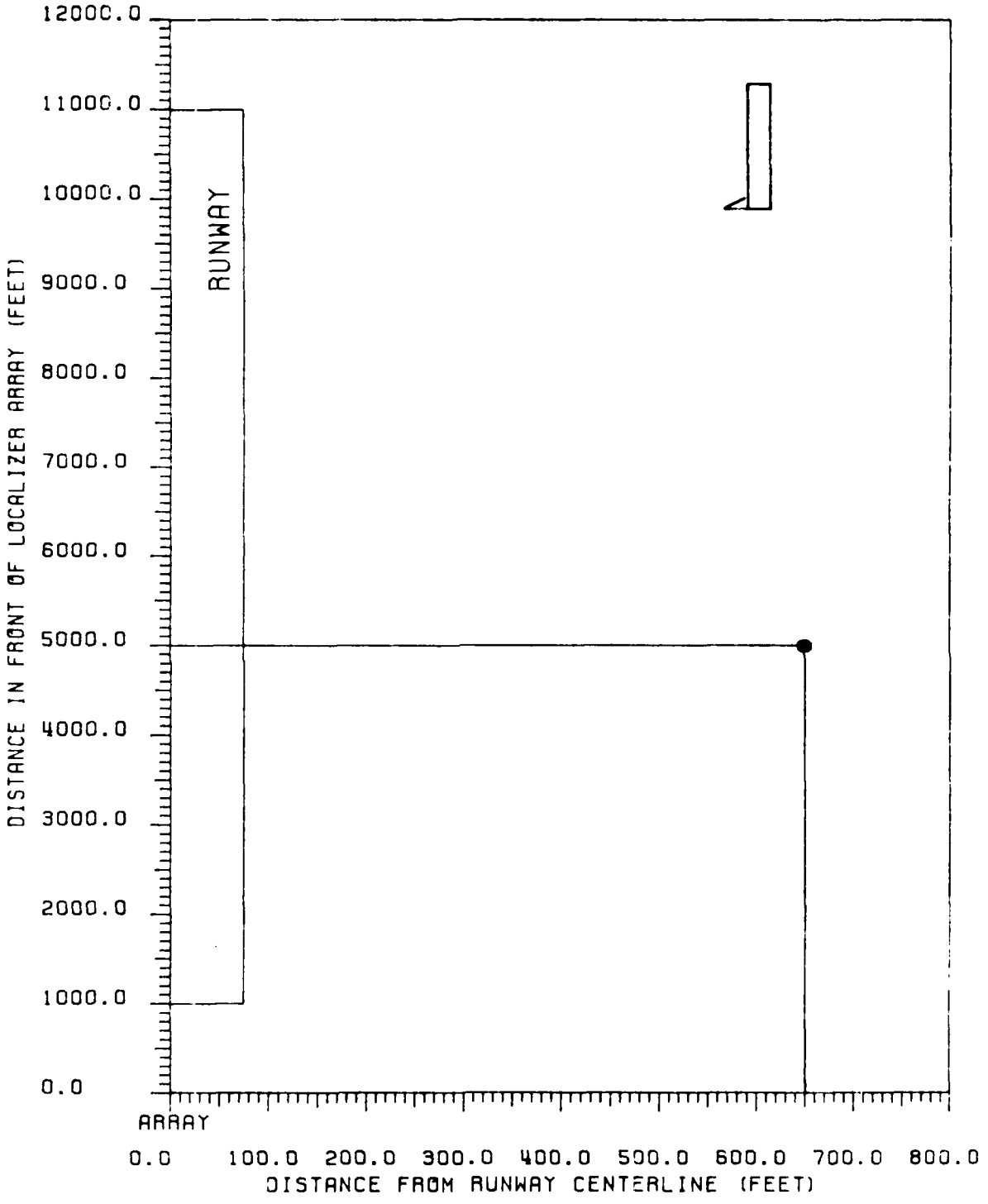

Figure 93 Critical area map for CAT II tolerances relating to B-747 aircraft. B-747 fuselage is parallel to runway centerline with tail towards the array. 8-element single-frequency array, LPD antennas.

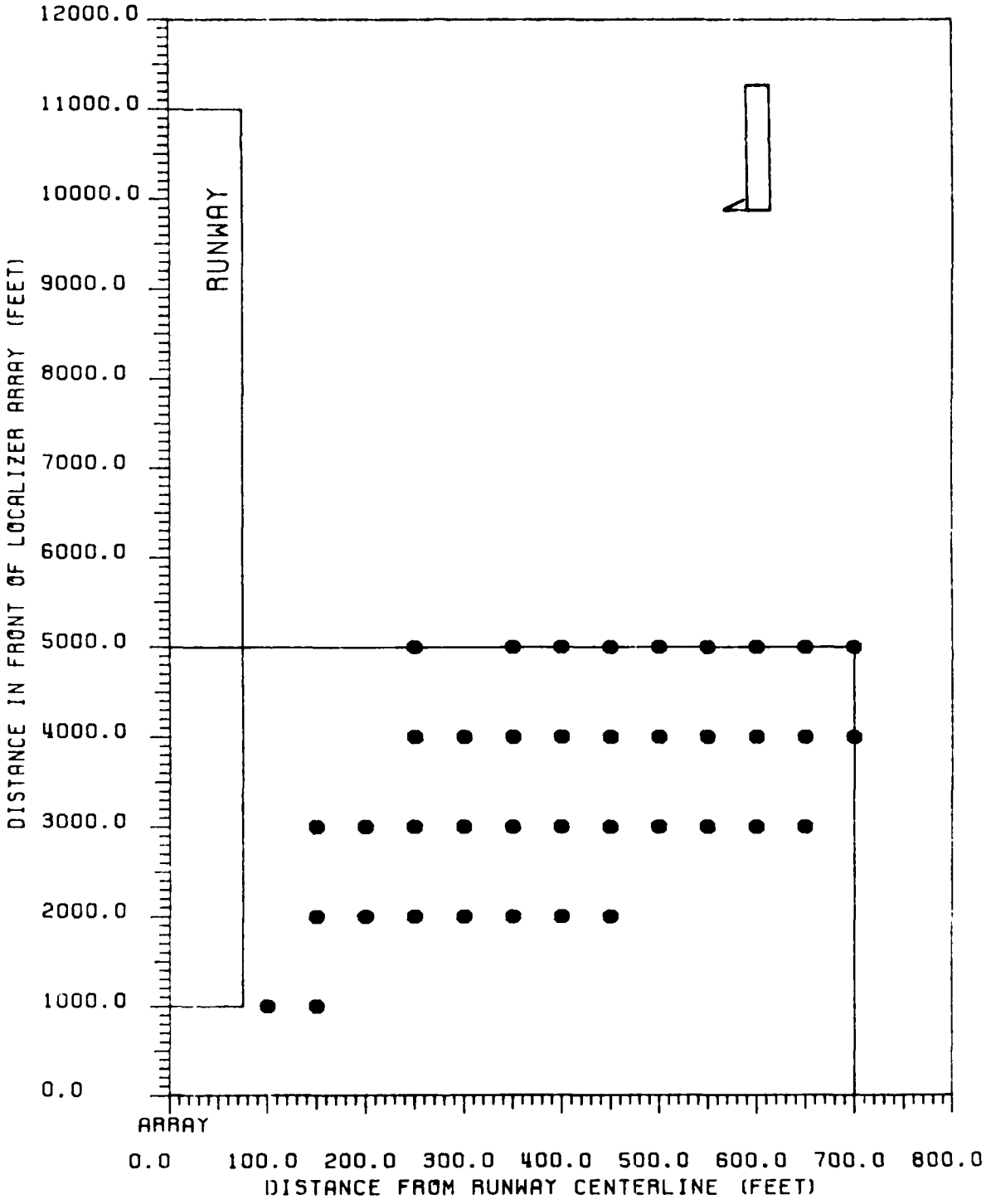

Figure 94 Critical area map for CAT III tolerances relating to B-747 aircraft. B-747 fuselage is parallel to runway centerline with tail towards the array. 8-element single-frequency array, LPD antennas.

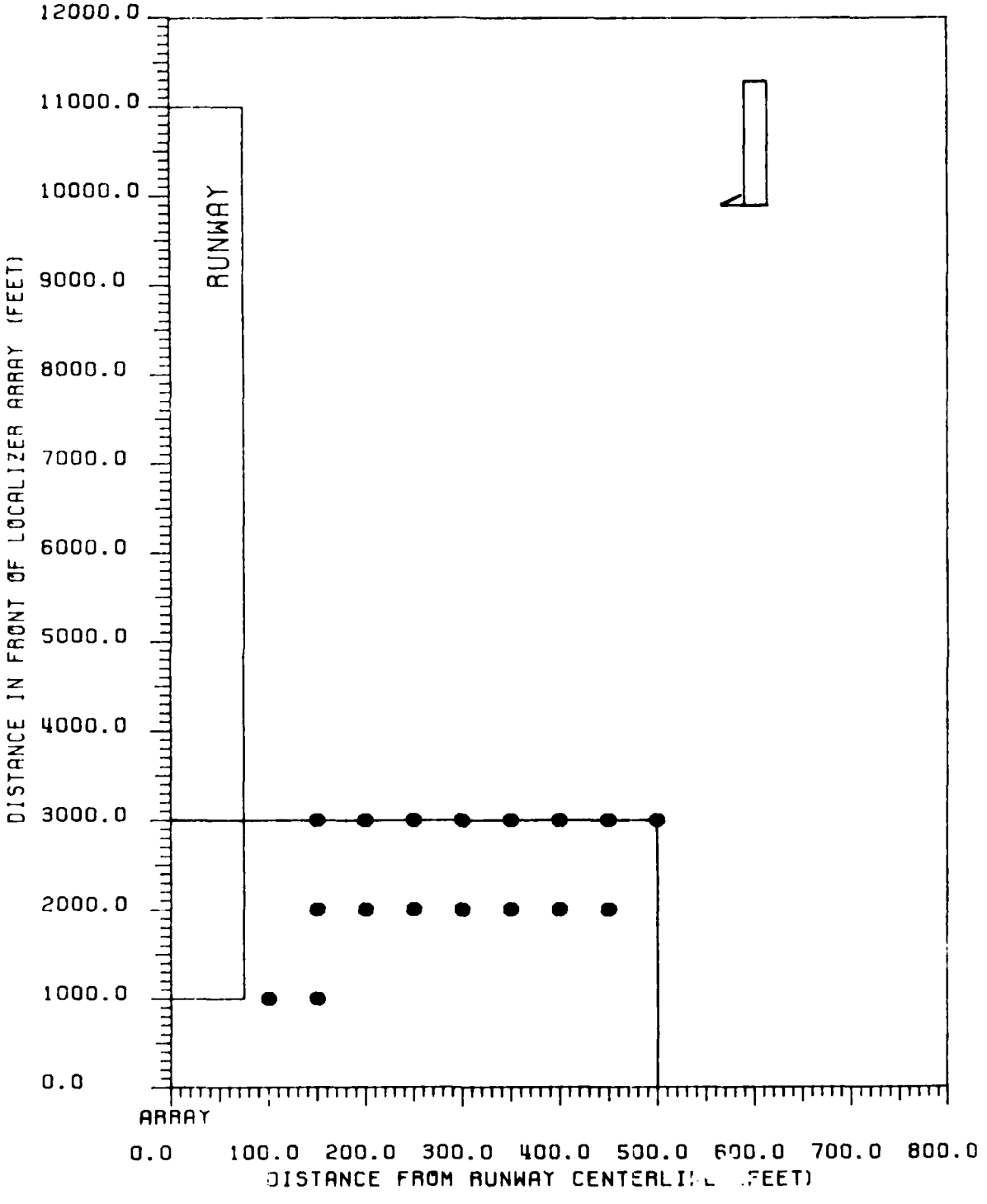

Figure 95 Critical area map for CAT III-X tolerances relating to B-747 aircraft. B-747 fuselage is parallel to runway centerline with tail towards the array. 8-element single-frequency array, LPD antennas.

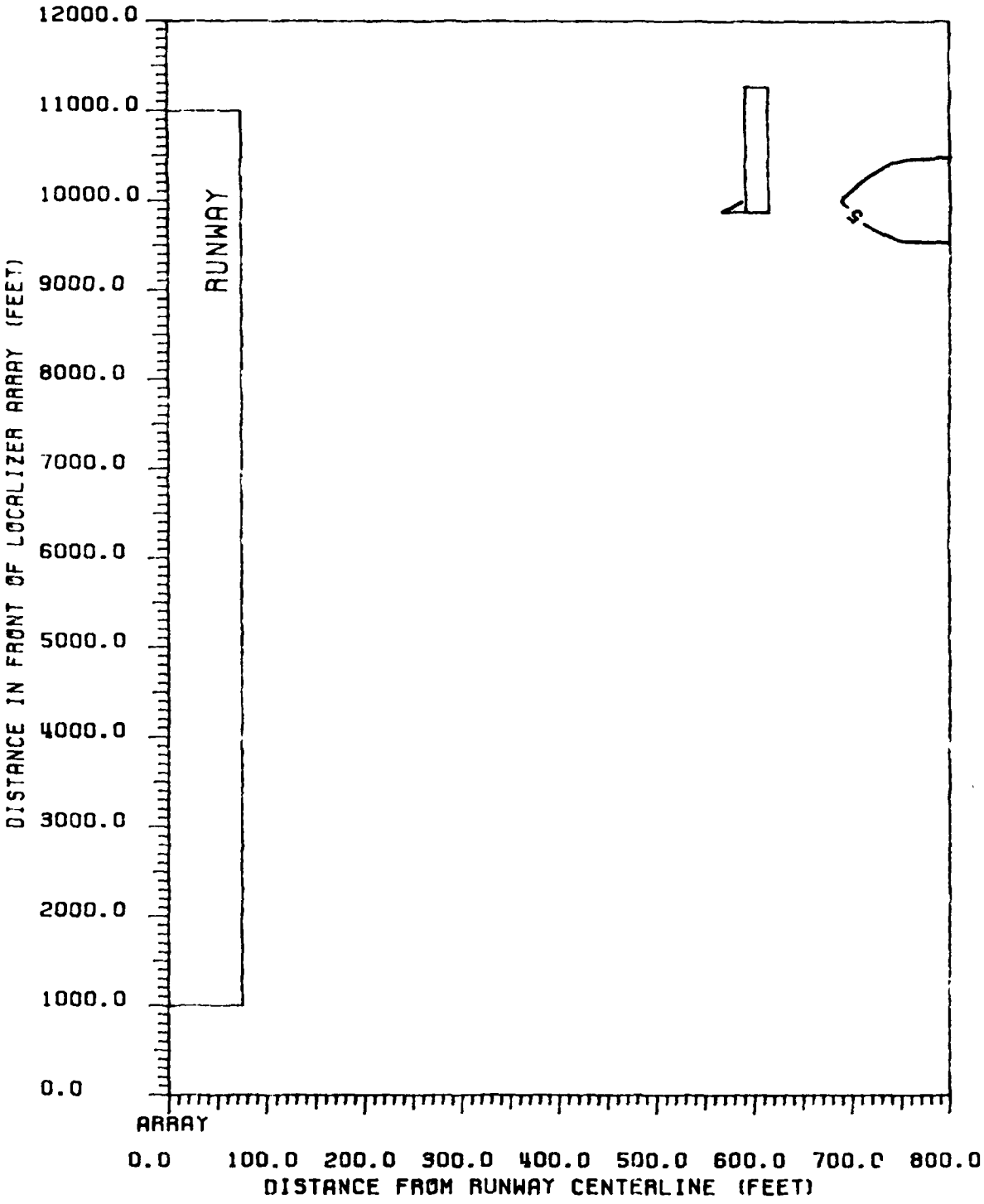

Figure 96 Contours of peak CDI values produced in ILS Zone 3 to Threshold for a B-747. B-747 fuselage is parallel to runway centerline, with tail towards the array. 8-element single-frequency array, LPD antennas.

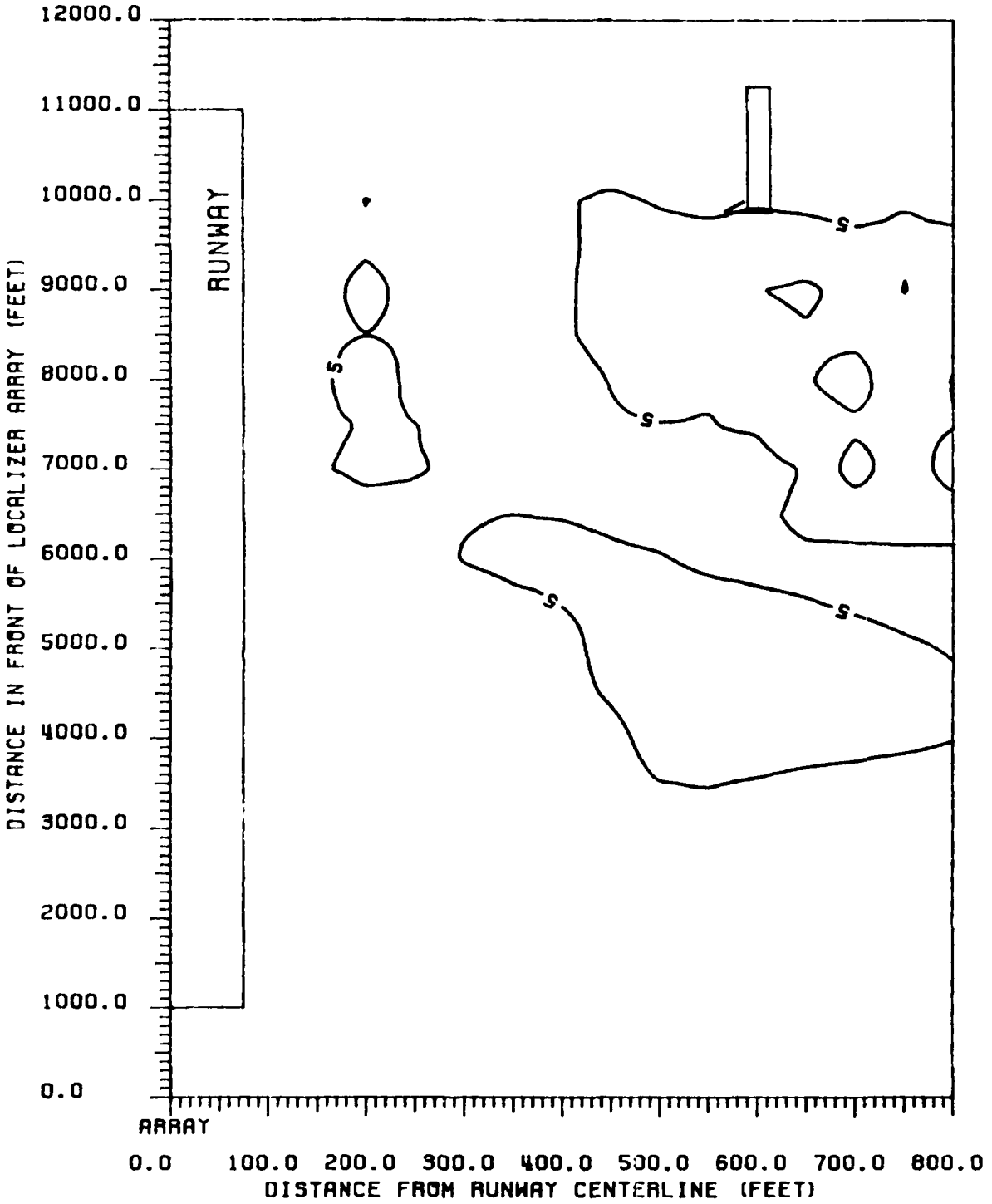

Figure 97 Contours of peak CDI values produced in ILS Zone 4 for a B-747. B-747 fuselage is parallel to runway centerline, with tail towards the array. 8-element single-frequency array, LPD antennas.

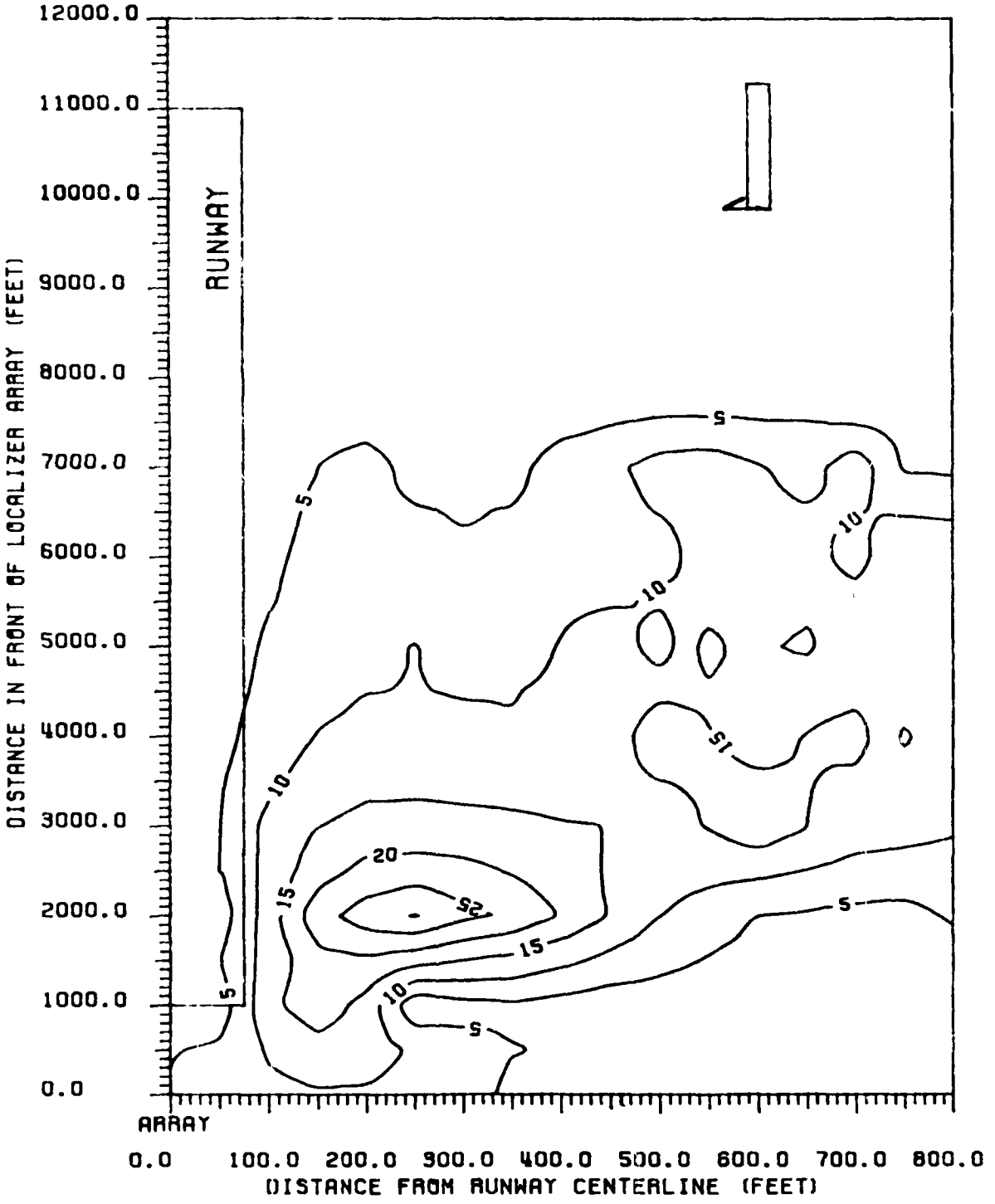

Figure 98 Contours of peak CDI values produced in ILS Zone 5 for a B-747. B-747 fuselage is parallel to runway centerline, with tail towards the array. 8-element single-frequency array, LPD antennas.

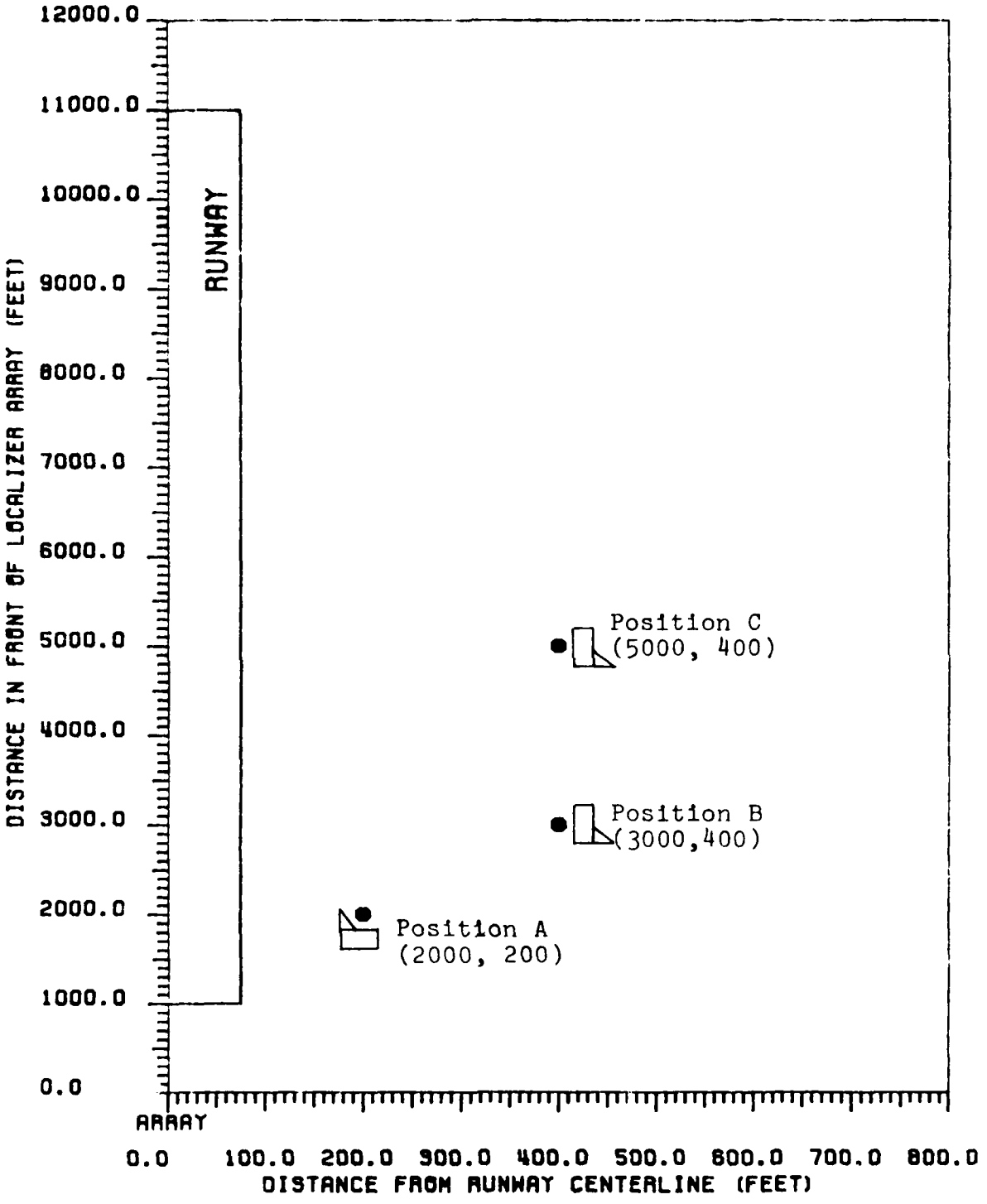

Figure 99 Positions and orientations of three L-1011 aircraft used to examine the impact of multiple reflectors.

through 105 show the localizer course structure for a specific position of scatterer(s). Category III tolerances are drawn on each plot for comparison purposes.

Figure 100 shows the localizer course structure with an L-1011 aircraft located at position A. This is intended to represent an aircraft that has just landed, and is turning off the runway at the last taxiway. The structure obviously exceeds CAT III tolerances. Figure 101 shows the localizer course structure with an L-1011 positioned at location B, while figure 102 shows the structure with an L-1011 at position C. These structures also exceed CAT III tolerances, though by lesser amounts. Figures 103 through 105 demonstrate the effects of combining scatterers A, B, and C. Figure 103 is the localizer structure resulting from scatterers A and B simultaneously. Figure 104 shows the effects of combining scatterers A and C, while figure 105 demonstrates the combination of scatterer B and C. In each case, the resulting CDI is basically the sum of the individual CDI values. All combinations of these three scatterer locations exceed CAT III tolerances by a larger amount than any individual scatterer. Several other cases of multiple reflectors are studied. No cases are identified in which the combined scatterers have less effect than any individual scatterer, suggesting that cancellation of the electromagnetic fields is probably more rare than their addition. However, there are also no cases identified in which the combination of scatterers causes a greater perturbation than N times the effect of an individual scatterer.

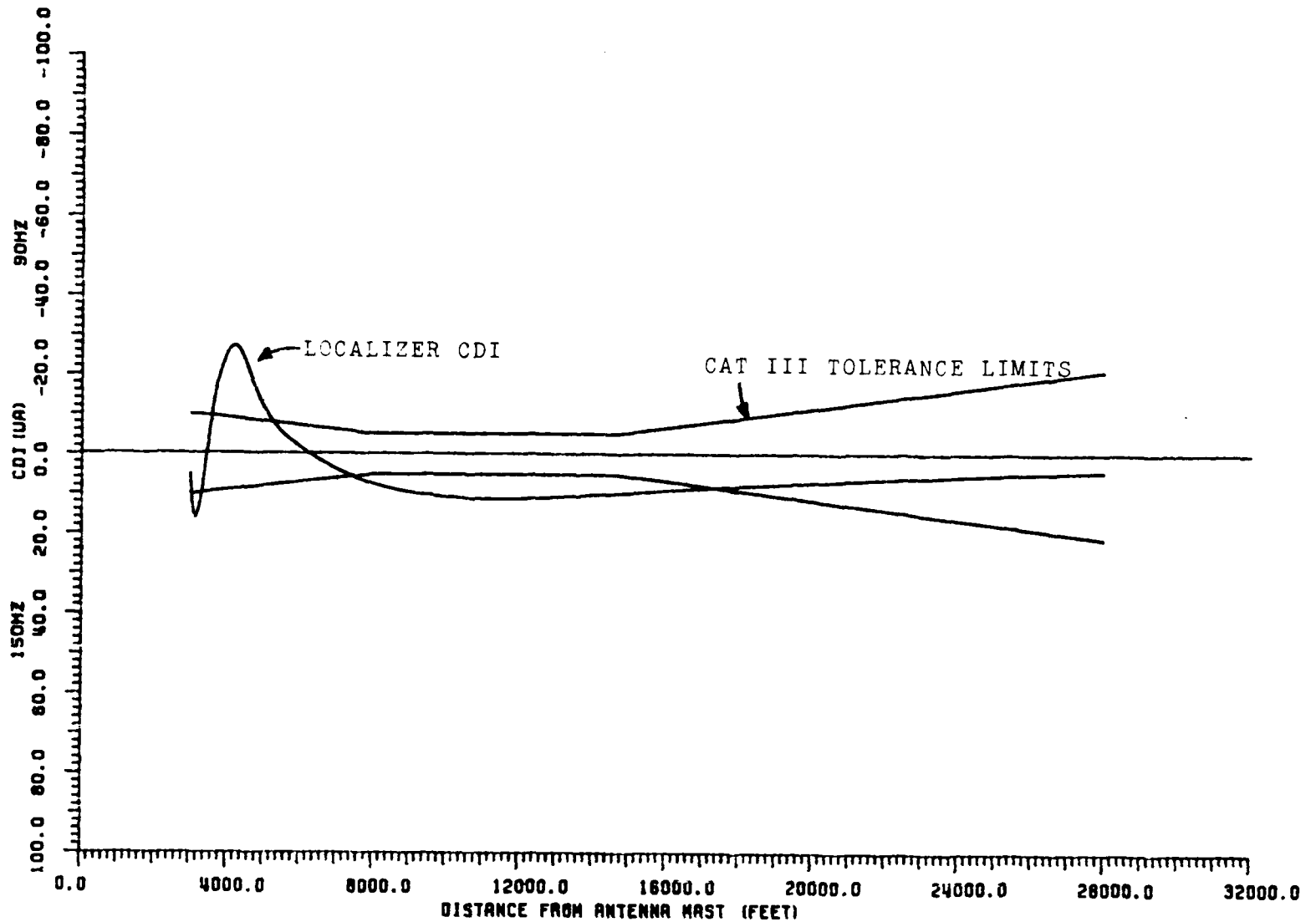

Figure 100 CDI plot with CAT III tolerance limits. Perturbations are caused by a single L-1011 aircraft located at position A.

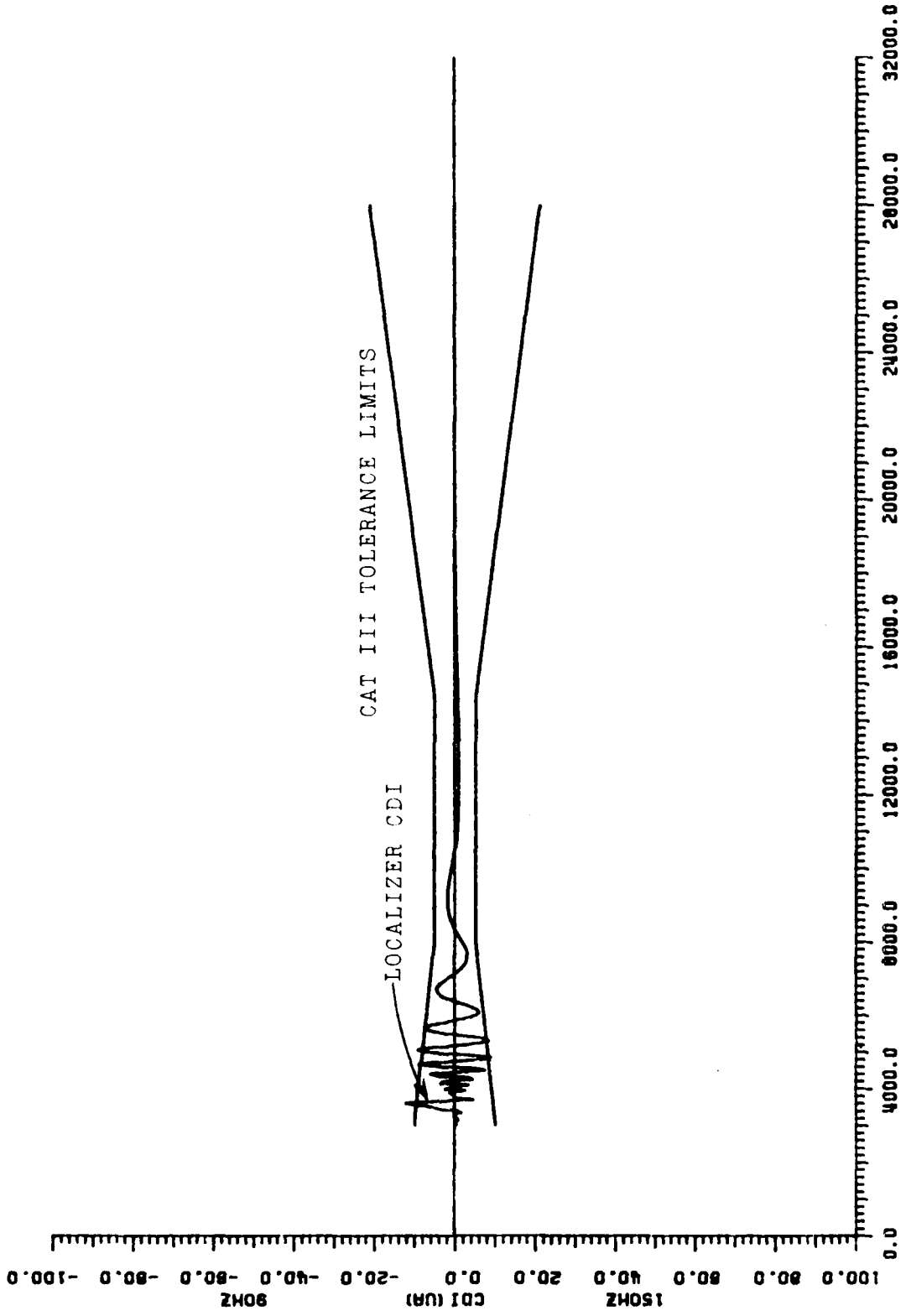

Figure 101 CDI plot with CAT III tolerance limits. Perturbations are caused by a single L-1011 aircraft located at position B.

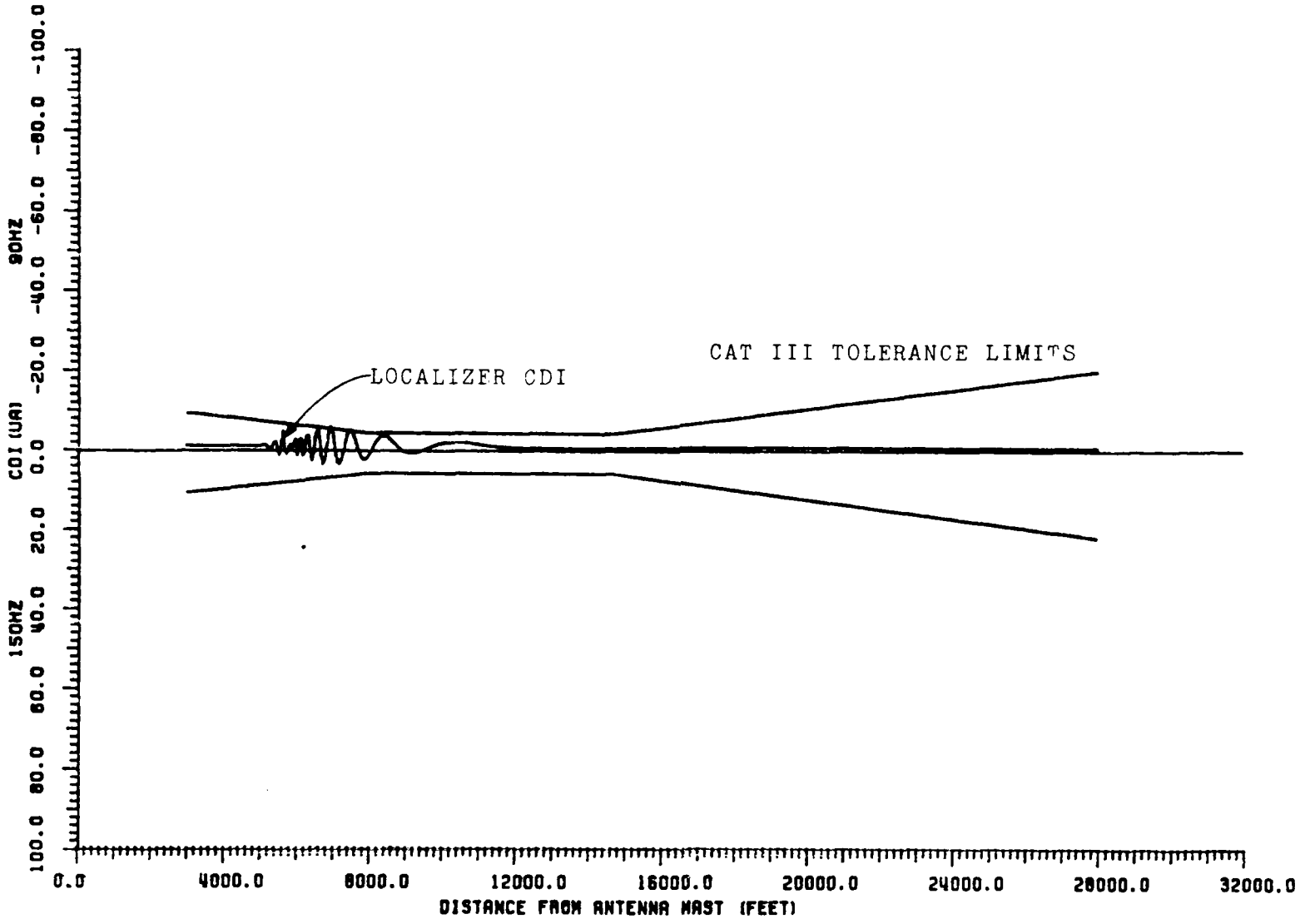

Figure 102 CDI plot with CAT III tolerance limits. Perturbations are caused by a single L-1011 aircraft located at position C.

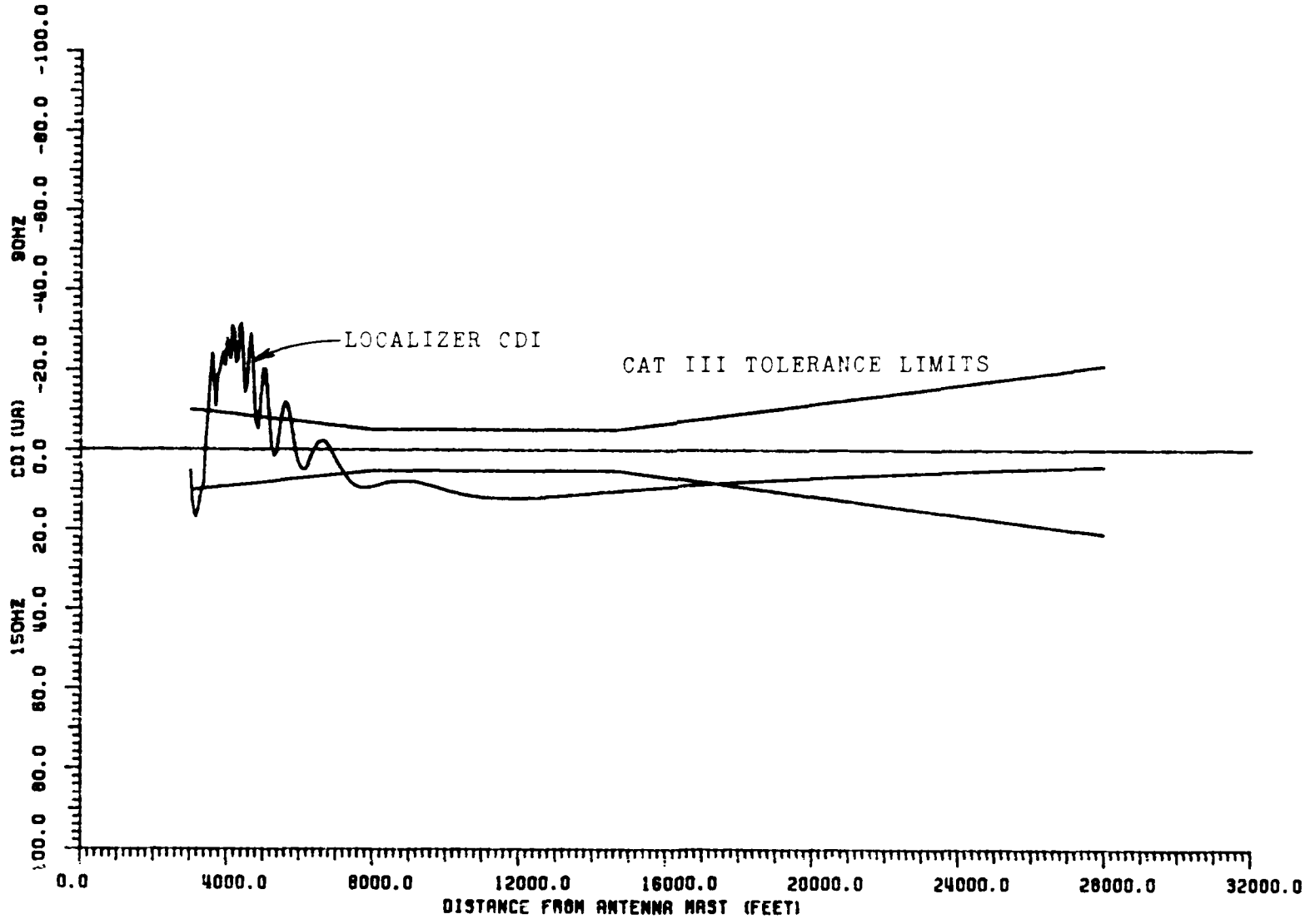

Figure 103 CDI plot with CAT III tolerance limits. Perturbations are caused by two L-1011 aircraft. One is located at position A, the other at position B.

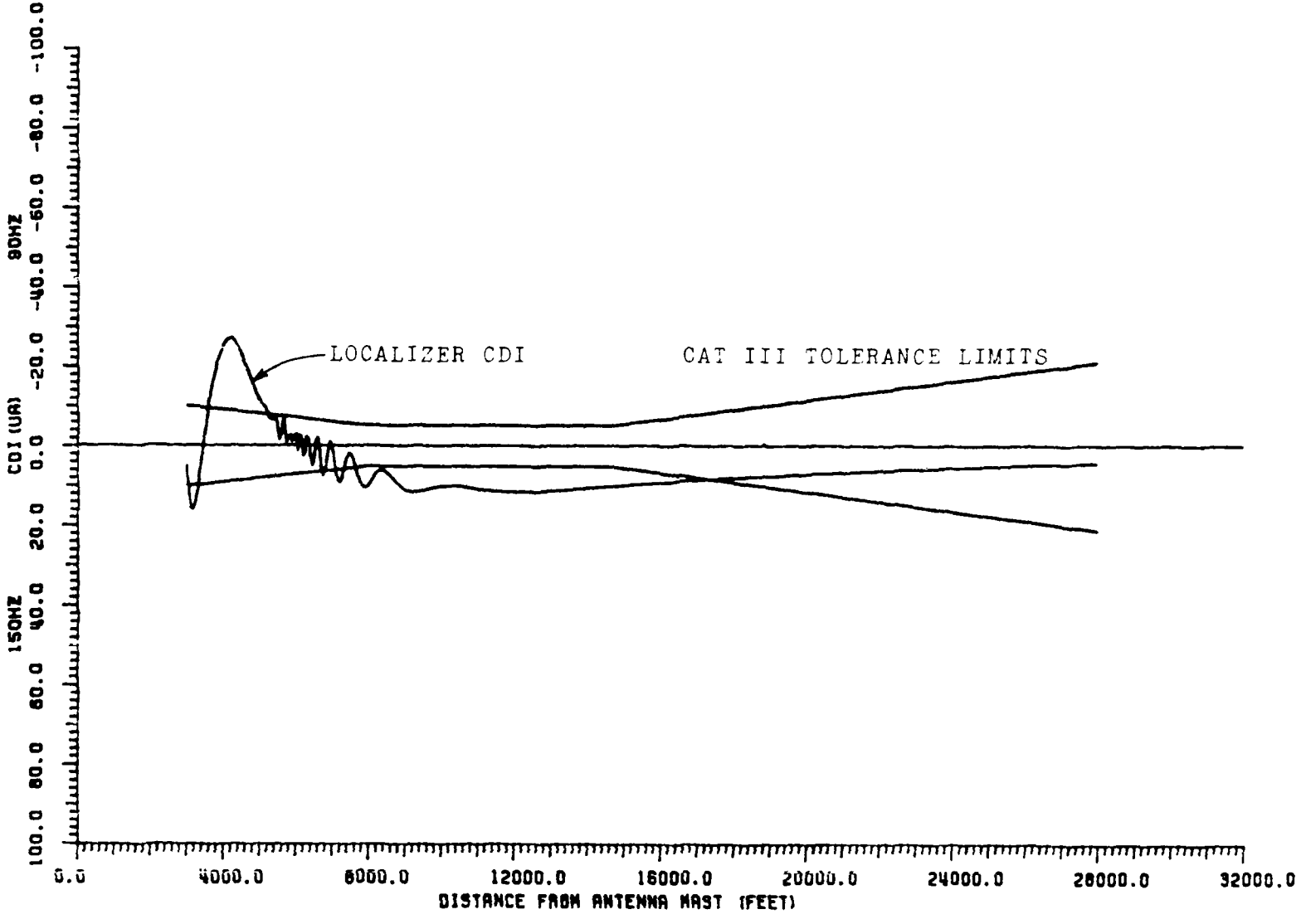

Figure 104 CDI plot with CAT III tolerance limits. Perturbations are caused by two L-1011 aircraft. One is located at position A, the other at position C.

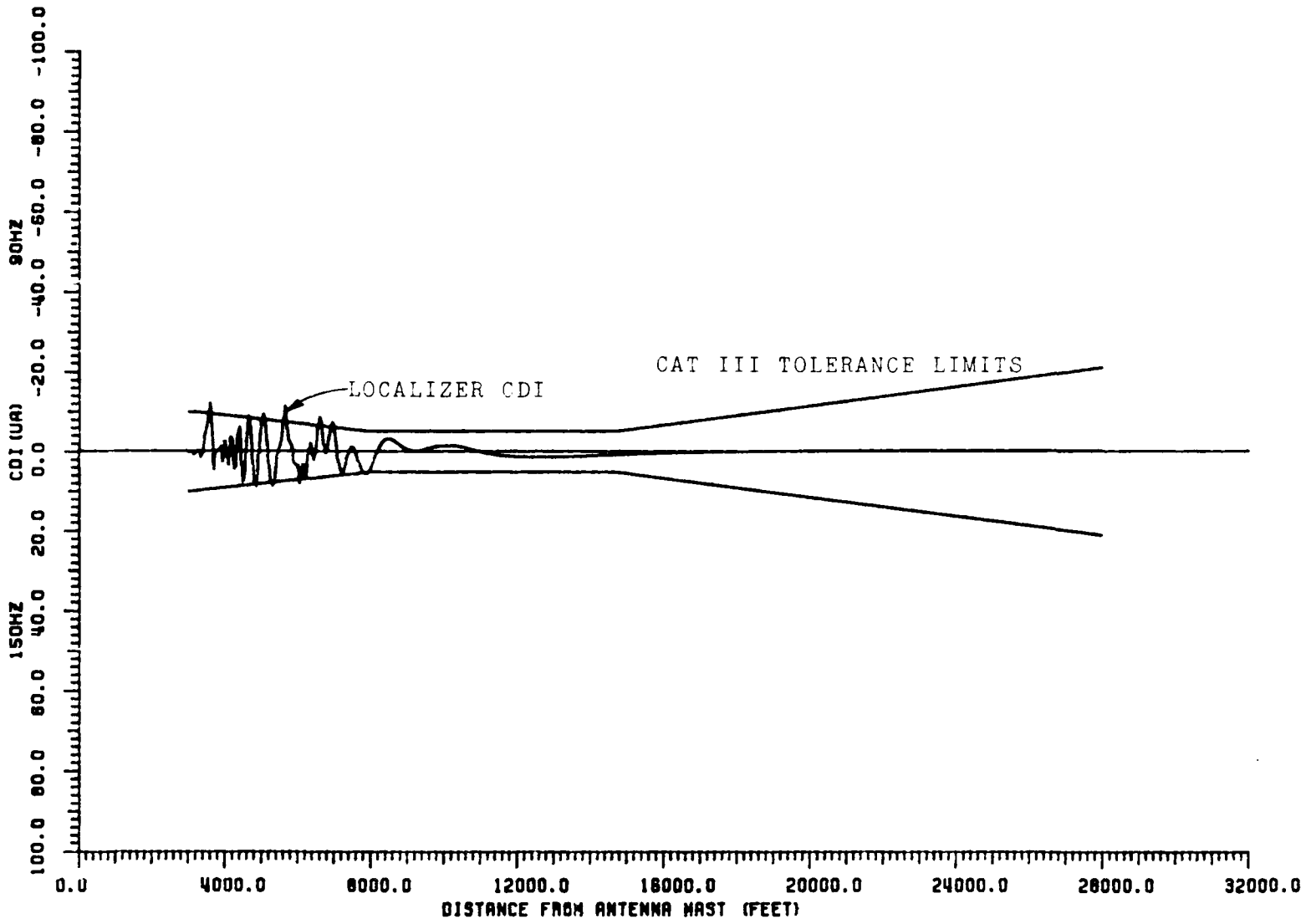

Figure 105 CDI plot with CAT III tolerance limits. Perturbations are caused by two L-1011 aircraft. One is located at position B, the other at position C.

VII. COMPARISONS WITH 14-ELEMENT, SINGLE-FREQUENCY ARRAY

Many of the earlier studies of localizer critical area have been limited in their scope, dealing only with one specific type of reflector, or using input data based on a specific airport. In the interests of standardizing the process of calculating localizer critical areas, a re-examination has been conducted of previous work dealing with 14-element, single-frequency localizers. The critical areas have been calculated using identical input data and assumptions that are used for the 8-element, single frequency localizer. The only exception is the actual array information. Table 10 provides the array data for the 14-element localizer.

It should be noted that significant improvements have been made in techniques for mathematical modeling of critical areas since previous reports were published. The method of filtering data, and the process of automatically analyzing every simulated approach in terms of flight check structure tolerances provide for more accurate determination of critical areas than previous efforts. This has led to correction and refinement of previously calculated and reported data, specifically [19].

Calculations have been completed for the 14-element array using the same scatterer aircraft as those used for the 8-element array. Several scatterer orientations are included in table 11, but plots are only presented for the worst case orientation. This is with the scatterer fuselage perpendicular to runway centerline, with tail towards the runway.

Table 11 summarizes the results of the 14-element single-frequency localizer calculations, and can be directly compared with the 8-element, single-frequency localizer results summarized in table 7. Dashes represent conditions for which there is no identified out-of-tolerance location. No contour maps are shown for ILS Zone 1.

ELEMENT	CSB LEVEL	CSB PHASE	SBO LEVEL	SBO PHASE	WAVELENGTH SPACING (λ)
7R	.060	0.00	.138	0.00	-4.80
6R	.060	0.00	.379	0.00	-4.05
5R	.212	0.00	.276	0.00	-3.30
4R	.212	0.00	.586	0.00	-2.55
3R	.394	0.00	.414	0.00	-1.80
2R	.394	0.00	.759	0.00	-1.05
1R	1.000	0.00	1.000	0.00	-.30
1L	1.000	0.00	1.000	180.00	.30
2L	.394	0.00	.759	180.00	1.05
3L	.394	0.00	.414	180.00	1.80
4L	.212	0.00	.586	180.00	2.55
5L	.212	0.00	.276	180.00	3.30
6L	.060	0.00	.379	180.00	4.05
7L	.060	0.00	.138	180.00	4.80

Table 10. Nominal values used to represent a 14-element single-frequency localizer.

	CAT I x, y*	CAT II x, y*	CAT III x, y*	CAT III-X x, y*
DC-9 perp, tail away CL	--	--	--	--
DC-9 perp, tail to CL	--	--	--	--
DC-9 para, tail away array	--	--	--	--
DC-9 para, tail to array	--	--	--	--
DC-9 60°, tail to array	--	--	--	--
B-727 perp, tail away CL	--	--	1000,0	1000,0
B-727 perp, tail to CL	--	1000,100	1000,100	1000,0
B-727 para, tail away array	--	--	--	--
B-727 para, tail to array	--	--	--	--
B-727 60°, tail to array	--	--	--	--
B-707 perp, tail away CL	--	1000,0	1000,0	1000,0
B-707 perp, tail to CL	--	1000,100	2000,150	1000,150
B-707 para, tail away array	--	--	--	--
B-707 para, tail to array	--	--	--	--
B-707 60°, tail to array	--	950,75	950,75	950,25
L-1011 perp, tail away CL	1000,0	3000,125	3000,125	2000,0
L-1011 perp, tail to CL	1000,125	5000,275	5000,275	3000,225
L-1011 para, tail away array	--	--	--	--
L-1011 para, tail to array	--	--	--	--
L-1011 60°, tail to array	925,0	2925,125	2925,125	1925,75
B-747 perp, tail away CL	1000,0	7000,150	7000,150	4000,50
B-747 perp, tail to CL	2000,200	9000,400	9000,400	5000,250
B-747 para, tail away array	--	--	1900,200	1900,200
B-747 para, tail to array	--	--	2900,250	2900,250
B-747 60°, tail to array	925,0	5925,200	5925,250	3925,100

* x = distance in front of localizer array to nearest point on aircraft longitudinal axis

y = distance perpendicular to runway centerline to nearest point on aircraft longitudinal axis

-- = no identified out-of-tolerance locations X > 1000' and Y > 0'

Table 11. Critical area vs. aircraft orientation for 14-element single-frequency array.

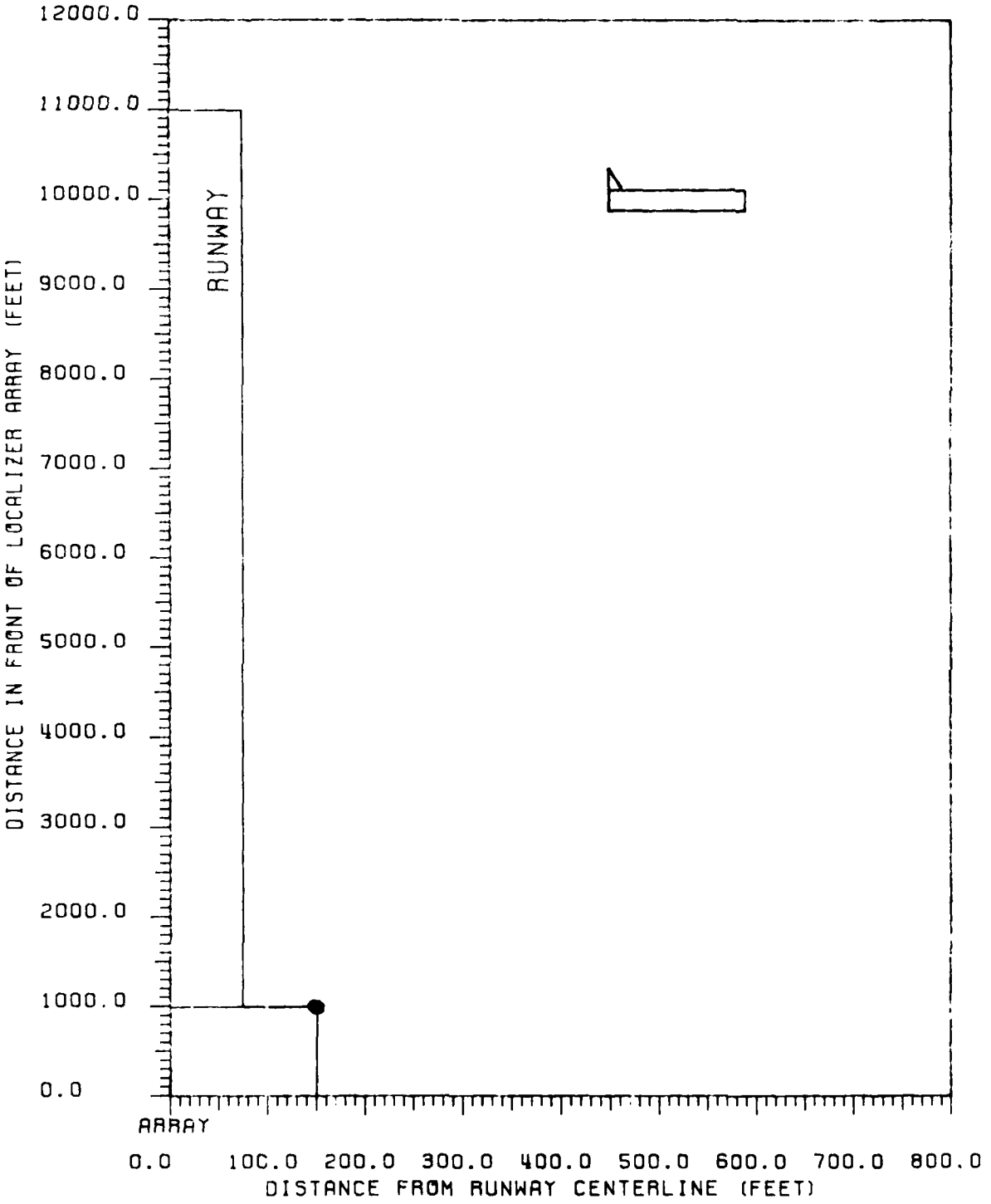

Figure 106 Critical area map for CAT II tolerances relating to B-727 aircraft. B-727 fuselage is perpendicular to runway centerline with tail towards the runway. 14-element single-frequency array, LPD antennas.

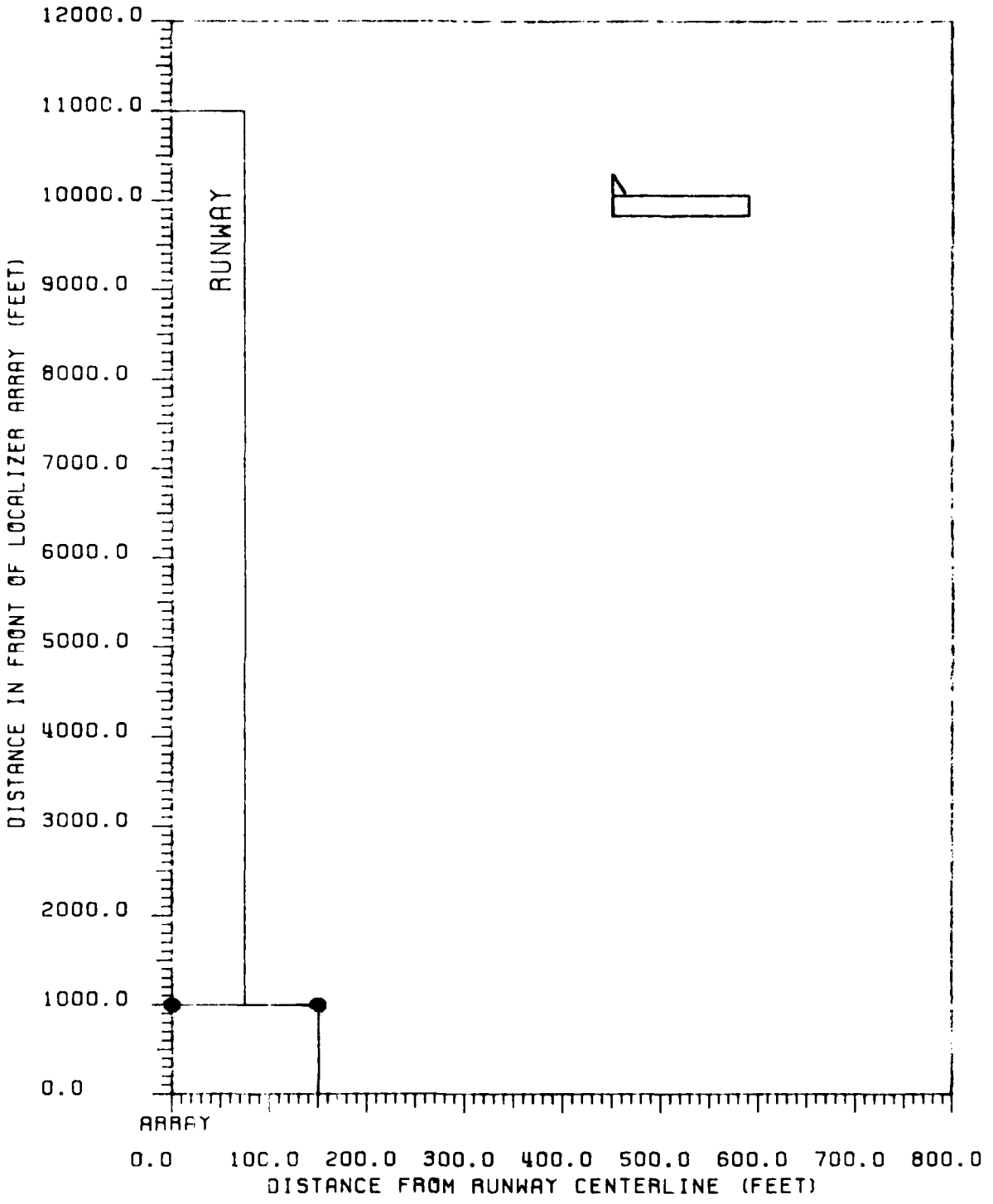

Figure 107 Critical area map for CAT III tolerances relating to B-727 aircraft. B-727 fuselage is perpendicular to runway centerline with tail towards the runway. 14-element single-frequency array, LPD antennas.

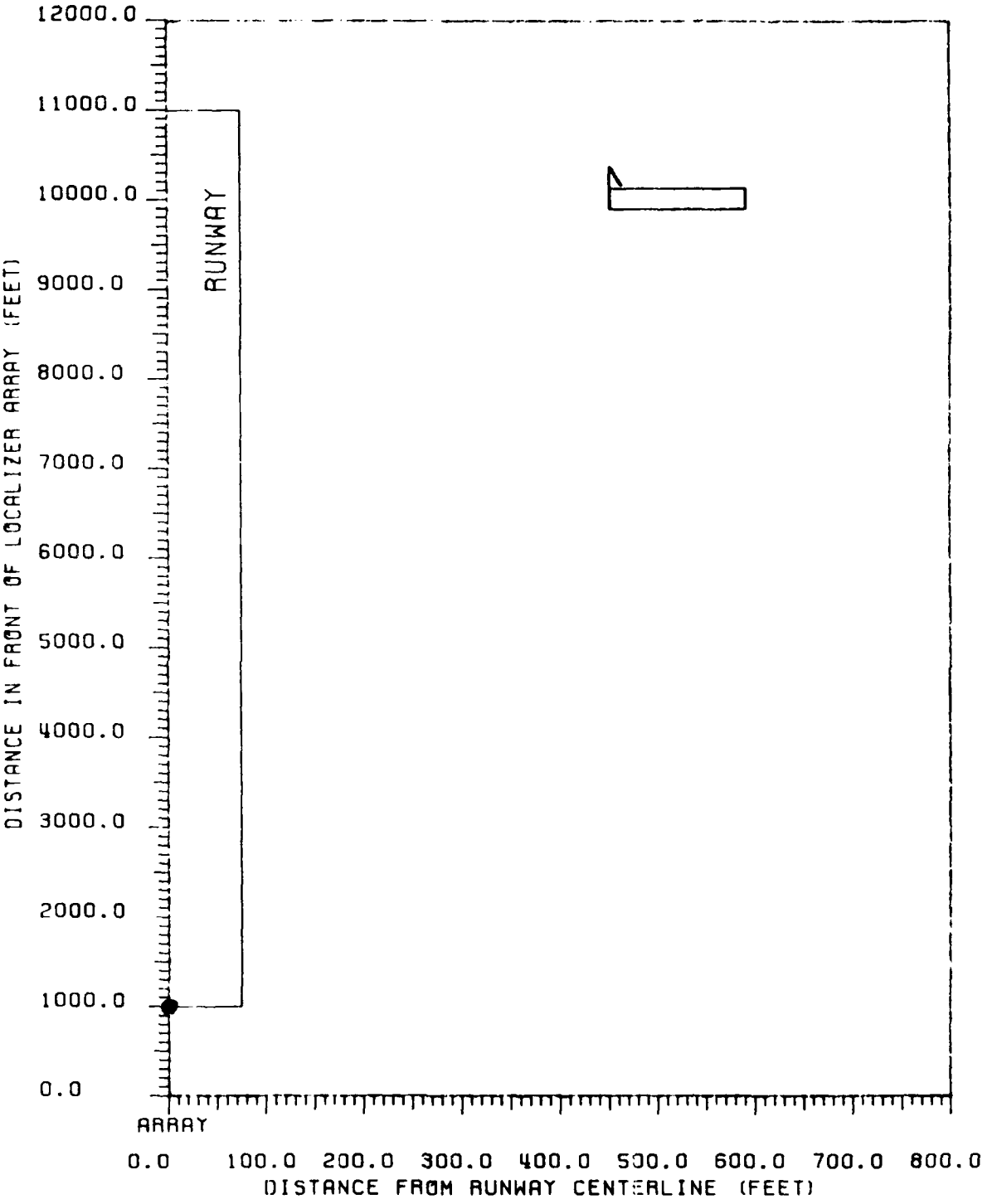

Figure 108 Critical area map for CAT III-X tolerances relating to B-727 aircraft. B-727 fuselage is perpendicular to runway centerline with tail towards the runway. 14-element single-frequency array, LPD antennas.

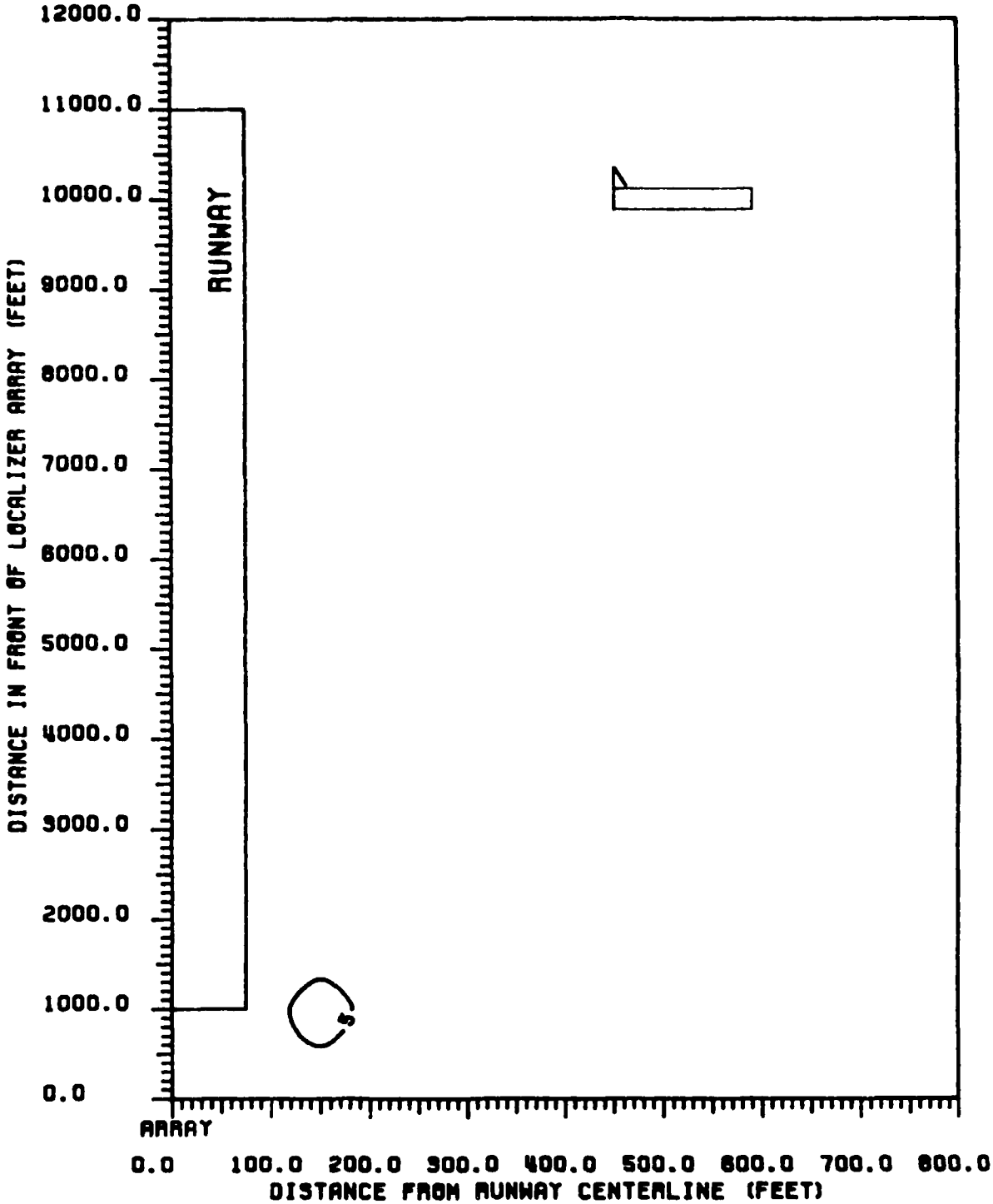

Figure 109 Contours of peak CDI values produced in ILS Zone 2 for a B-727. B-727 fuselage is perpendicular to runway centerline, with tail towards the runway. 14-element single-frequency array, LPD antennas.

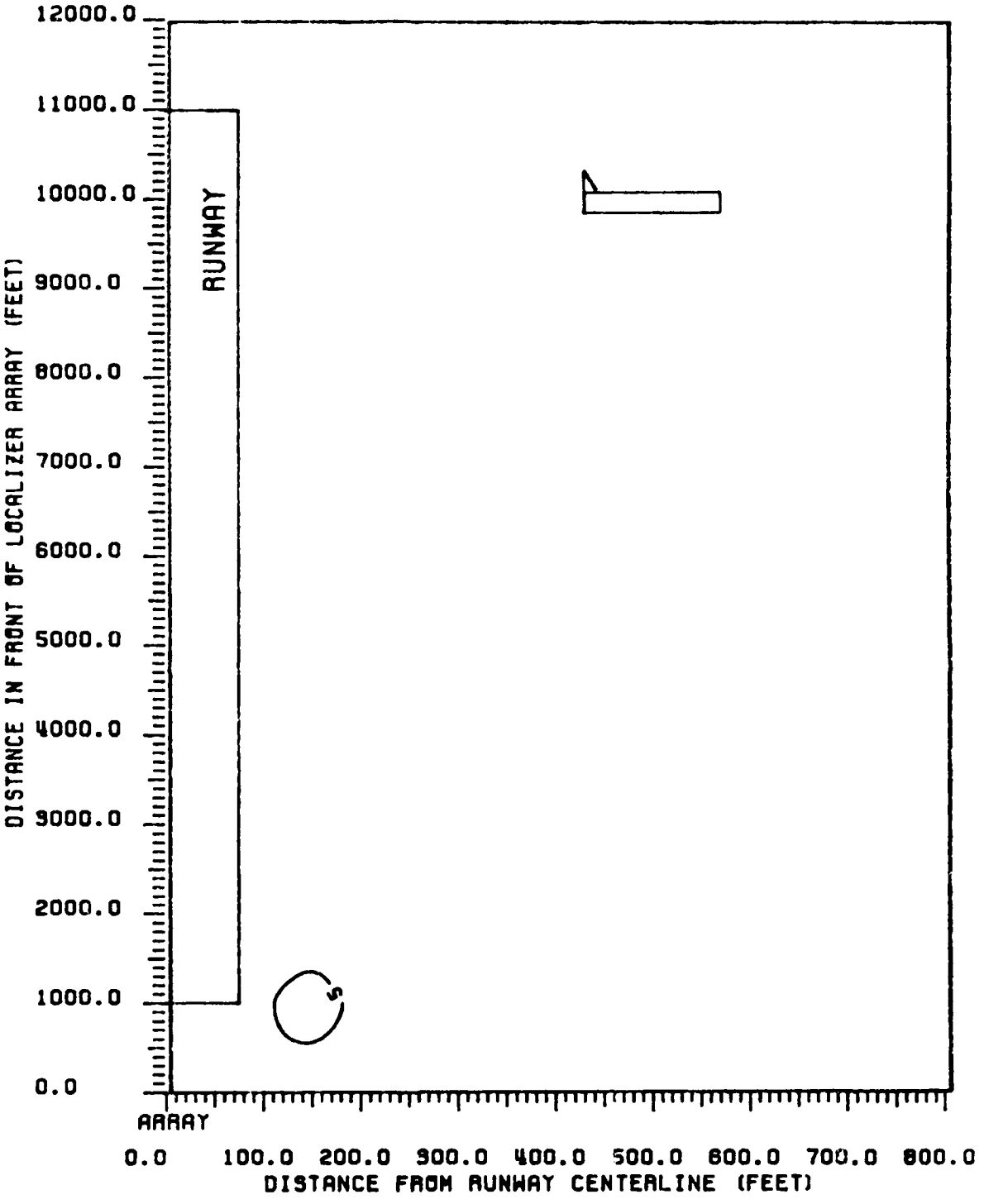

Figure 110 Contours of peak CDI values produced in ILS Zone 3 to Threshold for a B-727. B-727 fuselage is perpendicular to runway centerline, with tail towards the runway. 14-element single-frequency array, LPD antennas.

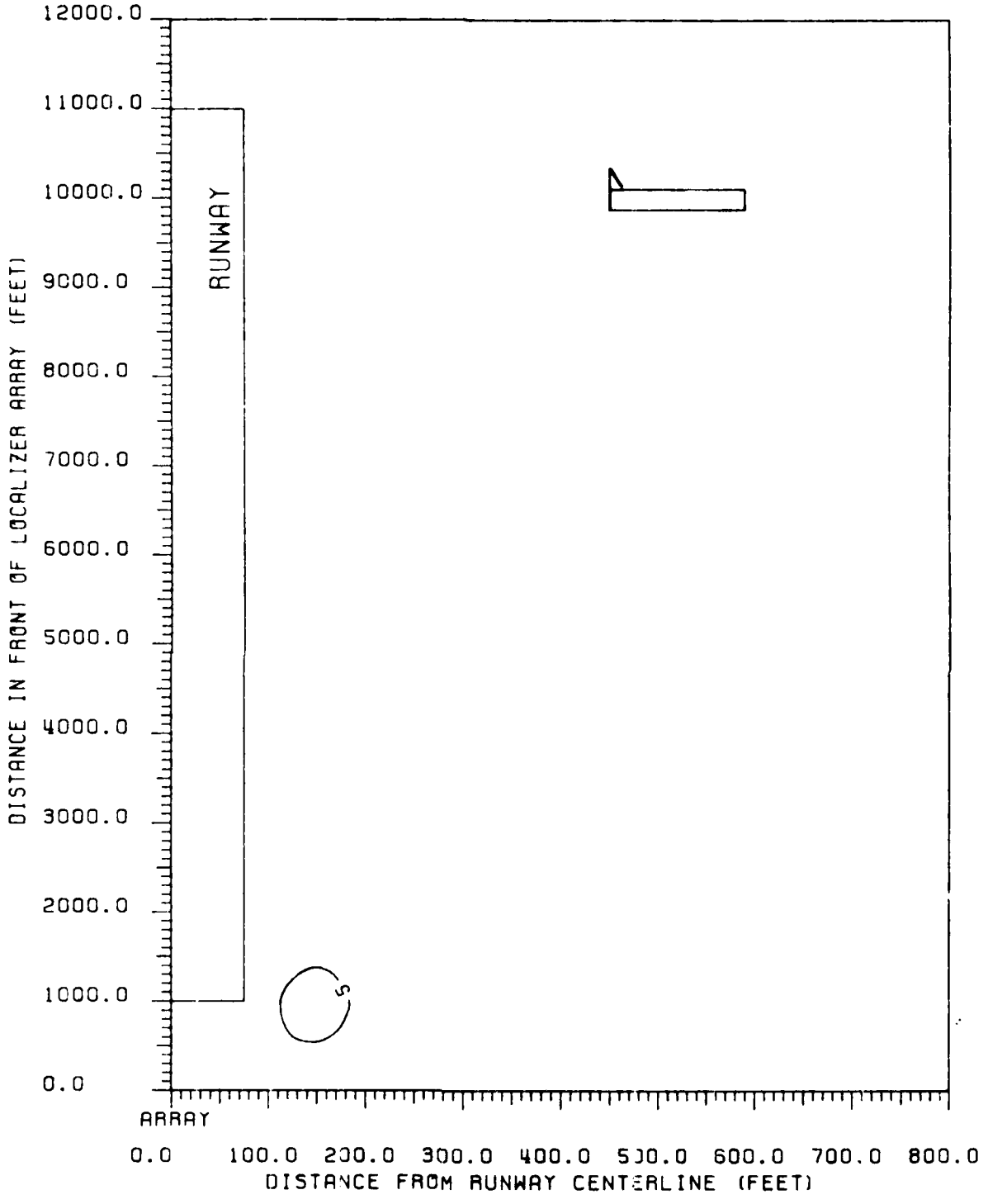

Figure 111 Contours of peak CDI values produced in ILS Zone 4 for a B-727. B-727 fuselage is perpendicular to runway centerline, with tail towards the runway. 14-element single-frequency array, LPD antennas.

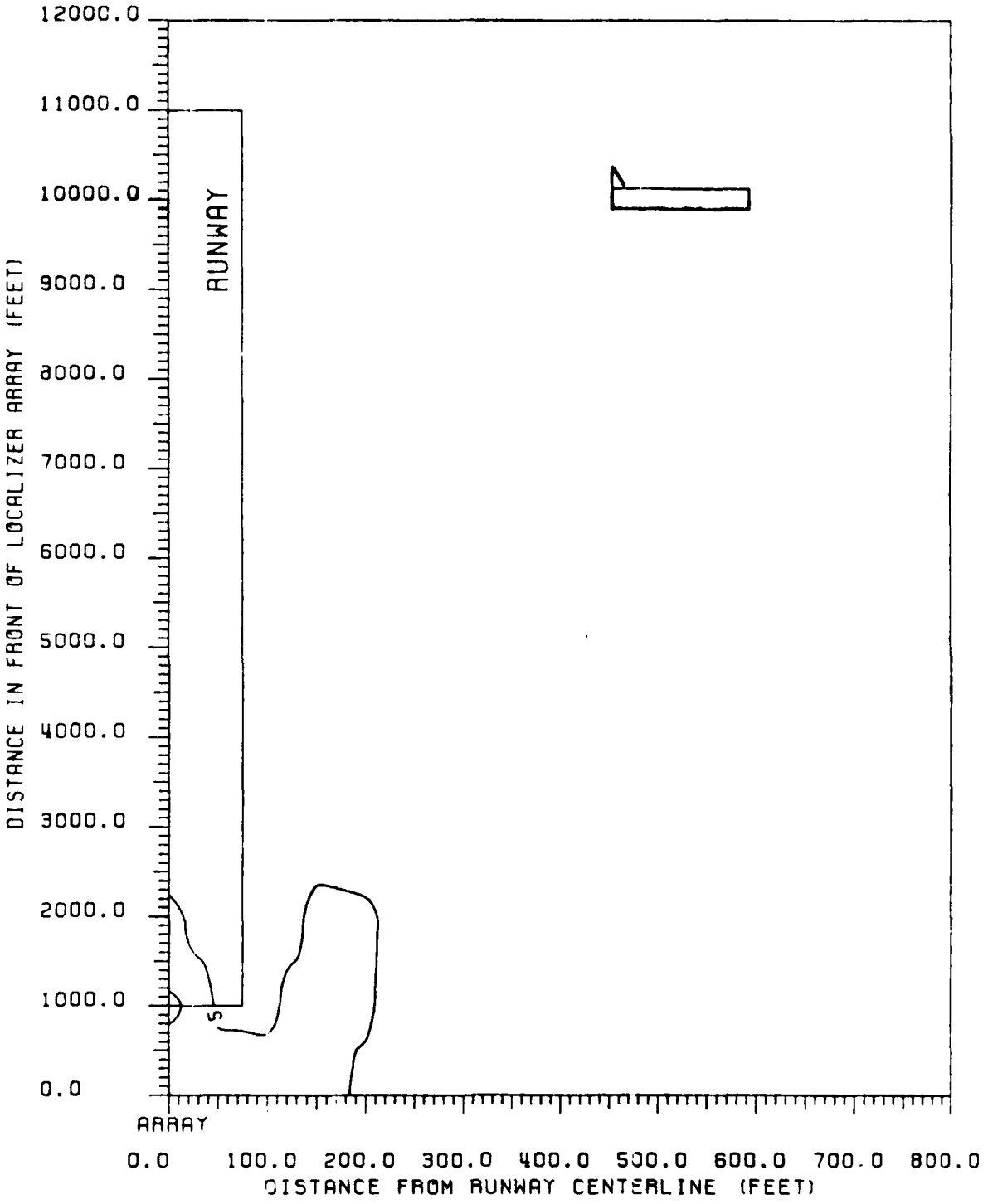

Figure 112 Contours of peak CDI values produced in ILS Zone 5 for a B-727. B-727 fuselage is perpendicular to runway centerline, with tail towards the runway. 14-element single-frequency array, LPD antennas.

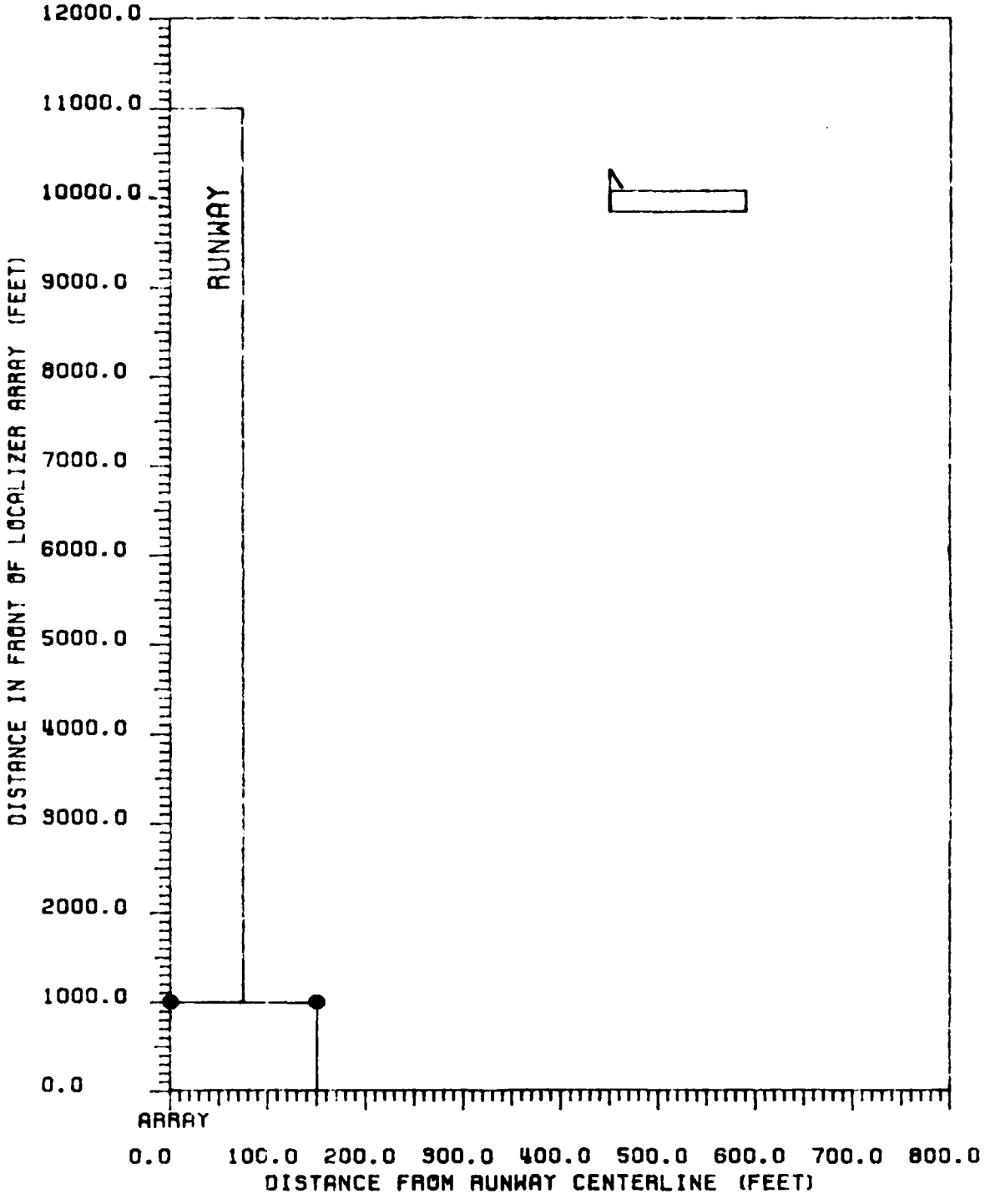

Figure 113 Critical area map for CAT II tolerances relating to B-707 aircraft. B-707 fuselage is perpendicular to runway centerline with tail towards the runway. 14-element single-frequency array, LPD antennas.

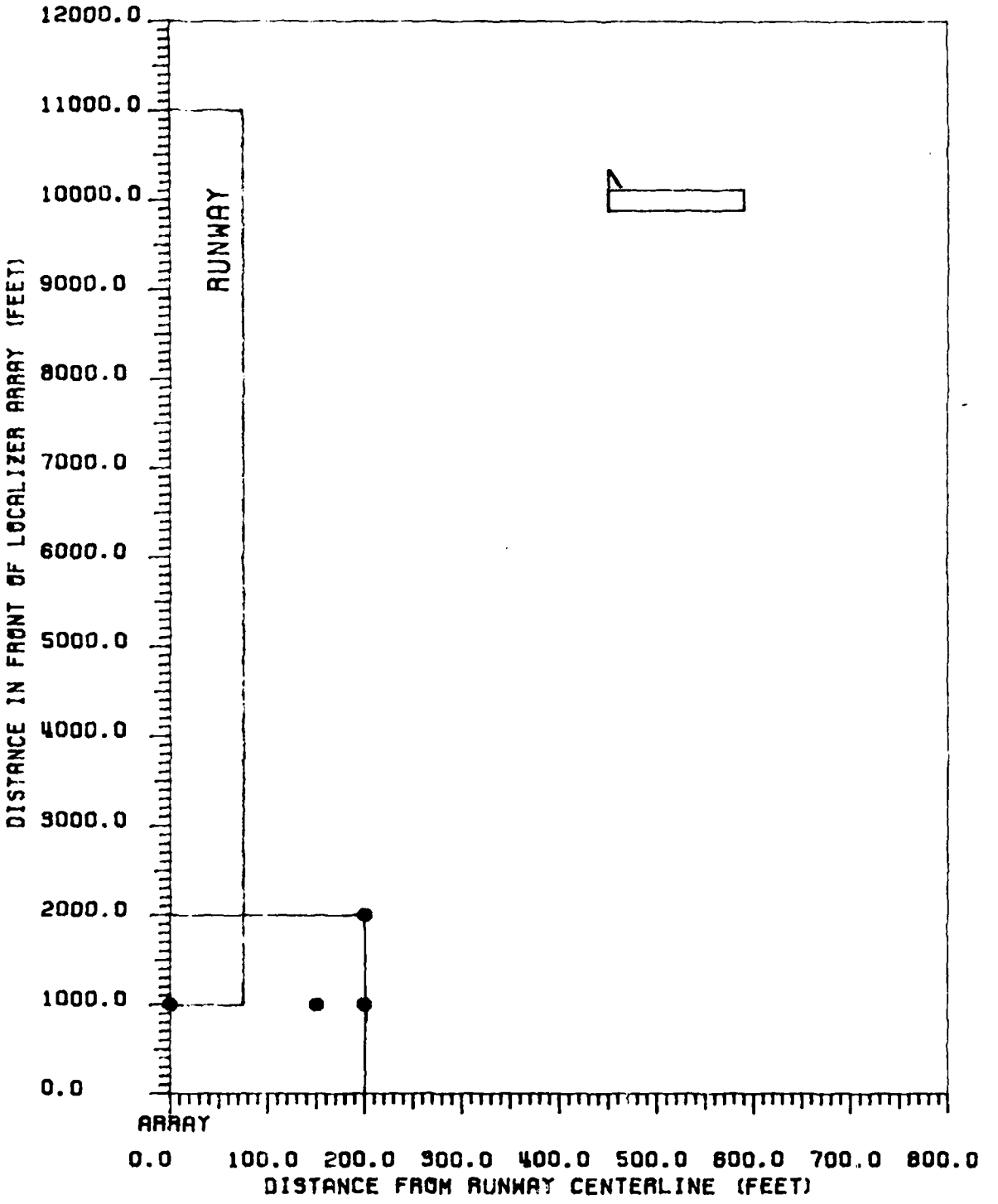

Figure 114 Critical area map for CAT III tolerances relating to B-707 aircraft. B-707 fuselage is perpendicular to runway centerline with tail towards the runway. 14-element single-frequency array, LPD antennas.

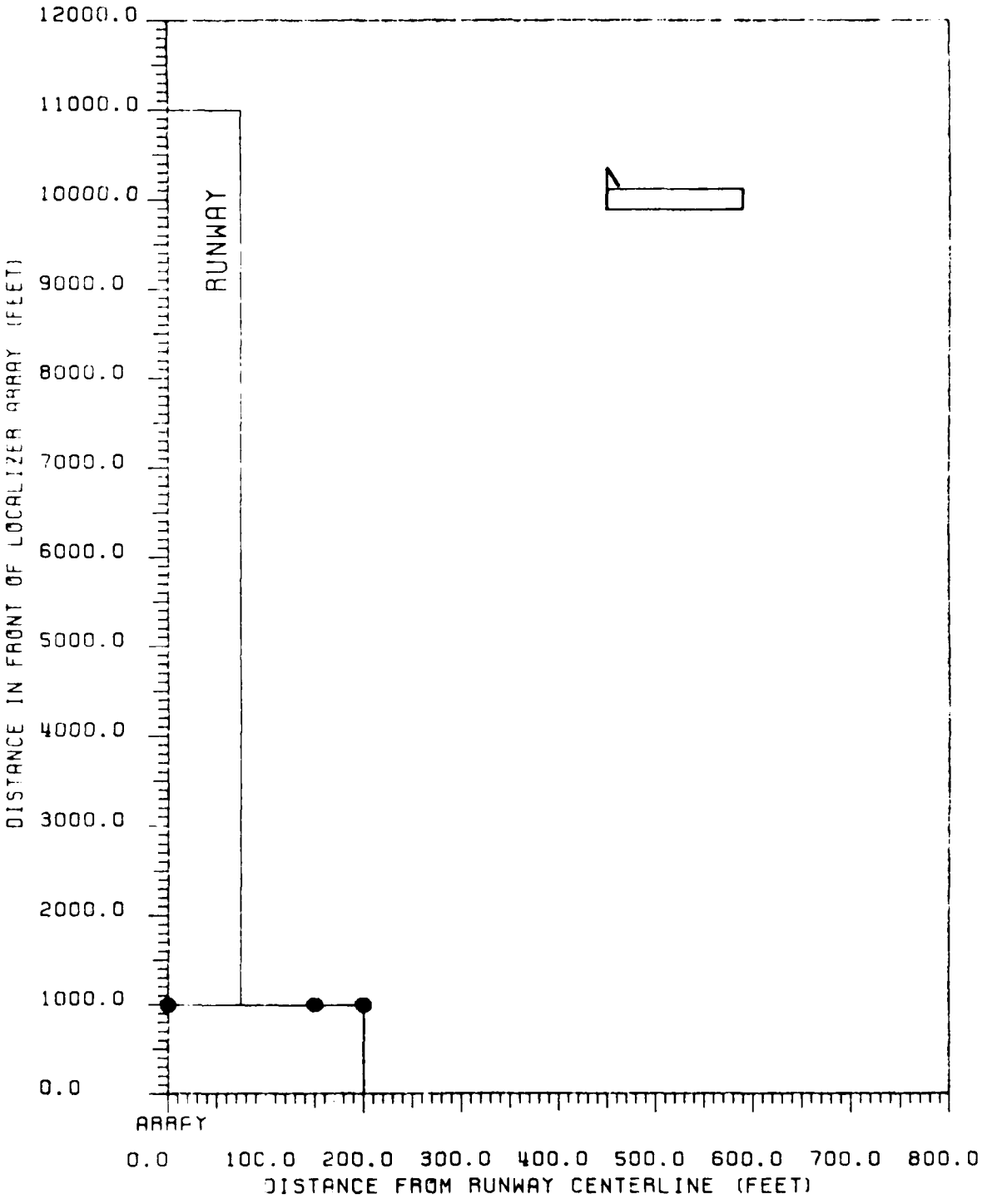

Figure 115 Critical area map for CAT III-X tolerances relating to B-707 aircraft. B-707 fuselage is perpendicular to runway centerline with tail towards the runway. 14-element single-frequency array, LPD antennas.

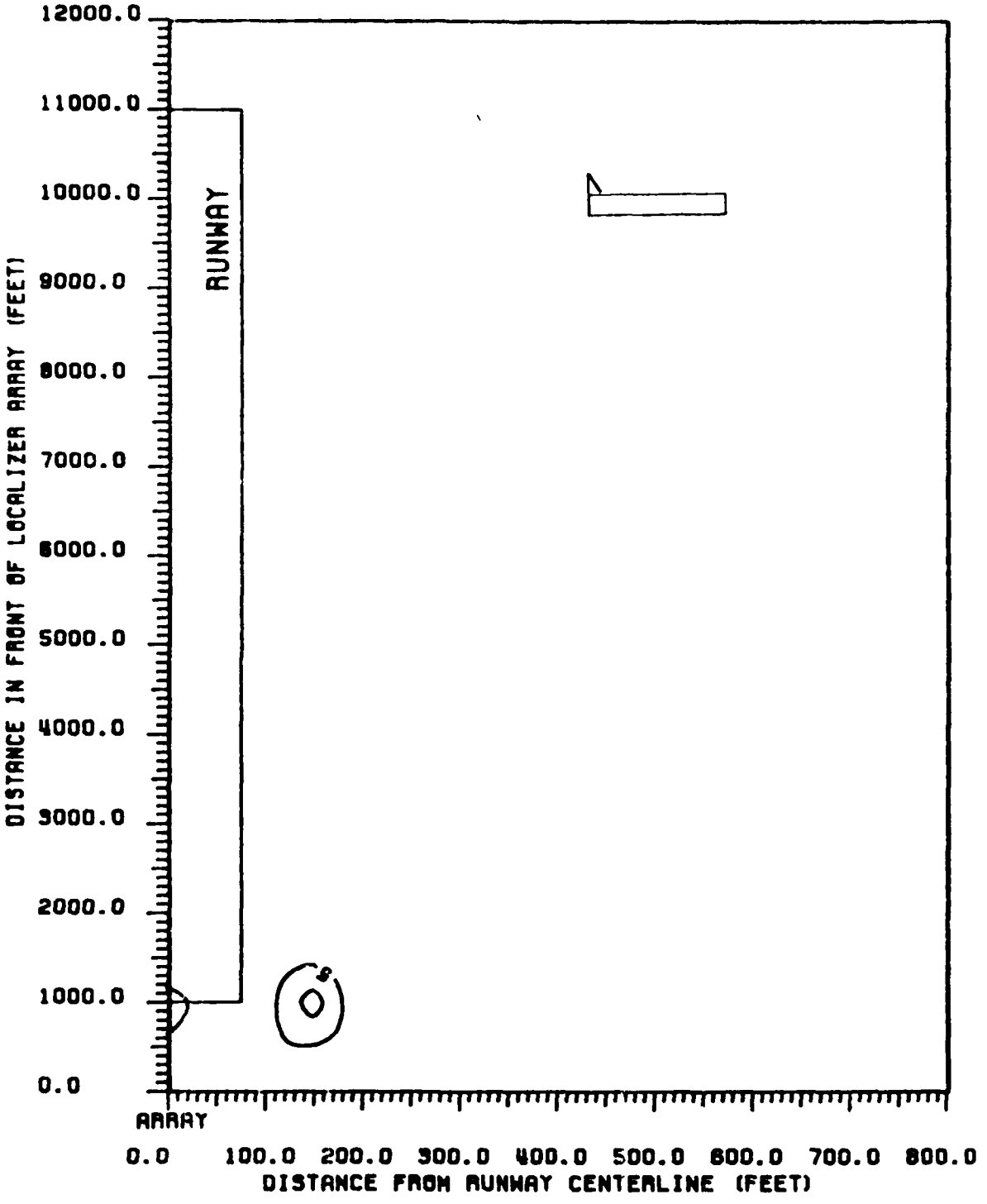

Figure 116 Contours of peak CDI values produced in ILS Zone 2 for a B-707. B-707 fuselage is perpendicular to runway centerline, with tail towards the runway. 14-element single-frequency array, LPD antennas.

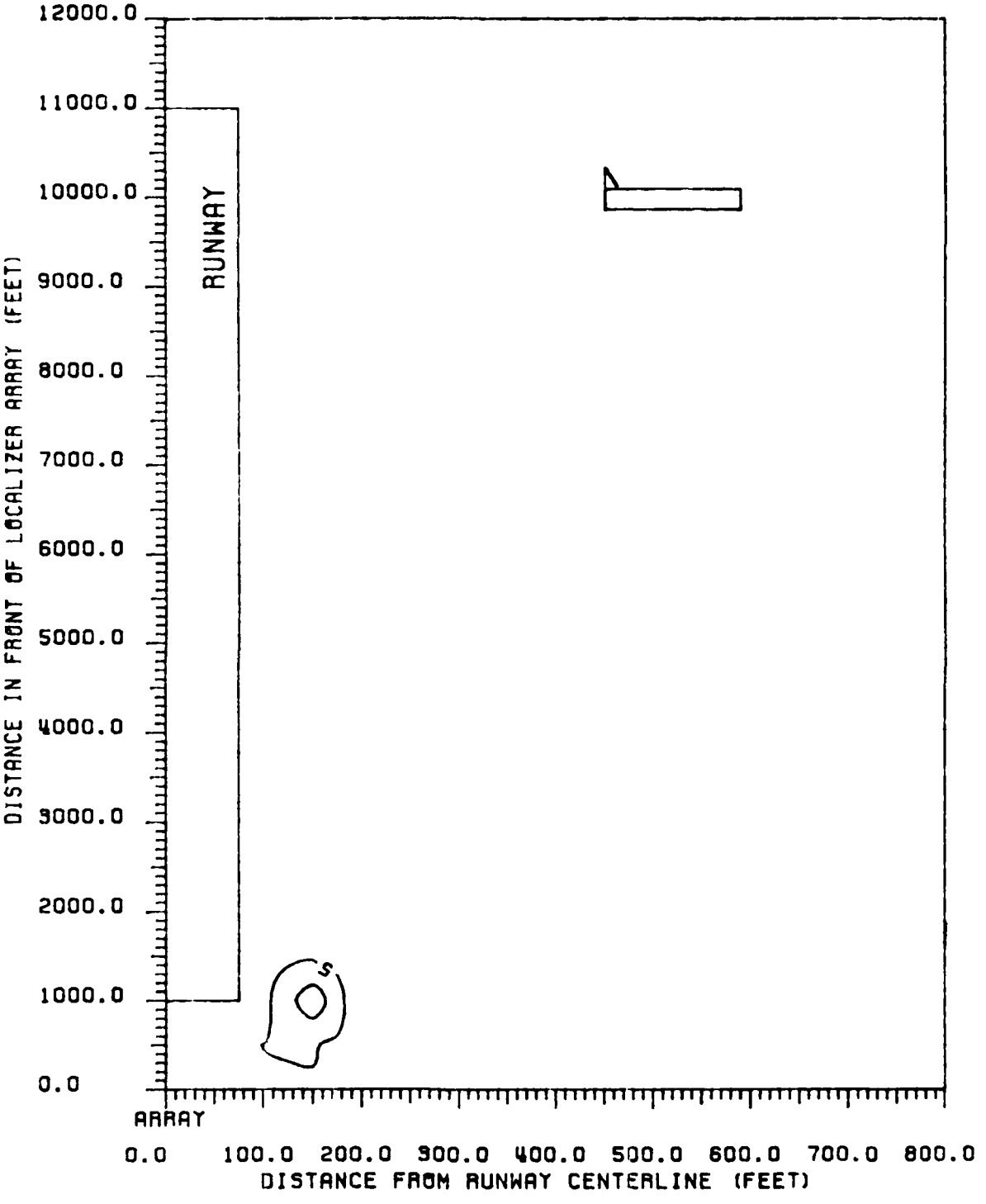

Figure 117 Contours of peak CDI values produced in ILS Zone 3 to Threshold for a B-707. B-707 fuselage is perpendicular to runway centerline, with tail towards the runway. 14-element single-frequency array, LPD antennas.

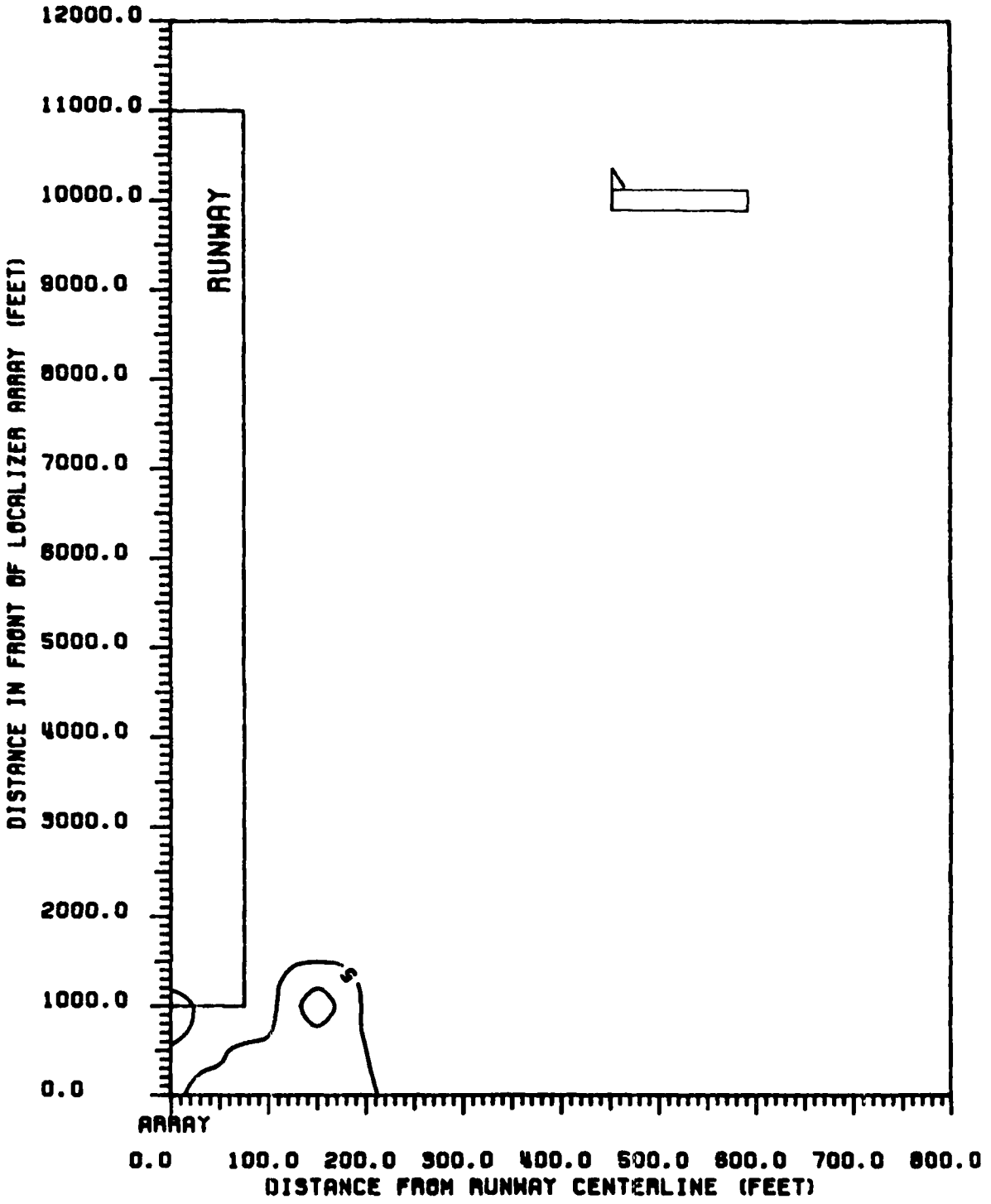

Figure 118 Contours of peak CDI values produced in ILS Zone 4 for a B-707. B-707 fuselage is perpendicular to runway centerline, with tail towards the runway. 14-element single-frequency array, LPD antennas.

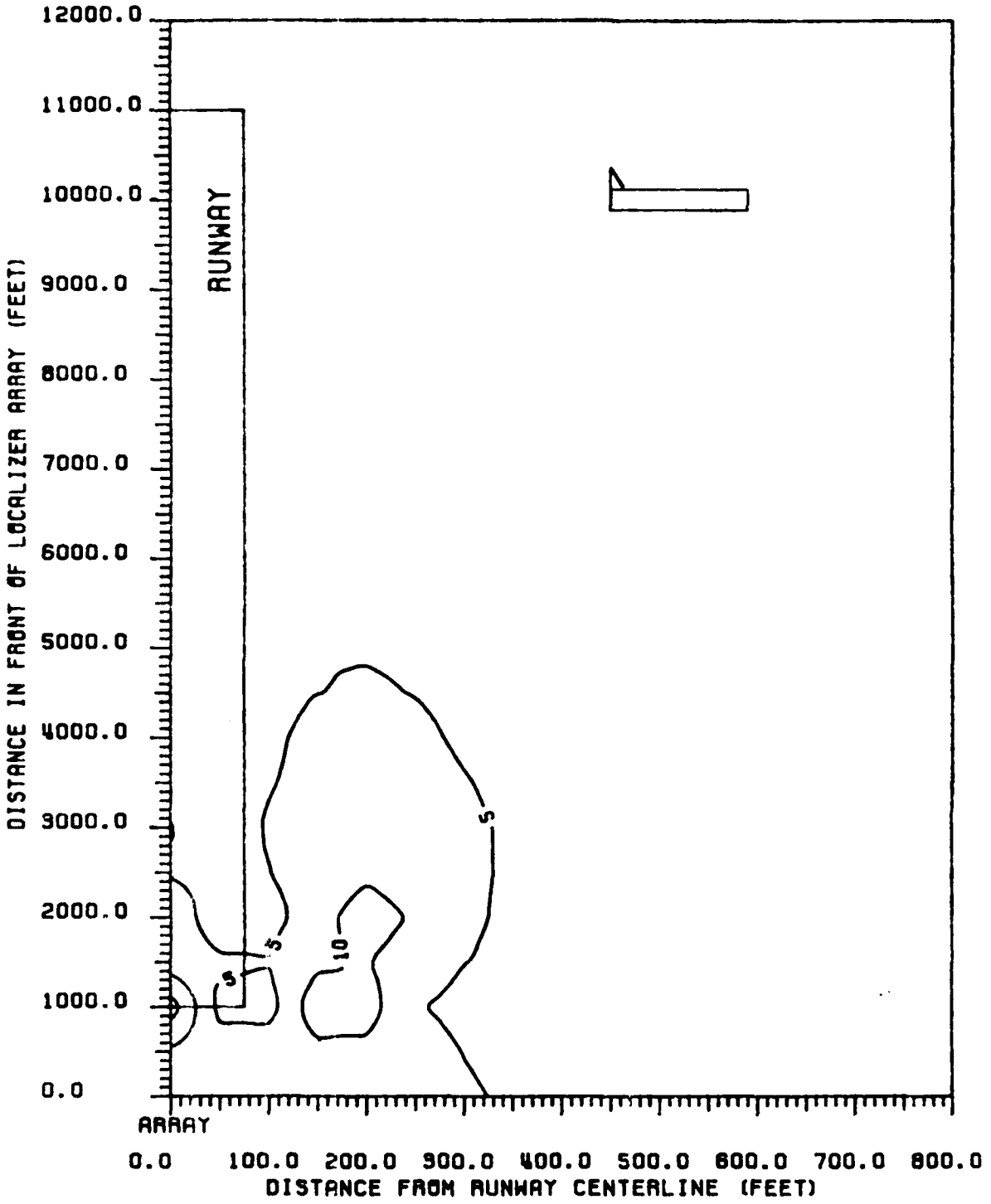

Figure 119 Contours of peak CDI values produced in ILS Zone 5 for a B-707. B-707 fuselage is perpendicular to runway centerline, with tail towards the runway. 14-element single-frequency array, LPD antennas.

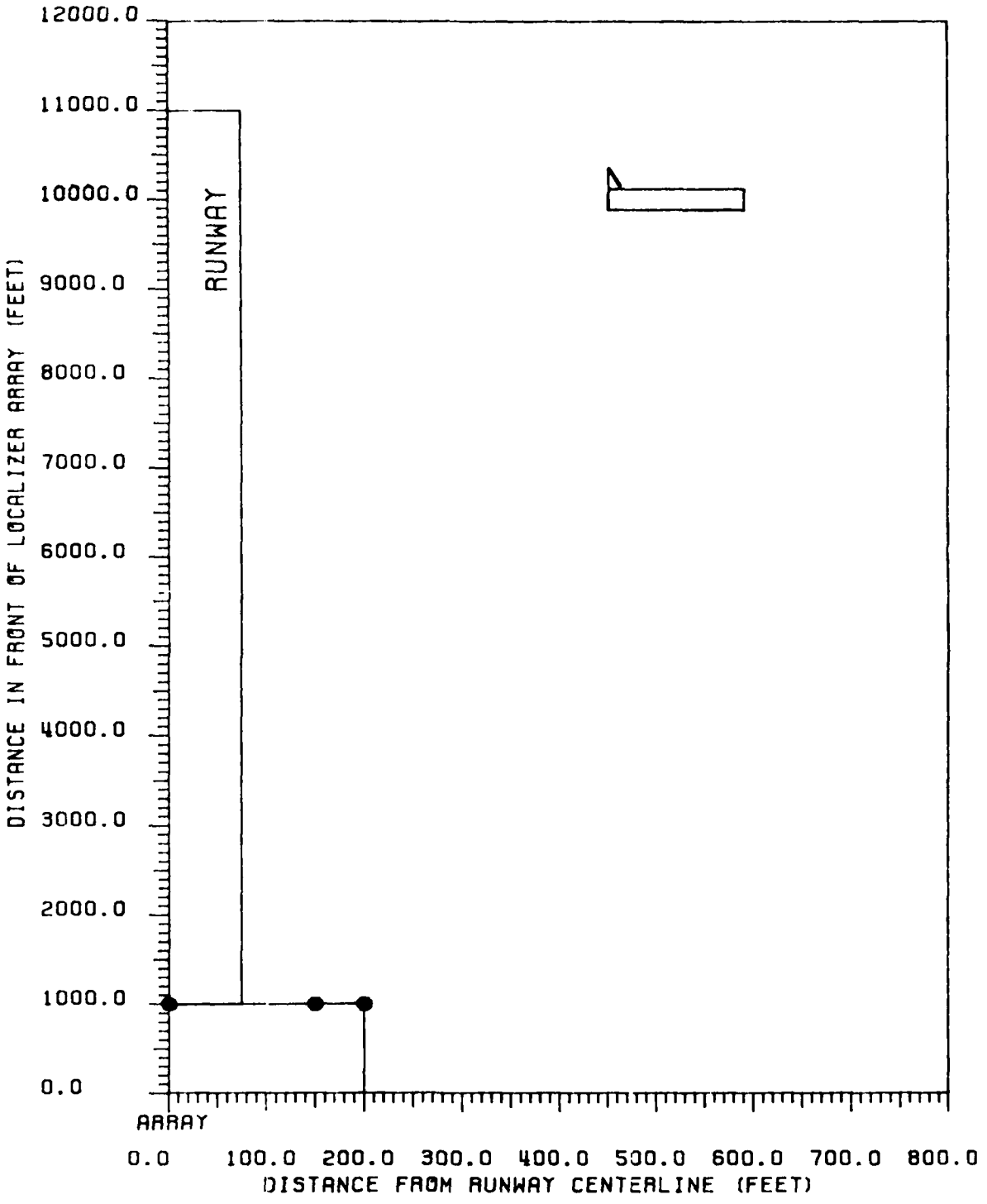

Figure 120 Critical area map for CAT I tolerances relating to L-1011 aircraft. L-1011 fuselage is perpendicular to runway centerline with tail towards the runway. 14-element single-frequency array, LPD antennas.

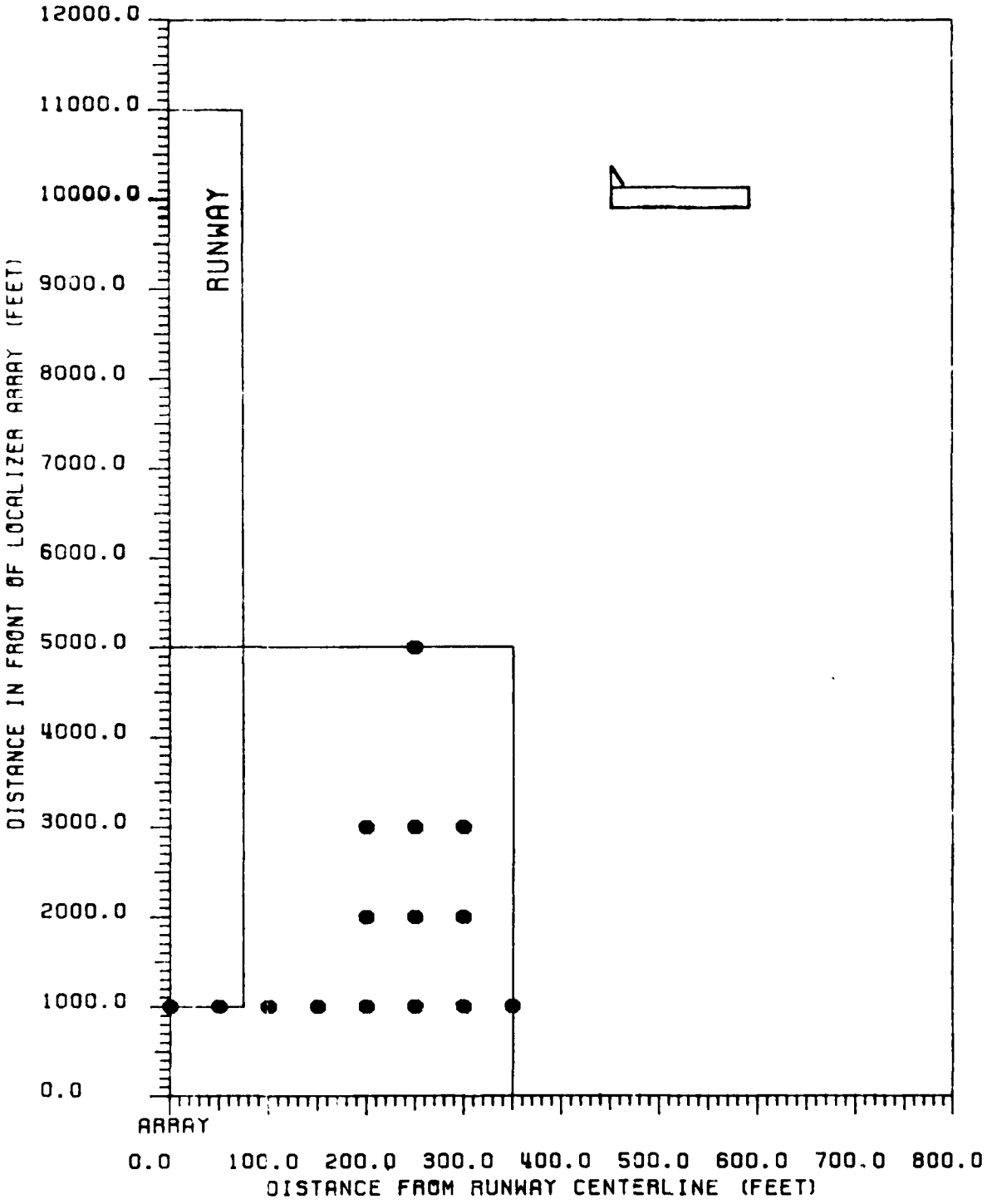

Figure 121 Critical area map for CAT II tolerances relating to L-1011 aircraft. L-1011 fuselage is perpendicular to runway centerline with tail towards the runway. 14-element single-frequency array, LPD antennas.

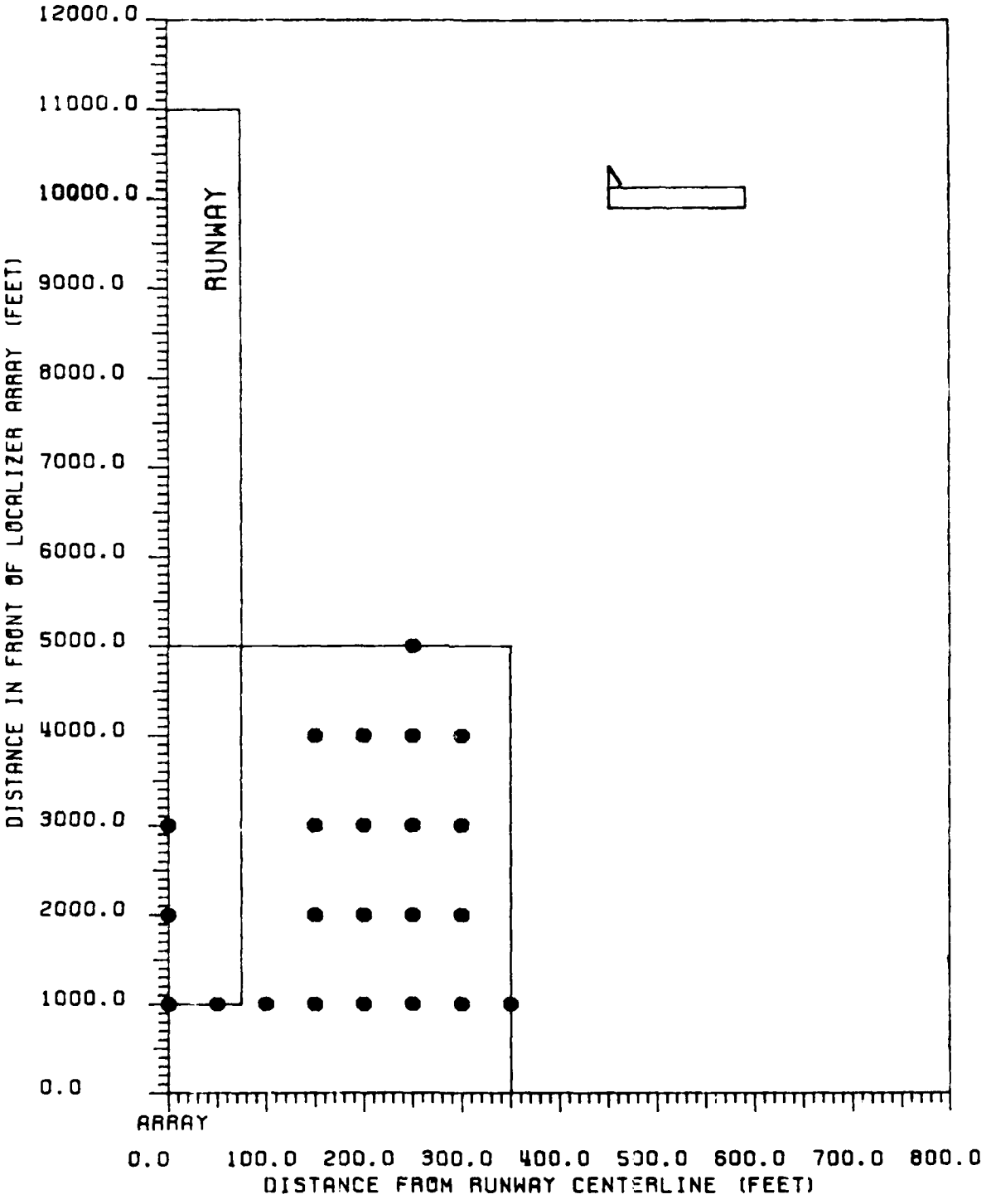

Figure 122 Critical area map for CAT III tolerances relating to L-1011 aircraft. L-1011 fuselage is perpendicular to runway centerline with tail towards the runway. 14-element single-frequency array, LPD antennas.

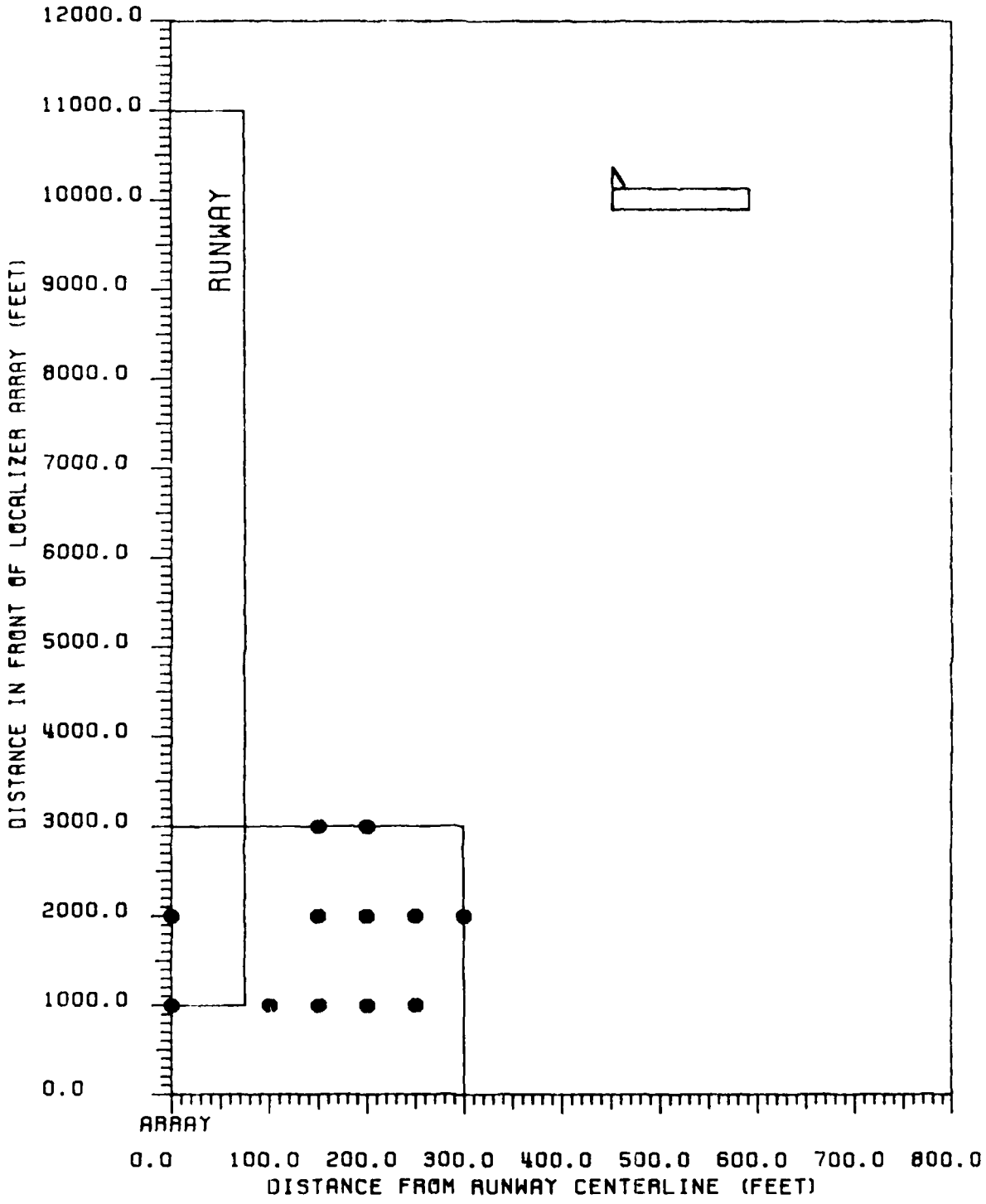

Figure 23 Critical area map for CAT III-X tolerances relating to L-1011 aircraft. L-1011 fuselage is perpendicular to runway centerline with tail towards the runway. 14-element single-frequency array, LPD antennas.

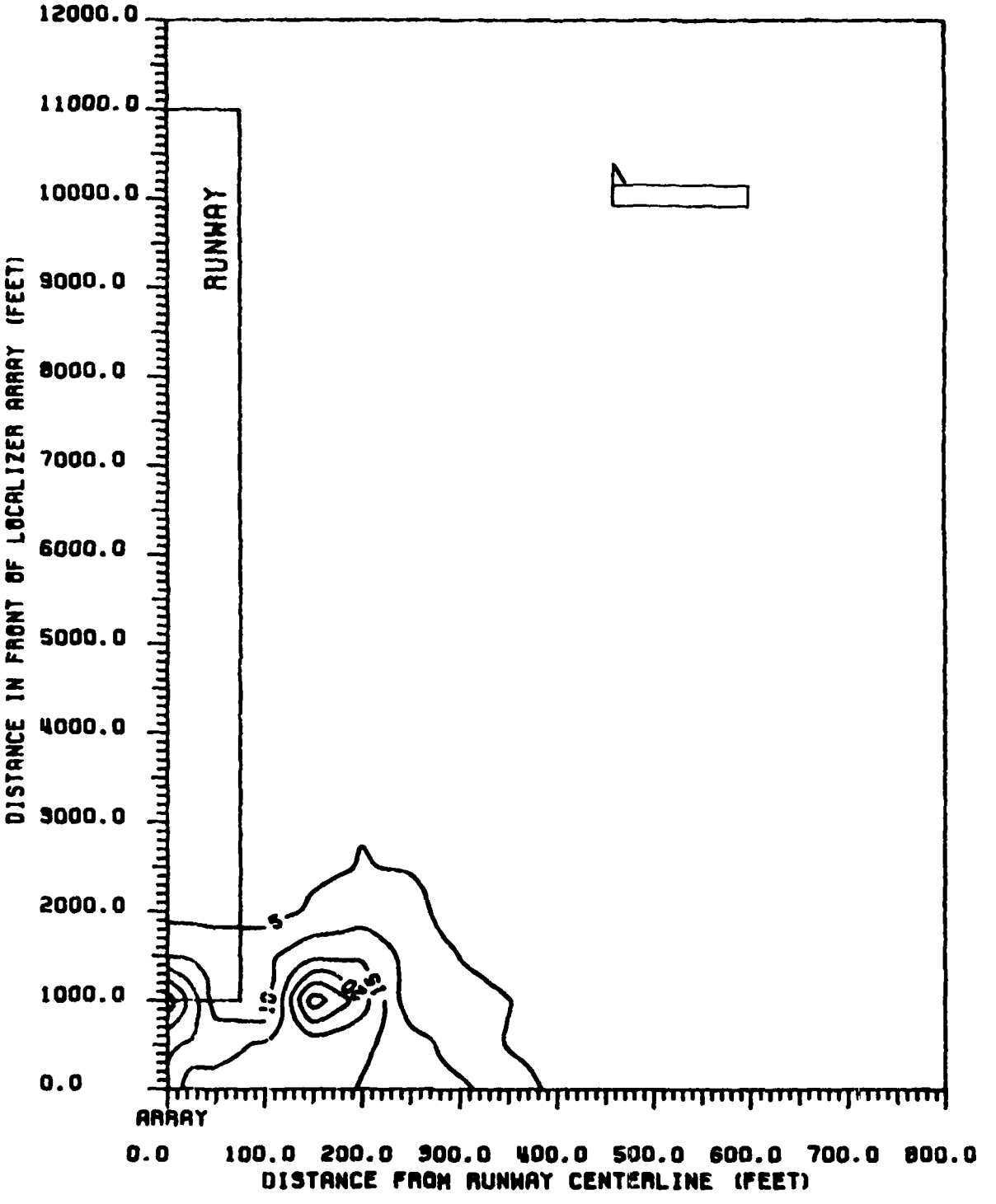

Figure 124 Contours of peak CDI values produced in ILS Zone 2 for a L-1011. L-1011 fuselage is perpendicular to runway centerline, with tail towards the runway. 14-element single-frequency array, LPD antennas.

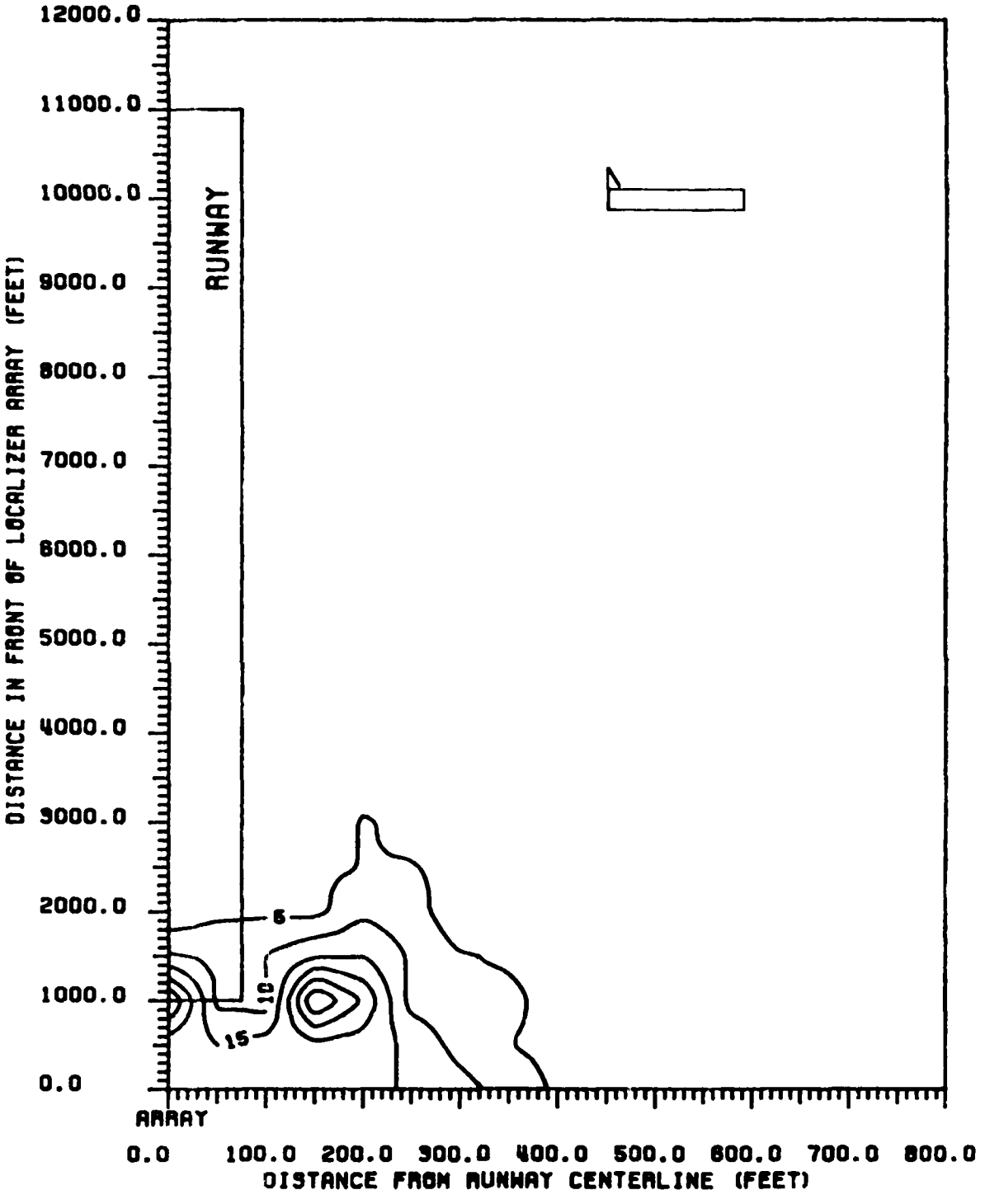

Figure 125 Contours of peak CDI values produced in ILS Zone 3 to Threshold for a L-1011. L-1011 fuselage is perpendicular to runway centerline, with tail towards the runway. 14-element single-frequency array, LPD antennas.

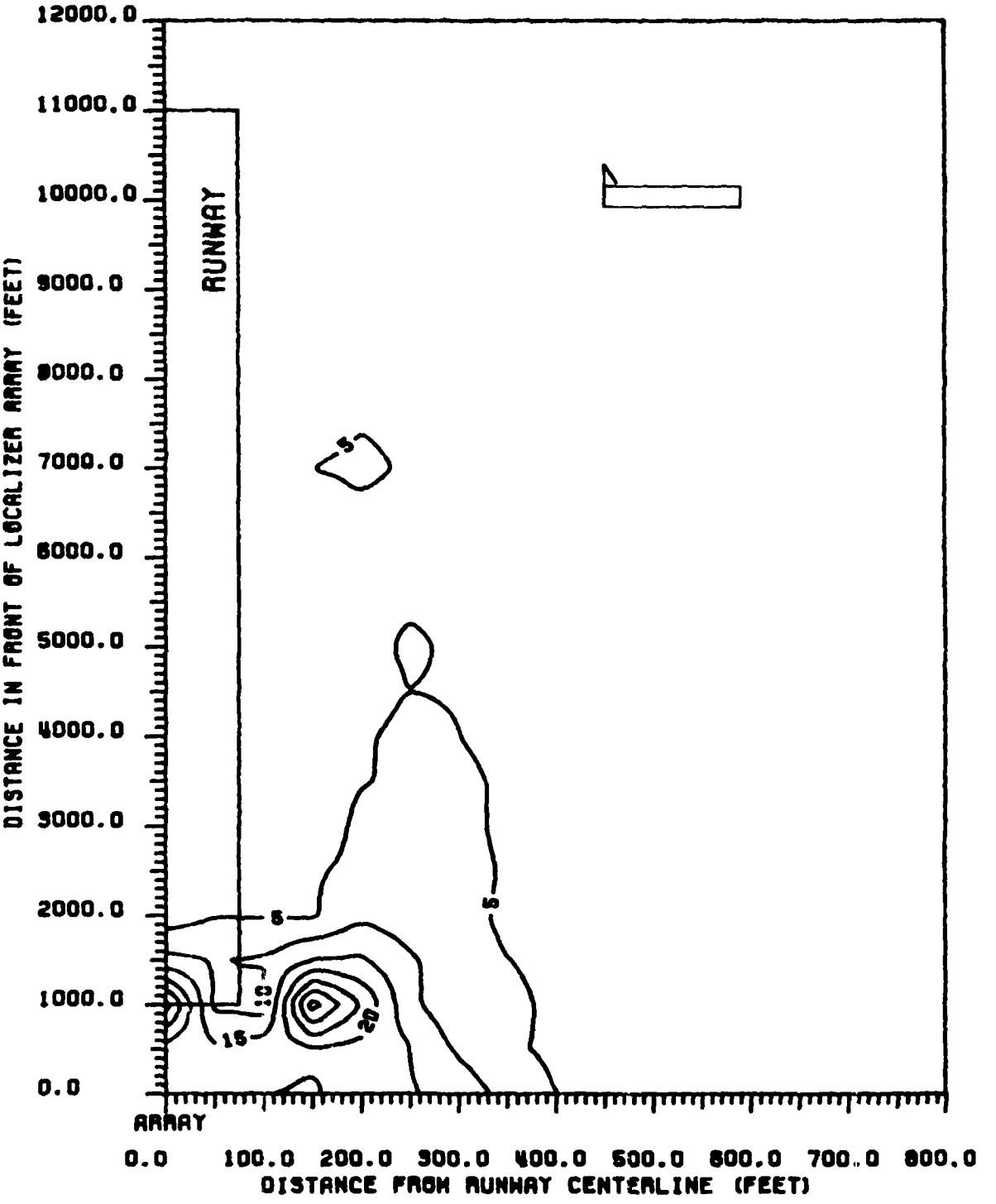

Figure 126 Contours of peak CDI values produced in ILS Zone 4 for a L-1011. L-1011 fuselage is perpendicular to runway centerline, with tail towards the runway. 14-element single-frequency array, LPD antennas.

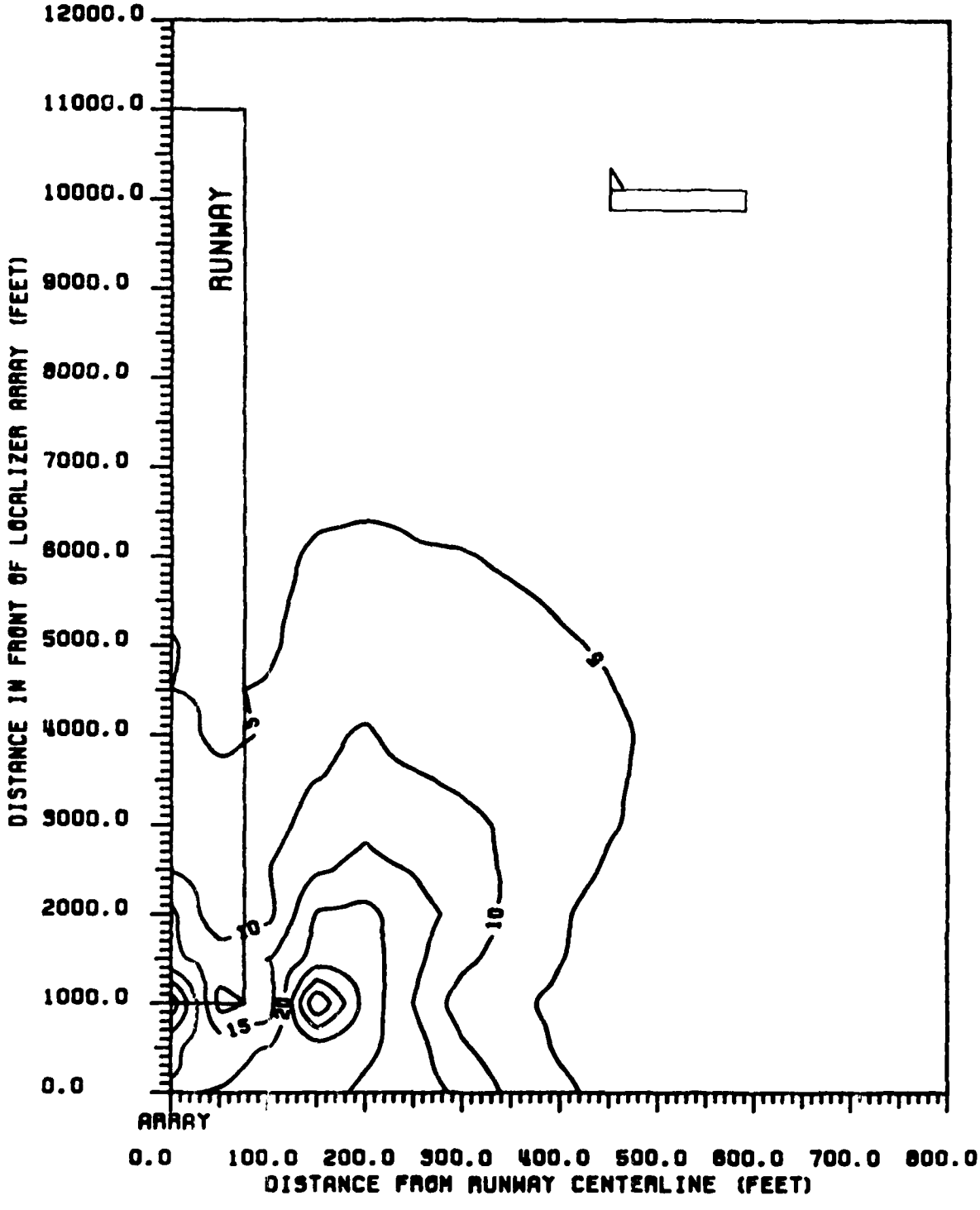

Figure 127 Contours of peak CDI values produced in ILS Zone 5 for a L-1011. L-1011 fuselage is perpendicular to runway centerline, with tail towards the runway. 14-element single-frequency array, LPD antennas.

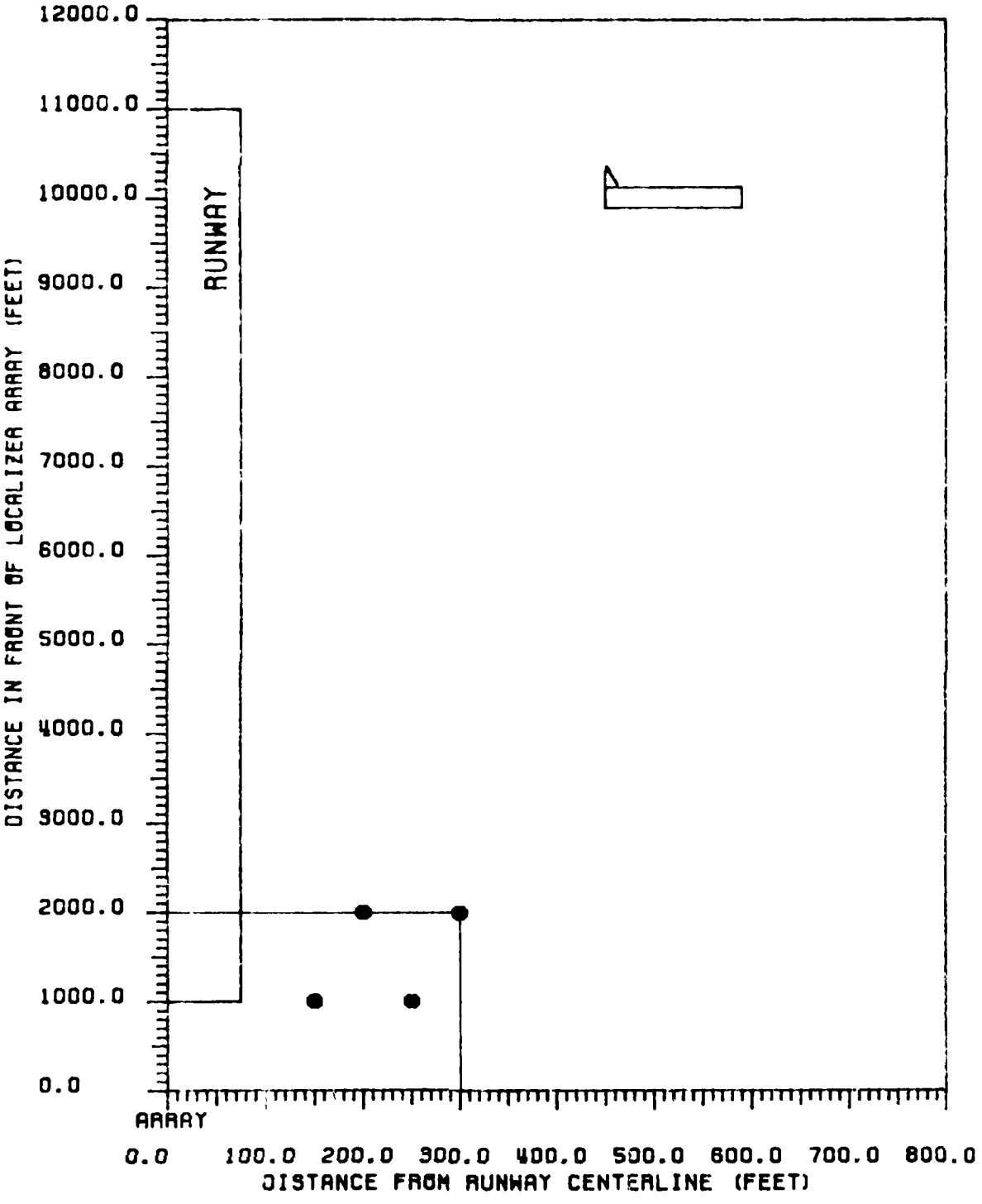

Figure 128 Critical area map for CAT I tolerances relating to B-747 aircraft. B-747 fuselage is perpendicular to runway centerline with tail towards the runway. 14-element single-frequency array, LPD antennas.

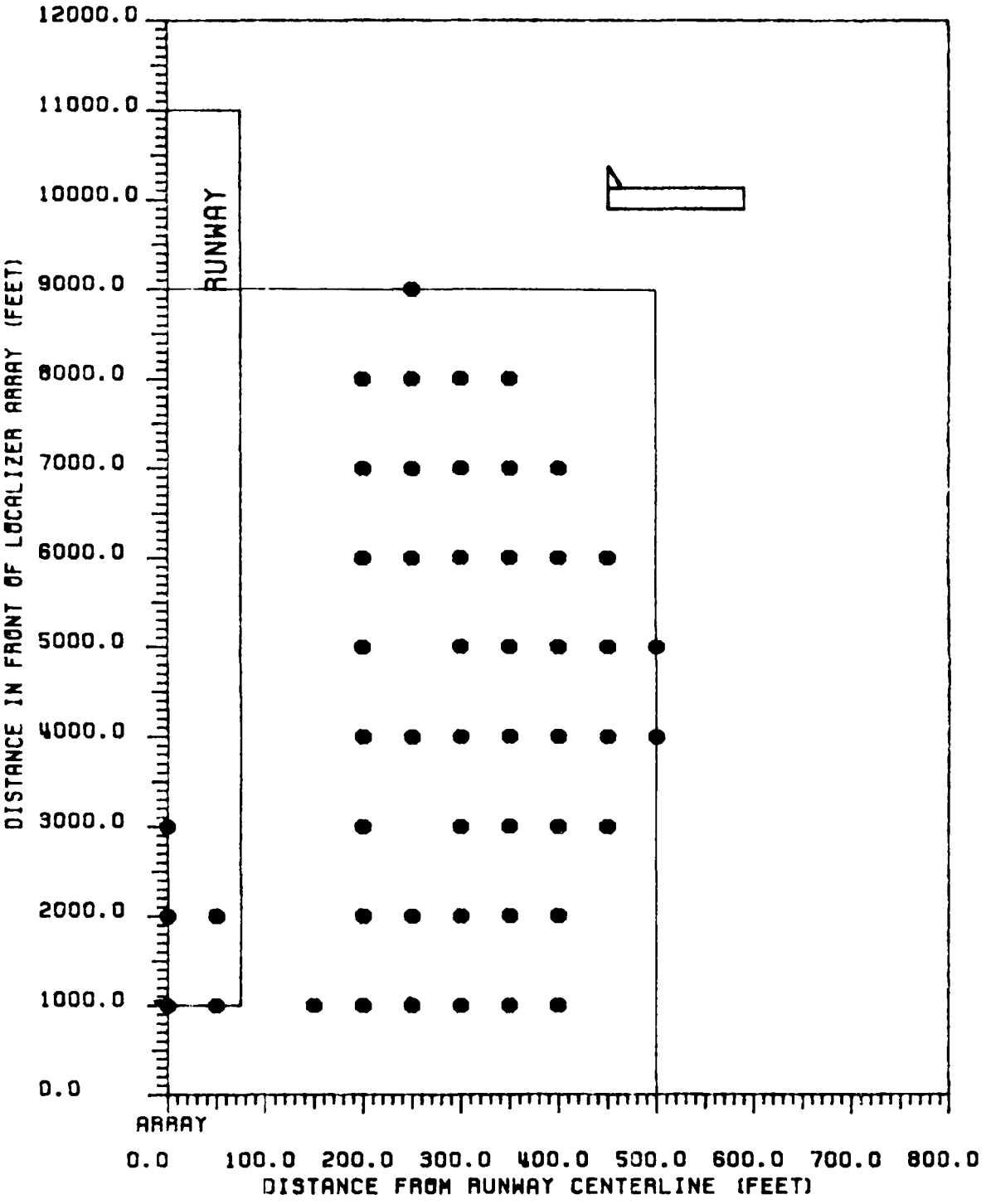

Figure 129 Critical area map for CAT II tolerances relating to B-747 aircraft. B-747 fuselage is perpendicular to runway centerline with tail towards the runway. 14-element single-frequency array, LPD antennas.

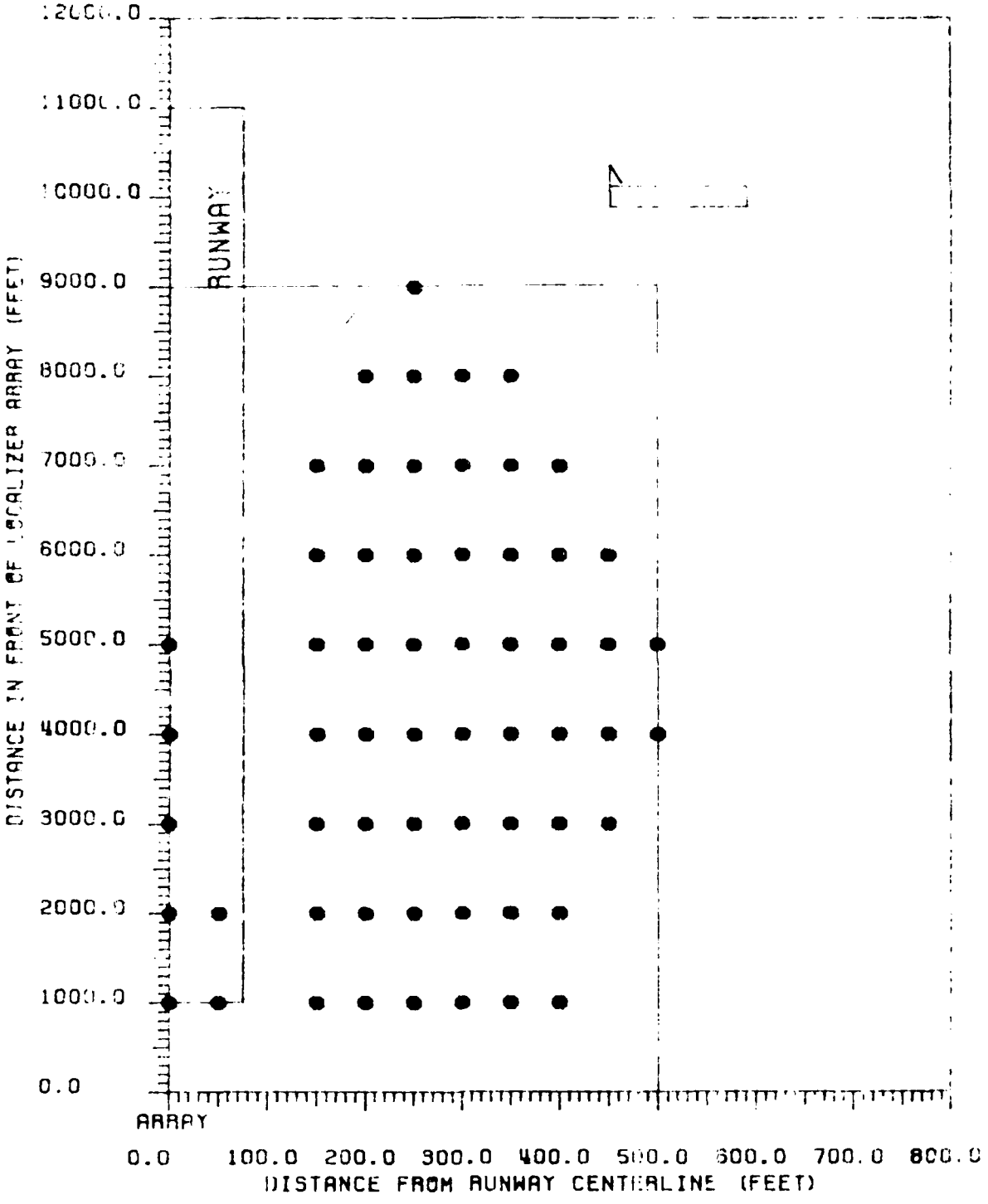

Figure 130 Critical area map for CAT III tolerances relating to B-747 aircraft. B-747 fuselage is perpendicular to runway centerline with tail towards the runway. 4-element single-frequency array, LPE antennas.

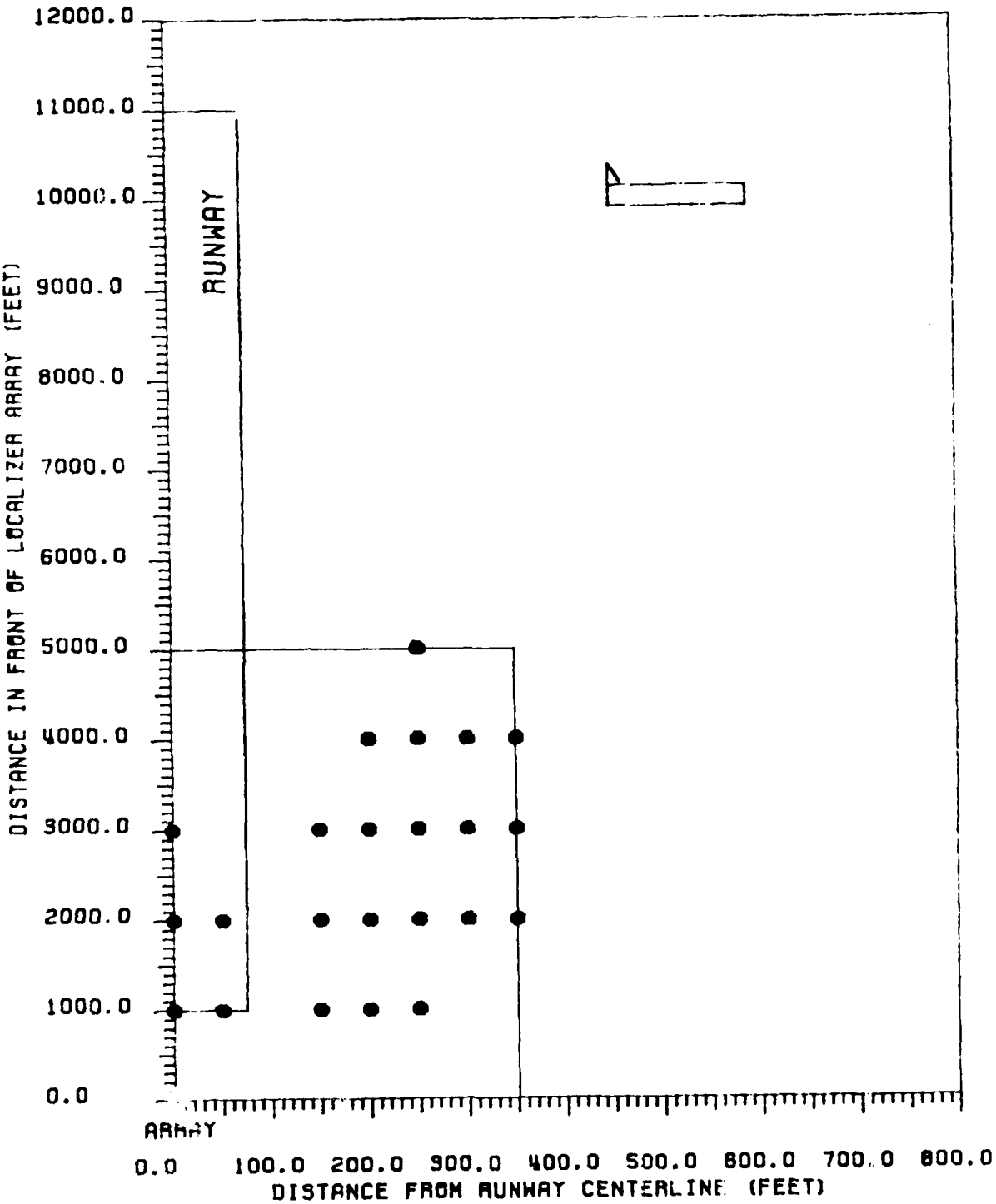

Figure 131 Critical area map for CAT III-X tolerances relating to B-747 aircraft. B-747 fuselage is perpendicular to runway centerline with tail towards the runway. 14-element single-frequency array, LPD antennas.

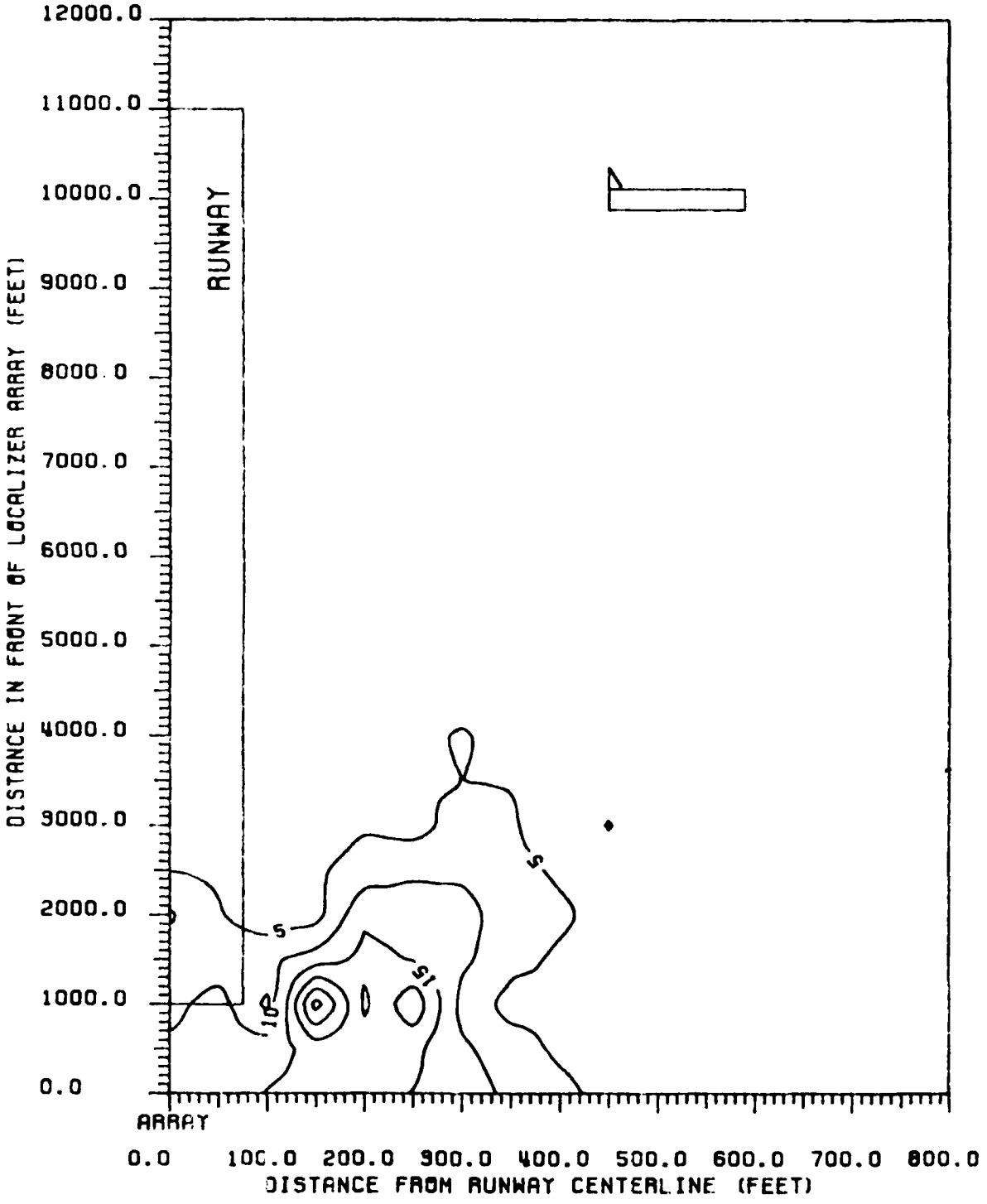

Figure 132 Contours of peak CDI values produced in ILS Zone 2 for a B-747. B-747 fuselage is perpendicular to runway centerline, with tail towards the runway. 14-element single-frequency array, LPD antennas.

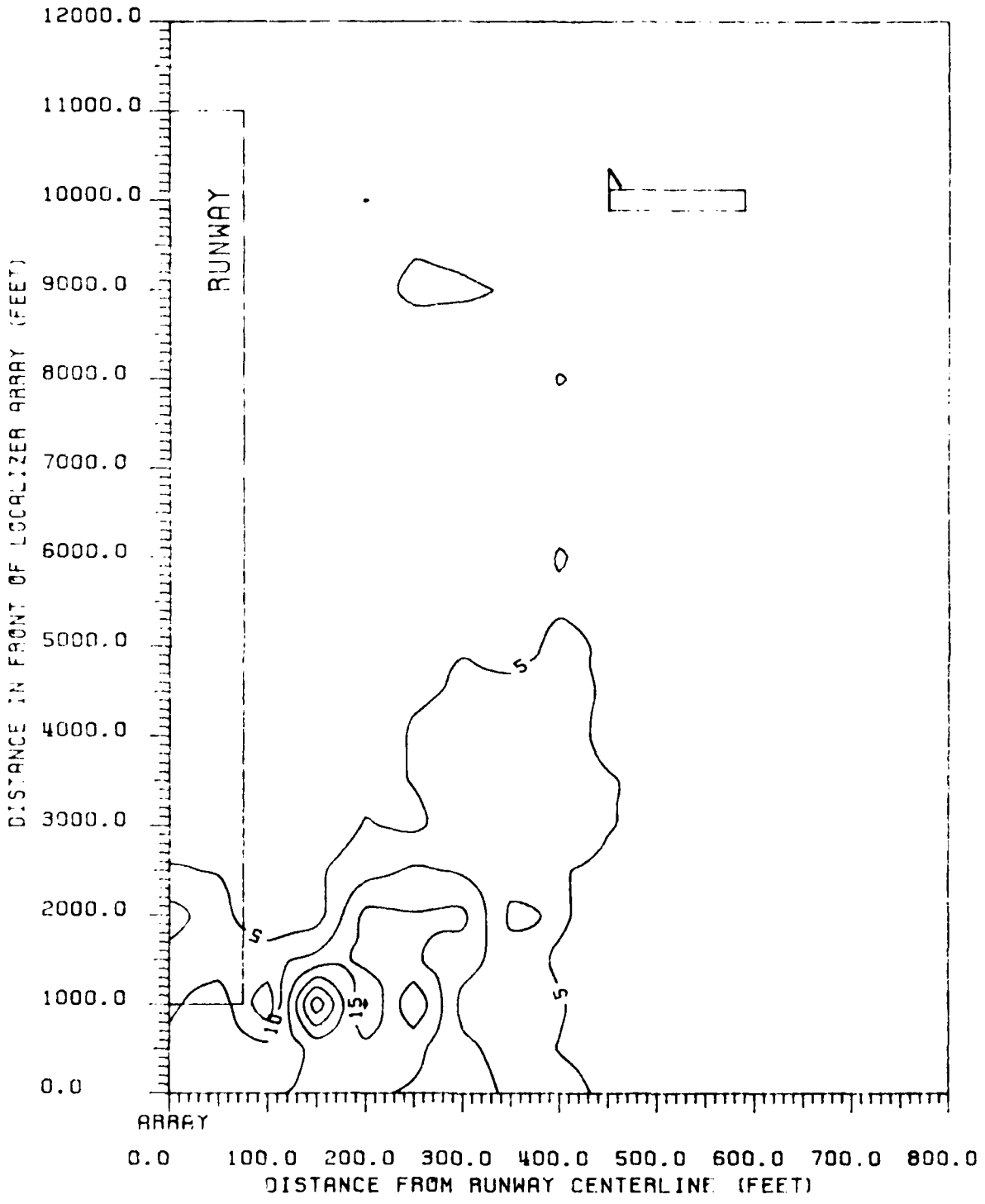

Figure 133 Contours of peak CDI values produced in ILS Zone 3 to Threshold for a B-747. B-747 fuselage is perpendicular to runway centerline, with tail towards the runway. 14-element single-frequency array, LPD antennas.

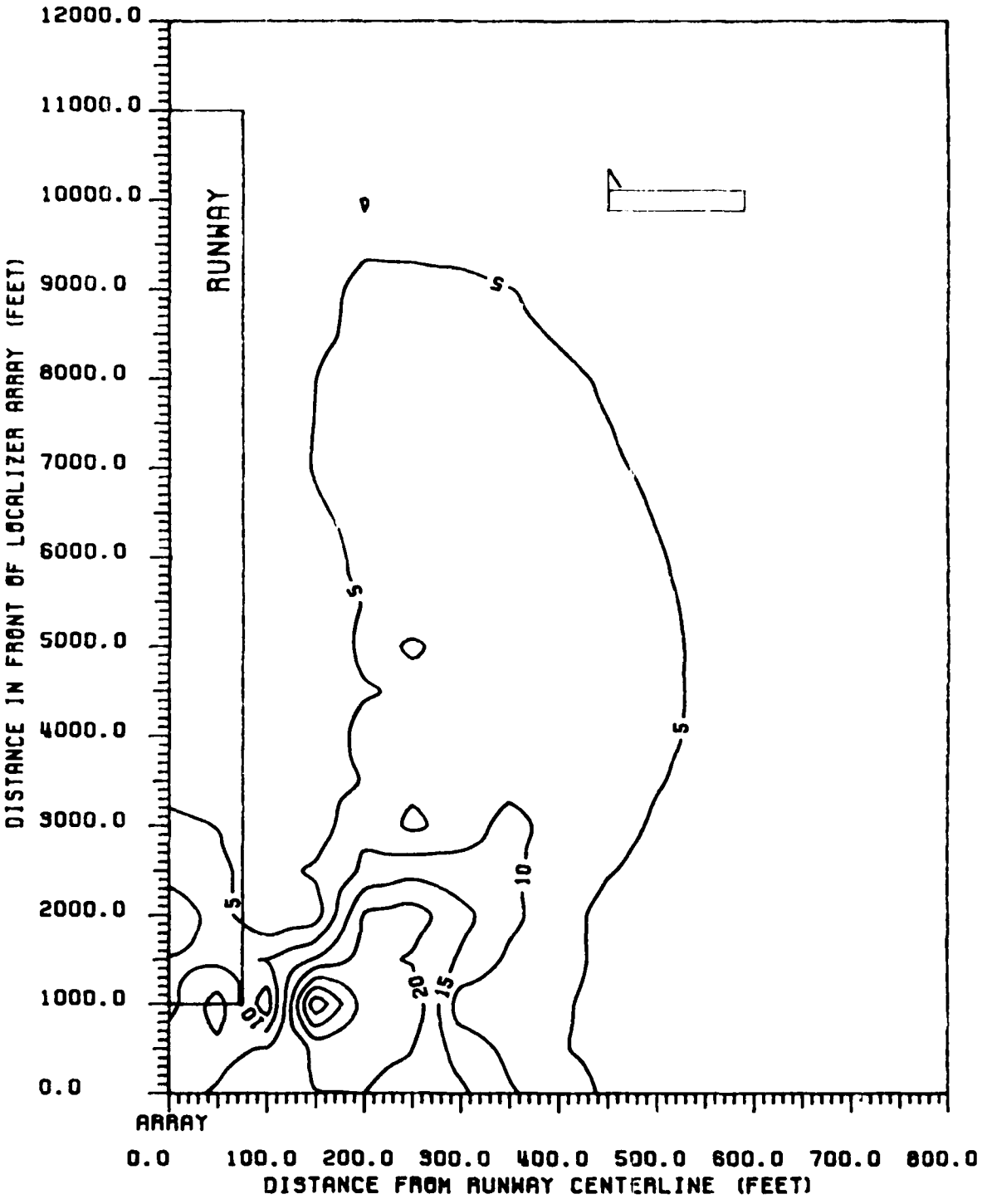

Figure 134 Contours of peak CDI values produced in ILS Zone 4 for a B-747. B-747 fuselage is perpendicular to runway centerline, with tail towards the runway. 14-element single-frequency array, LFD antennas.

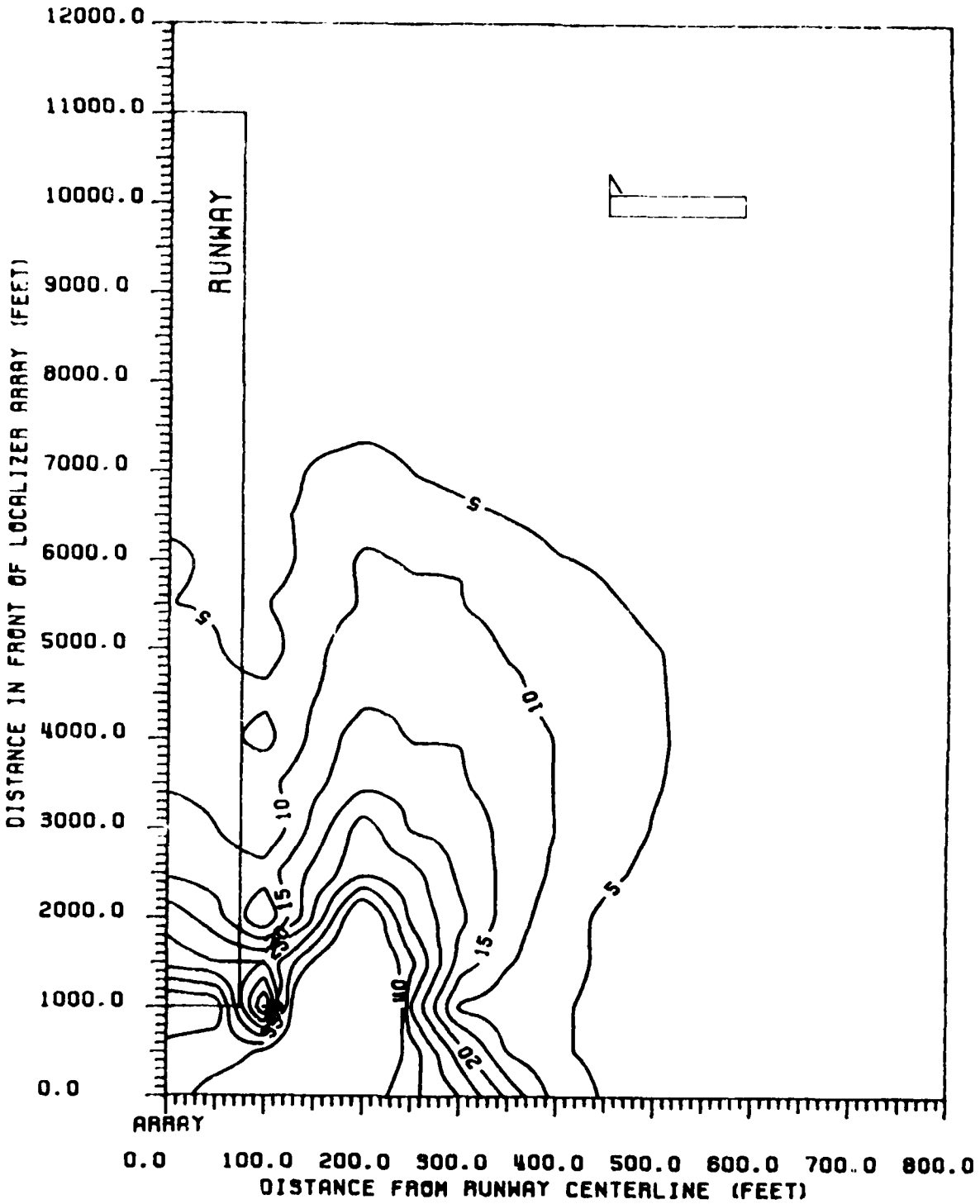

Figure 13. Contours of peak CDI values produced in ILS Zone 5 for a B-747. B-747 fuselage is perpendicular to runway centerline, with tail towards the runway. 14-element single-frequency array, LPD antennas.

VIII. RECOMMENDATIONS

The following recommendations are based principally on the theoretical calculations just completed which has identified areas in the vicinity of an 8-element, single-frequency localizer where the presence of various sizes and orientations of scatterers will cause the localizer path structure to exceed tolerances specified in U.S. Flight Inspection Manual 8200.1, Section 217.5.

1. The user should identify the inherent noise present in the localizer path structure of interest. The results in this study are based on this noise being zero. Since this is not true for practical sites, the results are not directly applicable for localizer structures having high noise levels already. The perturbations produced by the scatterer aircraft must be added to the base level of inherent noise.

2. Since the inherent noise can increase the size of the critical area, efforts should be made to reduce this noise by fundamental site improvement.

3. At sites where inherent noise is a problem, the contour maps should be used to identify the contours which will cause the path structure to exceed tolerance limits when the contour is added to the inherent noise.

4. Assuming inherent noise is not a problem, the critical area maps should be used to identify the boundaries which should be protected from the presence of scatterer aircraft during instrument approaches.

5. Critical area size increases so drastically with very large aircraft (L-1011 and larger) that consideration should be given to specifying critical area in more than one category. Smaller airports which are unlikely to serve jumbo jets can use other than worst case critical areas.

6. Critical area size for a given airport should also be based on the ILS category of operation. Critical area limits based on CAT III tolerances should not be specified for airports having only CAT II operations.

7. An additional study should be performed to examine all types of localizers which have not been covered by previous reports. There are several remaining localizer arrays for which there is no critical area information available. This study should tie together all information currently available on localizer critical areas in one study, with all calculations performed on a common input data base. This will allow comparisons to be made between all localizer array types and thus provide almost universal guidelines towards specification of localizer critical area. It should be noted that a similar effort for determining glide slope critical area is already underway.

IX. ACKNOWLEDGEMENTS

The author wishes to acknowledge the contributions provided for this localizer critical area study by various members of the Avionics Engineering Center staff. First, to Dr. Richard H. McFarland for providing technical direction on this project, and to Dr. Robert W. Lilley for providing management and allocation of the computer resources essential to a project of this type. Additional thanks is due to Mr. Dave Quinet, who developed the computer software necessary to do automatic application of flight inspection tolerances to the localizer data; and to Dr. Kent Chamberlain, who provided general assistance and advice on the ILS modeling process. Thanks also to Mr. Sammy Puleo, Mr. Godfrey Eze, and Mr. Ejiroghene Edeja who all assisted at various times with preparation of the plots. Ms. Alicya Shade prepared the final manuscript. Finally, a special thanks to Mr. Randall Smith, who made significant and substantial contributions to all phases of this study.

X. BIBLIOGRAPHY

[1] Rondini, R. A. and McFarland, R. H., "Experimental Validation of Boeing 747 ILS Signal Scattering Calculations for Critical Area Determination," Final Report, FAA-RD-74-57 (EER 18-1), Avionics Engineering Center, Ohio University, Athens, Ohio; January, 1974.

[2] Reifter, D. R., "Instrument Landing System for CAT III Operation, Multipath Interference Effects Due to Ground Movement of a Boeing 747 Aircraft on Heathrow Airport, London," TELS 34/2/069; January, 1971.

[3] Gorman, James T., "The Effects of Scattering from a 747 Aircraft Fuselage on the Operation of the Glide Path Portion of an Instrument Landing System," Master's thesis (supported by Federal Aviation Administration), Avionics Engineering Center, Ohio University, Athens, Ohio; March 20, 1971.

[4] Kwon, Young S., "The Effects of Reflection from Boeing 747 on Image Glide-Path Systems," Master's thesis (supported by Federal Aviation Administration), Avionics Engineering Center, Ohio University, Athens, Ohio; June 10, 1972.

[5] Rondini, Robert A., "A Study of Diffraction of Electromagnetic Waves Around Large Stationary Aircraft and Its Effects on Instrument Landing System Guidance Signals," Dissertation (supported by Federal Aviation Administration), Avionics Engineering Center, Ohio University, Athens, Ohio; June, 1976.

[6] Longworth, Joe L., "Instrument Landing System Critical Area Studies: Phase I, Theoretical and Experimental Investigation of Boeing 747 Dual-Frequency Localizer Signal Scattering for CAT III Critical Area Determination," (EER 59-3), Avionics Engineering Center, Ohio University, Athens, Ohio; November, 1983.

[7] Longworth, Joe D., "Instrument Landing System Critical Area Studies: Phase II, Theoretical Investigation of Wide-Body Aircraft Single-Frequency 8- and 14-Element Localizer Signal Scattering for Category III Critical Area Determination," (EER 59-3), Avionics Engineering Center, Ohio University, Athens, Ohio; November, 1983.

[8] Op. cit., Longworth, Phase I, pp. 13, 21.

[9] "Manual on Testing of Radio Navigation Aids," ICAO Document 8071, Vol. I, p. 62A, (3rd Edition, January, 1974).

[10] U.S. Flight Inspection Handbook OAP 8200.1 217.2, Figure 217-1A (Change 32)

[11] Op. cit., Longworth, Phase I.

[12] Op. cit., Longworth, Phase II.

[13] McFarland, R. E., "Instrument Landing Critical Area Studies: Phase III, Critical Area Determination for Null-Reference Glide Slope Considering General Aviation Aircraft," (EER 59-3) Avionics Engineering Center, Ohio University, Athens, Ohio; September, 1969.

[14] Op. cit., Koodini.

[15] Chun, E., et. al., "Users Manual for ILSLOC: Simulation for Derogation Effects on the Localizer Portion of the Instrument Landing System," Report No. FAA-RD-73-76, Department of Transportation Transportation Systems Center, Cambridge, MA; August, 1973.

[16] Op. cit., McFarland, pp. 99, 91.

[17] Op. cit., Chun, et. al.

[18] Op. cit., Longworth, Phase II, pp. 38, 79.

[19] Op. cit., Longworth, Phase II.

APPENDIX I

ILS FILTERING TECHNIQUES

The following discussion describes the analysis and realization of a first order recursive digital filter used to simulate the effects of a typical RC filter used in standard ILS receiver installations. The RC filter defines the frequency response of the ILS localizer and glide slope CDI signals as they are displayed on cross pointers and employed in automatic guidance systems. The desired time constant of such a filter is generally accepted to be 50/V seconds, where V is the velocity of the aircraft in knots. Given a typical speed of a landing aircraft of 117 knots, the TC (time constant) is calculated to be .424 seconds. The frequency associated with this time constant is 2.36 Hz. A low-pass filter selected for this frequency response can be represented by the schematic diagram shown in figure 136. Taking the nodal analysis @ node 1

$$I_1(t) + I_2(t) = 0 \qquad \text{(Kirchoff's current law)}$$

Initial conditions are $v_i(0)=0$, $v_o(0)=0$

$$I_1(t) = \{V_o(t) - V_i(t)\}/R$$

$$I_2(t) = C^* \left[\frac{dV_o(t)}{dt}\right]$$

where $dV_o(t)/dt$ is the derivative of $V_o(t)$

Therefore $I_1(t) + I_2(t) = \{V_o(t) - V_i(t)\}/R + C^* \left[\frac{dV_o(t)}{dt}\right]$

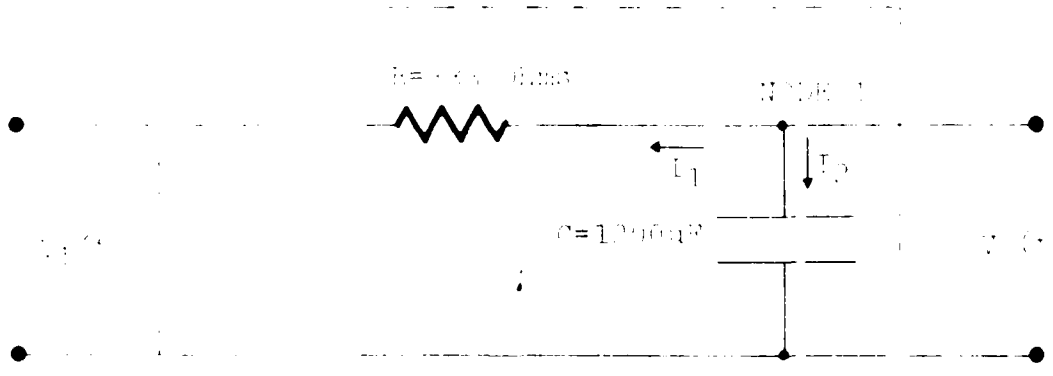

Figure 136 Schematic representation of an RC filter used in ILS receiver installations.

which implies that $V_o(t) - V_i(t) + R*C* \frac{dV_o(t)}{dt} = 0$ .... (Equation 1)

Transforming the differential equation (Equation 1) into the S-domain i.e. the Laplace Transform we have:

$$V_o(s) - V_i(s) + R*C\{sV_o(s) + v_o(0)\} = 0$$

where $s=jw$

$v_o(0) = 0$

$V_o(s)(1 + s*R*C) = V_i(s)$ ..... (Equation 2)

But transfer function of any given network is given by $H(s) = V_o(s)/V_i(s)$

Then from Eq. 2 $H(s) = \frac{V_o(s)}{V_i(s)} = \frac{1}{(1 + s*R*C)}$ ..... (Equation 3)

multiplying the R.H.S. of Equation 3 by $\frac{1}{RC} / \frac{1}{RC}$ yields

$$H(s) = \{1/ R*C)\}/\{s + 1/(R*C)\}$$

Let $\frac{1}{R*C} = w$

Therefore $H(s) = \frac{w}{s + w}$

Since a digital filter is desired, the Z-domain of H(s) is required.

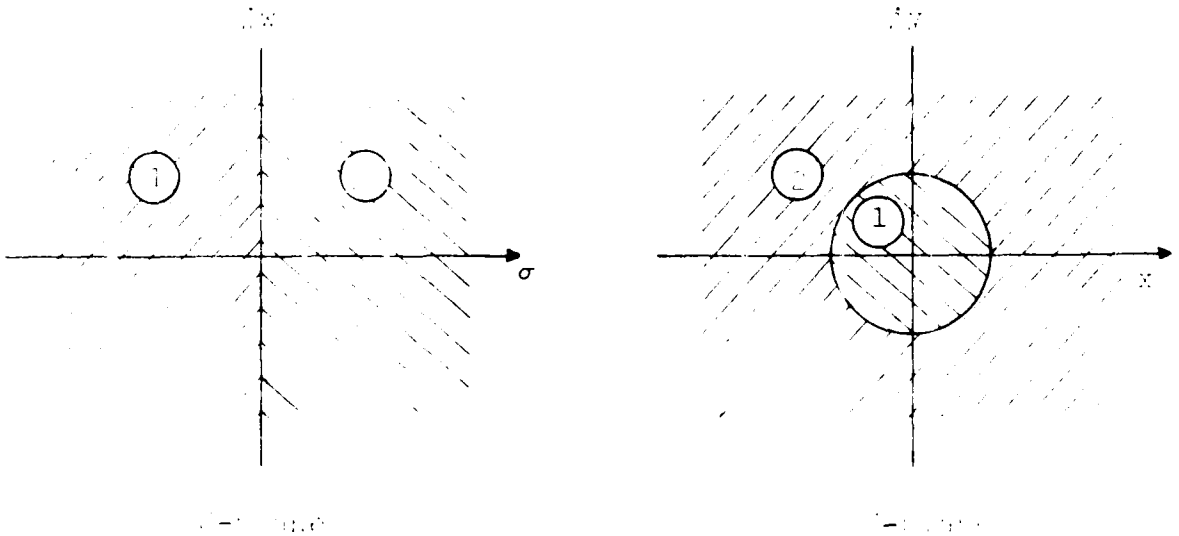

Figure 13/ Relationship of S-plane and Z-plane.

In the Z-domain $z = e^{sT}$ and $z^{-1} = e^{-sT} = e^{-jwT}$ (since $s = jw$)

The formula for mapping an S-domain function to a Z-domain function is given by:

$$\frac{1}{s+a} \rightarrow \frac{1}{1-e^{-aT}z^{-1}}$$

mapping of s to z

Therefore if $H(s) = \frac{w}{s+w}$

then

$$H(z) = w/(1-e^{-wT}z^{-1})$$

but $z = e^{-jwt}$

then $H(z) = w/(1-e^{-wT}e^{-jwt})$

The problem with this type of transformation is that of folding. This is caused by the overlapping nature of the samples, due to the nature of the approximation involved in the digitalization process. Thus a digital filter response of this type of transformation can be thought of as arising from the summation of the translated responses. If the out-of-band transmission of the continuous filter is small and the sampling frequency, f_s is large compared to the frequency of interest, then this effect of folding or aliasing will be small.

To avoid this problem the bilinear transformation is applied and samples are taken at high enough rate so that folding is greatly minimized.

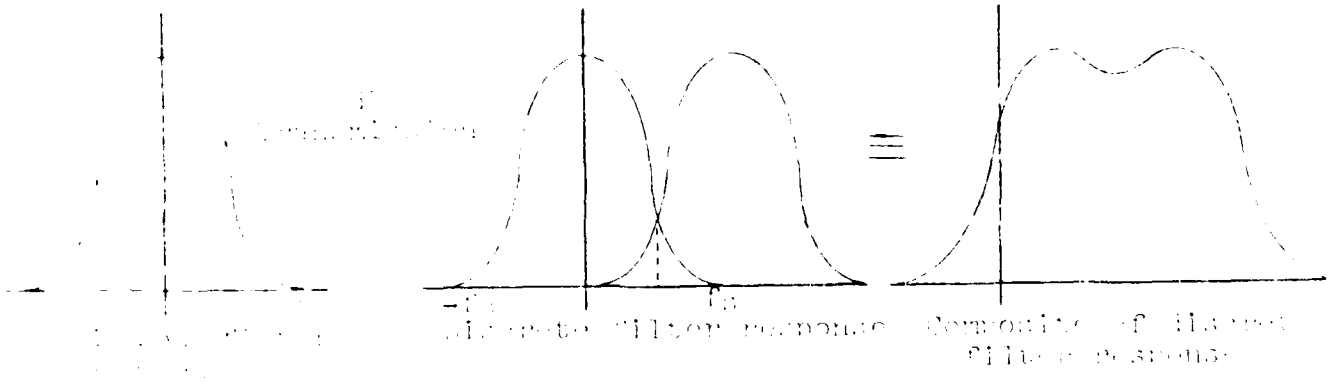

Figure 3.8 Effects of aliasing caused by under-sampling of input signal.

In this case (i.e. for bilinear transformation)

$$s = \frac{2}{T}\left[\frac{z-1}{z+1}\right]$$

$H(z)=H(s)$ evaluated at $s = \frac{2}{T}\left[\frac{z-1}{z+1}\right]$

$$H(z) \quad \frac{T*w(z+1)}{(2*(z-1)+T*w(z+1)} \qquad \text{(Equation 5)}$$

multiplying equation 5 by $\frac{z^{-1}}{z^{-1}}$

$$H(z) = T*w(z+1)*z^{-1}/((2*(z-1)+T*w(z+1))*z^{-1})$$

$$H(z) = T*w(1+z^{-1})/(2(1-z^{-1}) + T*w(1+z^{-1}))$$

$$V_o(z)/V_i(z) = H(z)$$

$$\frac{V_o(z)}{V_i(z)} = T*w(1+z^{-1})/(2*(1-z^{-1})+T*w(1+z^{-1}))$$

Cross-multiplying above equation,

$$V_o(z)*(z^{-1}(T*w-2)+(T*w+2)) = V_i(z)*(T*w(1+z^{-1})$$

$$V_o(z)*(T*w+2)+V_o(z)*(z^{-1}*(T*w-2)) = V_i(z)*(T*w(1+z^{-1}))$$

$$V_o(z)=(V_i(z)*T*w+V_i(z)*z^{-1}-V_o(z)*z^{-1}*(T*w-2)/(T*w+2)$$

Taking the inverse Z-Transform

$$Z^{-1}(V_o(z)) =$$

$$Z^{-1}\{T*w(V_i(z)+V_i(z)*z^{-1}-(T*w-2)V_o(z)*z^{-1}))/(T*w+2)\}$$

Therefore the inverse z-transform equals;

$$v_o(n) = (T*w*v_i(n)+T*w*v_i(n-1)-(T*w-2)*v_o(n-1))/(T*w+2) \quad \text{(Equation 6)}$$

where T = sampling period
w = 1/(R*C) = 1/(time constant (TC))
v_i = input signal
v_o = filtered output signal
n = position index number

The equation used in this computer analysis is given by

$$FX(i)=(SP*(x(i)+x(i-1))-FX(i-1)*(SP-2*TC))/(SP-2*TC) \quad \text{...(Equation 7)}$$

AD-A158 844 THEORETICAL INVESTIGATION OF SINGLE-FREQUENCY 8-ELEMENT 3/3
LOCALIZER SIGNAL (U) OHIO UNIV ATHENS AVIONICS
ENGINEERING CENTER W D PHIPPS MAY 85 OU/AEC/EER-59-4
UNCLASSIFIED DOT/FAA/PM-85/4 DTFA01-82-C-10050 F/G 17/7 NL

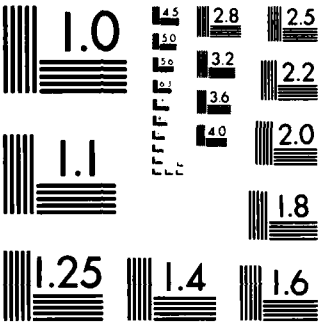

MICROCOPY RESOLUTION TEST CHART

DARDS-1963-A

where SP = sampling period
TC = time constant
x = input signal
FX = filtered(output signal)
i = position index number

Comparing the terms in equation 6 and 7 we see that

T in eq. 6	=	SP in equation 7
w in eq. 6	=	1/(TC) in equation 7
v_i in eq. 6	=	x in equation 7
v_o in eq. 6	=	FX
n	=	i
$v_i(n)$	=	x(i)
$v_o(n)$	=	FX(i)

NOTE: There is no direct relationship between T and TC
TC is the time constant defined by R*C
T is the sampling period defined by 1/(sampling freq)

A substitution of the equivalent parameters from equation 6 into equation 7 yields the formula using the mathematical model.

END

FILMED

10-85

DTIC